Seismic Coupling and Hydrological Responses

by

Shahid Rashid

A thesis
presented to the University of Waterloo
in fulfilment of the
thesis requirement for the degree of
Master of Science
in
Earth Sciences

Waterloo, Ontario, Canada, 2006

Author’s Declaration for Electronic Submission of a Thesis

I hereby declare that I am the sole author of this thesis. This is a true copy of the thesis, including any required final revisions, as accepted by my examiners. I understand that my thesis may be made electronically available to the public.

Abstract

In seismology, the capability of an earthquake to induce other seismic events has been widely accepted for decades. For example, the term aftershock involves a strong relation of such a seismic event with the incidence of a main shock. Moreover, hydrological changes (water level in wells and streams, geyser eruption and remote seismicity) in response to remote earthquakes have been reported for many years. A matter of current debate concerns the spatiotemporal scale of interaction among seismic events. However, there appears to be no clear image of what is the exact method of transmission of the triggering energy for the phenomena listed above. It appears that the P-wave and the S-wave are inadequate in terms of ground strain magnitudes at teleseismic distances, while the amplitude of the surface waves generally decreases exponentially with depth in the Earth and could not be responsible for triggering deeper earthquakes or deep-seated fluid flow fluxes in 3-5 km deep reservoirs. This leaves some other wave as a possible triggering energy sources.

This thesis is based on a diffusion-dynamic theory that predicts a low velocity displacement wave, called a soliton wave, propagating in liquid-saturated porous media with velocity ~100-300 m/s, analogous to a tsunami that travels with the loss of little energy. This is hypothesized to be the mechanism for energy transfer that could be sufficient to promote changes in local pore pressure and therefore to alter the ambient effective stresses. It is also hypothesized that a soliton wave packet is emitted by a primary seismic event and may trigger sympathetic secondary earthquakes at a remote distance, fluid level fluctuation in wells, changes in geyser eruption behaviour, and changes in microseismic frequency, amplitude and patterns in appropriate places (e.g. under water reservoirs, in areas of active hydrothermalism, in tectonically active areas, and so on).

This thesis undertakes a review of some of these phenomena, and finds that the evidence as to what is the triggering mechanism is not clear. Also, it appears that the soliton hypothesis is not at all disproved by the data, and there may be some evidence of its existence.

To reveal the evidence of this kind of wave (soliton) in nature, real sequence and K-Q cases velocity data bases of earthquake interactions in the year of 2003 have been constructed by using information from Incorporated Seismological Research Institute (IRIS). The qualitative and quantitative analysis demonstrates that interactions between seismological and hydrological systems due to soliton waves are a definite possibility. However, the growth of fluid fluxes, geysers eruption and remote seismicity are controlled by both the principal stresses and the pore pressure. Hence, this interaction depends on the hydromechanical properties of rock such as permeability, compressibilities, and viscosities of fluids, saturations, and porosity. Perhaps the strongest argument in favour of a low-velocity soliton trigger is that the other seismic waves seem to be inadequate, and there is no evidence for their actions as a trigger.

The practice of detection and analysis of a soliton is not undertaken in this work. Because current devices are incapable to measure such a wave as they are on the surface and insensitive to liquid-solid coupling, sensitive and precise sensors in the low frequency range must be installed within the liquid saturated zone, preferably under the water table, to advance further work.

Acknowledgements

I would like to express my gratitude to my supervisor Dr. Maurice Dusseault for his precious direction, conversation and financial support.

I would like to thank Dr. Tim Spanos for his valuable input which greatly assisted in the completion of my research work.

I would also like to thank to my thesis and defence committee members Dr. Anthony L. Endres and Dr. Giovanni Cascante.

Finally I am grateful to my family who facilitated and pray for me to complete my aspiration.

Dedication

To my adoring mother and late father

Table of Contents

List of Figures

List of Tables

Chapter – 1

Introduction

1.1 Introduction

Earthquake prediction is a great challenge for scientists; they are not well predicted, but numerous observations accumulated during the past 40 years demonstrate that earthquakes may alter water and oil production behaviour (Beresnev and Johnson 1994). Moreover, hydrological changes associated with earthquakes have been noted for decades and have occurred both near and far from the epicentre of the earthquake (Sneed 2003).

Interactions between seismological and hydrological domains have a potential to help determine temporal and spatial changes in hydrological systems and help interpret alterations in behaviour or special events at scales of pores to continents (Montgomery and Manga 2003). It is hard to imagine how a rock mass 5000-8000 km away from earthquake could behave in any other way but elastic, and in an elastic rock mass, there should be no permeability alterations or effects associated with small strains. Apparently, from the documentation in the literature, this is not the case.

Seismic waves generated during earthquakes have clearly affected (increased) pore pressure and changed stress fields that have led to the occurrence of secondary fractures or faults, aftershocks and possible even secondary earthquakes of significant magnitude. Seismic coupling evidenced as changes in hydrological systems and alterations in the incidence of microseismicity at remote sites is reported in numerous publications. The fluid fluxes in streams and in wells are associated with expulsion or intrusion of fluids, stress changes, alterations in strain distribution and pore pressure diffusion (perhaps under altered pressure gradients); these effects also are recorded to have taken place at teleseismic distances after a remote earthquake of large magnitude.

Geilikman et al. (1993) derived a mathematical expression for a porosity diffusion process that is shown to radiate from seismic events in fluid-saturated media. This process would lead to a wave-like excitation that can cause a change in pressure as it transits through the saturated porous medium. It is associated with a moving wave of

porosity dilation, and is a logical candidate mechanism for variations in fluid levels in the earth's crust, as well as other effects, following an earthquake.

Spanos (2002) proposed a general theory of wave transmission in multiphase porous media accounting rigorously for the compressibilities and energy conservation laws in all of the phases, at the appropriate scales. This theory is a coupled diffusion-dynamic theory that accounts for not only the small-strain aspects of classical wave propagation treated in the Biot-Gassmann formalism (dynamic), it also accounts for the effect of liquid movement in the pores during dynamic excitation at any frequency, even the slow frequencies associated with pressure changes handled by Darcy's Law (diffusion). His full mathematical formulation led to a new solution that was linked to a "porosity dilation" wave, a slow and long wavelength wave analogous to a tsunami that can transit the porous liquid-saturated medium and travel great distances because it is conservative. It is of interest to try and find evidence for the existence of this wave.

According to a broad interpretation of the theoretical work of Spanos, combined with other publications related to his work, the porosity (pressure) diffusion wave mentioned by Geilikman et al. (ibid.) (now called a porosity dilation waver or a soliton) can enhance the fluid flux in wells, affect remote seismic activity and may even trigger secondary earthquakes at remote distance, as Geilikman et al. (ibid.) implied. It is also note in some of the work that the time of propagation for the transit of the triggering energy that causes these phenomena is far slower than the velocity of seismic waves such as the compressional, shear, stoneley, or other common waves that are adequately conservative to travel hundreds of kilometres (Spanos 2002). Note finally that it is unlikely that surface waves could be responsible at any time for triggering deep earthquakes or flow alterations into deep-seated oil wells (>1000 m deep).

This research work is based on a hypothesis that seismic coupling may instigate variations in hydrological systems, fluid flow, remote seismicity, geyser eruption, and oil production. It is hypothesized that a soliton wave packet is emitted by a primary event, and that this can, because of the physical nature of the process, trigger sympathetic secondary earthquakes at a distance. Theory predicts that such a soliton travels with

much lower velocity than other seismic waves such as body and surface waves. Generally, body waves are too fast and surface waves lose energy exponentially with depth into earth. The soliton wave propagates with the velocity of 100-300 m/s and is considered to be a likely mechanism for energy transfer that could lead to changes in the local pore pressure and alter stress fields.

The soliton wave is described as a displacement wave (rather than a strain wave) with a large amplitude, low frequency and highly conservative so that it can travel long distances with little loss of energy or structure, similar to a tsunami in the open ocean that can travel 10,000 km with very small energy loss if circumstances are appropriate. In this thesis, interactions between fluid flow and porous media deformations due to the hypothesized soliton wave packet transit (slow displacement wave) are examined. Research work in this field herein is taken on the basis of a historical review of evidence and in some cases the development of new evidence. Hence, phenomena are re-examined in the context of the hypothesis that such a wave exists.

Its detection and analysis in practice is left for others, as current devices are ill-suited to measure such a wave. It must be measured at very low frequencies, from 10^{-2} to 10^{0} Hz, two orders of magnitude below common seismic needs, and sensors must be within the liquid saturated zone, not at the surface or in the phreatic zone. Preferably, sensors should be seated in porous bedrock as well.

1.2 Approach

The research goal is to try and find any evidence to support the existence of a soliton wave propagating with velocity ~100-300 m/s that could be responsible for altering fluid levels in wells, geyser eruption changes, and remote seismicity. Also, an attempt will be made to analyse public-domain earthquake data, where primary earthquakes may perhaps trigger secondary earthquakes at teleseismic distances (i.e. not local aftershocks) through interaction of the secondary system with a passing seismic wave train. More specifically, the intent is to:

- Examine whether effects that have been well-reported could be reasonably attributed to a soliton-like body displacement wave arising from liquid-solid coupling, perhaps affecting behaviours such as:
    - Microseismic swarms
    - Geyser activity
    - Pressure levels of production rates in wells
- Clarify the nature of triggering of sympathetic earthquakes
- Study the timing of water level or water pressure responses to earthquake excitation that might be due to the effect of a soliton wave
- Examine earthquake wave trains (CODA) from appropriately sited seismic stations for evidence of long wavelength, low frequency, slow waves (soliton wave, although note above that such seismic stations are ill-suited in general for this)

The nature of triggering of earthquakes after a major seism can be analyzed by looking the records of earthquakes. This section can be achieved by collection of data and calculations of velocities between foci of the major and the triggered earthquake, and examining the nature of the swarms of post-seismic events at teleseismic distances.

The velocity of energy transfer can be calculated by exploring the timing of pressure data or water level data related to earthquakes. It can be timed with reasonable accuracy (e.g. even 10 minutes or more would suffice for distant earthquakes).

Coda analysis involves looking for digital or analog data that can be digitized for analysis. Low velocities for the soliton wave means that the time lag after the arrival of the P-wave will be approximately 20-25 times the Δt for the P-wave (this can also be expressed as a function of the time delay between the P and S waves).

1.3 The Organization of the Thesis

This thesis consists of seven chapters and one appendix. After the general introduction to the soliton wave research, possible earthquakes interactions and hydrological changes,

the entire research process is defined herein in Chapter 1, and the studies are reported starting in Chapter 2.

Chapter 2 contains the theory, which restrains the hypotheses that are possible. Because the writer is not a mathematical physicist, a more intuitive and descriptive approach is taken.

In Chapter 3, literature observations of the fluid level changes in wells in response to seismic waves are studied. Fluid fluxes in wells in response to earthquakes are consistent with earthquake magnitude and depth, the distance from the epicentre, the hydrological environment, and whether the rock mass is a consolidated rock or an unconsolidated sediments.

Reservoir induced seismicity (RIS) during and after filling water reservoir behind a hydroelectric dam is examined in Chapter 4. Induced earthquakes are triggered due to rapid changes in water level after impoundment of the dam and decay with time. Delayed RIS can happen from pore pressure diffusion and fluid flux outside the strict reservoir volume, coupled also with the effect of an elastic load.

Chapter 5 investigates geysers activities and remote seismicity associated with earthquakes. Microseismicity activity is associated with stress, pressure, and temperature changes in the geyser or the underlying geothermal reservoir. Geyser activity can be changed by the transit of seismic waves which perhaps have changed the permeability by unclogging existing fractures, leading to pressure and stress changes.

Chapter 6 contains some evidence for the existence of slow soliton waves based on earthquake timing data. Graphs are drawn and cases are discussed of plausible interactions of earthquakes and variations in hydrological systems in response to the slow soliton-like displacement wave.

Conclusions and future work are given in chapter 7.

Appendix I is a data base of possible earthquakes interactions for large earthquakes in one year at interaction velocities of 100-300 m/s, which is the assumed speed of the soliton wave.

Chapter – 2

Displacement Wave Theory

2.1 Introduction

The existence of coupled diffusion-dynamic processes in porous media is well known. Earthquakes have altered (usually enhanced) production from reservoirs of modest porosity (elastic conditions without potential for compaction), as published in Russian literature (Beresnev and Johnson 1994). Water level variations in wells and increase in the flow of streams after earthquakes have been well documented (Manga et al. 2003). Sympathetic secondary earthquakes triggered at a remote area is a well-acknowledged possibility (Geilikman et al. 1993), and it is also known that for the triggering of secondary earthquakes, the time of propagation is slower than the velocity of body and surface waves or other common waves that are observed to travel hundreds of kilometres (Geilikman et al. 1993).

Based partly on the work of numerous predecessors such as Raleigh, Love, Gassmann, a comprehensive theory for elastic wave propagation in liquid-saturated porous media was developed by Biot in 1956 and is called Biot-Gassmann theory. The poroelastic terms derived by Biot have long been considered as standard and his Biot parameter, derived for static pressure changes of a stressed porous medium, has been the basis for resolving particular problems in poroelasticity (e.g. Rice and Cleary, 1976).

A soliton (displacement) wave theory for a porous medium must involve two coupled and interacting continua, which are assumed to be a liquid saturating a porous solid where the pores are all interconnected and the system is under a static confining stress. It is necessary to suppose that the liquid is compressible, in contrast to Darcy theory where the fluid is assumed to be incompressible. It is also necessary, as in Darcy theory, to stipulate that the pore liquid may flow relative to the solid matrix, causing a viscous resistance to arise (Spanos et al. 2003), and leading to possible out-of-phase inertial effects (where the solid and liquid are not moving in unison). However, the Biot-Gassmann theory of wave propagation does not consider viscous dissipation within the fluid element, nor does it consider any thermoelastic effect, such as might arise, for example, with compression and decompression of the liquid phase. On the other hand, in the basic Darcy flow theory for liquid diffusion through a porous medium, there are no terms of second order in time that

can provide any inertial effect. Therefore, Darcy theory is actually a static (or quasi-static), not a dynamic theory.

Porosity diffusion in porous media processes was suggested by Geilikman et al. (1993), who also showed that a low velocity wave can be postulated as a trigger for secondary earthquakes, perhaps by causing a pressure change in the pore liquid at a distance. In line with this, it is well documented that some form of wave excitation is responsible for earthquake induced changes in fluid flow in porous media.

Spanos revisited the problem of fluid flow and inertial wave propagation in porous media. Using the basic continuity equations and careful volume averaging methods, without unnecessary assumptions (such as assuming that porosity is a fixed quantity, as Biot did), Spanos (2002) developed a set of equations that couple diffusion and inertial processes in porous media. Because of the additional degrees of freedom introduced by not treating porosity as a fixed value, extra eigenvalue solutions (characteristic solutions) were found. One of these had not been treated before, and it appears to be a long wavelength, low frequency displacement wave (a soliton) that propagates slowly outward in liquid-saturated porous media.

Classical wave propagation theory in porous media is based on two widely accepted but seemingly restrictive assumptions:

- Porosity is assumed to be a constant scalar quantity
- "The energy state for a representative elementary volume can be described by a unique energy function" (Spanos et al. 2003)

These two restrictions are not necessary, and they lead to imperfect (incomplete) thermodynamic statements for porous media transport processes. This incompleteness, particularly in the cases of low frequency excitation and multiphase fluids, leads to results that obstruct theoretical improvements in thermomechanics (Spanos et al. 2003).

It is hypothesized that a soliton wave packet, generated by an earthquake and travelling great distances with little energy loss, is the agent that causes teleseismic phenomena

such as fluid level variations in wells, triggering of remote seismicity, changes in geyser eruption patterns, and even the initiation of sympathetic secondary earthquakes (not after shocks).

2.2 Seismic Waves

Seismic waves are packets of elastic strain energy that propagate outwards from a seismic source such as an earthquake or an explosion. Seismic waves are propagating pulses that may contain a wide range of frequencies, and they carry elastic energy away from the earthquake region. Of course seismicity, in particular small-scale seismicity (microseismicity), can be triggered by magmatic movements, eruptions, fluid movements, and man-induced activity such as fluid injection or underground mining.

Seismic pulse techniques are used to explore for oil and natural gas, as well as to study the nature of the subsurface geology. In natural seismic events, the measurements are recorded globally by real-time monitoring stations, usually placed on dry ground, and registering the solid-body strains associated with the transit of the waves. Strains associated with the passage of a seismic wave are small, at least several orders of magnitude below the levels associated with plastic deformation, and may be assumed to be elastic in nature (Kearey and Brooks 1996). The propagation speed (velocity, celerity) of seismic waves is determined by the elastic moduli and densities of the materials through which they pass. In the conventional view (neglecting the possible existence of the soliton mentioned above), there are two groups of seismic waves, body waves, and surface waves.

2.2.1 Body Waves

Body waves can propagate through the body of an elastic solid and can therefore travel through the interior of the earth, as well as along its surface. Body waves are further divided into two major types, one is known as the compressional wave or primary wave (P-wave) and the other is called a shear wave or secondary wave (S-wave) (Kearey and Brooks 1996).

The P-wave propagates in the direction of the particle oscillation. The vibration generated by P-waves is a minuscule volume change, alternating from compression to dilatation (rarefaction) in the direction that the wave is travelling, as shown in Figure 2.1. P-waves travel through all types of media such as solid, liquid, and gas (Kearey and Brooks 1996), although gas is a highly attenuative medium, particularly for higher frequencies.

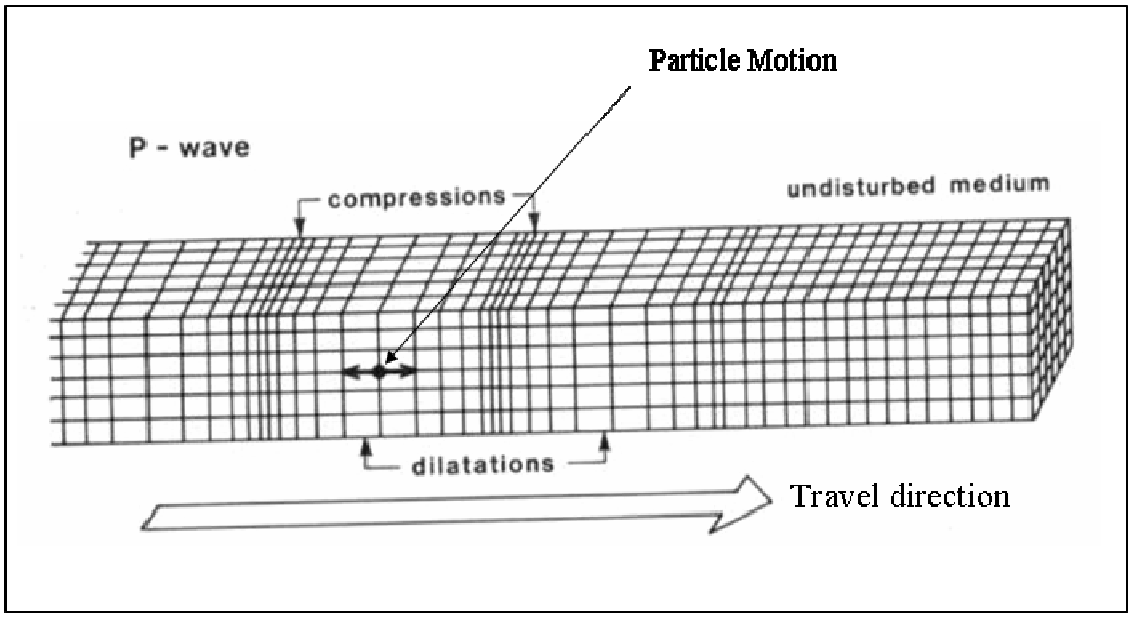

Figure 2.1: Elastic deformations and ground motions associated with the passage of P waves (modified after Kearey and Brooks1996).

The S-wave propagates perpendicular to the direction of particle oscillation as shown in Figure 2.2 and travels slower than P-waves (Kearey and Brooks 1996).

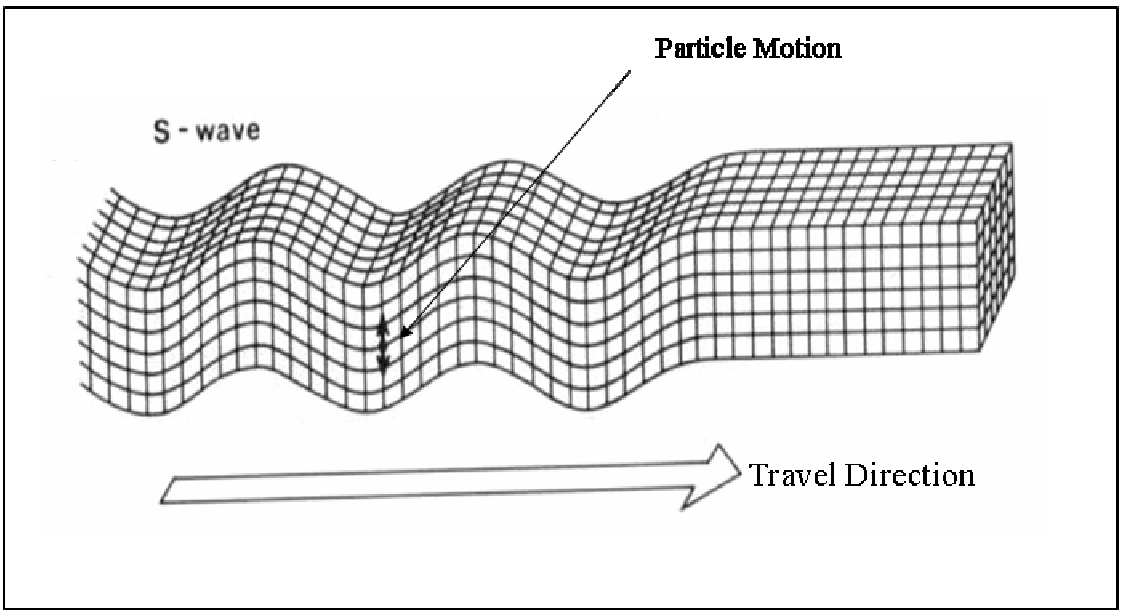

Figure 2.2: Elastic deformations and ground particle motions associated with the passage of S-waves (modified after Kearey and Brooks1996).

A distinctive characteristic of the S-wave is its incapability to propagate through a fluid or a gas because fluids and gasses cannot transmit shear stress and S-waves are waves that shear the material. In general, earthquakes generate larger amplitude shear waves than compressional waves because the release of the stored elastic energy in the earth is mostly through sudden shear displacement along a fault plane. Much of the damage close to an earthquake is the result of strong shaking caused by shear waves (Braile 2004).

2.2.2 Surface Waves

In a bounded elastic solid, seismic waves known as surface waves can propagate along the boundary of the solid. Though surface waves penetrate to some depth below the surface of the earth, they do not travel directly through the earth's interior because of the lack of a free surface.

Surface waves are further divided into two kinds. The Rayleigh wave is a surface wave that propagates along a free surface or along the boundary between two dissimilar solid media. The solid particles' motion is elliptical in the plane, perpendicular to the surface,

and containing the direction of propagation, as shown in Figure 2.3 (Kearey and Brooks 1996).

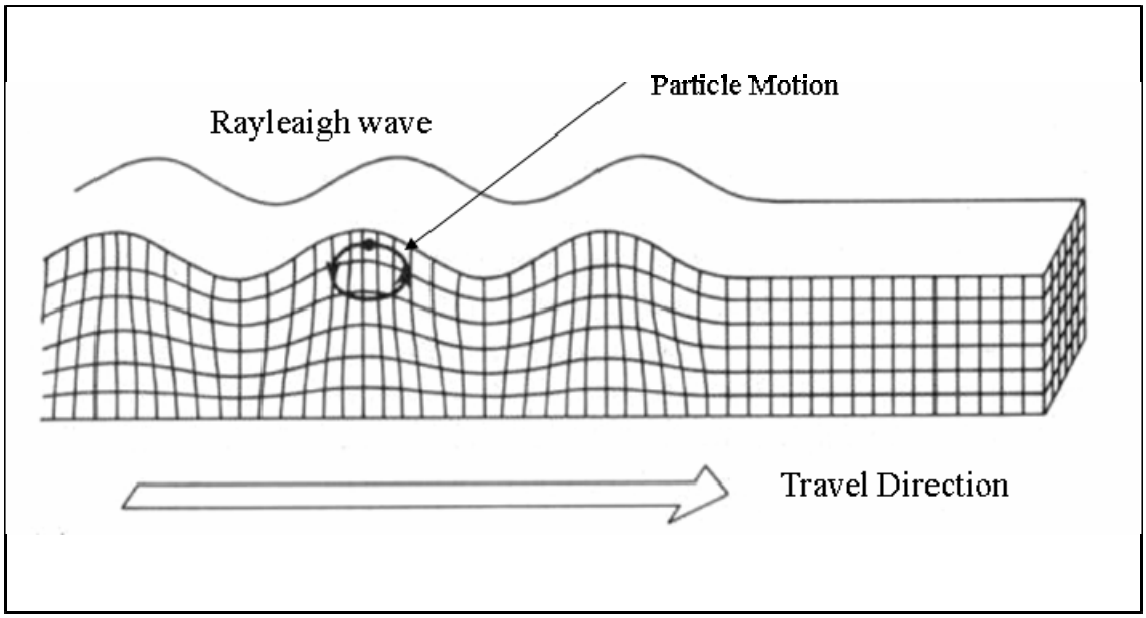

Figure 2.3: Elastic deformations and ground particle motions associated with the passage of Rayleigh wave (modified after Kearey and Brooks1996).

In a layered solid, a second set of surface waves, known as Love waves, can propagate with particle motion parallel to the free surface and perpendicular to the direction of wave motion, as shown in Figure 2.4.

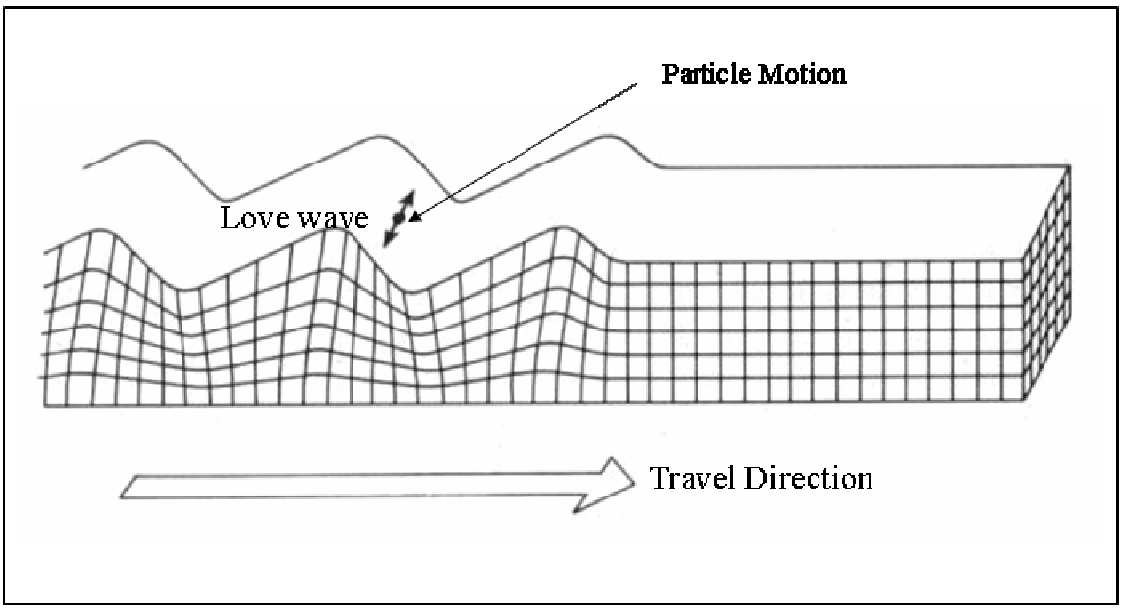

Figure 2.4: Elastic deformations and ground particle motions associated with the passage of Love waves (modified after Kearey and Brooks1996).

In general, surface waves are larger in amplitude and longer in duration than the body waves. Furthermore, surface waves with longer wavelength (longer period and low frequency) provide more information about the subsurface velocity structure than surface waves with shorter wavelength (short period and high frequency), which tend to contain information only about shallow structures (Braile 2004). P-waves, S-waves, R-waves and L-waves can be identified on the seismogram of distant earthquakes, as shown in Figure 2.5.

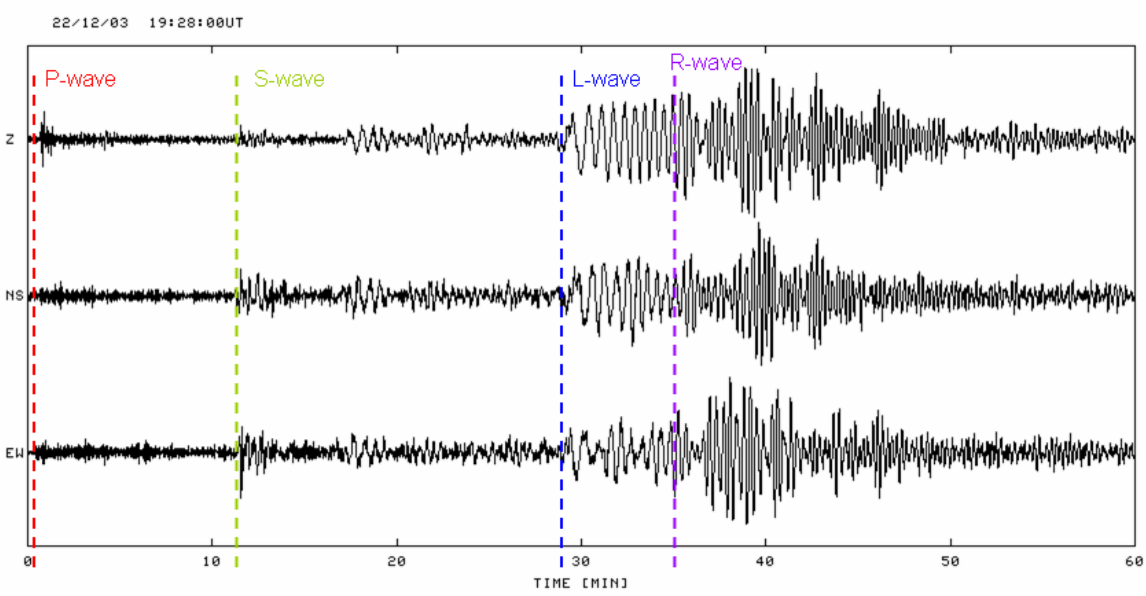

Figure 2.5: Seismogram shows seismic waves records (Braile 2004)

The first significant wiggle will register the arrival of the P-wave, as P-waves are the fastest seismic waves. The next set of seismic waves on the seismogram will be the S-waves. If S-waves have not been recorded on a large earthquake seismogram, then there are two possibilities: one is that the earthquake is on the other side of the planet (shielded), and second possibility is that S-wave disappeared because it cannot travel through a liquid zone. Surface waves arrive on the seismogram after the shear wave and usually have larger amplitude. Surface waves propagate a little slower than S-waves (which are slower than P-waves). The surface waves may possibly be the largest waves recorded by the seismograph for shallow earthquakes (earthquakes with a focus near the surface of the earth) (Braile 2004).

It is important to remember that the seismometers (or geophones or accelerometers) used to detect and record the seismic waves are almost always set up at the surface of the earth, relatively far from the saturated zone. Therefore, these devices are extremely well-positioned to record the maximum amplitude of the surface waves, but ill-equipped to record any changes in pressure at depth, or any waves that require propagation through a liquid-solid medium. If a geophone, accelerometer, or pressure sensor with an extremely broad range of frequency sensitivity is placed deep in the earth, well below the water

table, it would record far weaker surface wave effects, and would be well-positioned to pick up any low-frequency waves such as the soliton wave discussed above. Unfortunately, detailed data from this type of recording station is very rare.

2.2.3 Seismic Wave Speed

Seismic waves propagate fast, on the order of kilometres per second (km/s). The precise speed that a seismic wave travels depends on several factors such as stress, temperature, elastic properties and density of the rock (Kearey and Brooks 1996). Increased temperature tends to lower the speed, whereas increased stress tends to increase the speed of seismic waves. Pressures and stresses increase with depth in earth due to the weight of the rocks and the column of connected water. In general, the speed of seismic waves increases with depth in earth (Braile 2004).

Rocks can be characterized as elastic, ductile or brittle. When external forces are applied to a rock body, internal forces are balanced within it, for example, through grain contact loads or fluid pressures. The averaged effect of the applied forces is referred to stress and the resulting deformation caused by a change in stress is called a strain. The stress is deemed compressive if the forces are directed towards each other and tensile if the forces are directed away from each other. The rock body behaves elastically (recoverable) to a small change in stress, or it can yield permanently (non-elastic deformation) if a strength limit, a certain limit value of stress, is surpassed. In an ideal solid, the strain response to a stress change is linear (Hooke's Law), and if stress is removed, the elastic strain is fully recovered, so that elastic strain is reversible (Kearey and Brooks 1996). If the stress is increased above some limit, the strain becomes non-linear and partly irreversible. That portion that is non-recoverable is called ductile or plastic strain. If the stresses are increased even more, above some strength limit, the internal structure of the rock breaks down, this is known as the brittle point or shear fracture point. The relationship between the stress and strain that a material displays is known as a stress-strain curve, as shown in Figure 2.6. Rocks are typically ductile at high temperature and pressure (Kearey and Brooks 1996), but there is also a component of velocity: rapid loading, as in an

earthquake, generates elastic waves, but very slow loading, as at the crust-mantle boundary, generates very slow ductile deformation.

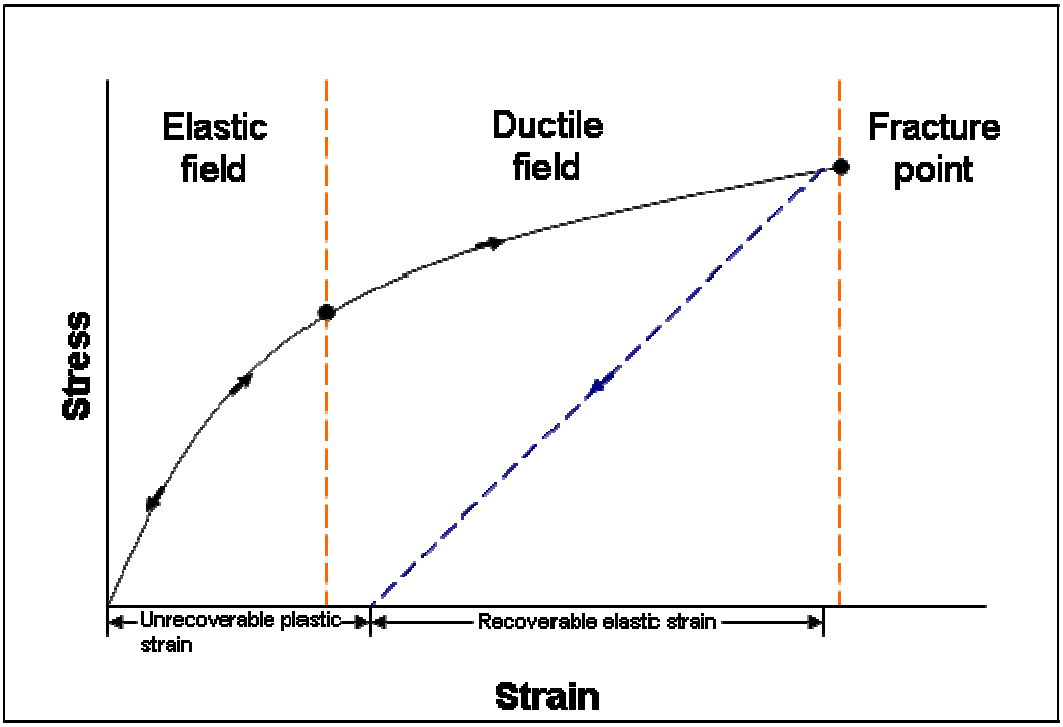

Figure 2.6: A typical stress – strain curve for a solid body (modified after Kearey and Brooks 1996).

Seismic body wave velocity is determined by the rigidity to compression, the rigidity to shear, and the density of the medium (Kearey and Brooks 1996):

$$\mu = \frac{E}{2(1+\upsilon)} \tag{2.1}$$

$$K = \frac{E}{3(1-2\upsilon)} \tag{2.2}$$

Where,

μ = rigidity (shear) modulus (N/m^2)

E = Young's modulus of elasticity (N/m^2)

υ = Poisson's ratio (dimensionless)

K = bulk modulus (N/m^2)

The velocity of propagation of a body wave in any material depends on the elastic properties and density and mathematically expressed as (Kearey and Brooks 1996).

$$V = \sqrt{\frac{appropriate.elastic.\mathrm{mod}ulus.of.material}{density \rho.of.material}} \tag{2.3}$$

Where,

ρ = density of a material

The velocity of a P-wave (V_p), which involves a uniaxial compressional excitation and strain in the direction of propagation, is expressed mathematically as (Kearey and Brooks 1996).

$$V_p = \sqrt{\frac{K + \frac{4}{3}\mu}{\rho}} = \sqrt{\frac{E}{\rho}\frac{1-\upsilon}{(1+\upsilon)(1-2\upsilon)}} \tag{2.4}$$

The velocity of the S-wave (V_s) in a solid body, which involves a pure shear strain, is described mathematically as (Kearey and Brooks 1996):

$$V_s = \sqrt{\frac{\mu}{\rho}} = \sqrt{\frac{E}{\rho}\frac{1-\upsilon}{2(1+\upsilon)}} \tag{2.5}$$

It can be seen from these equations that V_p always travels faster than V_s in the same medium. V_s is zero if the rigidity modulus is zero; so V_s does not propagate in a liquid medium. Since Poisson's ratio for consolidated rocks is typically about 0.25, $V_p \approx 1.7 V_s$ (Kearey and Brooks 1996).

Descriptions of wave characteristics and velocity for four types are given in Table 2.1. Table 2.1 describes the different seismic wave types and ranges of speed to indicate the range of values which has been observed in common terrestrial rocks. However, the specific speed in the earth will depend on composition, temperature, and pressure because of its heterogeneity (Braile 2004).

Table 2.1: Description of wave characteristics and velocity for four types of seismic waves (after Braile 2004).

Wave Type (and names)	**Typical Velocity**	**Other Characteristics**
P, **Compressional**, Primary, Longitudinal	V_P ~ 5 – 7 km/s in typical Earth's crust; >~ 8 km/s in Earth's mantle and core; ~1.5 km/s in water; ~0.3 km/s in air.	P motion travels fastest in materials, so the P-wave is the first-arriving energy on a seismogram. Generally smaller and higher frequency than the S and Surface-waves. P waves in a liquid or gas are pressure waves, including sound waves.
S, **Shear**, Secondary, Transverse	V_S ~ 3 – 4 km/s in typical Earth's crust; >~ 4.5 km/s in Earth's mantle; ~ 2.5-3.0 km/s in (solid) inner core.	S-waves do not travel through fluids, so do not exist in Earth's outer core (inferred to be primarily liquid iron) or in air or water or molten rock (magma). S waves travel slower than P waves in a solid and, therefore, arrive after the P wave.
L, **Love**, Surface waves, Long waves	V_L ~ 2.0 - 4.4 km/s in the Earth depending on frequency of the propagating wave, and therefore the depth of penetration of the waves. In general, the Love waves travel slightly faster than the Rayleigh waves.	Love waves exist because of the Earth's surface. They are largest at the surface and decrease in amplitude with depth. Love waves are dispersive, that is, the wave velocity is dependent on frequency, generally with low frequencies propagating at higher velocity. Depth of penetration of the Love waves is also dependent on frequency, with lower frequencies penetrating to greater depth.
R, **Rayleigh**, Surface waves, Long waves, Ground roll	V_R ~ 2.0 - 4.2 km/s in the Earth depending on frequency of the propagating wave, and therefore the depth of penetration of the waves.	Rayleigh waves are also dispersive and the amplitudes generally decrease with depth in the Earth. Appearance and particle motion are similar to water waves. Depth of penetration of the Rayleigh waves is also dependent on frequency, with lower frequencies penetrating to greater depth.

2.2.4 Attenuation of Seismic Energy

As seismic waves propagate, the original energy (E) moving outward from the source becomes distributed over a spherical wave front of growing radius. If the radius of the wave front is r, the amount of energy contained within a unit area of the wave front is $E/4\pi r^2$. As a result, the energy per unit decreases as $1/r^2$ due to the effect of the geometrical spreading of the energy. Wave amplitude, in a homogenous material, is directly proportional to the square root of the wave energy, which subsequently drops as $1/r$ (Kearey and Brooks1996).

Another cause of energy loss along a ray path takes place because the earth is not perfectly elastic in its response to seismic wave propagation. Due to internal frictional losses and adiabatic compression effects (usually ignored), elastic energy is steadily absorbed by the medium, leading ultimately to reducing the energy to the level of being undetectable. The absorption coefficient (α) is used to describe the amount of energy lost during wave transmission; it is the loss over a distance corresponding to one complete wavelength λ. Values of α range from 0.25 to 0.75 $dB\lambda^{-1}$ for common earth material (Stein and Wysession 2003).

Over the narrow range of frequencies commonly used in seismic analysis, α is assumed to be independent of frequency. This leads to the conclusion that if the amount of energy absorption per wavelength is constant, lower frequency waves attenuate less slowly than high frequency waves as a function of distance. To amplify this point, assume two waves with frequencies of 10 Hz and 100 Hz propagating through a rock, where v_p = 2.0 km/s and α = 0.5 $dB\lambda^{-1}$. The 100 Hz wave (λ = 20m) is attenuated due to absorption by 5 dB over a distance of 200 m, while the 10 Hz wave (λ = 200 m) is to be attenuated by only 0.5 dB over the same distance (Stein and Wysession 2003).

2.3 Soliton (pressure) Wave Theory

A soliton wave is a low-frequency displacement wave with high amplitude (energy) that propagates outward from an earthquake (or other suitable excitation source) just like any other seismic wave, although it travels much more slowly. It is shown as a propagating source in a rough sketch (isotropic medium) in Figure 2.7. Spanos has explored the nature of the soliton solution to his equations and has suggested that the soliton wave propagating through a liquid-saturated porous medium travels with a velocity ~100-300 m/s.[1] Therefore at 0.1 Hz, the wavelength is 1-3 km, and at a frequency of 0.5 Hz, the expected wavelength would be 200-600 m. It also travels long distances with little loss of energy or dispersion because it is a very long wavelength displacement wave, analogous to a tsunami (a liquid displacement wave) that can propagate thousands of kilometres with little loss of energy in the open ocean. In principal, the soliton wave should be measurable and detectable on full bandwidth seismograms taken with devices of sensitivity ranging from 0.01 to >100 Hz, but placed deep within the saturated zone and fully coupled to both the solid and the liquid phase. Finding suitable seismograms and executing such analysis is reserved for later work.

The soliton wave velocity is associated with the dynamic frequency at which pore liquid starts to behave incompressibly. It is well known that at low frequencies, liquids act incompressibly (according to Darcy flow, $<10^{-3}$ Hz); at high frequencies (sound frequencies, $>10^{1}$ Hz), liquids can compress and convey a compressional wave. Therefore, there must be some excitation frequency somewhere in between where the liquid starts to perform incompressibly and at that limit, a soliton wave is the result. Its velocity relies on the compressibility and viscosity of the phases, as well as the stresses and density (Dusseault et al. 2000).

---

[1] A number of the comments in this section remain unpublished or incompletely published because the coupled diffusion-dynamic theory has not been extensively studied in practice at this time. These comments are partly from personal communications with Spanos and Dusseault.

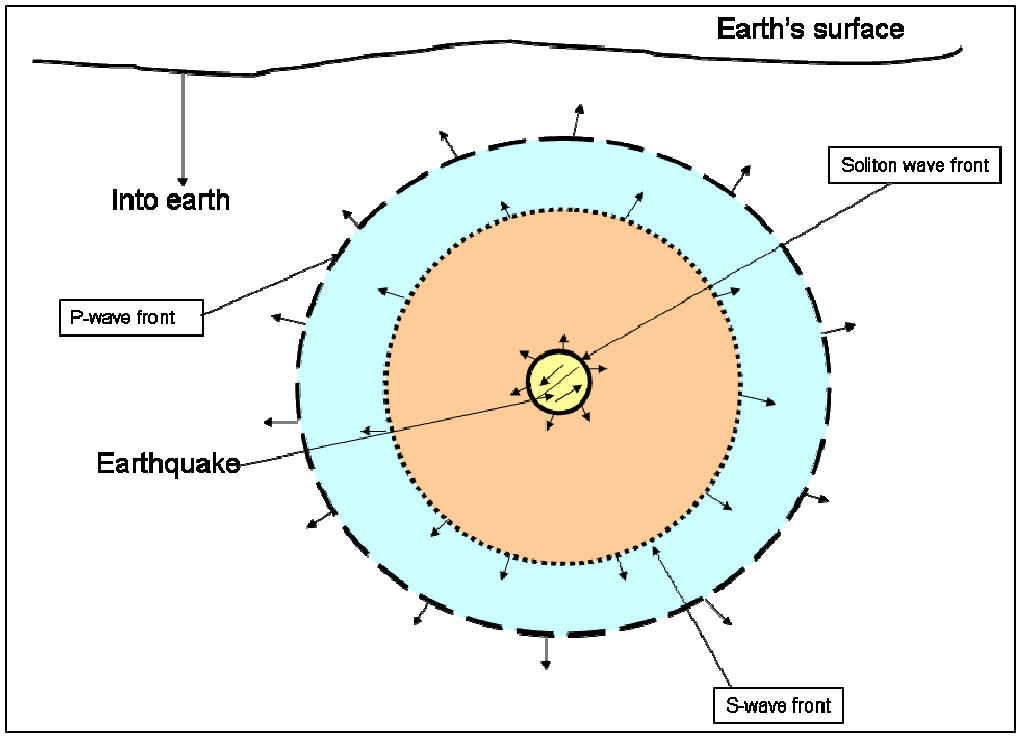

Figure 2.7: A rough sketch illustrates a soliton wave front after an earthquake (modified after Ammon 2006).

The soliton wave theory appears to be significant in earthquake mechanics as a mechanism for triggering of more distant earthquakes in critically stressed areas by increasing pore pressure (Spanos 2002). In addition, it is hypothesized to likely also be responsible for the alteration of fluid level in wells, inducing remote microseismicity and changing geysers eruption pattern.

2.3.1 Development of the Soliton (pressure) Wave Theory

Spanos (2002) wrote down the outlines of a rigorous theory of thermoporoelasticity of fluid-saturated porous media under a broad range of conditions. Previous simplifications and presumptions were studied, and discrepancies were eliminated, resulting in a theory that is more vigorously consistent than either Biot-Gassmann theory for wave propagation or Darcy's theory for non-dynamic. In fact, a strong test of the theory is that in the high frequency limit the Biot-Gassmann wave equation is recovered (in a slightly different form), and at the zero frequency limit, Darcy diffusion theory is recovered.

Spanos found that porosity plays a significant role in both the thermomechanics and thermodynamics of porous media, and it is not appropriate to treat it as a fixed quantity. To be rigorous, it should be considered as a thermodynamic state variable, analogous to pressure and temperature, and not as a dynamically constant quantity (Spanos et al. 2003). It must therefore enter into the time differentials in a manner similar to other thermodynamic variables and be differentiated with respect to time.

As mentioned, this theory leads to a prediction of a soliton wave (Spanos, 2002), but the mathematical treatment is complex and difficult to understand. Spanos et al. (2002, 2003) attempted to present the theory for a single phase liquid case only to simplify it. Even then, there are complex terms including viscosity, compressibility and first and second-order differentials that are challenging to understand. Thus, the discussion here is qualitative in nature.

In a solid isotropic body mass without porosity, the two recognized body waves are the compressional and shear waves. Now imagine a liquid-saturated porous medium where the liquid and the solid phase are in full continuity throughout. If the pressure in a small volume is abruptly changed, a local porosity change (+ve or –ve) arises. This creates an unbalanced force, which triggers a wave if the impulse is sharp. This wave is not a strain wave, it is a displacement wave that propagates through the physical displacement of the liquid (as in a tsunami), and this passes through the deformable porous medium as a soliton. The movement of liquid into and out of the pores as the wave passes is controlled by the permeability and the viscosity, and this defines a pore-scale diffusion process. That is why the theory contains diffusion terms, which are terms of ∂-/∂t, as well as wave terms, ∂^2-/∂t^2 (Spanos et al. 2003). The dependent variable in these differentials can be pressure, porosity, or displacement.

2.3.2 Darcy Flow and Biot-Gassmann Theory

Consider a range of mechanical excitation frequencies in a liquid-saturated porous medium, as shown in Figure 2.8. Two paradigms are typically used, Biot-Gassmann wave mechanics is used for high frequencies and Darcy flow mechanics without inertial effects

is used for low frequencies (Spanos et al. 2003). There noticeably must be more or less three orders of magnitude in between where both inertial and diffusion effects are consistently significant because the possible frequencies of excitation are continuous. No coupled interial-difussion theory presented before the work of Spanos allowed general analysis of the whole range of frequencies (Spanos et al. 2003).

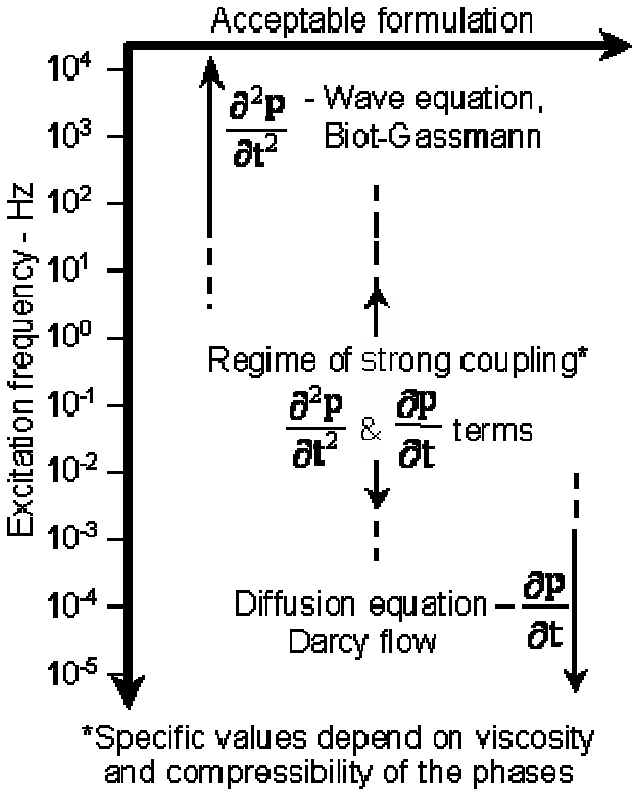

Figure 2.8: Excitation frequencies and theories (Spanos et al. 2003).

In the Biot paradigm, there exist several postulations that restrict its generality and make formulating true liquid-solid coupling impossible. Biot supposed that for a representative elementary volume (REV) in a multiphasic porous media, a single continuous thermodynamic function would be sufficient to express the energy state (neglecting any phase changes). This leads to an ambiguity that may be exhibited by a simple example. If a single function is enough, there can be only one value and direction of maximum gradient, and if the energy is exclusively a function of pressure, this implies that there may be only one direction of flow (Spanos et al. 2003). On the other hand, scientists have

performed flow experiments for decades where two continuous immiscible fluid phases, such as oil and gas, are instigated to flow at 90° or in opposite directions. This means that a single energy functional is inadequate. In fact, recent research work has demonstrated that if N continuous adjacent phases are present (physically continuous and linked together by the laws of physics and properly scaled), N energy functionals are required to fully describe behaviour (Spanos 2003). For an example, simultaneously, two immiscible systems such as oil and water can flow relative to one another in two directions as shown in Figure 2.9. This also happens at low seismic frequencies, resulting in out-of-phase liquid motion, with water and oil moving at different velocities with respect to each other.

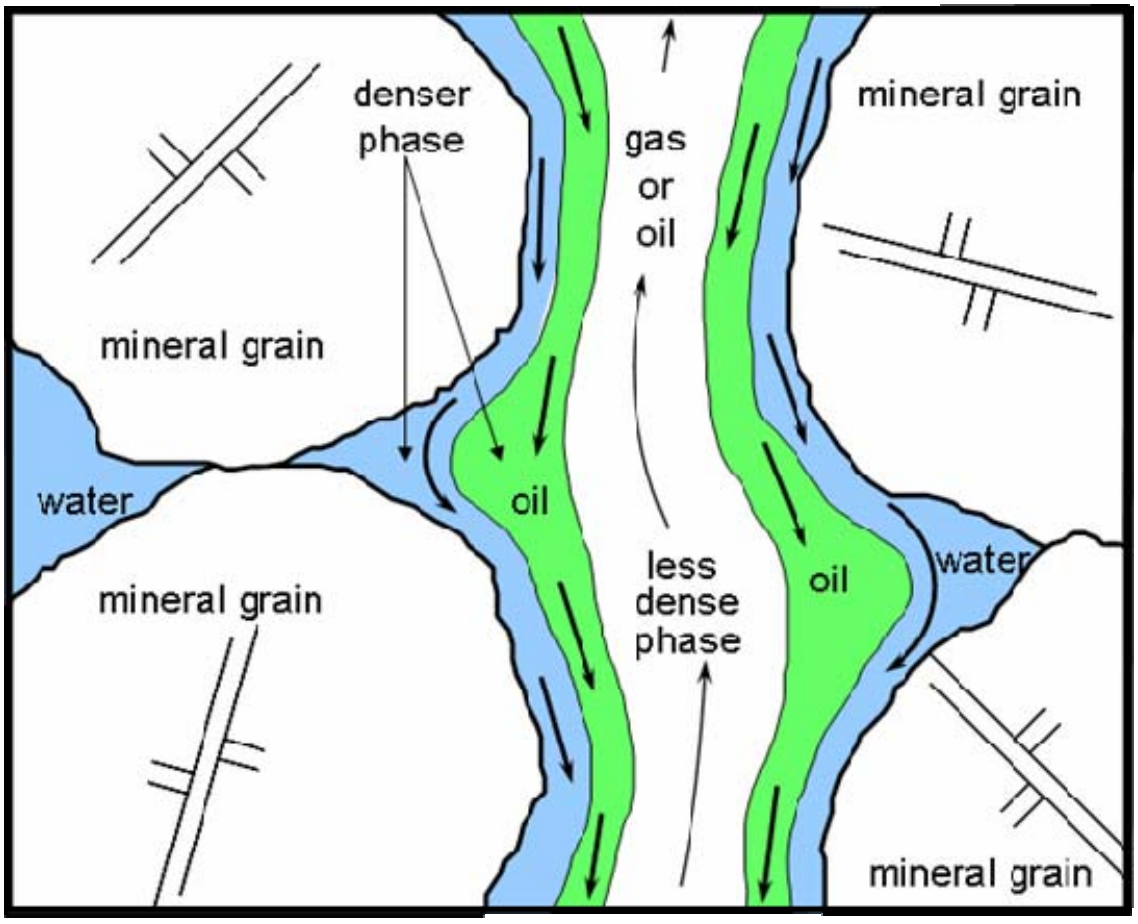

Figure 2.9: A micromodel of 3-phase gravitationally segregating flow (in a 2-phase system, oil and water only, oil may be the lighter phase that is rising) (Dusseault 2004).

It is clear that Biot considered that porosity (ϕ) was a fixed parameter, but this must be an approximation only because any strain that takes place (seismic P and S-waves are strain waves) means that both solid and liquid are compressed slightly, but because they have different compressibilities, they must change volume in different manners, therefore there is a small change in porosity. This means that the porosity change, for the temporal development of volume changes in a porous medium must be expressed as a balance equation over time:

$$\frac{\partial \eta}{\partial t} = \delta_s \overline{\nabla} \bullet \overline{\mathbf{v}}_s - \delta_f \overline{\nabla} \bullet \overline{\mathbf{v}}_f \tag{2.6}$$

Where

$\frac{\partial \eta}{\partial t}$ = porosity diffusion

δ_s and δ_f = densities of solid and fluid phases

v_s and v_f = velocities of solid and fluid phases

The porosity change with time (porosity diffusion) is identified by the deviation of the velocities, multiplied by the densities.

As the constant porosity postulation and the single energy function are not consistent with the physical reasoning above, it is not possible to specify details such as wave attenuation in Biot wave mechanics from first principles of thermodynamics that have to be part of any complete theory. Biot considered wave attenuation (no spatial scattering) empirically, instead of accounting for energy losses during compression and rarefaction cycles of the liquid and solid phases (Spanos et al. 2003).

It is implicit in wave mechanics that the liquids distort by straining, and that no distinct flow happens during dynamic excitation. Efforts to overcome this shortcoming through the use of empirical “squirt flow” notions have not been absolutely satisfactory and seem also to point out that Biot theory is not complete (Spanos et al. 2003).

In the low-excitation-frequency spectrum, the Darcy paradigm treats flow through porous media with the following postulations (Spanos et al. 2003):

- No dynamic (inertial) effects present; hence all motion may be explained by a set of diffusion equations.
- Liquids are incompressible and strains are small. Amendments exist to analyze gas flow to wells.

Clearly, Darcy flow theory is a quasi-static theory and does not contain dynamics effects. It may be a reasonable approach for excitation frequencies less than $\sim 10^{-4}$ Hz, because liquids act as incompressible in this range, instigating a pure displacement procedure (diffusion) through the pores (Spanos et al. 2003).

Therefore, it seems necessary to incorporate both diffusion and inertial terms (e.g. $\partial p/\partial t$ and $\partial^2 p/\partial t^2$) for a complete theory of flow in porous media with dynamic-diffusive coupling as shown in Figure 2.8 (Spanos et al. 2003).

2.4 Summary

Darcy theory is applied to flow mechanics and Biot-Gassmann theory is applied to wave mechanics in porous media. Biot-Gassmann theory is based on a set of postulations that have lately been shown to be insufficient by Spanos. Biot-Gassmann theory assumes that porosity is a fixed thermodynamic parameter, and for a REV in a multiphase porous media, a single function can express the energy state.

Biot-Gassmann and Darcy theories do not predict the existence of a soliton wave because of the constant porosity assumption (Biot-Gassmann theory) and no inertial effects (Darcy theory). Therefore, Spanos included both diffusion ($\partial p/\partial t$) and inertial ($\partial^2 p/\partial t^2$) terms.

The soliton wave cannot be generated without liquid-solid coupling and frequency of excitation between 0.1 – 1 Hz, because the pore liquid starts to behave incompressibly in this range. The soliton wave is a displacement wave, similar to a tsunami (a liquid

displacement wave) and propagates approximately $1/20^{th}$ the velocity of the P-waves. Furthermore, it spreads away from the event (earthquake) geometrically just like other seismic waves. Its velocity is associated with the compressibility of the phases, viscosity of the liquids, and the stresses and density.

It is hypothesized that soliton wave packet, travelling at a velocity of ~100-300 m/s, is a likely mechanism of energy transfer that increases the local pore pressure, and allows highly stressed faults to be "triggered" by the remote major event that set off the soliton packet.

Chapter – 3

Earthquake Induced Fluid Level Changes in Reservoirs

3.1 Introduction

Although a reliable process has not yet been developed to predict earthquakes, one of the most common indicators often discussed in this regard is a co-seismic fluid level change in wells. During the last 40 years, many observations have shown that earthquakes may alter water and oil production behaviour (Beresnev and Johnson 1994). Moreover, hydrological changes associated with earthquakes have been known for more than 2000 years (Sneed 2003).

Over the past several decades, interactions between earthquakes and hydrological process have been studied extensively. It has been observed that earthquakes have caused fluid levels to fluctuate, both in close proximity to as well as thousands of kilometers from epicenters. Further observations related to earthquakes have been made of water levels in wells which sometimes rise and dip, increases of stream flow, liquefaction of granular materials, formation of new springs, and alterations or degradations of well water and surface water (Montgomery and Manga 2003.)

In the United States, water level fluctuations were recorded in 716 wells after the Alaska earthquake of magnitude of 8.5 in 1964. (Note that the Alaska earthquake was the largest earthquake in the Northern Hemisphere in the previous century.) It is well-documented that the Alaska earthquake also had effects on water level recorders in many other countries, such as Canada, England, Denmark, Belgium, Egypt, Israel, Libya, The Philippines, South-West Africa (now Namibia), and Northern Australia (Beresnev and Johnson 1994). Many other cases have also been documented; some of them are listed here:

- Water level or pressure data changes were recorded in 16 wells of the Tono Mine in Gifu Prefecture, central Japan, after a local earthquake of magnitude of 5.8 that occurred 50 km south of Tono (King et al. 1999).
- The Chi-Chi earthquake of magnitude of 7.3 that occurred in Taiwan in 1999 caused groundwater level changes that were observed in 158 monitoring wells

located approximately 12 to 78 km away from the epicenter in the Choshui River alluvial fan (Chia et al. 2002).

- In the Mojave Desert, California (USA), water levels fluctuated in many wells after the Landers earthquake in June 1992, after the Northridge earthquake in January 1994, and after the Hector Mine earthquake in October 1999.
- Following the Denali fault earthquake in Alaska in November 2002, a rise in water level was observed in a well in Wisconsin, USA at a distance of several thousand kilometers from the epicenter (Sneed et al. 2003).

In oil wells, production rates have occasionally dramatically changed in response to earthquakes. For example, in the Northern Caucasus of the former USSR, an increase of 45 percent in the production rate followed an earthquake in January 7, 1938. In another example, following a Southern California earthquake (July 21, 1952), several wells in Kern County showed a substantial variation in oil production (Beresnev and Johnson 1994).

Since the early 20th century, scientists from all over the world, particularly Russia, Germany, Armenia, Japan, China, Mexico, Italy, Turkey and the USA, have observed and analyzed physical and chemical changes in groundwater of active tectonic zones before and after earthquakes (Simsek 2003).

As a general conclusion from these and other studies, the magnitude and persistence of liquid level fluctuations in wells following earthquakes are associated with the earthquake magnitude and depth, the distance from the epicenter, the hydrological environment, and whether the rock mass is a consolidated rock or an unconsolidated sediment.

3.2 Earthquake and Hydrological Processes

Observed hydrological processes related to earthquakes include changes in both stream flow (surface water) and ground water level in wells. These and other observations have resulted in a variety of proposed mechanisms to explain the correlation of these

hydrological responses and earthquakes, as shown in Figure 3.1 (Montgomery and Manga 2003).

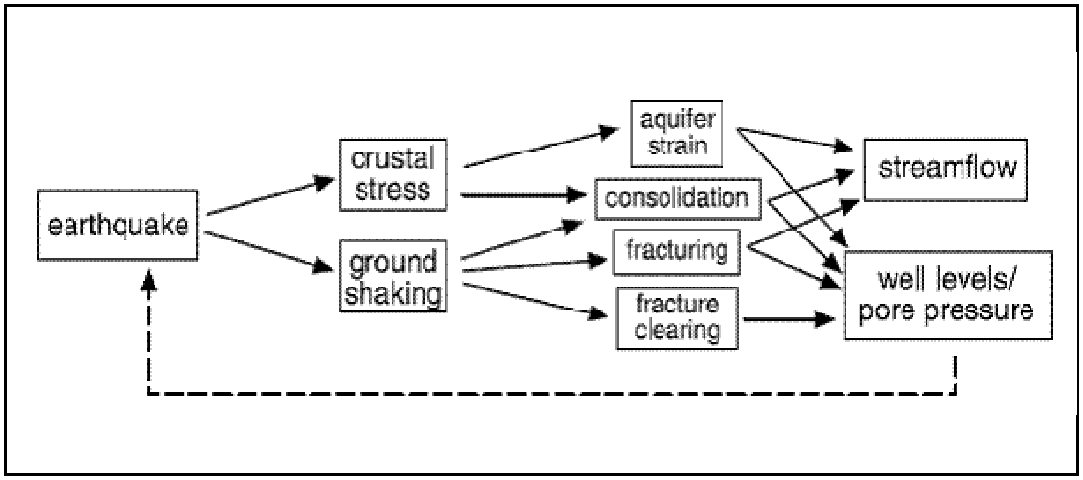

Figure 3.1: Interactions between earthquake and hydrological processes (Montgomery and Manga 2003).

The above flow chart (Figure 3.1) illustrates how an earthquake is considered to affect a hydrological system. The changes in stream flow and water levels in wells are associated with expulsion or intrusion of fluids, stress changes, strain distribution, and pore pressure diffusion (perhaps under altered pressure gradients). The permeability is purportedly increased by the opening of fractures after vibration of surficial deposits and decreased by the consolidation of surficial deposits in shallow aquifers. Moreover, it is stated that seismological and hydrological interactions have a potential to determine "…temporal and spatial variability of hydrological properties and processes at scales ranging from pores to continents…" (Montgomery and Manga 2003). Elastic material there should be no permeability changes from small strains and also it is hard to observe how a rock mass 5000 – 8000 km away from the epicenter could behave in any other way but elastic. Unfortunately, there is no independent measurement available, so this interpretation remains "unverified hypothesis". This scrutiny also applies to other "hypotheses" that are made by Montgomery, Manga, Nur and others. It makes for better science if these issues are clearly pointed out.

Different records of the hydrological responses to earthquakes may be classified by considering "…near-field versus far-field, transient versus sustained, and rapid versus delayed responses…" (Montgomery and Manga 2003). More specifically, these authors define near-field effects as those that range within about one fault rupture length from the ruptured area, intermediate-field effects as those that range from 1 to 10 rupture lengths away from the fault, and far-field effects are those at greater distances. It is also useful to differentiate between the transient response because of the passage of various waves and the permanent (sustained) responses that take place because of aquifer compression or dilation. Transient responses increase water level in wells and stream flows that last for weeks, whereas sustained responses can be observed for more than months, and sometimes can be attributed to changes in aquifer properties that are permanent. Rapid response begins during ground shaking (coseismic) and delayed responses occur thereafter (postseismic), once the dynamic waves have passed. These different scales and types of hydrological response may demonstrate different mechanisms that are related to the proximity of the epicenter and the geological environment (Montgomery and Manga 2003).

Generally, it is believed that large earthquakes cause a pore pressure increase in areas of compressional strain and a decrease in areas of dilational (extensional) strain. Liquefaction and consolidation also may occur from the interaction of aquifer properties and transient strain in response to seismic waves (Montgomery and Manga 2003). Consolidation is a permanent loss in porosity that occurs as grains adopt denser packing in response to a change in effective stress or in response to a dynamic excitation that temporary destabilizes the grain contact force structure. Consolidation can occur in granular materials of any grain sizes, but liquefaction seems to be limited to coarse-grained silts to medium-grained sands.

To understand the strain associated with earthquake cyclic excitation that may open or close pre-existing fractures, one may consider a schematic model as shown in Figure 3.2 (Wood and King 1993). Interseismic time represents the time between one earthquake to another, and coseismic time shows time of arrival of a wave train during an earthquake.

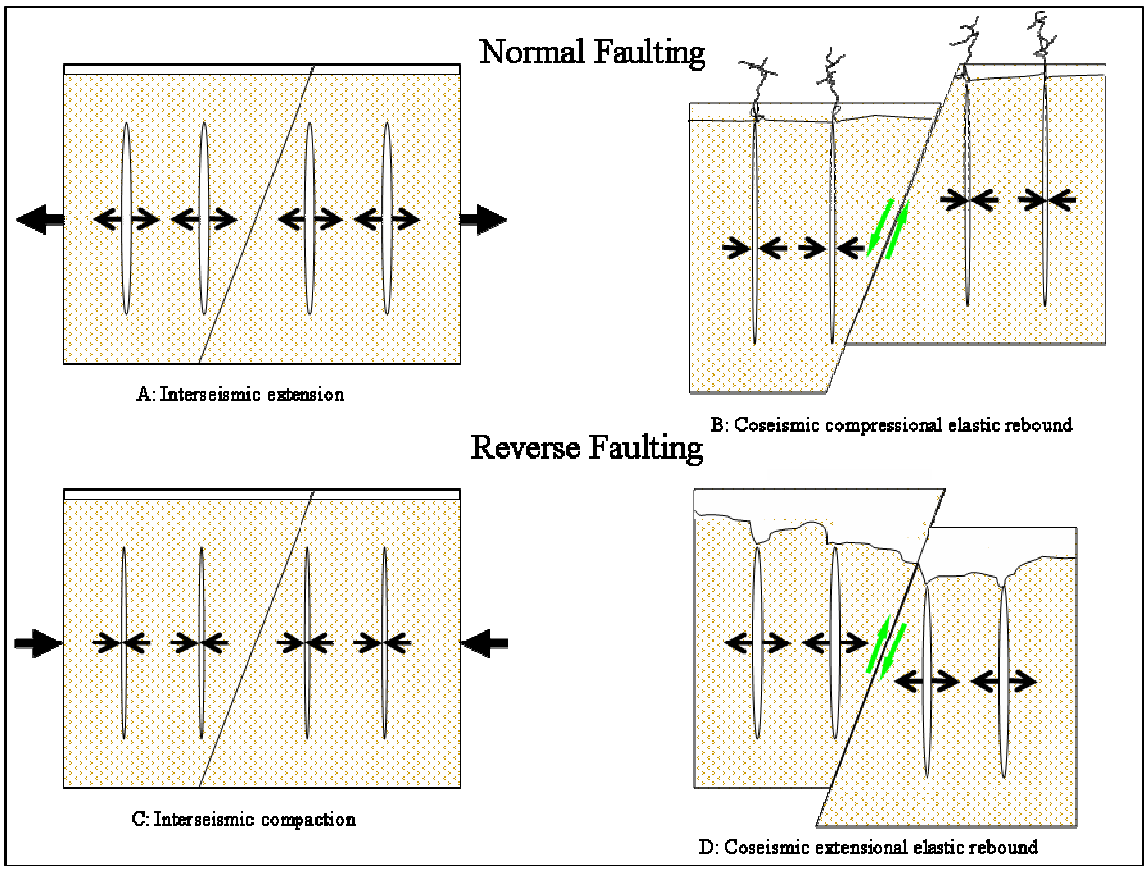

Figure 3.2: A model to explain interseismic accumulation and coseismic release of strain in extensional and compessional tectonic environments (modified after Wood and King 1993).

For extensional faulting, the interseismic time is related to fracture opening and increase of effective porosity, as shown in Figure 3.2A, whereas Figure 3.2B shows the case when fractures are closed and water is expelled during an earthquake. For compressional cases, the interseismic period is related to fracture closure and expulsion of water as shown in Figure 3.2C, whereas Figure 3.2D shows the case during the earthquake when fractures open and water is drawn in. In other words, in normal (extensional) faulting, water can be ejected under substantial pressure toward the surface during an earthquake and therefore immediately affect river flow (surface fountains), as shown in Figure 3.2B. In the case of reverse faulting, fractures must be filled from the water table, a slower process that may not be evidenced by detectable changes in river flow. In the above model, only vertical fractures are shown of course, but the authors believe that if pre-existing fractures are

present, opening and closing of the vertical ones may be the leading effect in changing porosity and expelling or imbibing water (Wood and King 1993).

Two significant recent normal faulting earthquakes in the USA are the Hebgen Lake earthquake in Montana with magnitude of 7.3 on August 17, 1959, and the Borah Peak earthquake with magnitude of 7.0 on October 28, 1983. Substantial fluctuations in surface hydrological conditions were observed following each earthquake, as shown in Figure 3.3 and Figure 3.4 (Wood and King 1993).

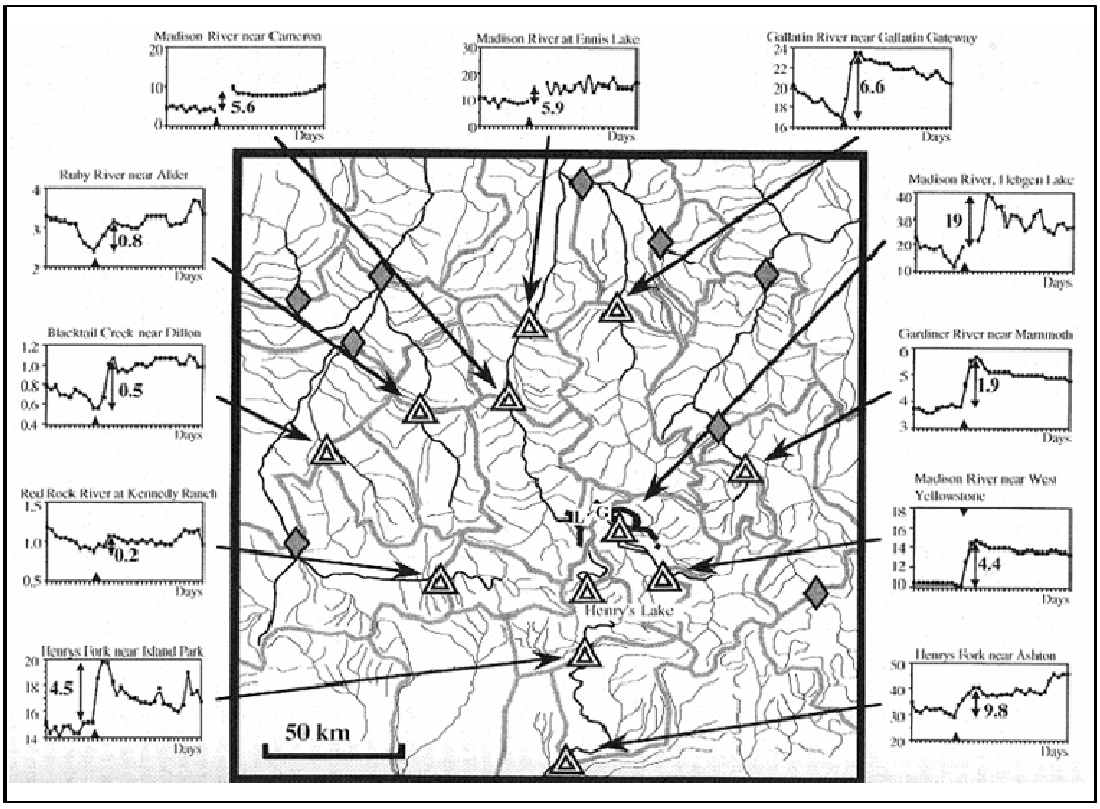

Figure 3.3: River basins and daily flow data in the area surrounding the Hebgen Lake earthquake (modified after Wood and King 1993).

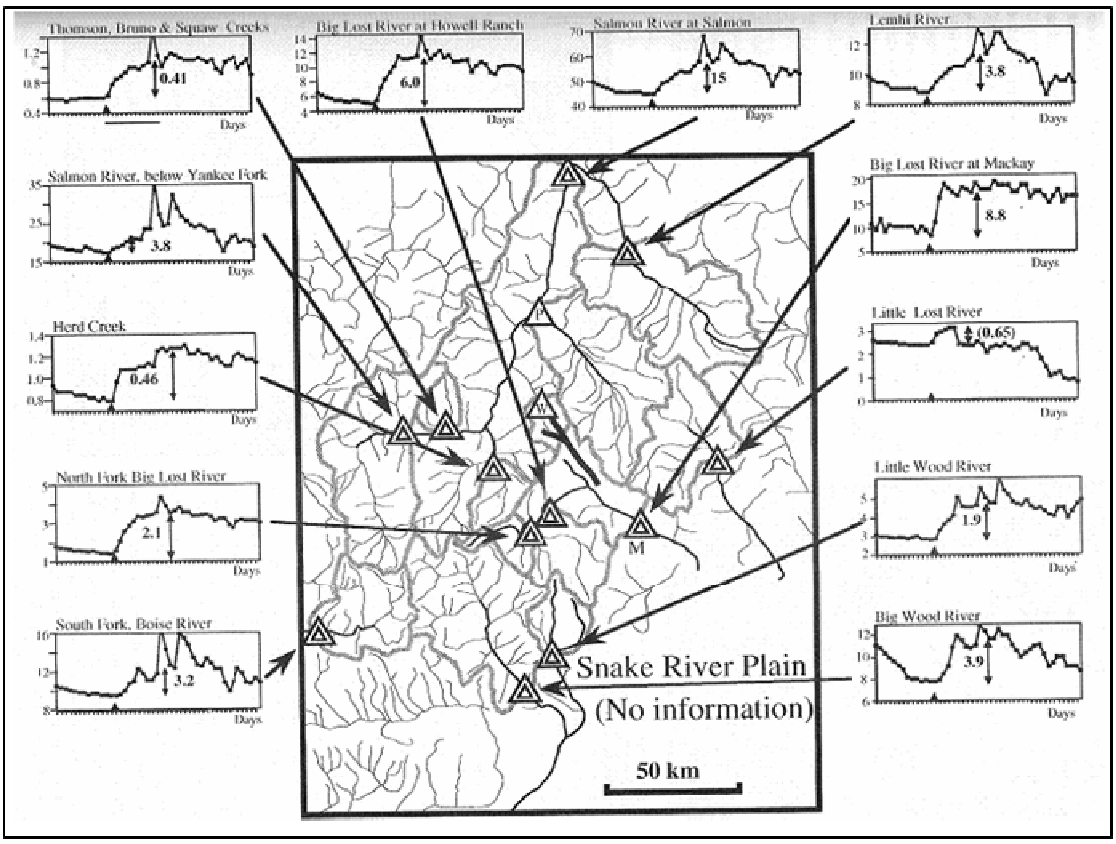

Figure 3.4: River basins and daily flow data in the region surrounding the Borah Peak earthquake (modified after Wood and King 1993).

Water variations in reservoirs due to reverse faulting earthquakes have been observed in the USA, such as following the Alaska earthquake of March 27, 1964 with magnitude of 8.5 (Figure 3.5), the Kern County earthquake, California of July 21, 1952 with magnitude of 7.5 (Figure 3.6), Loma Prieta, California of October 17, 1989 with magnitude of 7.1 (Figure 3.7), and so on (Wood and King 1993).

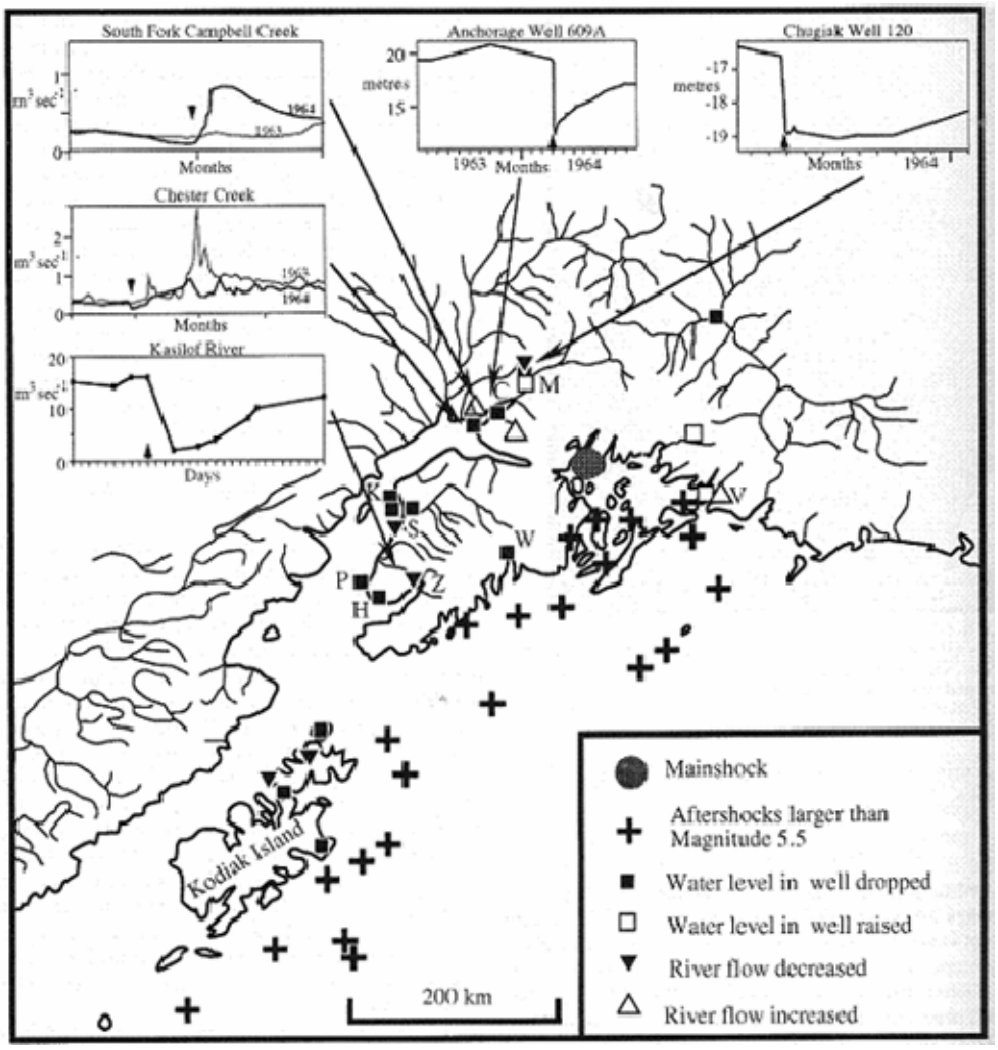

Figure 3.5: Records of river flow and water level in wells in the vicinity of the great Alaska earthquake (modified after Wood and King 1993).

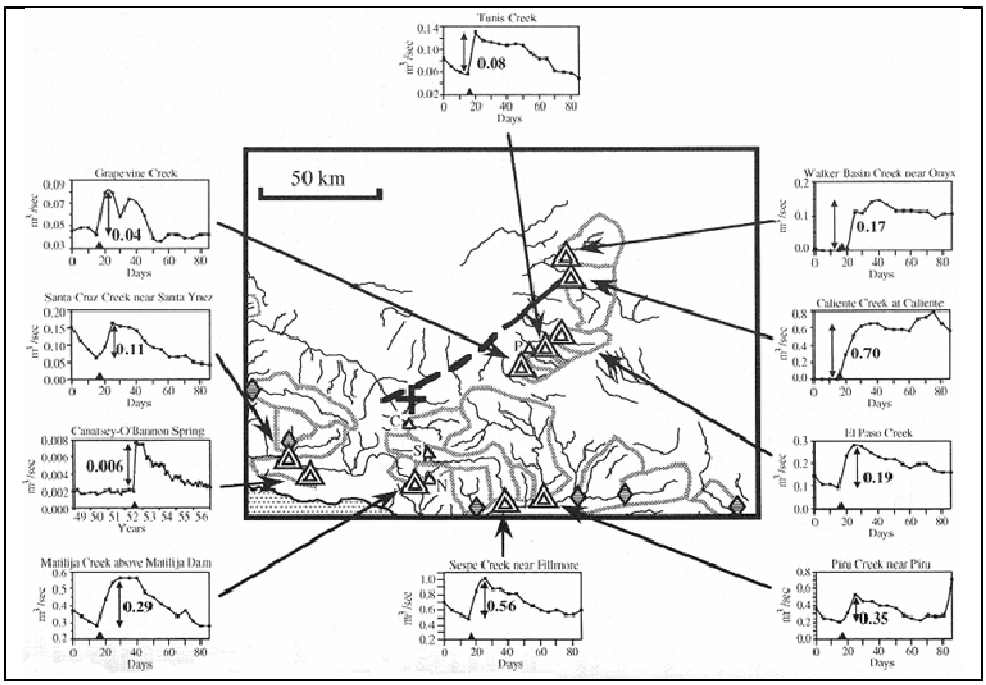

Figure 3.6: Streams flow rates in the neighbouring area of the Kern County earthquake, California (modified after Wood and King 1993).

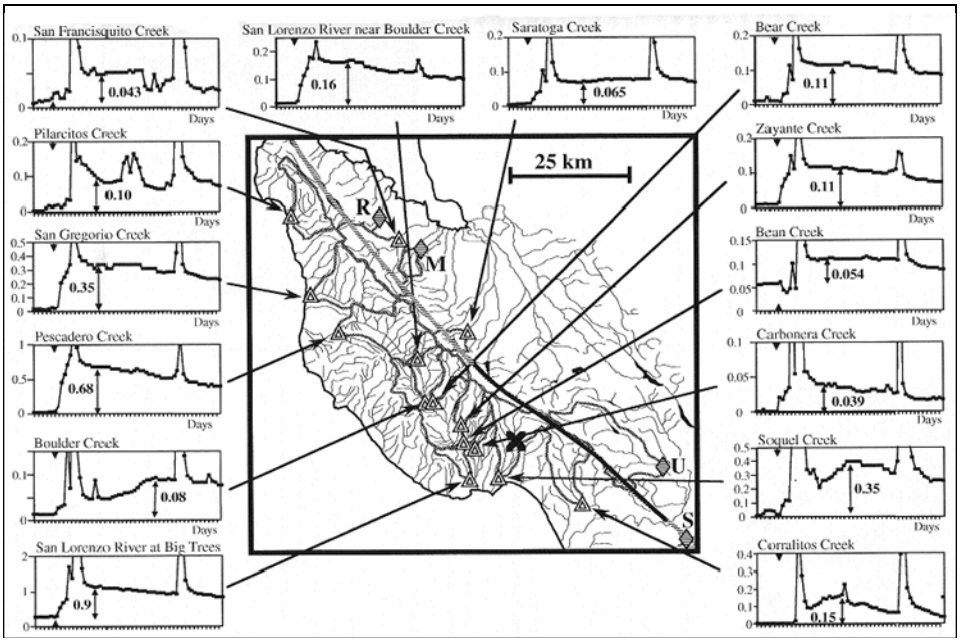

Figure 3.7: Flow rates in streams in the vicinity of the Loma Prieta earthquake, California (modified after Wood and King 1993).

From Figure 3.3 to 3.7, symbols refer to local geographical features and their names can be found in the original article (Wood and King 1993). All the above Figures have small graphs which show that earthquakes play a significant role in altering the hydrological system, as demonstrated by factors such as flow rates in rivers and streams, and water level changes in wells.

3.3 Physical Changes

A number of physical changes associated with earthquakes, such as liquefaction and changes in groundwater level, temperature, turbidity and flow rates, have been observed.

3.3.1 Induced Liquefaction

Liquefaction is a physical process that may lead to a land failure, and it has been often observed during earthquakes. Liquefaction is triggered by a large amount of cyclic dynamic strain in loose, water-saturated granular soil because of an earthquake excitation. It involves a total loss of effective stress that occurs when the quasi-stable granular structure undergoes enough shaking to allow the grains to adopt a denser structure, but only in cases where the permeability is low enough so that the pore water pressure cannot drain away in the same time frame as the densification. It is generally accepted that fine-grained materials (less than perhaps 50 μm) are insensitive to dynamic liquefaction, and coarse-grained sands (greater than ~500 μm) have such a high permeability that the excess pore pressures generated can quickly dissipate. As a result of the liquefaction, clay-free soil deposits, mainly sand and silts, become temporarily transformed into viscous fluids that can flow (Hays 1981). Figure 3.8 illustrates liquefaction associated with an earthquake.

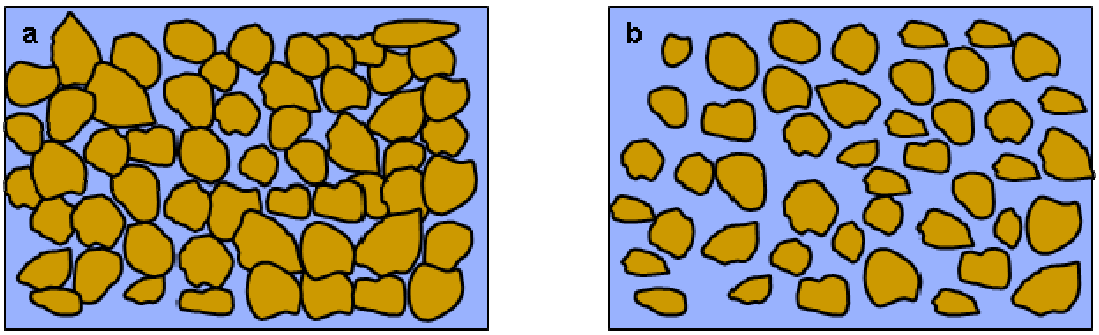

Figure 3.8: Liquefaction in water-saturated soil deposits due to an earthquake. The height of the blue column represents pore water pressure in the soil, (a): Sediments are shown before an earthquake, (b): During the earthquake the sediments lost strength and behaved as liquids (modified after Berkeley 2003).

Liquefaction usually occurs in response to seismic strain waves, most likely the surface waves, passing through a saturated granular soil stratum. Earthquakes deform the granular structure and soil particles lose contact with each other in an attempt to find a denser equilibrium state. This transfers grain-to-grain contact forces in the soil stratum to the pore water, hence the pore pressure increases as forces are lost between grains. Continued ground shaking increases pressure in the pore water, either causing drainage to take place in cases with high permeability or good drainage, or to an abrupt rise in the pore pressure if drainage is impaired or if the permeability is too low. The pore pressure can increase only to about the total stress produced by the vertical weight of the column of soil, at which point the granular soil stratum performs like a fluid rather than a solid because of the total loss of frictional strength. In this situation, failure of the land can take place as the substratum flows away, and this may cause major subsidence (Berkeley 2003) as well as other phenomena.

An example of widespread liquefaction has been observed in Niigata, Japan due to the 1964 Niigata earthquake that damaged many buildings, as shown in Figure 3.9. In this case, the liquefied sand flowed away from the high loads under the building foundations, leading to settlement, tilting and tipping.

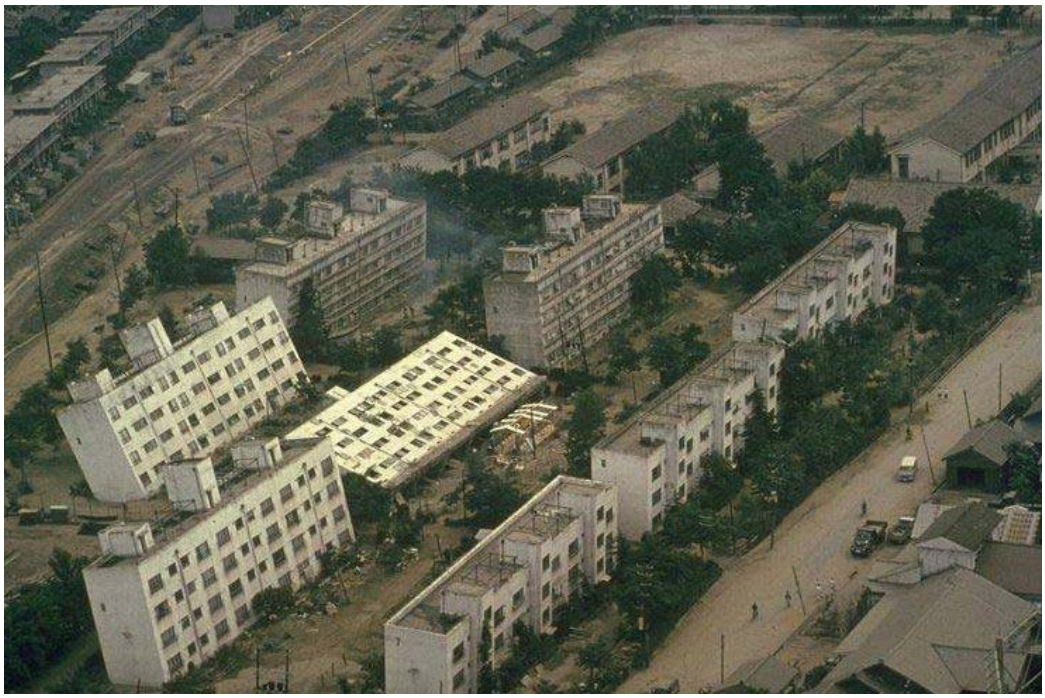

Figure 3.9: 1964 Niigata earthquake caused widespread liquefaction in Niigata, Japan, destroying many buildings (Hays 1981).

Liquefaction is observed only in saturated soil and in low-lying areas near or in water bodies such as rivers, lakes, bays, and oceans. In these areas, sediments were deposited in a loose state, and as the sediments were buried, the grain-to-grain friction forces impeded the sediments from adopting a denser (lower porosity) state. They became "quasi-stable" for the stress conditions, and susceptible to strong shaking. Thus, liquefaction is controlled by the geologic and hydrologic environments and is found mostly in areas where sand and silts deposits have been slowly laid down for many years (Hays 1981).

Generally, the magnitude of an earthquake and the extent and size of related phenomena are closely linked. The stronger the event (earthquake), the larger the distance from the epicenter where liquefaction and enhanced stream flow will be observed, and the size of the response will be accordingly larger as well. For example, an earthquake with a magnitude of 9 can certainly produce liquefaction and stream flow up to 600 kilometers away (Berkeley 2003). This does not indicate an enhanced stream flow due to

liquefaction. It rather demonstrates that both phenomena occur because of the same process that is related to processes involving dynamic strain (Berkeley 2003).

3.3.2 Temperature Changes

Earthquakes may induce temperature changes in reservoirs. Groundwater temperature changes associated with seismic activity have been noticed mostly in high heat flux areas such as in geyser or geothermal spring regions. Usually, short-term and seasonal fluctuations are features for groundwater initiating from regional flow systems. Groundwaters originating from local flow systems, such as geyser systems, generally do not display any short-term variations and are assumed to represent stable state conditions (Simsek 2003).

In geothermal areas where a local groundwater flow system plays a dominant role, the cap rock of the geothermal reservoir may possibly break due to stress accumulation before an earthquake. This initiates a convective heat flow to the non-thermal reservoirs by hot fluids of the thermal reservoir such as water, steam, and gas. Regional groundwater temperature is increased by the convective transport of heat. In addition, pressure increases in geothermal springs before seismic activity cause increased flow rates in the geothermal reservoir and decreased mixing of cold groundwater with the hot reservoir. This can cause the temperature of geothermal reservoirs to increase before seismic activity (Simsek 2003).

For example, a few hours before the Kobe earthquake in Japan with magnitude (M) of 8.1 in 1994, the temperature of the Amina thermal reservoir increased 2 to 4ºC. Kyoto University researchers have observed groundwater temperature variations in the reservoir before other earthquakes (e.g. December 28, 1998, M: 7.5); whereas other geothermal reservoirs in the same area have not shown any temperature changes (Simsek 2003).

3.3.3 Turbidity

Earthquakes cause a rapid release of energy which results in physical changes both in the subsurface as well as at the surface. When groundwater is affected by an earthquake,

turbidity of the water can occur. Turbidity is caused by sudden mixing of water with fine-grained particles (silt, clay, algae, plankton etc) which leads to a change in colour and taste. It is observed in geothermal reservoirs in active tectonic zones before earthquakes (Simsek 2003). Turbidity also occurs because of breaching of the cap rock due to stress accumulation before earthquakes, allowing ingress of particles to the hydrogeological system (Simsek 2003).

3.3.4 Groundwater Level Changes

Earthquakes may cause physical and chemical variations in hot and cold groundwater either before or after an event (earthquake). Physical and volumetric (dilation) deformation have occurred due to the changes of stresses in the crust. This process generates new micro-cracks and fractures as well as expanding (dilation) the existing ones.

In porous and fractured media, stress changes on the formation may lead to changes in porosity and permeability and, thus, affect groundwater among grains. Furthermore, a decrease or an increase in porosity and permeability has resulted in water level fluctuations in a reservoir (King et al. 1995).

Water level changes associated with seismic activity may take place even at very remote points from an epicenter. These changes can occur before, during or after an earthquake. Groundwater level changes are associated with reservoir properties, the magnitude of the seismicity and characteristics of the seismic waves (Simsek 2003).

After the Hyogo-ken Nambu (Kobe) earthquake of 1995 in Japan, variations have been reported in groundwater system of the region. Though it was dry season, groundwater levels and the flow rates of reservoirs were increased (Simsek 2003). Also, in the Tokai area, the water level dropped up to 13.6 and 3.5 cms in two monitoring wells after the Kobe earthquake. In the Tono mine before an earthquake of magnitude 5.8 near Gifu (Japan), water levels of the observation wells decreased abruptly and after the earthquake the level of water wells increased (Simsek 2003). In California, a few weeks before the Loma Prieta earthquake with magnitude of 7.1 on January 17, 1989 and ending a few

months after, levels of groundwater dropped about 21 meters at the high altitude of the San Lorenzo and Pescadero drainage basins (Simsek 2003).

A monitoring well (8N/10W-1Q1) in the Mojave Desert, California has fluctuated in response to the Landers earthquake in June 1992, the Northridge earthquake in January 1994, and the Hector Mine earthquake in October 1999 as shown in Figure 3.10 (Sneed et al. 2003), though the latter effect is not clear.

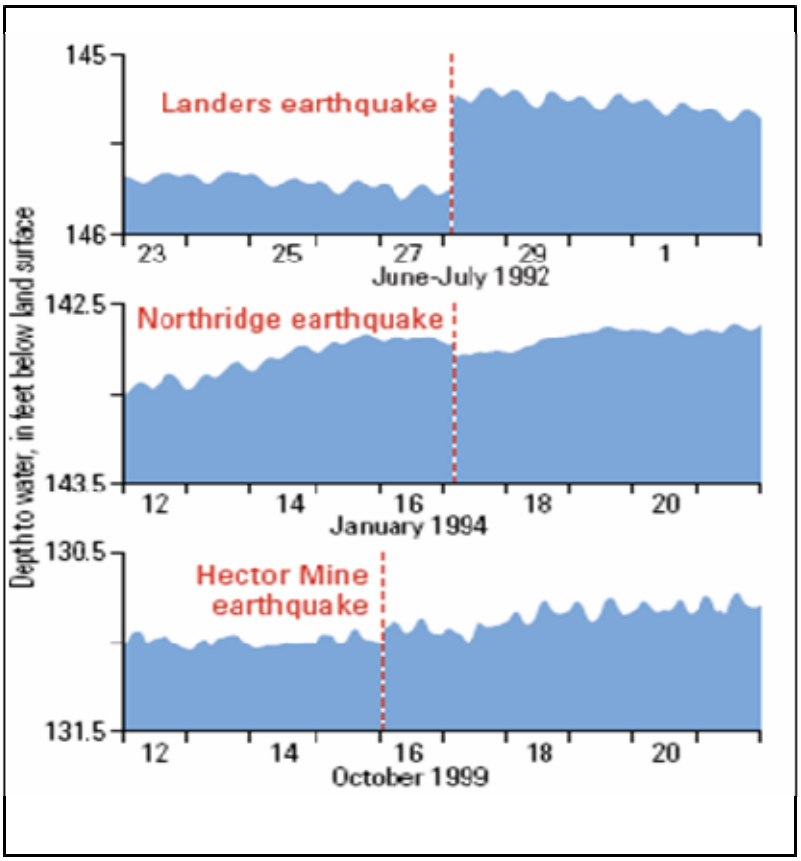

Figure 3.10: Well 8N/10W-1Q1 in the western Mojave Desert, California responded to several southern California earthquakes (Sneed et al. 2003).

A rise of 2 feet in water level has been recorded in well MO-18/02W/29-0017 at Wisconsin, USA in response to the Denali fault earthquake, Alaska on November 2002, as shown in Figure 3.11, even though it (the well) was located at about more than 4300 km distance from the epicenter (Sneed et al. 2003).

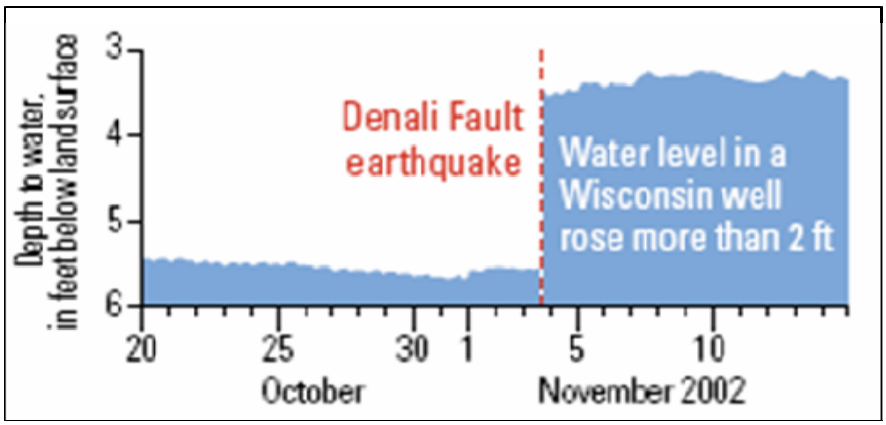

Figure 3.11: Well MO-18/02W/29-0017 in Winconsin responded to the remote Denali Fault earthquake in Alaska (Sneed et al. 2003).

In California, the BV well, shown in Figure 3.12, has been observed on a regular basis, and water level variations have been observed as described in Table 3.1 (Roeloffs 1998).

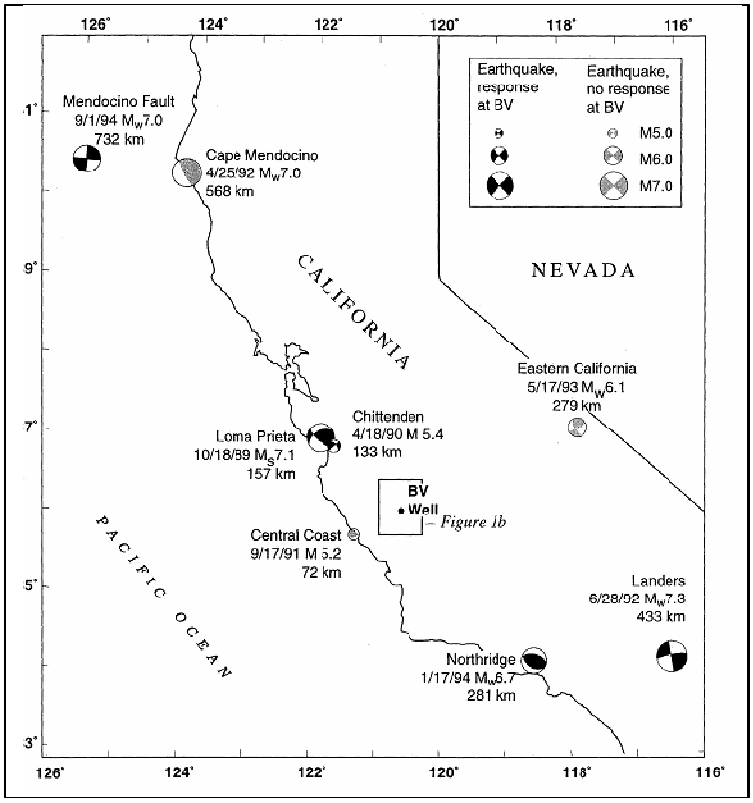

Figure 3.12: A map shows the location of the BV well and various earthquakes (Roeloffs 1998).

Table 3.1: Earthquake and water level responses in the BV well (modified after Roeloffs 1998).

Location	Date & Time, UT	Magnitude (M)	Latitude, Longitude	Depth, (km)	Distance from BV well, (km)	Expected water level changes (cm)	Observed water level change (cm)
Loma Prieta	Oct. 18, 1989, 0004	7.1	37.04N, 121.88W	18.5	157	74.4	85
Chittenden	April 18, 1990, 1354	5.4	36.93N, 121.66W	5.8	133	4.7	5.5
Central Coast	Sept. 17, 1991, 2110	5.2	35.82N, 121.33W	6.0	72	8.6	0
Cape Mendocino	April 25, 1992, 1806	7.1	40.33N, 124.23W	10.0	568	4.3	0
Landers	June 28, 1992, 1157	7.3	34.20N, 116.44W	3.2	433	34.5	34.0
Parkfield	Oct. 20, 1992, 0528	4.7	35.93N, 120.47W	10.0	23.3	18.4	14.0
Eastern California	May 17, 1993, 2321	6.1	37.17N, 117.79W	7	279	6.0	0
Parkfield	Nov. 14, 1993, 1225	4.8	35.95N, 120.49W	11.5	20.9	26.9	36.0
Northridge	Jan. 17, 1994, 1230	6.7	34.21N, 118.54W	18	30.8	6.6	19.0
NE of Parkfield	March 31, 1994, 2000	4.4	36.18N, 129.31W	11.5	30.8	6.6	0
NE of Parkfield	April 21, 1994, 1637	4.3	36.30N, 120.43W	9.6	30.2	5.5	0
Mendocino fault	Sep. 1, 1994, 1515	7.0	40.44N, 126.89W	7.0	732	5.3	9.1
Parkfield	Dec. 20, 1994, 1027	5.0	35.92N, 120.47W	8.9	24.0	32.4	33.0

As another example, local as well as distant earthquakes have induced water level fluctuations persisting for days to weeks at Long Valley caldera, California. Monitoring wells are shown in Figure 3.13; unfortunately, specific data is unavailable but the wells have recorded groundwater level changes in response to local and distance earthquakes, shown in Figure 3.14 (Roeloffs et al. 2003).

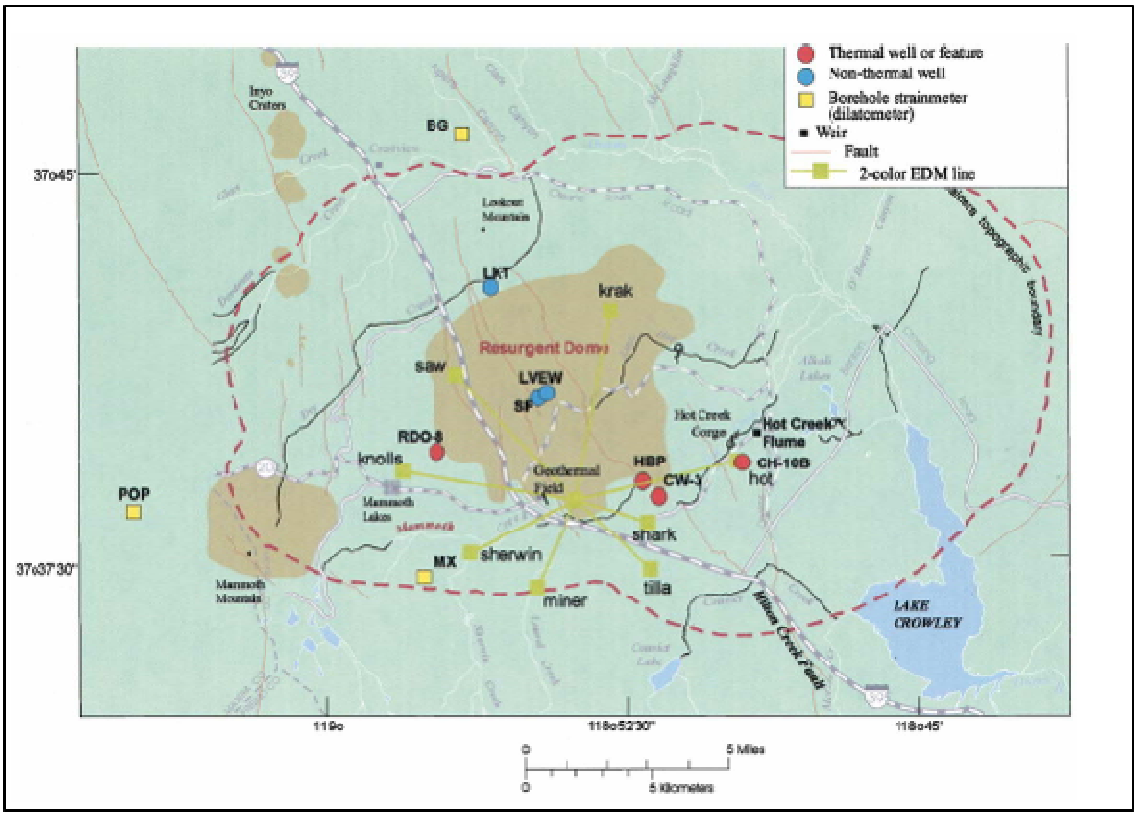

Figure 3.13: Map of the Long Valley area showing observation wells, the two-colour electronic distance measuring (EDM) network (modified after Roeloffs et al. 2003).

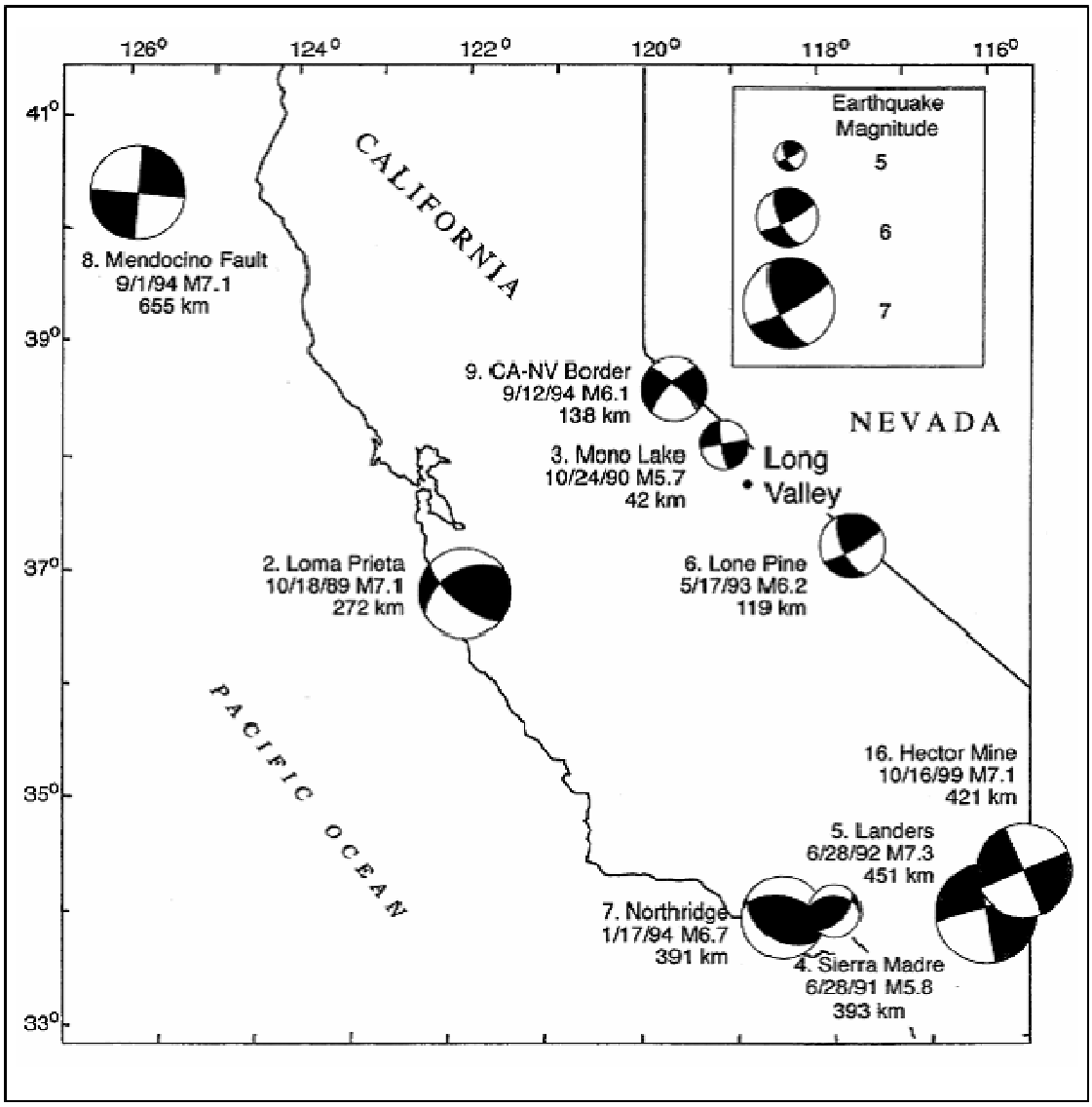

Figure 3.14: Map of California showing locations of earthquakes in vicinity of Long Valley area that produced water level changes (modified after Roeloffs et al. 2003).

In Central Japan, water level fluctuation records associated with earthquakes in 16 wells have been examined. These wells were installed around the region of a relatively impermeable fault. From one of the 16 wells, the data of one well, No. SN-3 is described in Table 3.2 (King et al. 1999), though why the water level dropped down in association with earthquakes in the well (SN-3) is unclear.

Table 3.2: Coseismic water level changes associated with earthquakes at SN-3 well (modified after King et al. 1999).

No.	Year	Month	Day	Time*	Longitude	Latitude	Depth (km)	Magnitude (M)	Hypodistance (km)	Drop (cm)	Precursory
1	1989	5	2	1608	136.60E	35.33N	39	4.7	70	20	
2	1989	11	2	0325	143.06E	39.85N	0	7.1	714	9	
3	1990	2	20	1553	139.23E	34.76N	5	6.5	195	28	
4	1990	9	24	0613	138.63E	33.10N	60	6.6	290	22	Yes
5	1991	9	3	1744	138.83E	33.68N	33	6.3	242	12	
6	1992	2	2	0404	139.79E	35.23N	92	5.9	249	6	
7	1992	6	8	1341	137.05E	35.79N	12	4.2	49	5	
8	1992	7	30	2016	136.51E	35.51N	37	5.3	77	42	
9	1993	1	11	0958	137.19E	35.19N	56	4.8	63	15	
10	1993	2	7	2227	137.65E	37.65N	24	6.6	253	12	
11	1993	4	23	0518	137.50E	35.81N	7	5.1	53	12	
12	1993	9	23	1552	137.01E	35.03N	48	4.3	66	17	
13	1994	5	28	1704	136.28E	35.32N	44	5.2	97	30	
14	1994	10	4	2222	147.68E	43.37N	28	8.1	1257	6	Yes
15	1994	11	20	1722	136.89E	35.43N	14	4.4	35	17	
16	1994	12	28	2119	143.75E	40.43N	0	7.5	800	-	Yes
17	1995	1	17	0546	135.04E	34.59N	17	7.2	219	4	yes
18	1995	3	17	0008	137.57E	35.74N	10	5.3	51	9	
19	1996	12	7	1413	137.11E	35.75N	12	4.5	43	6	
20	1996	9	5	0315	139.94E	31.41N	13	6.1	509	-	yes
21	1996	9	11	1137	141.22E	35.64N	52	6.4	365	7	
22	1997	3	16	1451	137.53E	34.92N	39	5.8	70	29	
23	1997	10	21	1955	138.23E	35.12N	33	4.3	101	6	
24	1998	2	10	0120	137.13E	35.73N	11	4.2	40	16	
25	1998	4	22	2032	136.57E	35.17	10	5.4	65	13	

* Japan local time

At Haibara, in central Japan, groundwater level changes in one well in response to 28 earthquakes during the period April 1987 to December 1997 are shown in Table 3.3 (Matsumoto 2001). The three largest coseismic changes decreased the level in the Haibara well in response to earthquakes number 10, 15, and 27 (Table 3.3) with magnitudes of 6.8, 6.5, and 5.8 respectively (Figure 3.15) (Matsumoto 2001).

Table 3.3: Earthquakes that induced changes in groundwater level at Haibara well, Japan (modified after Matsumoto 2001).

No.	Date	Hypodistance (km)	Magnitude (M)	Drop (cm)	Latitude	Longitude	Depth (km)
1	August 15, 1981	41.9	4.8	6.4	34.80N	138.05E	40
2	July 23 1982	375.0	7.0	3.5	36.18N	141.95E	30
3	December 28, 1982	155.9	6.4	3.6	33.87N	139.45E	20
4	March 16, 1983	65.9	5.7	4.4	34.79N	137.61E	40
5	May 26, 1983	621.9	7.7	1.8	41.26N	139.00E	14
6	August 8, 1983	113.1	6.0	2.6	35.52N	139.03E	22
7	October 3, 1983	150.4	6.2	-	34.00N	139.03E	15
8	November 24, 1983	57.0	5.0	1.9	34.73N	137.71E	36
9	March 6, 1984	741.6	7.9	-	29.34N	139.21E	452
10	September 14, 1984	127.9	6.8	14.9	35.82N	137.56E	2
11	June 24, 1986	241.7	6.5	1.3	34.82N	140.72E	73
12	November 22, 1986	126.2	6.0	3.1	34.55N	139.53E	15
13	December 17, 1987	226.7	6.7	3.5	34.37N	140.50E	58
14	October 14, 1989	122.1	5.7	1.7	34.82N	129.50E	21
15	February 20, 1990	95.9	6.5	8.1	34.76N	139.23E	6
16	September 24, 1990	199.7	6.6	1.3	33.1N	138.21E	60
17	April 25, 1991	43.9	4.9	1.1	35.06N	138.83E	32
18	September 3, 1991	139.9	6.3	3.0	33.68N	138.83E	33
19	July 12 1993	888.8	7.8	1.0	42.78N	139.18E	35
20	October 4, 1994	1253.7	8.1	7.4	43.37N	147.71E	23
21	December 28, 1994	794.3	7.5	1.3	40.43N	143.75E	0
22	January 17, 1995	289.8	7.2	3.9	34.59N	135.04E	18
23	February 1, 1996	13.2	3.6	0.8	34.76N	138.33E	1
24	March 6, 1996	104.4	5.8	2.2	35.47N	138.95E	20
25	May 27, 1996	33.7	4.2	3.1	34.96N	138.21E	28
26	October 5, 1996	36.2	4.3	1.1	34.97N	138.05E	28
27	March 16, 1997	73.3	5.8	8.8	34.92N	137.53E	39
28	October 11, 1997	54.4	4.9	6.2	34.42N	138.23E	36

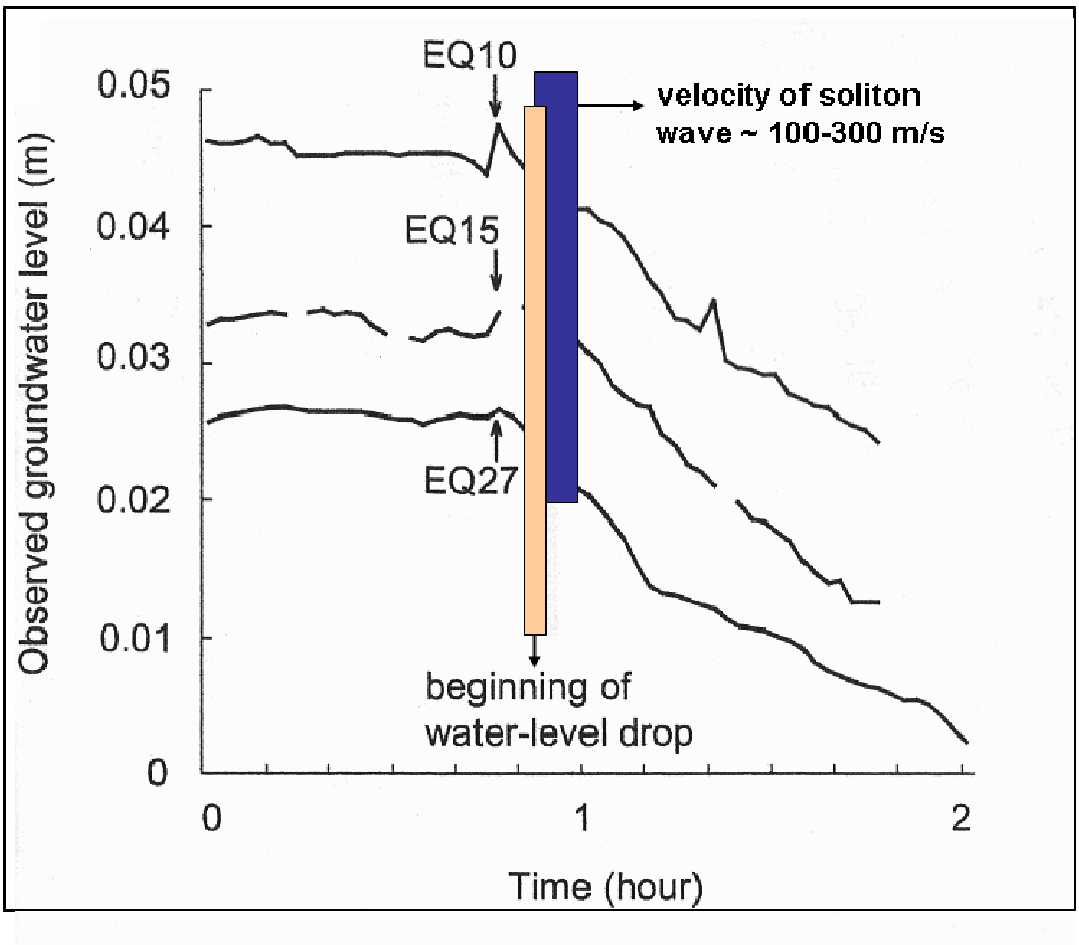

Figure 3.15: The three largest coseismic drops in the Haibara well. The sampling rate is 2 minutes; the blue line bar represents the soliton wave arrival time range (modified after Matsumoto 2001).

The above figure (3.15) shows that coseismic drops in Haibara well may be due to soliton wave because the water level dropped in the range of the soliton wave velocity range, and a long time after the surface waves had passed. Therefore, these data seem to support the hypothesis of a slow soliton wave as the source of the energy causing changes in water levels.

3.3.5 Fluid Flow Rate Changes

Fluid flow rate change associated with seismic activity in springs or aquifers due to earthquakes have been recorded. Fluid flow rates have been observed to change in

streams, rivers or lakes during or after earthquakes. The Antofagasta earthquake in Chile with a magnitude of 8 occurred on July 30, 1995. The fluid flow rate variation in this active fault zone is shown in Figure 3.16. In Figure 3.16.A, thick grey lines show the level of the seismogenic zone and the arrow represents high stress in response to a subducting oceanic plate. In Figure 3.16.B, an earthquake completely breaks the seismogenic zone and destroys the permeability barrier, allowing fluid flow after earthquake. This alters the stress field and pore pressure (Kissling 2001).

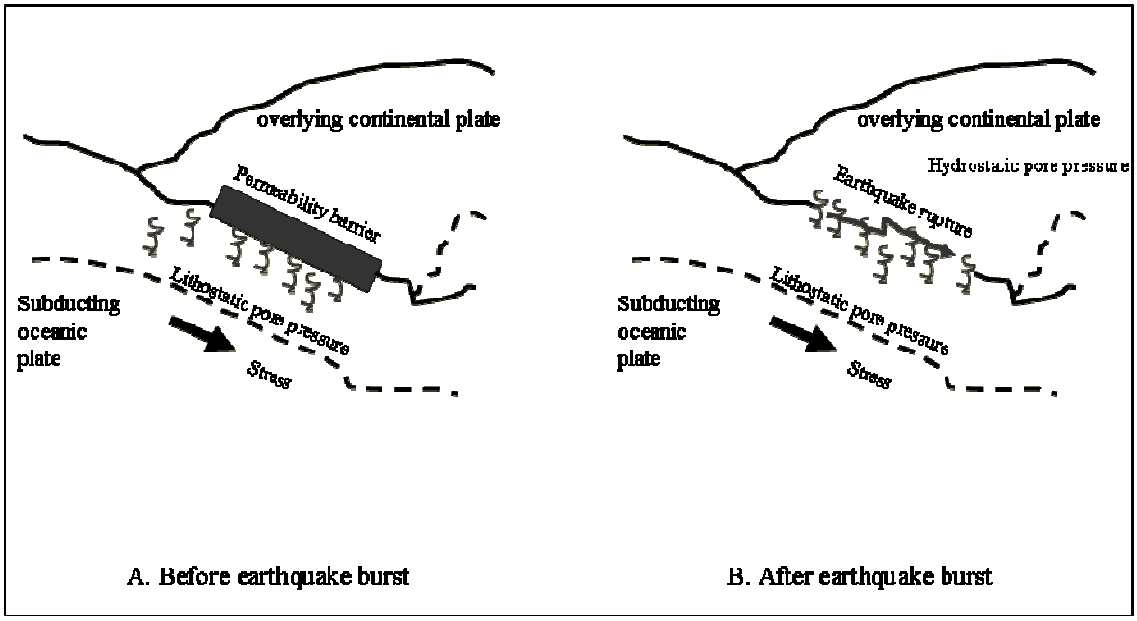

Figure 3.16: Schematic proposed explanation of fluid flow after an earthquake (modified after Kissling 2001).

3.4 Mechanism of Coseismic Changes

Coseismic changes are associated with the arrival of wave trains produced by earthquakes. Two types of earthquake induced water level fluctuations are observed; dynamic change and static change.

3.4.1 Dynamic Change

Dynamic change is associated with seismic vibration following an earthquake. During earthquakes, dynamic changes may cause soil liquefaction in loose sand or silt formation at shallow depth. For example during the Chi-Chi earthquake with magnitude of 7.3 on September 21, 1999 (time 01:47 a.m.) in Taiwan, oscillatory water level changes in the TC well of amplitude up to 6 m were observed, approximately as shown in Figure 3.17. The TC well is in an unconfined aquifer. Dynamic change of the groundwater level recovered rapidly after the earthquake; however, the earthquake did cause a widespread soil liquefaction hazard in surrounding area of the TC well (Chia et al. 2002).

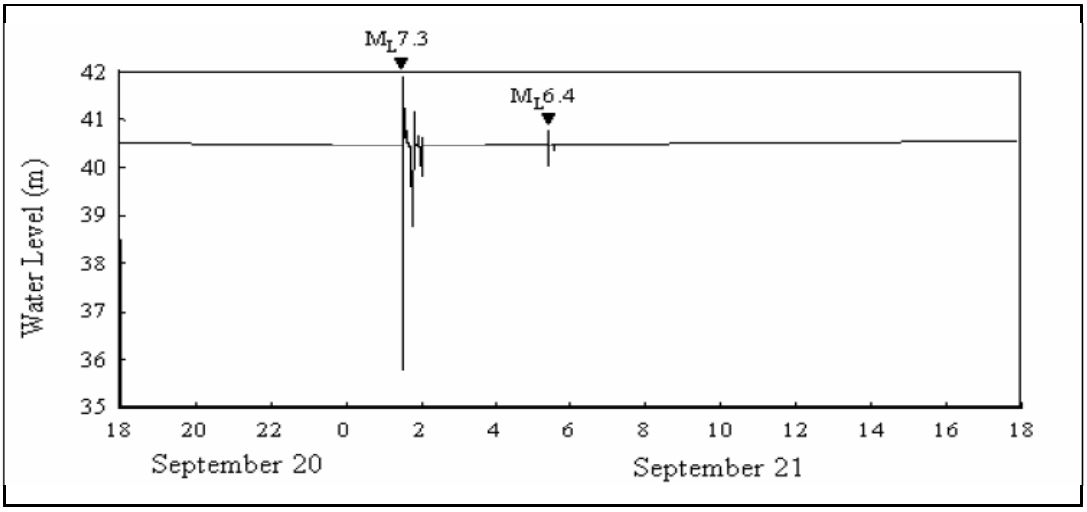

Figure 3.17: Analog records at the TC well are showing oscillatory groundwater level fluctuations at the main shock and a few aftershocks in an unconfined aquifer (Chia et al. 2002).

Because of the lack of time data on analog records, it is difficult to observe detailed oscillatory water level changes in many records. Recently, a piezometer has been installed in a monitor well to record water level changes every 3 seconds at the National Taiwan University. The oscillatory response to an earthquake with magnitude of 6.2, triggered on May 29, 2002, about 59 km east of Hualian city, is shown in Figure 3.18 (Chia et al. 2002). The distance between the epicenter and the monitoring well is

approximately 200 km. The largest amplitude recorded was around 7 cm and the oscillation persisted for 1 minute.

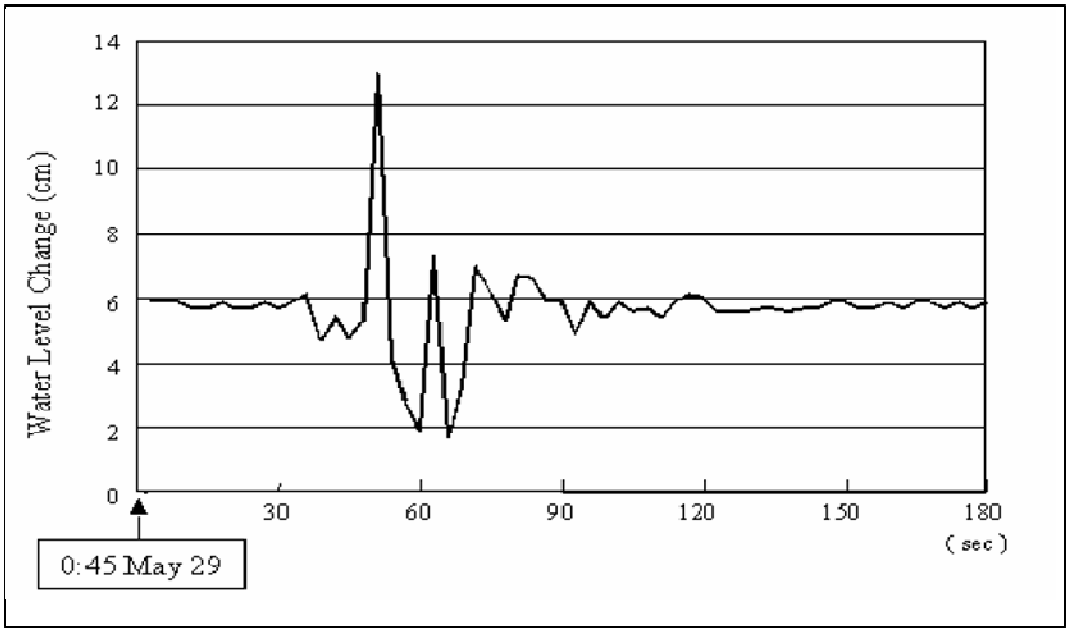

Figure 3.18: Digital records showing the detailed process of oscillatory groundwater level change in response to the M 6.2 earthquake at 0:45 AM on May 29, 2002 (Chia et al. 2002).

The above digital record (Figure 3.18) is drawn in the frequency-amplitude spectrum by using the Fourier transform function in the MathCAD program. A peak is shown at a frequency of 0.08 Hz, which suggests that the groundwater level fluctuation in the well could be in response to a soliton wave, as its assumed frequency range is from 0.1 to 1 Hz. Of course, there are many complications that are not addressed here such as high frequency damping in a water filled tube, and so on.

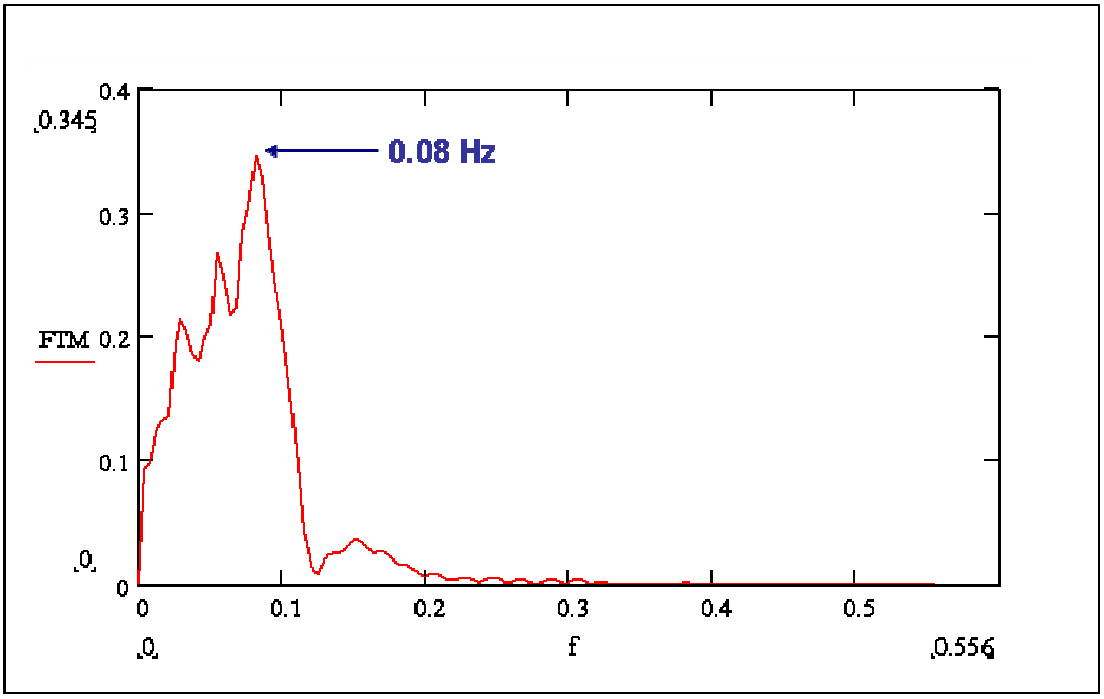

Figure 3.19: Graph shows the frequency content of the water level changes of Fig 3.18

3.4.2 Static Changes

Response of groundwater to the redistributed tectonic stress field caused by fault movement is considered as a static (long-term) change. The redistribution of tectonic stress can occur due to an abrupt change of pore pressure and effective stress in the formation, resulting in groundwater pressure changes. Most of the tectonic stress change was evidenced by a sudden change of pore pressure during the earthquake, as shown in Figure 3.20 (Chia et al. 2002). After an earthquake, recovery of the pore pressure and effective stress may occur slowly (static response) and lead to a volumetric strain of the formation. For example, the stress field in Taiwan and its nearby area must have experienced a rapid change during the Chi-Chi earthquake due to the thrust of the Chelungpu fault, Taiwan. Figure 3.20 shows the assumption that the effective stress and the pore pressure are directly linked (Terzaghi's effective stress principal) during an earthquake (Chia et al. 2002).

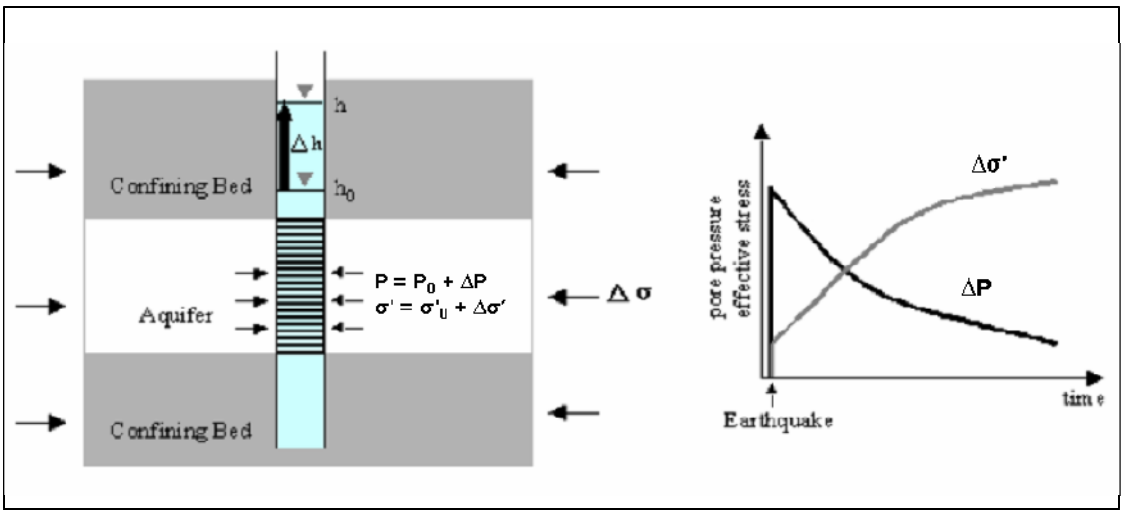

Figure 3.20: Schematic diagram showing the static response of groundwater level change to tectonic stress adjustment (modified after Chia et al. 2002).

In Figure 3.20, h is hydraulic head, p is pore pressure, and σ′ is effective stress.

Groundwater level changes in a reservoir can be recorded at a monitoring well before an earthquake, and then groundwater may flow between the well and its connected reservoir during the earthquake. If a well is installed in a less permeable reservoir or covered with a blocked screen, it may require a few days to analyse a full scale coseismic groundwater level change. For example YL4 well in Taiwan recorded during the Chi-Chi earthquake a rise of 1.20 m, but as time passed it changed by 2.1 m, as shown in Figure 3.21. Most of the monitoring wells in the vicinity of the YL4 well recorded a full scale coseismic groundwater level change instantaneously after the earthquake, because reservoirs in the Choshui River alluvial fan, Taiwan are mainly in highly permeable sediments (Chia et al. 2002).

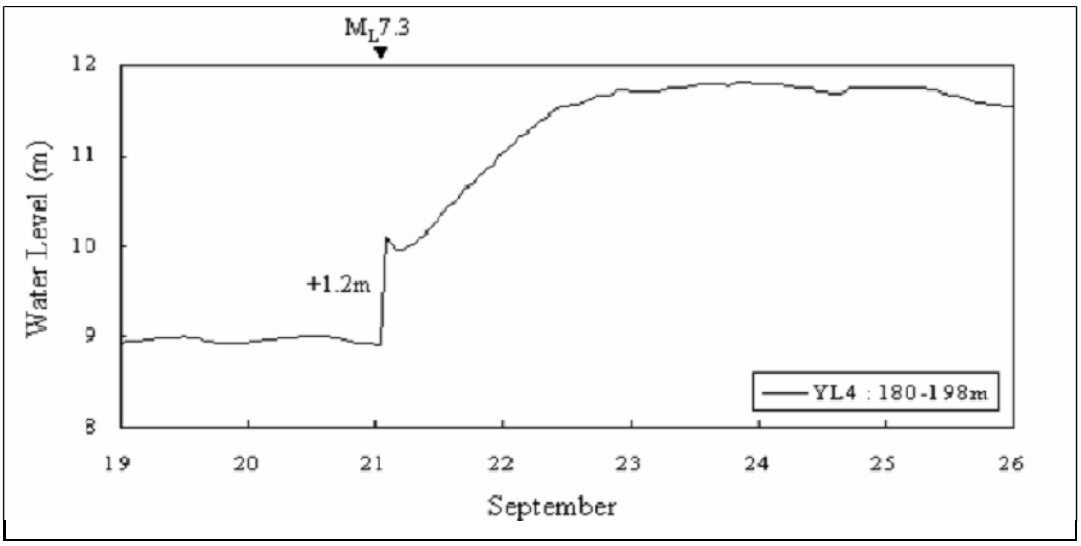

Figure 3.21: Groundwater level records at the YL4 well related to Chi-Chi earthquake (modified after Chia et al. 2002).

3.5 Direction of Coseismic Changes

Coseismic groundwater level alterations should be in the directions assumed for responses to the redistribution of tectonic stress due to the fault movement. For example, due to the thrust of the Chelungpu fault in Taiwan in response to the Chi-Chi earthquake, coseismic groundwater level increased in regions of increased compressive stress state and decreased in regions of tensile stress state at monitoring wells (Chia et al. 2002).

The direction of coseismic groundwater level changes may provide subsurface information for estimating the dispersion (distribution) of the volumetric strain in unconsolidated deposits by recording at many monitoring wells. It has been proposed by Wakita (1975) that coseismic groundwater level changes based on the quadripolar pattern (radiation pattern) of increasing and decreasing strain may be used to study changes in tectonic strain (Chia et al. 2002). Generally, groundwater level changes have been analysed on the basis of such a strain radiation pattern.

3.5.1 Radiation Pattern

Earthquakes usually occur on faults, but can also be due to processes such as volcanic eruptions, mine collapse or underground rock burst and so on. All large earthquakes, however, occur as slip on fault surfaces. When an earthquake is triggered, the seismic waves are generated and scattered, but not necessarily of the same strength (amplitude) in every direction. Commonly the amplitude of a seismic wave depends on the size of source, source receiver distance, and direction of the receiver from the source (Parnell 1994). This direction dependence of response is called the radiation pattern. Seismic stations that record elastic wave patterns from an earthquake show that the amplitude of P and S wave arrivals may be plotted into a form of radiation pattern, as shown in Figure 3.22.

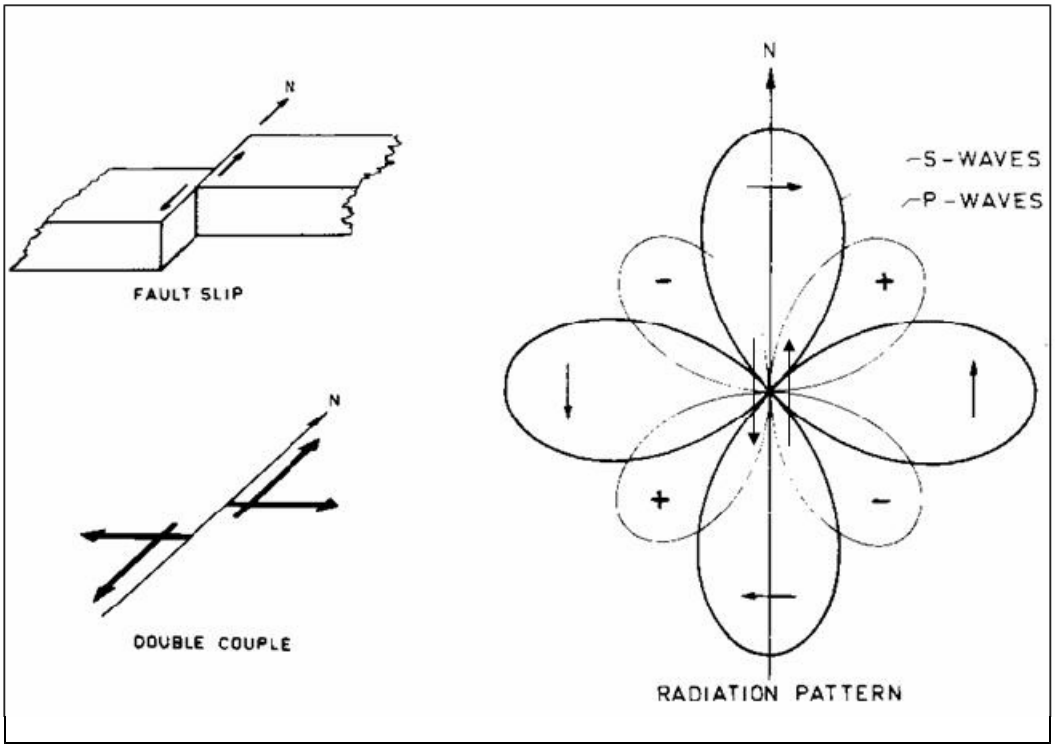

Figure 3.22: A fault shows its radiation pattern according to arrival of P and S waves (modified after Parnell 1994).

Another way it can be represented is as shown in Figure 3.23 in which the radiation pattern is quadrantal with compressional and dilatational quadrants. Dark arrows show stresses critical to generate the slip.

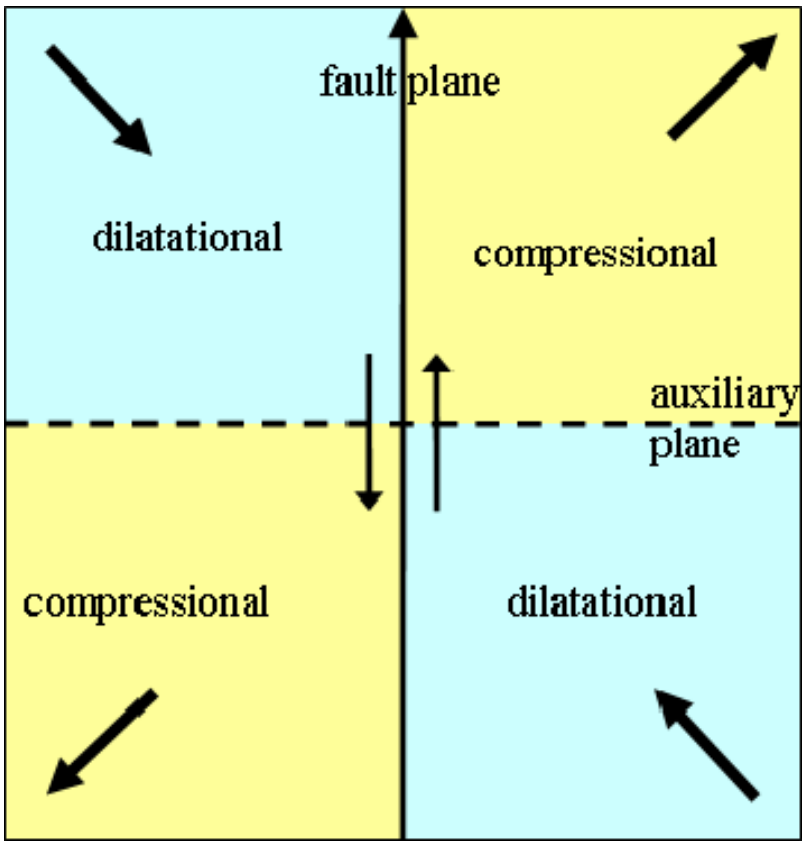

Figure 3.23: Fault shows the radiation pattern with compressional and dilatational quadrants (modified after Parnell 1994).

General fault orientations (actually motion diagrams) are shown by use of a “beach ball”, as shown in Figure 3.24. The shaded part of the beach balls represents the compressional quadrants, and the block diagrams exhibit the primary and auxiliary fault planes.

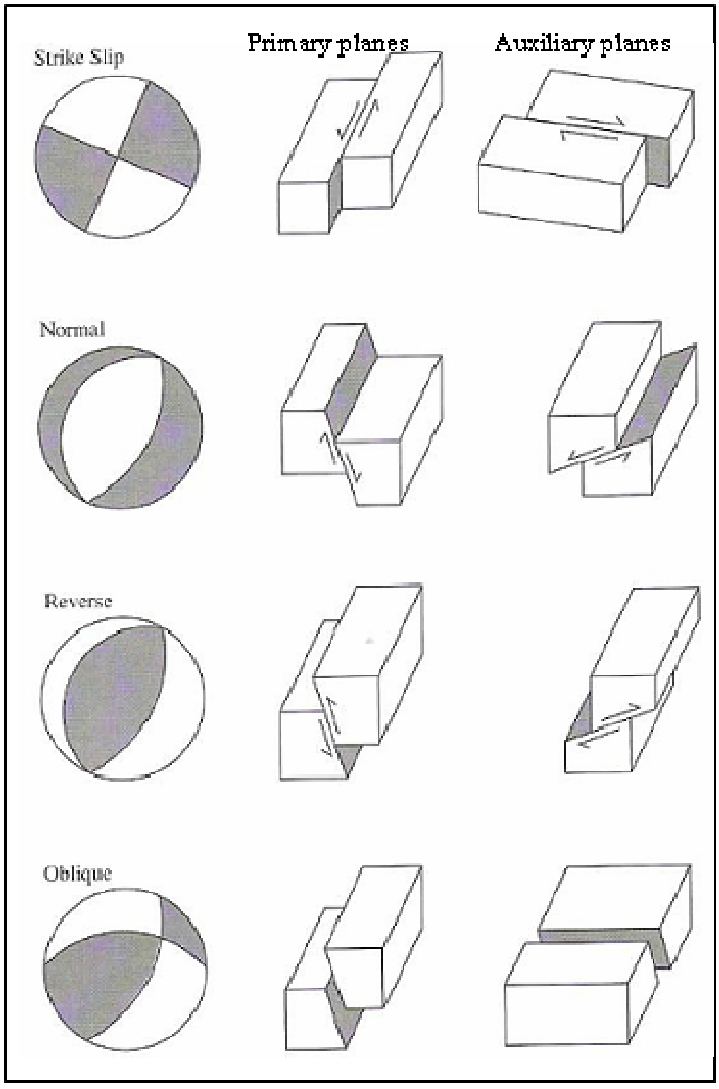

Figure 3.24: “Beach balls” show the radiation pattern corresponding system of faults (modified after Sleep and Fujita 1997).

Rough sketch shows, in Figure 3.25, that seismic waves cause dilatational strain and compressional strain changes in an aquifer that may rise and drop the water level (Huang et al. 2004).

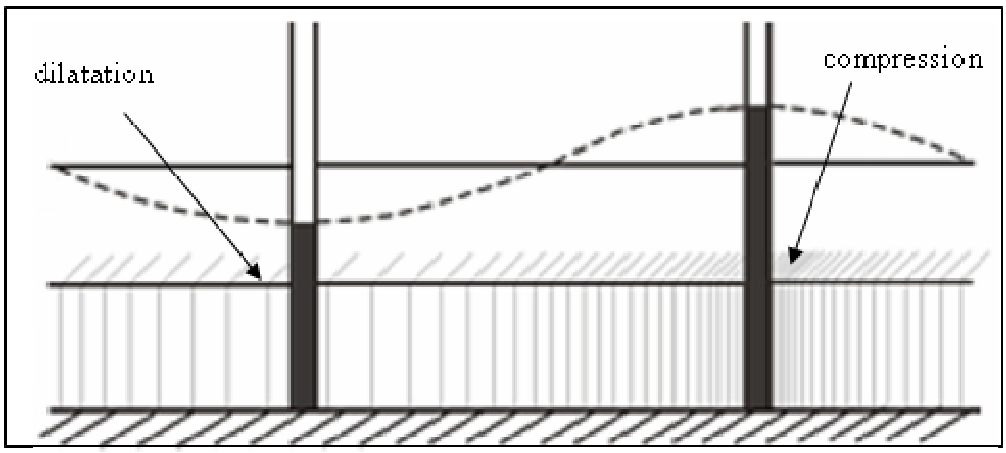

Figure 3.25: Map of water level response to seismic waves (modified after Huang et al. 2004)

3.6 Oil Production Changes

Several examinations also demonstrate the effects of an earthquake on oil production, as shown in Table 3.4 (the 12-point intensity scale has been used as described by the original reference, but there are at least three kinds of definitions for the scale, it was not mentioned which definition was used). The data is provided in chronological order. During the Southern California earthquake, triggered on July 21, 1952, Beresnev and Johnson (1994) explained fluctuations in oil production in Kern County. A number of wells demonstrated significantly increased the oil production in the first couple of days following the earthquake. However, in the same field, many wells did not show changes, reflecting a complex nature to the effect. For example, two adjacent wells behave very differently: oil production of one well increased from 20 bbl/day to 34 bbl/day (1 bbl of oil = 42 US gallons or 153 x m^3) instantly after the earthquake, whereas oil production dropped from 54 bbl/day to 6 bbl/day in an adjacent well.

Another example of an increase in oil production rate is an increase of up to 45 percent in response to the earthquake of January 7, 1938 in Starogronznenskoye oil field, Northern Caucasus as shown in Figure 3.26 (Beresnev and Johnson 1994). Unfortunately, no other quantitative details are available.

Table 3.4: Summary of case studies of influence of earthquakes on oil production (modified after Beresnev and Johnson 1994).

No.	Field location	Earthquake magnitude (M)	Seismic intensity in oil field (12 pt. scale)	Distance from epicenter (km)	Observed effect	Duration of effect
1	Kern County, California, USA.	7.6	8-11	80	Mixed effects of increased and decreased oil production, increased casing pressure.	Less than a month
2	Cudermes field Northeastern Caucasus.	3.5 and 4.5 45. and 4.2	5-7 5	10-15 10-15	Increased oil production, largest effects near fault. Increased oil production.	Less than a month.
3	Different fields in Daghestan and Northern Caucasus.	6.5	4-7	50-300	Large changes in oil production, renewed production in abandoned in production associated with passive faults	Several months to three years
4	Anapa Northern Caucasus	5.5	3-5	100	Increased oil production from some wells, pronounced near anticline, increased reservoir pressure	
5	Starogrozenenskoye field, Northern Caucasus	4.8	6	30	45% increase in oil production	

In the Daghestan Republic (former USSR as shown in Figure 3.26), an earthquake with a magnitude of 6.5 (8-9 intensity at epicenter) occurred on May 14, 1970 (Beresnev and Johnson 1994). This region has several productive oil fields, and changes in oil production, occurrence of earthquake and its aftershock effects have been studied thoroughly. Instantly following the earthquake, oil production increased rapidly, though it decreased as the aftershock activity reduced. Variations were observed in oil yield related to seismicity for a few months. The wells that showed the largest changes in oil production were located in the surrounding areas of known fault regions. Moreover, abandoned wells displayed an oil and water flow within the region of seismic intensity of 7 following the earthquake of May 14, 1970. Outflow of oil from these wells had finished many years before the earthquake, but this renewed outflow was sustained through 1974 (Beresnev and Johnson 1994).

Figure 3.26: Map of part of the former USSR showing oil production and earthquake regions (Beresnev and Johnson 1994).

The wells have behaved differently in numerous oil fields associated with the earthquake of May 14, 1970, shown in Figure 3.27. The oil and gas field of Gasha is located 50 km from the epicenter. Figure 3.27 displays the Well No. 23 activity due to the earthquake; oil production increased rapidly due to the main shock, whereas the water production increased by three times from the same well, as shown in Figure 3.27 (Beresnev and Johnson 1994). Scientists do not understand the delayed response of water flow as compared to oil production very well.

In another observation, in the Eldar oil and gas field, the distance is 220 km from the epicenter. Well No. 58, drilled in the surrounding area of a fault, showed a sharp rise in production, yielding a rate of production feature of the whole field before the earthquake.

The 3.3-3.4 × 10^6 kg/day production reported in the early half of May 1970 increased after several shocks up to 4.3 x 10^6 kg/day. It was analysed that the production increased about 15 percent in this well, No 58, but unfortunately, data was absent to show how long the effect remained (Beresnev and Johnson 1994).

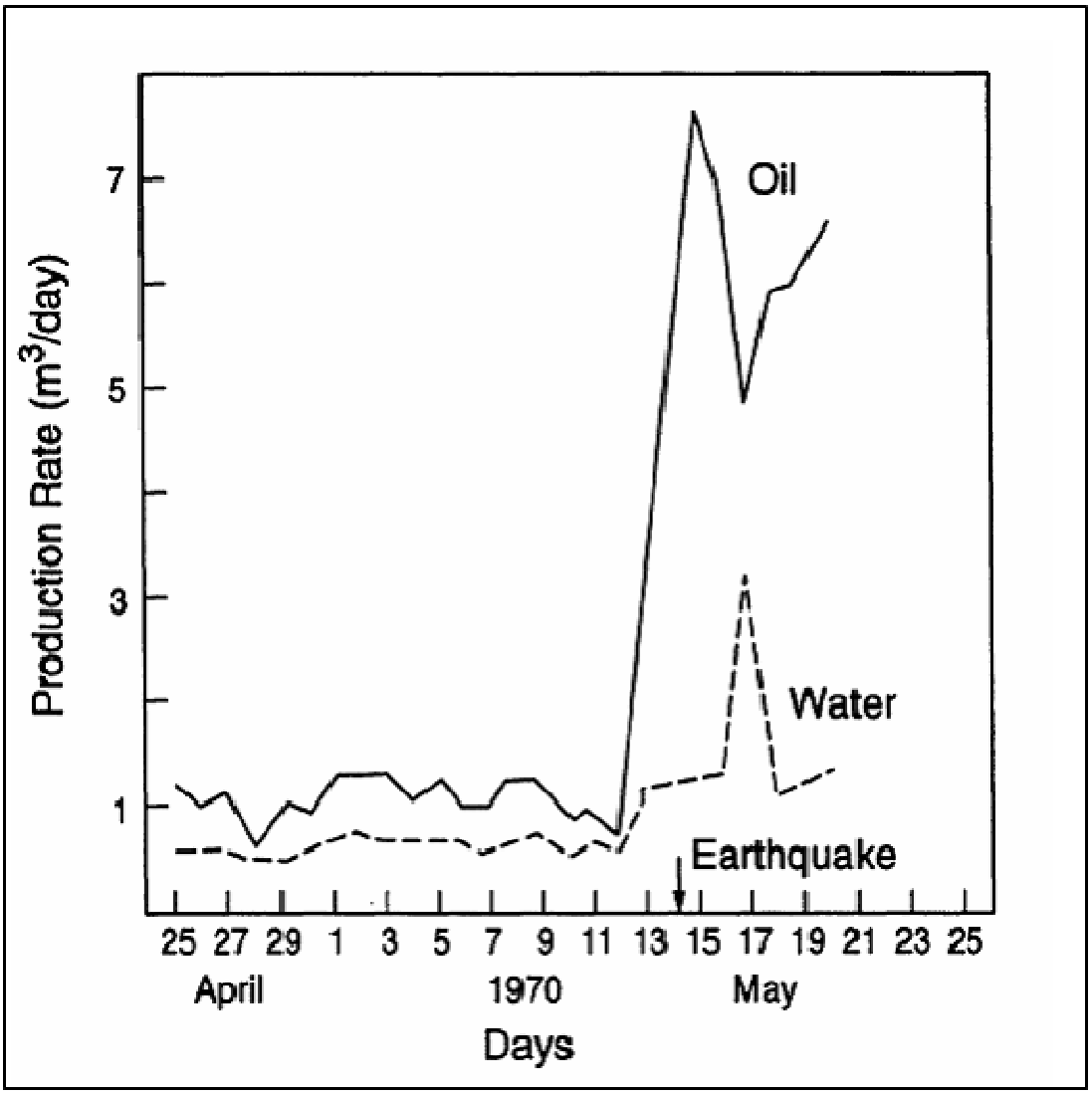

Figure 3.27: Daily response oil and water production at well no.23, which is located 50 km away from the Daghestan earthquake (modified after Beresnev and Johnson 1994).

Osika D.G. (1981) analysed data from a few other earthquakes in the Caucasus (Beresnev and Johnson 1994). For example, an earthquake occurred in 1966 at the Black Sea near Anapa; the intensity was 6-7 at its epicenter. Effects of this earthquake were noticed in

the Abino-Ukrainkaya oil field, 100 km away from the epicenter, where a few wells exhibited increased production. Osika emphasized that the hydrodynamic effect of the earthquake occurred even in those zones where seismic intensity was as small as 3 and 4, such as in Kolodeznove oil field which is situated 300 km from the Daghestan earthquake epicenter (Daghestan earthquake May 14, 1970). In Well No. 5 of the Kolodeznove oil field, the oil production was boosted from 51.8 to 73 m^3/day instantly after the earthquake. Also, in well No. 130, the level of liquid increased by 9 m, and then slowly returned to the early level. Not all wells responded to the earthquake, and effects were more prominent near the anticline domes (Beresnev and Johnson 1994).

Smirnova, in 1968, examined the effect of several earthquakes on oil production in the Gudermes Field near the Northern Caucasus (Beresnev and Johnson 1994). A monitoring well is situated 10-15 km far from the epicenter of two earthquakes which occurred on March 23, 1950 with magnitudes of 3.5 and 4.5. Oil production increased up to 30 percent during the two earthquakes. Another two earthquakes which occurred on August 1955 with magnitudes of 4.5 and 4.2 affected almost all wells in the Gudermes Field through rapid or delayed changes in oil production. The effect of the earthquakes remained for a month (Beresnev and Johnson 1994). The studies showed remarkable oil production fluctuations associated with the earthquakes in the oil field area. A few wells exhibited increased oil production, whereas a few of them showed decreased oil production.

3.7 General Description of Mechanism

A number of publications such as, Bodine, 1954a, 1954b, 1955; Duhon, 1964; Surguchev et al., 1975; Gadiev, 1977; Wallace, 1977; Kuznetsov and Efimova, 1983; Kissin and Stklianin, 1984; Vakhitov and Simkin, 1985; Sadovskiy et al., 1986; Simkin and Lopukhov, 1989; Kuznetsov and Simkin, 1990; Kissin, 1991; Simkin and Surguchev, 1991, as described in Beresnev and Johnson 1994 research journal, have been issued on the subject of suggested mechanisms of the effect of low-frequency elastic waves on saturated media. In general, these publications support (or at least do not disprove) the hypothesis of a soliton wave theory, as discussed in this thesis (chapter 2). This

mechanism clearly has the ability to enhance the flow of fluids in porous media in response to the dynamic excitation of an earthquake excitation, and it is also clear that because of the great distances involved, the effect is at least in substantial part elastic in nature (i.e. no permanent changes in porosity or permeability).

Basically, the writers claim that gravitational and capillary forces are predominantly responsible for the flow of fluids in the reservoir (Beresnev and Johnson 1994). Gravitational forces act because of "…the difference in density between phases saturating the medium…" (Beresnev and Johnson 1994). Remaining oil in a typical subsurface reservoir is usually contained in the shape of droplets scattered in water. The separation of oil from water is due to their capillarity (they are immiscible), not their density differences. But, when there is an excitation, some additional force is applied at the scale of the droplets (or to the pore throats which provide capillary blockage), and then the densities can help lead to upward flow of the less dense phase (gas or oil), and downward flow of the denser phase (water or oil). Pore scale process, shows the 3-phase system, where a denser phase (water or oil) flow downward, and a less dense phase (gas or oil) flow upward due to the applied additional force, as shown in 2.9 (chapter 2, page 26).

Mineral wetness and capillary forces play significant roles in restricting or affecting liquid percolation through fine pore channels. Liquid films are adsorbed onto minerals, and in a pore throat, these films decrease the normal percolation rate by decreasing the effective diameter of pore throats (usually, water is the wetting phase and oil or gas is the permeating, mobile phase). The boundary film may severely retard percolation, and in a small pore, there may be only one phase, such that a capillary barrier exists to flow of an immiscible phase such as oil and gas. In this case, the immiscible phase is stopped from flow through the pore by the capillary blockage, which requires a high local force to overcome the surface tension ($\Delta p = \gamma/2r$, where r is the degree of curvature of the capillary interface and /2r, where r is the degree of curvature of the capillary interface and γ is the surface tension). Percolation may continue again if some significant additional pressure can be introduced, as shown in Figure 3.28, and this pressure increase can perhaps be generated by the excitation of an earthquake. This pressure increase or "pulse" has the ability to move the oil blob further, or to help generate a vertical

gravitational segregation if the fluids are of different density (Beresnev and Johnson 1994).

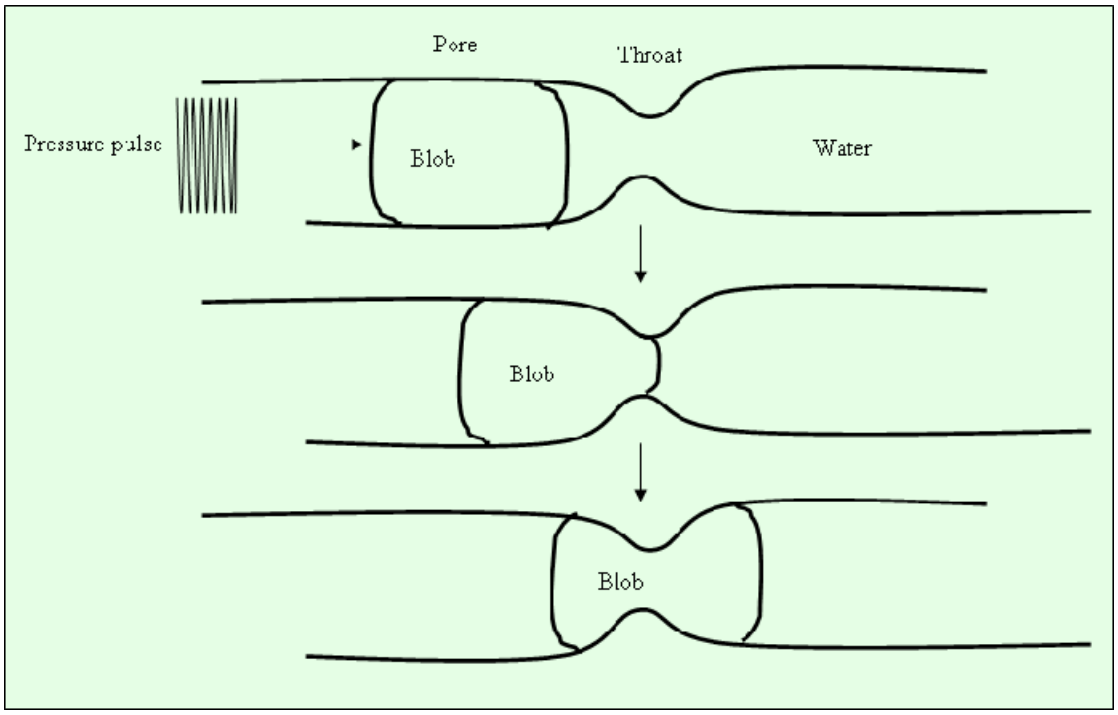

Figure 3.28: A model shows immiscible two phase flow through a porous channel with a constriction, under the effect of external pressure pulse wave (modified after Beresnev and Johnson 1994).

3.8 Summary

Water level changes associated with an earthquake can fluctuate differently for different wells, even those situated very close to one another. Reasons for this behaviour are not precisely known, but the water level fluctuations seem to depend on the magnitude and direction of the seismic waves, as well as on the structure of the reservoir in which the well is located (King et al. 1999). For example, the water level in wells drilled into bedrock may fall as water percolates into newly formed rock cracks if the earthquake is of sufficient energy level to generate new cracks. Distant effects cannot create new cracks, so changes in water level at great distance have been ascribed to dilation or contraction of pre-existing cracks.

The water levels in wells drilled into loose ground, such as valley-bottom deposits, may rise as the unconsolidated ground becomes more compact during earthquake excitation; compare this with the shaking of a bowl of loose dry flour, noting the settlement of the flour. This consolidation shrinks aquifers and compresses water, thereby increasing the pressure (or water level). However, differences between adjacent wells often cannot be clarified by existing displacement models for earthquakes, but has to be assigned to different hydrological environments for the different wells (Montgomery and Manga 2003).

The precise mechanism between hydrogeologic changes and earthquakes is not fully understood, but monitoring these changes improves perception into the responsible mechanisms, and may help diminish the ambiguity. It is necessary to collect the timing, magnitude, and impact of earthquakes (Sneed et al. 2003), and relate the excitation to accurate and high frequency pressure or water level measurements, and there is little data that fulfils all these requirements.

Changes in oil production associated with earthquake occurrence have been widely noted, but again, accurate measurements of production at short time intervals, are not published and supposedly not recorded. Consequently, investigators note discrepancies in the observed effects, so that the response of a particular well can hardly be predicted in advance. Furthermore, if increased production is found in response to a local earthquake, it remains indistinct whether it is stimulated by the actual elastic wave effect or an inelastic effect, by surface waves or body waves, or by some other associated sequence of events (Beresnev and Johnson 1994). If a strong theory with a robust physical basis were available, it should be possible to make predictions about well level, pressure, or oil production response. However, it seems that the state of the science is not yet at this point because the micromechanisms are not fully understood.

Chapter – 4

Fluid Induced Seismicity in Reservoirs

4.1 Introduction

Reservoir induced seismicity (RIS) has often been observed during and after filling the water reservoir behind a large dam. Dams are often built in active earthquake areas (Muco 1998) where there is substantial relief, and dams are always built in valleys, which in turn are often fault-controlled because faulting yields weakened, more erodable rock, leading to a negative geographic feature. It seems more likely that the rock under a fault-controlled valley in a tectonically active area is closer to a state of rupture than the rock away from the valley, all things considered. These induced earthquakes are apparently triggered by changes in pore pressure due to water flow such as occurs during diffusion because of the increased hydraulic head, or shear stress and pressure increases in response to the compressive loads imposed by the filling of the reservoir (Rastogi 1995).

Microseismic activity which precedes a larger earthquake in these cases occurs most likely as the result of the gradual changes (increases) in pore pressure which cause the effective stresses on the fault plane to be altered, reducing the frictional resistance of the fault plane. The first known example of reservoir-induced seismicity was documented at Lake Mead Reservoir, created by Hoover Dam on the Colorado River in the United States of America during the late 1930's. During the 1960's, several earthquakes greater than magnitude 6.0 occurred as the result of reservoir filling, such as in the vicinity of the water reservoirs at Xinfengjiang, China (1962), Kariba, Zambia-Zimbabwe border (1963), Cremasta, Greece (1966), and Koyna, India (1967) (Gupta 1992). Other reservoir-filling induced earthquake examples have been documented at Oroville, California, and Aswan, Egypt. These magnitude 6.0 induced earthquakes are large enough to cause damage in nearby towns and villages. A significant site of reservoir-induced earthquakes is the Koyna reservoir in India, where earthquakes began to occur soon after the impoundment of Shivajisagar Lake in 1962 and continued to occur for some time, the latest reported being on the 12^{th} and 13^{th} of March, 1995, when earthquakes exceeding magnitude 4.0 were documented (Rastogi 1995).

In addition to earthquakes induced by reservoir filling, other causes of man-made seismicity have been documented, such as during the injection of fluids under high pressure and temperature, large-scale underground mining, large surface excavations, oil production and reservoir pressure depletion, geothermal energy extraction, massive solidwaste disposal by slurry injection, and so on.

Understanding the role of fluids in weakening fault zones has long been recognized as an important aspect in studying the mechanism of earthquakes (Piccinelli et al. 1995). Using sophisticated instrumentation and measurements in boreholes, many observations of these seismic events have been recorded, and a large body of knowledge has been accumulated.

The mechanics of seismicity, as observed in the above mentioned dam reservoir cases, is considered mainly due to the change in pore pressure which leads to an altered effective stress field underneath the reservoir and within its surrounding area. The pore pressure can increase in two ways: undrained behaviour of the pore fluid in rocks that are subjected to an increase in compressive stress, implying a low permeability, and pressure increase through the diffusion of elevated pore pressures arising because of the increased hydraulic head in the impounded area, implying hydraulic connectivity of the reservoir to the stressed fault plane. Therefore, in the sense that elevated pore pressures can reduce the frictional strength of a fault zone below the value needed for stability, pore pressure change is an important mechanism for triggering earthquakes (Knoll 1992).

4.2 Types of Seismicity

Generally two types of RIS have been observed. The first type is related to initial filling of the reservoir or water level changes, whereas the second type is related to delayed strength changes that are coupled to water level fluctuations and diffusion.

4.2.1 Initial Seismicity (Type 1)

Initial seismicity (Type 1) is associated directly with the reservoir impoundment, a process which causes a rapid change in water level (from +15 m to as much as +100 m change in a year or two). Seismic activity is of the “swarm” type; it is usually associated

with a volume of rock rather than on specific fault surfaces, and it is characterized by a low magnitude and a shallow hypocenter depth. This activity is linked strictly with changes in water level of the reservoir and it arises because of the increase in elastic stress under the impoundment basin as a response to the increase in surface loads (100 m of water increases the stress on the ground surface by 1 MPa, and a large impoundment can contain several cubic kilometers of water, therefore a large area is loaded). There may also be an increase of pore pressure arising from the undrained behaviour of the rock that arises because of pore compressibility and low permeability (as in clays), and this is coincident with the direct increase of stress under the reservoir during impoundment and occurs with only a slight delay or no delay at all (Piccinelli et al. 1995). This is because stress changes, in contrast to water pressures, are transmitted almost instantaneously.

4.2.2 Protracted Seismicity (Type 2)

Protracted seismicity (Type 2) is associated with the kind of earthquakes that occur a substantial period of time after the beginning of reservoir impoundment. The magnitude is variable and often high, the hypocenters are deeper than in Type 1, and the hypocenters can extend over an area wider than the basin borders, maybe by 10 km or more for large reservoirs. It has been most frequently observed in reservoirs which show evidence of a correlation with active fault zones crossing the impoundment basin (Piccinelli et al. 1995). “The delayed response can arise from the diffusion of the pore pressure and the water flux outside the basin coupled with the elastic load” (Piccinelli et al. 1995). These phenomena can show a considerable time delay from the moment at which the surface load starts to be applied during primary impoundment, and these earthquakes may even reflect seasonal changes in water levels.

4.3 Seismicity and Reservoir Level

Generally in RIS, seismicity is related to impoundment and level changes in the large reservoirs created behind the dams. Intensity of the RIS is associated with hydro-mechanical properties of the underlying rocks, the nature of stress fields in the rocks in the vicinity of the reservoir, presence of fractures and pre-existing faults, the geology of

the area, the size and depth of the reservoir, water level changes, and so on. The number and magnitudes of RIS events decrease with the passage of time and seismicity can be triggered again by repeated filling events until the maximum impoundment levels are reached. Some reservoirs continue to actively display RIS after several years, yet other reservoirs show no seismicity. It is observed that deeper and larger earthquakes are caused by long-period water level changes (months to years), as compared to short-period water level changes (days to weeks) (Talwani 1997). Larger reservoirs have more widespread and deeper seismicity than smaller ones, and the microseismic activity is observed both below the deepest part of the reservoir and also in the surrounding areas. The location of the seismicity is thought to be dominated by the nature of the pre-existing faulting below and in the surrounding area of the reservoir (Talwani 1997).

A nonparametric correlation analysis can be carried out in order to check the statistical significance of possible interrelations between seismicity fluctuation rates and the water level of the impoundment. This approach allows one to analyze the seismic time series data (temporal changes in seismicity and seismic attributes such as size, frequency content, spatial location…), recognise monotonic deterministic interrelations (such as a direct rise in mean seismic event magnitude with a rise in reservoir level), and assess the significance level of frequency distributions of the series (Piccinelli et al. 1995). However, this approach appears to be insensitive to monotonic transformations of the variables that are involved, so it makes little difference if one uses the intensity, the magnitude, the energy, or the strain release, as these quantities are related with each other (Piccinelli et al. 1995).

One of the most interesting features of RIS is how widespread it is. It is not restricted simply to cases in which reservoirs have been built over what one might recognize as an active fault. Among the cases mentioned previously are several that are far from any naturally occurring seismicity. Yet others, such as cases in Quebec, India, and Australia, are in mid-plate environments with no historical evidence of seismicity of any kind. A simple Mohr-Coulomb analysis shows that the effect of reservoir impoundment is to move the state of stress closer to the failure condition by an amount equivalent to an increase of shear stress of only about 1 MPa or less (for 100 m of water). The obvious

conclusion must be that a large part of Earth's lithosphere must be stressed that close to a failure state, even in regions not undergoing active tectonics deformation. In other words, it appears that strain energy can be stored in shallow rocks (RIS foci are shallow) for long periods of time, to be released only when a trigger of appropriate magnitude, even as low as 1 MPa, is applied. From this point of view, a study of the many cases of reservoirs that do not induce seismicity would be interesting (Talwani 1997).

The elastic effects can immediately increase seimicity around a reservoir. A good example of rapid response (elastic response) has been observed at Nurek Reservoir; Tadjikistan, USSR (Figure 4.1), where earthquake swarms have been triggered by increasing the water level (to 100 m) (Knoll 1992). The seismic activity first decreased but next year it rose again when water level increased to 120 m and the seismicity rate subsequently decreased. Later, when the water level reached 200 m, an abrupt burst of increased seismic activity rate took place, as shown in Figure 4.1. The seismicity increased as a result of the "instantaneous" filling of the reservoir, rather than as a delayed diffusion-controlled process.

Some other examples of rapid seismic response to filling a reservoir have been observed at Monticello Reservoir (USA), Manic-3 (Canada), Kariba (Zimbabwe), Karemasta (Greece), Talbingo (Australia), and so on (Simpson et al. 1988).

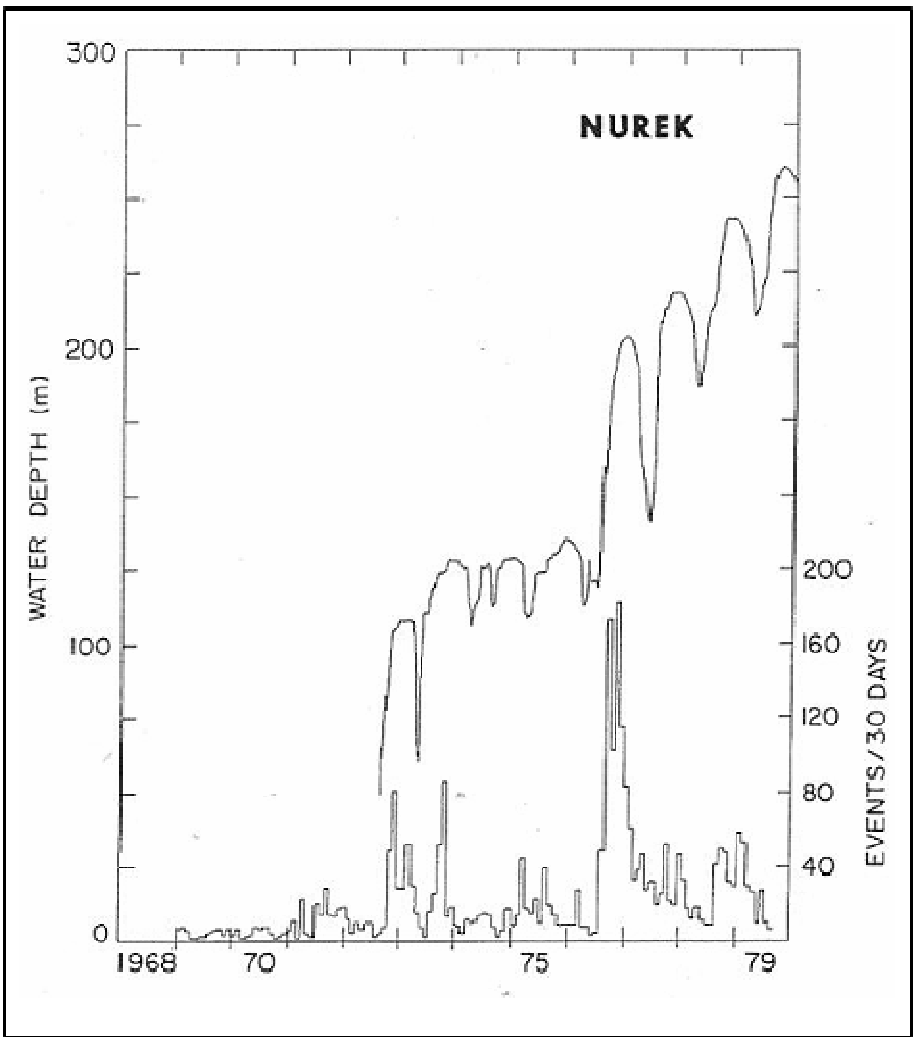

Figure 4.1: An example of induced seismicity with a rapid response at Nurek Reservoir, Tadijkistan, USSR (Knoll 1992)

A delayed response, such as at the Koyna dam in the west part of India, has also been noticed, as shown in Figure 4.2 (Knoll 1992). 1n 1962, the reservoir filling started, and after a while small magnitude earthquakes were recorded. Large earthquake events with magnitude of 5.5 and 6 occurred at depth (~ 5 km) in late 1967 once the reservoir level increased. The largest event caused significant damage and loss of life.

Some more examples of delayed response were noted at Oroville, California and Aswan Lake, Egypt. An earthquake of magnitude 5.7 was triggered seven years after impoundment in Oroville, California, whereas an earthquake of magnitude 5.3 occurred

in late 1981, some years after filling began in 1975 in Aswan Lake, Egypt (Simpson et al. 1988).

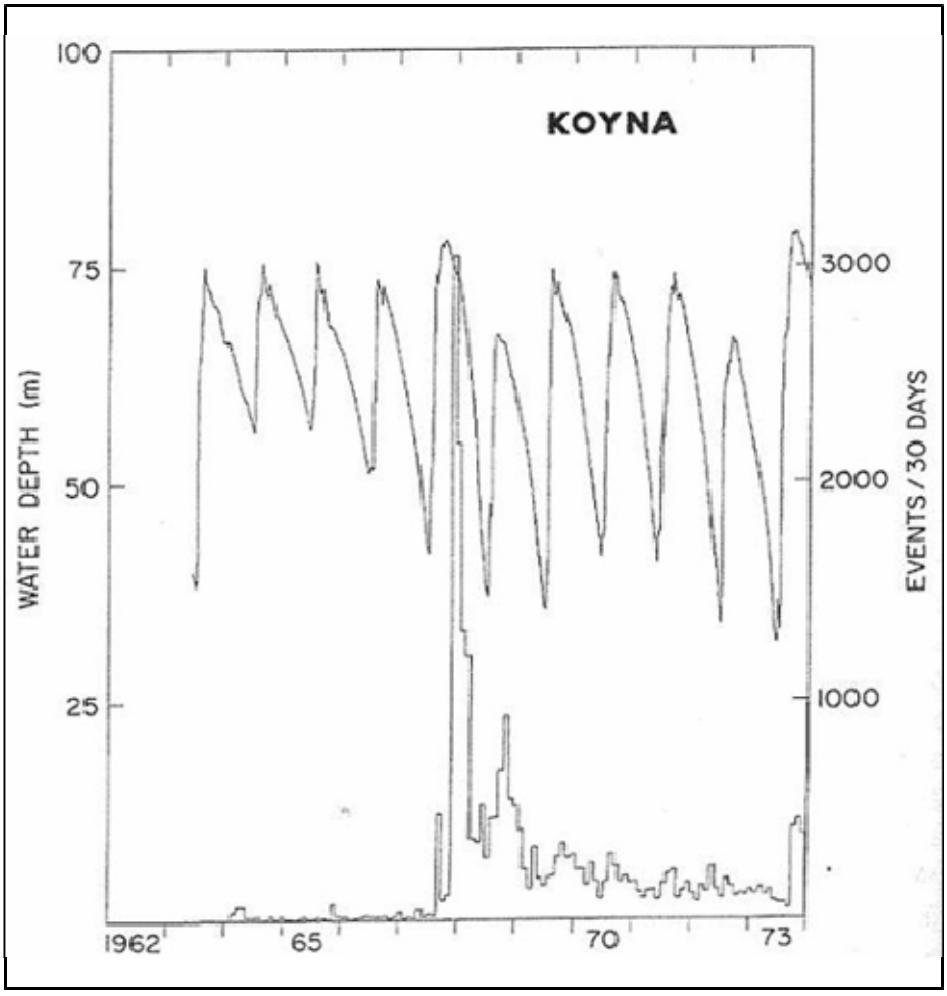

Figure 4.2: An example of induced seismicity with delayed response, at Koyna Reservoir, India (Knoll 1992)

Most cases are well known and noticeable examples of reservoir induced seismicity, such as the above mentioned instances, where impoundment depth was 100 m or more. On the other hand, induced seismicity with only a small rise in water level of a reservoir is also known, such as at the Monticello Reservoir (USA), where a remarkable increase in seismic activity began "immediately" after only 20 m increase in water level of the reservoir (Figure 4.3) (Simpson 1986). After January 1978, the seismicity has been not

observed when the water level curve remained at 130 m, suggesting that the stress has been relieved (released).

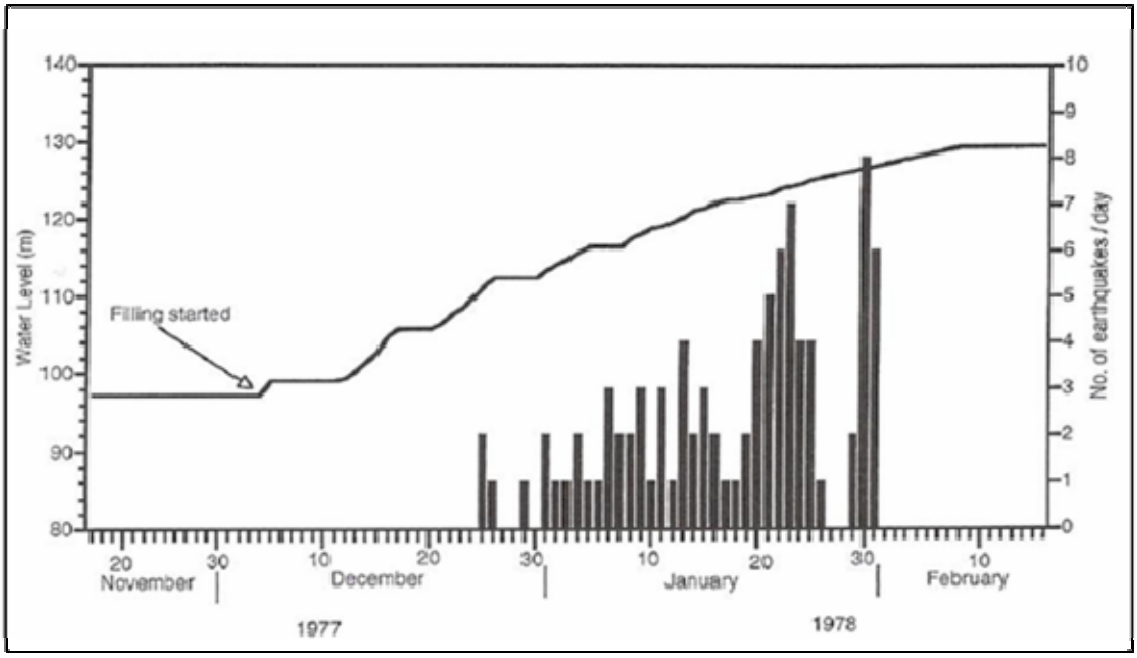

Figure 4.3: Seismicity associated with the filling of Monticello Reservoir (Scholz 2002).

4.4 Effective Stress Law

In porous rocks, flow, pressure, and pore fluid properties play significant roles in various crustal processes. The theory of effective stress developed by Terzaghi is commonly used to explain the pore fluid pressure effect on faulting, deformation, and earthquake generation or triggering (Chen 1992). Also, it is well known that porous rocks show typical responses in their compressional and shear wave velocities to confining stress and pore pressure variations. In general, higher pore pressures mean lower velocities and lower shear wave amplitudes.

The effective stress within a soil or rock is equal to the total stress minus the pore pressure. The effective stress principle is as fellows. Across any plane at element A within a rock, there are acting a total stress (σ) and a pore water pressure (p_p). Total stress (σ) can be visualized as the weight of a water-saturated column of rock. Two components

of that weight are the rock with empty pores and the weight of the water that fills the pores. The weight of the column of water, in the hydrostatic case, defines the pore pressure, and the effective stress (σ') is the difference between the two (Parry 1995):

$$\sigma' = \sigma - p_p \tag{4.1}$$

Distinguishing between the total vertical stress (σ_v) and the total horizontal stress (σ_h), which can be very different because of tectonics and geological stress history, the effective stresses can be defined as:

$$\sigma'_v = \sigma_v - p_p \tag{4.2}$$

$$\sigma'_h = \sigma_h - p_p \tag{4.3}$$

Where,

σ'_v = effective vertical stress

σ'_h = effective horizontal stress

Note that the maximum shear stress at a point is $(\sigma_v - \sigma_h)/2$, which is the same as $(\sigma'_v - \sigma'_h)/2$, is unaffected by changes in pore pressure. Therefore, as a first approximation (neglecting the effects of strain), an increase in pore pressure decreases the normal effective stress but has little effect on the shear stress.

4.4.1 Stress Relation

Rock strength varies with relations of shear stress (τ) and normal stress (σ) in soil mechanics. This is known as the Mohr-Coulomb law of failure, and a simple two-dimensional stress state can be plotted as a semicircle on a Mohr diagram. A change of stress increases or decreases the radius of Mohr-Coulomb, and the stress state moves towards or away from the failure condition, depending on the tectonic environment, on the stress change and on the pore pressure effect (Parry 1995). Generally, it is considered that increasing the pore pressure causes small-scale rock failure below the reservoir by

brining the stress circle tangent to the Mohr-Coulomb slip criterion. Figure 4.1 shows Mohr-Coulomb stress circles that are tangent to the slip criterion for several different stress conditions (Gupta 1992).

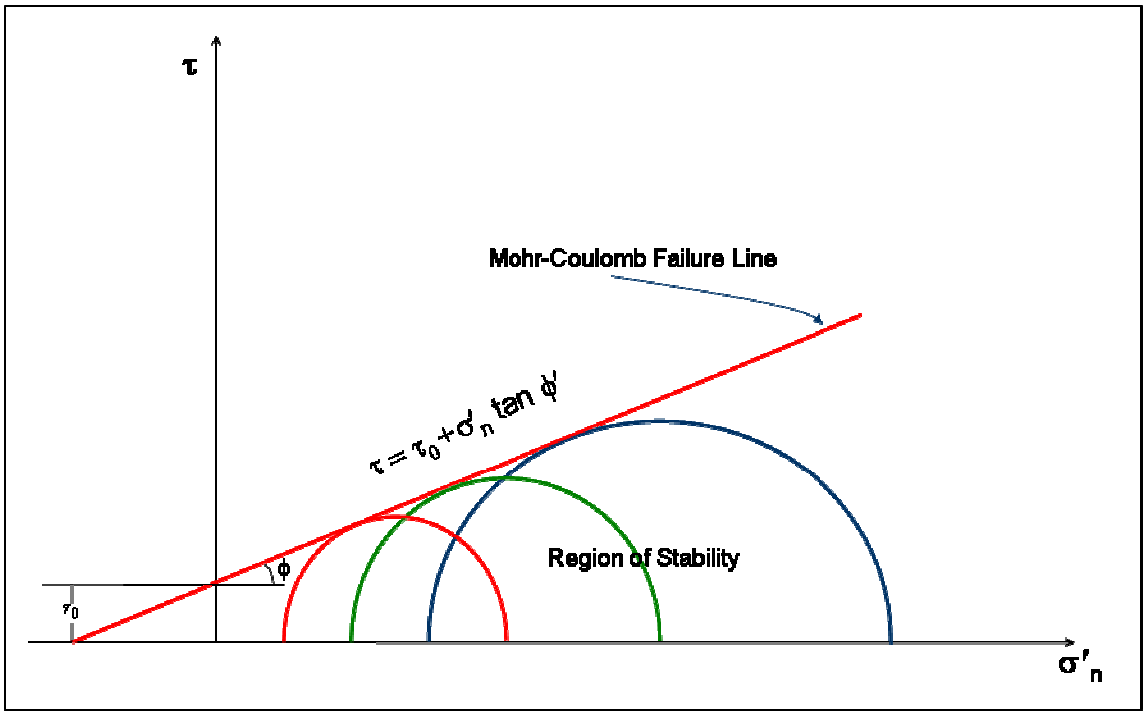

Figure 4.4: Mohr-Coulomb circle of stress showing failure for various values of confining pressures (modified after Gupta 1992).

Mathematically, the slip condition is described as (Gupta 1992):

$$\tau = \tau_0 + \sigma'_n \tan \phi' \qquad (4.4)$$

Where,

τ = shear stress at the slip point

τ_0 = basic shear strength (cohesion in soil and rock mechanics)

σ'_n = effective normal stress across a slip surface

ϕ' = effective angle of internal friction

4.4.2 Effect of Pore Pressure on the Stress Distribution in Rocks

Pore pressure plays a significant role to aid the rupture of highly stressed rocks by changing the effective stresses. Rocks within the outer few kilometers of the lithosphere have either an inter-granular or a fracture porosity, and below the depth of a few tens of metres the pores are filled with water or, exceptionally, with gas or oil (Scholz 2002). In the absence of any natural overpressure, injection or production, the pore pressure of water as a function of the depth *Z* is approximately (Gupta 1992):

$$p = \rho_w \mathbf{g} Z \tag{4.5}$$

Where,

p = pore pressure

ρ_w = density of water

g = acceleration due to gravity

Z = depth

However, Hubert and Rubey (1959) has mentioned that the actual pressures found at depth in drilled wells are distinctly different from the pressure given in equation (4.5). In the absence of strong geographical relief, the vertical stress is approximately given by:

$$\sigma_v = \rho_b \mathbf{g} Z \tag{4.6}$$

Where,

ρ_b = mean bulk density of water saturated rock

If hydrostatic conditions exist, then $\sigma'_v \sim (\rho_b - \rho_w)\mathbf{g}Z$. If not, the pore pressure must be measured and then used in the previous equation to estimate the effective stresses. The value of the horizontal stresses (σ_{HMAX}, σ_{hmin}) must be determined by measurements or by assessing the geological history of the site.

4.5 Poroelastic Effects in Reservoir Impoundment

Poroelastic effects during impoundment of reservoir can be divided into instantaneous effects and delayed effects. According to Rice and Cleary (1976), in the poroelastic approach the solid and fluid phases are assumed to be compressible (this is in contrast to the soil mechanics approach where the mineral phase itself and the water are assumed to be incompressible, although the soil skeleton – or matrix – has a compressibility). The instantaneous effects are due to the elastic loading, and the delayed effects are due to pore pressure changes arising by diffusion into the underlying rocks (Talwani 1997).

Bell and Nur (1978) defined the changes in rock (or fault) strength, ΔS, mathematically written as (Talwani 1997):

$$\Delta S = \mu_f (\Delta\sigma_n - \Delta p) - \Delta\tau \qquad (4.7)$$

Where,

$\Delta\tau$ = changes in shear stress

$\Delta\sigma_n$ = changes in compressive normal stress (total stress)

μ_f = co-efficient of friction of the fault surface

Δp = changes in pore pressure

It is noticed in equation (4.7), a decrease in rock strength (ΔS) may be caused by an increase in pore pressure or a decrease in the normal stress ($\Delta\sigma_n$) related to loading. This equation is similar to equation 4.4, and it is a version of the Mohr-Coulomb failure criterion relating the shear stress at slip to the product of the effective stress and a coefficient of friction (Talwani 1997).

4.5.1 Elastic Response

The elastic response (rapid response) of the subsurface is an instantaneous change in "normal and shear stresses on the fault plane by loading a reservoir" (Talwani 1997). In isotropic conditions, it is considered that stress ($\Delta\sigma$) (Figure 4.5b) simulates a loading curve for the reservoir (Figure 4.5a), and it is generally assumed that increased normal stress stabilizes the zone (increases ΔS), usually the case of reservoir loading. Substantial seismicity has been observed with reservoir elevation alterations at Lake Mead; induced seismicity swarms were observed after impoundment following the Hoover Dam construction in the 1930's and 40's (Talwani 1997).

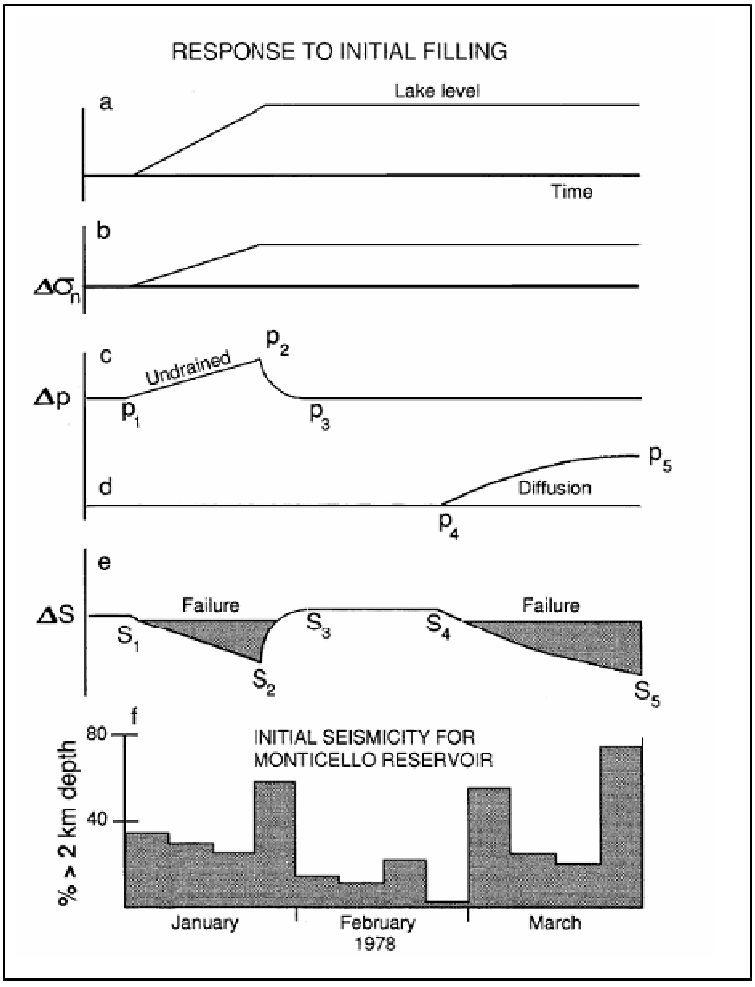

Figure 4.5: Schematic diagram to illustrate the processes of reservoir induced seismicity associated with the initial filling of Monticello Reservoir (Talwani 1997).

4.5.2 Undrained Response

Undrained response is associated with the pressure of fluids within the pores of a reservoir. According to soil mechanics principles, if the pore fluid cannot escape or enter because of low permeability (with respect to the loading rate) and the rock sample is subjected to alteration in total confining stress, the condition is called undrained, and the pore fluid can take some or all of the total stress change (depending on phase compressibilities). In the case of reservoir filling, it has been observed that an "immediate" increase (i.e. a rapid response) in pore pressure occurs in the bedrock because reservoir water added a load at the surface. If the flow of pore water is severely impeded, as perhaps in clay-filled fractures or a fault plane, it means an (undrained) increase in pore pressure (Δp_u) takes place. The increase in pore pressure will persist until it disperses into the surrounding rock mass through flow (Talwani 1997).

4.5.3 Drained Response

Drained response is defined as the condition where the pore fluid can respond rapidly to a change in pressure applied from, for example, the change of head in the reservoir. An undrained response at a short time becomes a drained response after all the excess pore pressure caused by the loading dissipates. A drained response to changes in pressure (e.g. from a change in reservoir level) is a relative issue: if the response time for drainage is slow (lower permeability case) with respect to the loading rate, the pore fluid may respond only slowly to a forcing pressure change. Nevertheless, a drained response can be assumed once the fluid leaves the pores and the excess pore pressure (Δp_u) decreases to zero such as (p_2 to p_3) in Figure 4.5c. A drained response is always somewhat delayed with respect to the stress-change-induced Δp_u arising from rapid primary impoundment and the delay depends on the hydromechanical properties of the rock (permeability, compressibilities, viscosities of fluids, saturations, porosity). However, it is also conceivable that chemical effects, perhaps even aided by pressure increases (stress corrosion or softening of rock material) can affect the strength. The combination of a pore pressure change and a strength change are included in the change in rock strength ΔS (S_2 to S_3) as shown in figure 4.5e, for the drained response (Talwani 1997).

4.5.4 Pore Pressure Diffusion

Diffusion of pressure occurs when the reservoir head is raised (p_4 to p_5) as shown in figure 4.5d. The pore pressure increase is related with a decrease in rock strength (S_4 to S_5), as shown in figure 4.5e, because the higher pore pressure causes a reduction in the effective stress across the slip plane. Further RIS can be induced by this decreasing strength, marked as failure in figure 4.5e (Talwani 1997).

4.5.5 Coupled Response

A coupled response is associated with including all of the phase compressibilities as well as the compressibility of the rock matrix in a consistent manner, so that the pore pressure change predictions are more rigorous. In 1976, Rice and Cleary derived the fully coupled response "…for isotropic fluid-saturated porous medium…" (Talwani 1997) and it can be written as (Talwani 1997):

$$\sigma_{ij} = 2G\varepsilon_{ij} + \frac{\nu}{1+\nu}\sigma_{kk}\delta_{ij} - \frac{3(\nu_u - \nu)}{B(1+\nu)(1+\nu_u)}p\delta_{ij} \tag{4.8}$$

Where,

ν, ν_u = drained and undrained Poisson's ratio

G = shear modulus

B = skempton co-efficient (fluid pressure divided by confining pressure under undrained conditions)

The fully coupled response is most important at the moment of a change in the total stress as it allows the prediction the magnitude of the undrained response in pressure and stresses as well, including all strains in the various phases. Once enough time has gone by and pressure diffusion acted, the pore pressure function p(z, t) will be dominated by permeation effects, generating a RIS lag to impoundment level change times (Talwani 1997).

The above comments are particularly applicable for isotropic rock conditions; however, because of fractures (cracks) where RIS often is observed, there are other factors associated with the compliance of the rock mass and time effects on diffusion. Anisotropy in elastic properties can also be the case, and this would change the form of the previous equation and also the RIS character. For example, with an increase in pore pressure, RIS can be observed "…on vertical fractures in a normal faulting and on horizontal fractures in a reverse faulting environment" (Talwani 1997).

4.6 Mechanism of RIS

The circumstances essential for causing induced sesimicity in the reservoir area are the accumulation of initial stress and water level (pressure) fluctuation. Apparently, the pore pressure effect is the most important effect for RIS. This takes into account that RIS events can be found in petroleum reservoirs associated with fluid injection into deep well-bores. Because in most cases the rock mass is saturated and the pores are filled with liquid in a natural manner even before filling the reservoir or injection of liquid into the ground, respectively (Knoll 1992), and injection production could change the pressures substantially, especially if there is no compressible fluid (i.e. free gas).

RIS is generally "…caused by shear failure on a pre-existing fault plane…" (Talwani 2000). ΔS, the strength change along a pre-existing fault plane in response to reservoir impoundment, according to Mohr-Coulomb's law, is described mathematically as (Talwani 2000):

$$\Delta S = \mu(\Delta\sigma_n - \Delta P) - \Delta\tau \tag{4.9}$$

$$\Delta P = \Delta P_i + \Delta P_{diff} \tag{4.10}$$

Where,

ΔS = change in strength

$\Delta\sigma_n$ = change in normal stress

$\Delta\tau$ = change in shear stress

μ = coefficient of friction

ΔP = total change in pore pressure

ΔP_i = change in pre pressure due to instantaneous effect

ΔP_{diff} = change in pore pressure due to diffusion

Negative values of ΔS imply weakening, while positive values signify strengthening. Ignoring nonlinear effects, the subsurface responds to the reservoir impoundment by alterations in shear stress and normal stress on the fault plane. Generally, an increase in shear stress (τ), an increase in pore pressure (P), or a decrease in normal stress (σ_n) may cause slip in the fault region. One possible explanation for low fault strength might be simply the hydromechanical reduction in strength because of the high fluid pressures present in the fault region (Rajendran and Harish 2000).

Protracted sesimicity usually shows a time lag in response to re-impoundment of the reservoir, thus pore pressure diffusion plays a significant role. The effect of diffusion in RIS is the following:

- Filling or draining the reservoir behind the dam changes the pressure head of the fluid in the rocks directly underneath the impoundment.
- This pressure increase moves through the rock mass gradually through the process of pressure diffusion, and is therefore rate-controlled by the hydraulic conductivity of the rock mass
- Because diffusion is a slow process if the rocks are of low permeability, head changes in the reservoir may take a long time (months to years) to reach the potential slip plane deep beneath the reservoir.
- Hence, seismic activity that is linked to this effect can be substantially delayed in time.
- Seasonal filling and draining of the reservoir creates a varying pressure (the forcing function) which may be reflected in the pressure response at depth as a varying response function, delayed in time and usually of reduced magnitude.

To understand the temporal and spatial pattern of induced seismicity using the mechanical effect of pore pressure diffusion, Talwani and Acree (1985) defined a term called 'seismic hydraulic diffusivity', signified as α_s, and demonstrated a simple relationship $\alpha_s = L^2/t$, where L = distance between the location of earthquakes and the source of the pore pressure front (reservoir), and t = delay between the onset of seismic activity and the time of filling. Using this relation, a range of values of α_s has been calculated and a characteristic value reported of about 5×10^4 cm^2/s, which was valid for most areas.

An example of the protracted sesimicity that can be observed in active reservoirs is given below (Fig. 4.6), where the lake level in the Koyna Reservoir fluctuated regularly (Rajendran and Harish 2000).

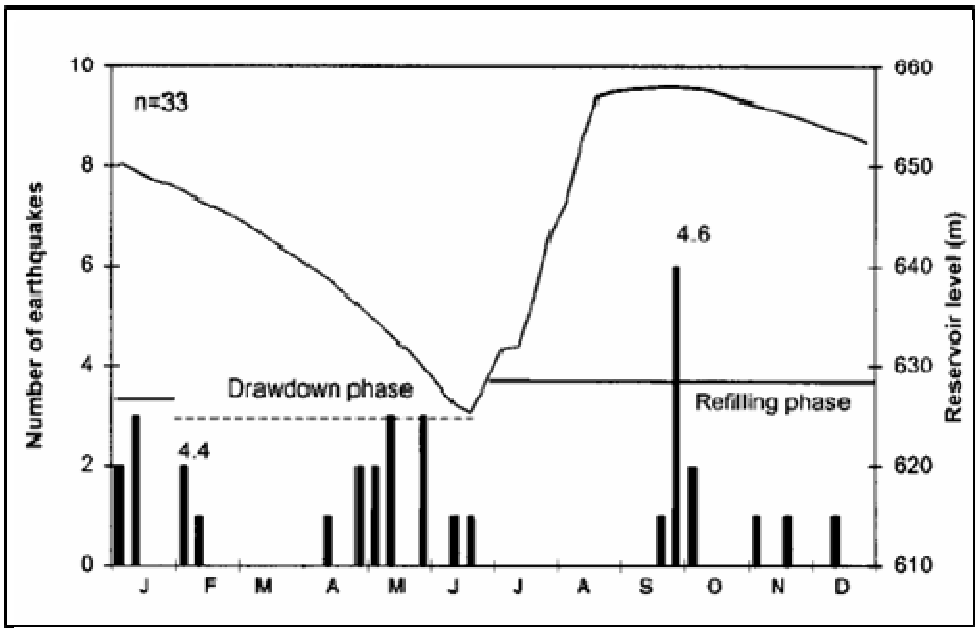

Figure 4.6: Lake level fluctuation and protracted seismicity at Koyna Reservoir during 1983 (Rajendran and Harish 2000).

4.7 Case Histories of Important RIS

More than one hundred cases of large-scale impoundment-induced seismicity have been observed all over the world, as shown in Table 4.1 (Guha and Patil 1992). The

geographical locations of the reservoirs are shown in Figure 4.7; whereas Figure 4.8 displays the distribution of RIS changes in seismicity in the world (Knoll 1992).

Table 4.1: Large water reservoir induced seismicity (up to 1990) (modified after Guha and Patil 1992).

No.	Name of Dam, Country	Dam Location	Reservoir Max. depth (m)	Magnitude (M) Max.	Date: d-m-y	Level of RIS
1	Akosombo, Ghana	07.50N 00.25E	109	5.3	11.64	II
2	Almendra, Spain	41.21N 06.16W	185	2		III
3	Arimine, Japan	N/A	N/A	>3.5	N/A	II
4	Asahi (GIFU)	N/A	N/A	>3.5	N/A	II
5	Aswan, Egypt	N/A	111	5.6	14.11.81	II
6	Bajina Basta, Yugoslavia	43.97N 19.37E	81	4.8	03.07.67	II
7	Benmoew, New Zealand	44.40S 170.23E	96	5	07.07.66	II
8	Bhatsa, India	19.51N 73.42E	58	4.8	15.09.83	II
9	Blowering, Australia	35.50S 148.00E	95	3.5	06.01.73	II
10	Cabin Creek, USA	39.62N 105.72W	46	2	68	III
11	Cajuru, Brazil	20.30S 44.70W	21	4.7	23.01.72	II
12	Camarillas, Spain	38.36N 01.65W	44	4.1	15.04.64	II
13	Canelles, Spain	42.03N 00.65E	132	4.7	09.06.62	II
14	Charvak, Uzbekistan	Near Tashkent	130	4	15.03.77	II
15	Clark Hill, USA	33.85N 82.38W	54	4.3	02.08.74	II
16	Contra, Switzerland	46.23N 08.83E	190	3	10.65	III
17	Coyote Valley, USA	39.23N 123.17W	22	5.2	06.06.62	II
18	Danjiangkou, China	32.69N 111.08E	86	4.7	29.11.73	II
19	Eguzon,. France	N/A	61	3.5	N/A	II
20	El Cenajo, Spain	38.38N 02.23W	75	N/A	73	III
21	El Grado, Spain	42.38N 00.17E	85	N/A	N/A	-
22	Emosson, Switzerland	46.09N 06.91E	170	3	73-74	III
23	Eucumbene, Australia	36.08S 148.72E	106	5	18.05.59	II
24	Fairfield, USA	34.34N 81.32W	49	2.8	10.78	III
25	Flaming Gorge, USA	41.25N 109.50W	139	Decrease in microseismicity	N/A	III
26	Foziling, China	N/A	74	4.5	11.08.73	II
27	Ghirni, India	18.37N 76.38E	15	2	N/A	III
28	Glen Canyon, USA	37.07N 11.22W	178	Decrease in microseismicity	N/A	III
29	Gordon River Power Development Storage, Tasmania, Australia	N/A	140	N/A	N/A	II

30	Grancarevo, Yugoslavia	42.75N 18.48E	105	3	68-70	III
31	Grandval, France	44.97N 03.10E	78	V	05.08.63	II
32	Hendrik Verwoerd, S.Africa	30.63S 25.78E	55	2	71	III
33	Hitotsuse, Japan	N/A	N/A	>3.5	N/A	II
34	Hoover, USA	36.13N 114.43W	191	5	10.03.40	II
35	Huangshi, China	N/A	40	2.3	21.09.74	III
36	Idukki, India	09.83N 76.97E	166	3.5	02.07.77	II
37	Ingouri, Russia	Caucasus	270	4.4	12.79	II
38	Itezhitezhi, Zambia	15.79S 25.07E	62	4.2	13.05.78	II
39	Izvorul Muntelui-Bicaz,Romania	N/A	127	2	N/A	III
40	Jocasse, USA	34.98N 82.94W	107	3.7	25.08.79	II
41	Kadana, India	23.30N 73.80E	58	2.5	N/A	III
42	Kamafusa, Japan	38.15N 140.50E	42	3	N/A	III
43	Kariba, Zambia/Zimbabwe	16.93S 27.93E	122	6.2	23.09.63	I
44	Kastraki, Greece	38.67N 21.70E	91	4.6	N/A	II
45	Keban, Turkey	38.82N 39.33E	182	3	06.73	III
46	Keowee, USA	34.80N 82.89W	53	3.8	13.07.71	II
47	Kerr, USA	47.70N 114.17W	54	4.9	28.07.71	II
48	Kinnersani, India	17.68N 80.67E	62	5.3	13.04.69	II
49	Koyna, India	17.62N 73.76E	100	7	10.12.67	I
50	Kremasta, Greece	38.90N 21.53E	120	6.3	05.02.66	I
51	Kurobe, Japan	36.53N 137.65E	180	4.9	19.08.61	II
52	Kuzuryu, Japan	N/A	N/A	>3.5	N/A	II
53	LaCohilla, Spain	43.21N 04.54W	98	N/A	75	III
54	Leroy Anderson, USA	N/A	72	Decrease in foreshocks and aftershocks	73	III
55	Makio, Japan	N/A	N/A	>3.5	N/A	II
56	Mangalam, India	10.63N 76.52E	29	3	63	III
57	Mangla, Pakistan	33.22N 73.68E	104	3.6	28.05.67	II
58	Manicouagan3, Canada	50.11N 68.65W	96	4.1	23.10.75	II
59	Marathon, Greece	38.18N 23.90E	60	5.7	20.07.38	II
60	Mica, Canada	52.07N 118.30W	191	4.1	05.01.74	II
61	Midono, Japan	N/A	N/A	>3.5	N/A	II
62	Miomote, Japan	N/A	N/A	>3.5	N/A	II
63	Mississippi River Valley, USA	N/A	N/A	Past earthquakes	N/A	II
64	Monteynard, France	44.90N 05.70E	125	4.9	25.04.63	II
65	Mula, India	19.37N 74.62E	44	1.5	72	III
66	Magarjunsagar, India	16.46N 79.20E	114	3.5	N/A	II
67	Nagawado, Japan	N/A	N/A	>3.5	N/A	II
68	Nanchong, China	N/A	45	2.8	25.07.74	III

69	Narugo, Japan	N/A	N/A	>3.5	N/A	II
70	Nurek, Tajikistan	38.42N 69.27E	285	4.6	27.11.72	II
71	Ohkura, Japan	N/A	N/A	>3.5	N/A	II
72	Oroville, USA	39.53N 121.43W	204	5.7	01.08.75	II
73	Ouedd Fodda, Algeria	36.02N 01.60E	83	3	05.33	III
74	Palisades, USA	43.23N 111.12W	67	3.7	10.06.66	II
75	Parambikulam, India	10.38N 76.80E	66	3	N/A	III
76	Piastra, Italy	44.21N 07.21E	84	4.4	07.04.66	II
77	Pieve de Cadore, Italy	46.45N 12.41E	98	V	13.01.60	II
78	Porto Colombia, Brazil	20.12S 48.35W	50	5.1	24.02.74	II
79	Qianjin, China	N/A	50	3	20.10.71	III
80	RockyReach, USA	7.78N 120.17W	53	N/A	N/A	-
81	Sainte-Croix, France	N/A	85	2.2	N/A	III
82	San Louis, USA	37.07N 121.13W	104	N/A	N/A	-
83	Sanford, USA	35.63N 101.67W	67	N/A	N/A	-
84	Schlegeis, Austria	47.07N 11.77E	113	2	04.73	III
85	Sefia Rud, Iran	36.75N 49.37E	80	4.7	02.08.68	II
86	Serre-Poncen, France	N/A	129	3.3	23.08.66	II
87	Sharavathy, India	14.10N 76.82E	38	2	N/A	III
88	Shasta, USA	40.77N 122.30W	152	2	N/A	III
89	Chenwo, China	N/A	50	4.8	02.12.74	II
90	Sholayar, India	10.31N 76.77E	59	2	N/A	III
91	Sriramsagar dam, India	19.00N 78.33E	43	3.2	21.07.84	II
92	Talbingo, Australia	35.72S 148.33E	142	3.5	06.01.73	II
93	Tarbela, Pakistan	34.13N 72.79E	137	3	N/A	III
94	Tohri, Japan	N/A	N/A	>3.5	N/A	II
95	Toktogul, Kyrgyzstan	41.74N 72.79E	185	2.5	N/A	III
96	Tsengwen, Taiwan	23.31N 120.65E	124	3	N/A	III
97	Uchkawa, Japan	N/A	N/A	>3.5	N/A	II
98	Ukai, India	21.25N 73.72E	64	3	N/A	III
99	Vajont, Italy	46.27N 12.38E	232	3	63	III
100	Varragamba, Australia	33.97S 150.42E	104	5.4	09.03.73	II
101	Vidra Lotru, Romania	N/A	121	2.8	N/A	III
102	Vidraru-Arges, Romania	N/A	167	2.8	N/A	III
103	Volta Grande, Brazil	20.14N 48.05W	32	5.1	24.02.74	II
104	Vouglans, France	46.42N 05.68E	112	4.4	21.06.71	II
105	Hsifengchiang, China	23.78N 114.58E	80	6.1	18.03.62	I
106	Yuda, Japan	N/A	N/A	>3.5	N/A	II
107	Zhelin, China	N/A	62	3.2	14.10.72	II

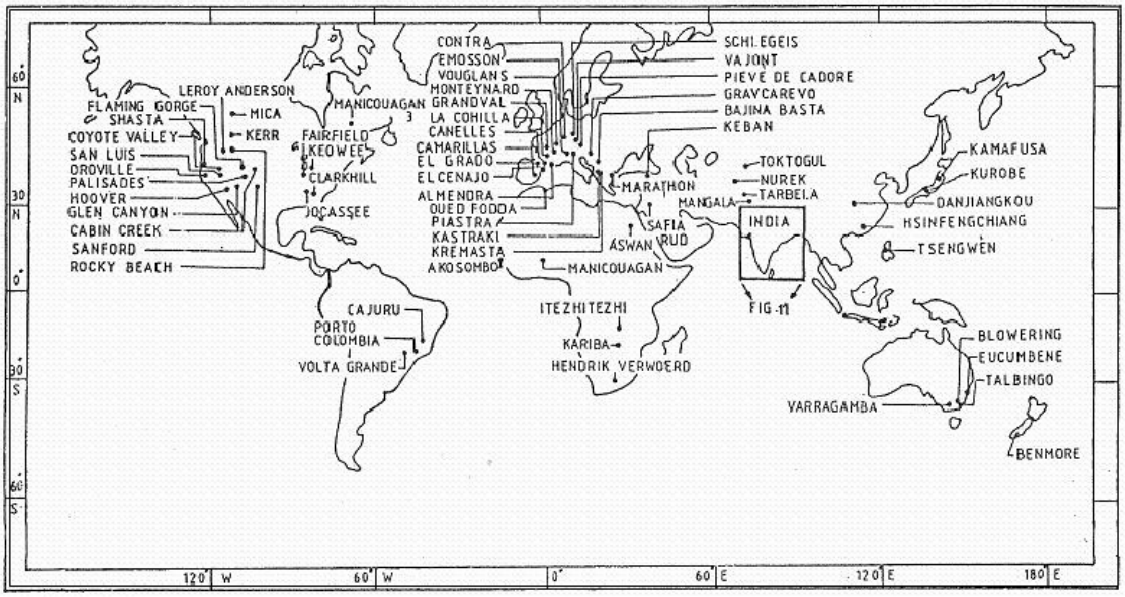

Figure 4.7: Geographical locations or reservoirs showing induced seismicity (after Knoll 1992).

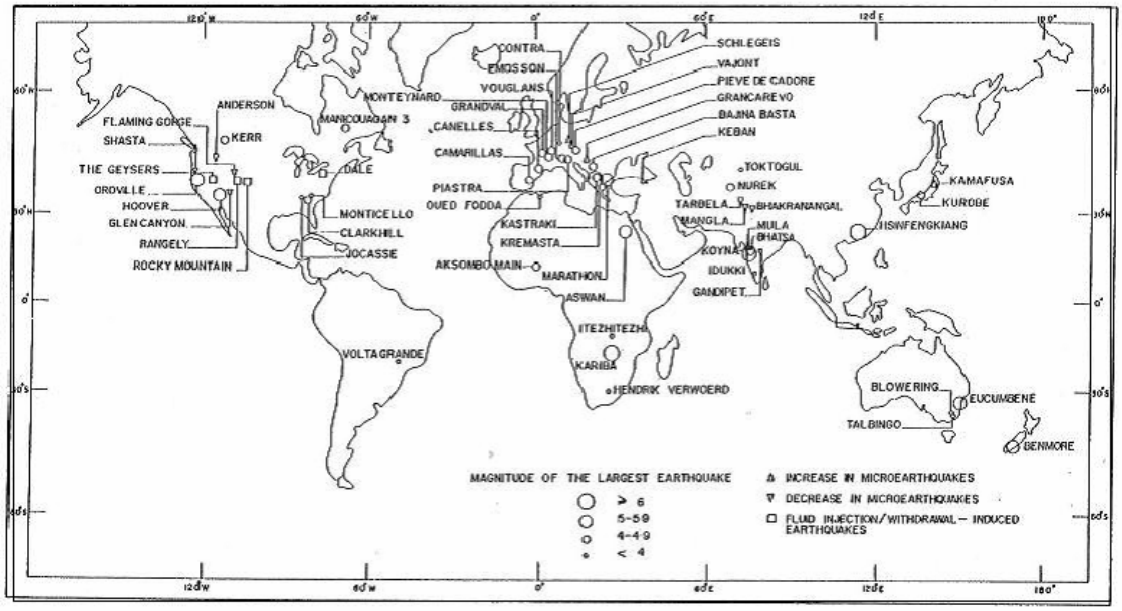

Figure 4.8: World wide distribution of RIS changes in seismicity (after Knoll 1992).

Table 4.2: Level of induced seismicity related to RIS cases, world over (from Knoll 1992).

No.	Nature/Intensity of Seismicity	Magnitude (M) Range	Number of Reservoirs	RIS level
1	Micro-level	≤ 3.0	35	III
2	Mild	3.1 – 3.9	30	II
3	Moderate	4.0 – 5.9	34	II
4	Intense	≥ 6.0	4	I

These reservoirs (Table 4.1) can be divided into three "categories" on the basis of maximum earthquake magnitudes (Table 4.2). RIS level I lies above magnitude (M) ≥ 6.0, RIS level II is M = 3.1 to 5.9, and RIS level III is M ≤ 3.0, respectively reflecting intense, mild to moderate, and micro-level seismicity. It is clear from Tables 1 and 2 that only four reservoirs, namely Hsinfengchiang, China in 1962; Kariba, Zambia-Zimbabwe border in 1963; Kremasta, Greece in 1966; and Koyna, India 1967 have shown RIS level I (M ≥ 6.0), as shown in Figure 4.9. Seven examples of RIS are given in the Figure 4.9 for magnitudes ranging from 5.0 to 6.5. Lake Nasser produced by the Aswan dam in Egypt is a relatively recent addition to this list; seventeen years after filling the lake, an earthquake with M = 5.5 took place on November 14, 1981 (Knoll 1992). The Figure 4.9 is drawn by using relative data, without the scales reflecting the earthquake magnitude.

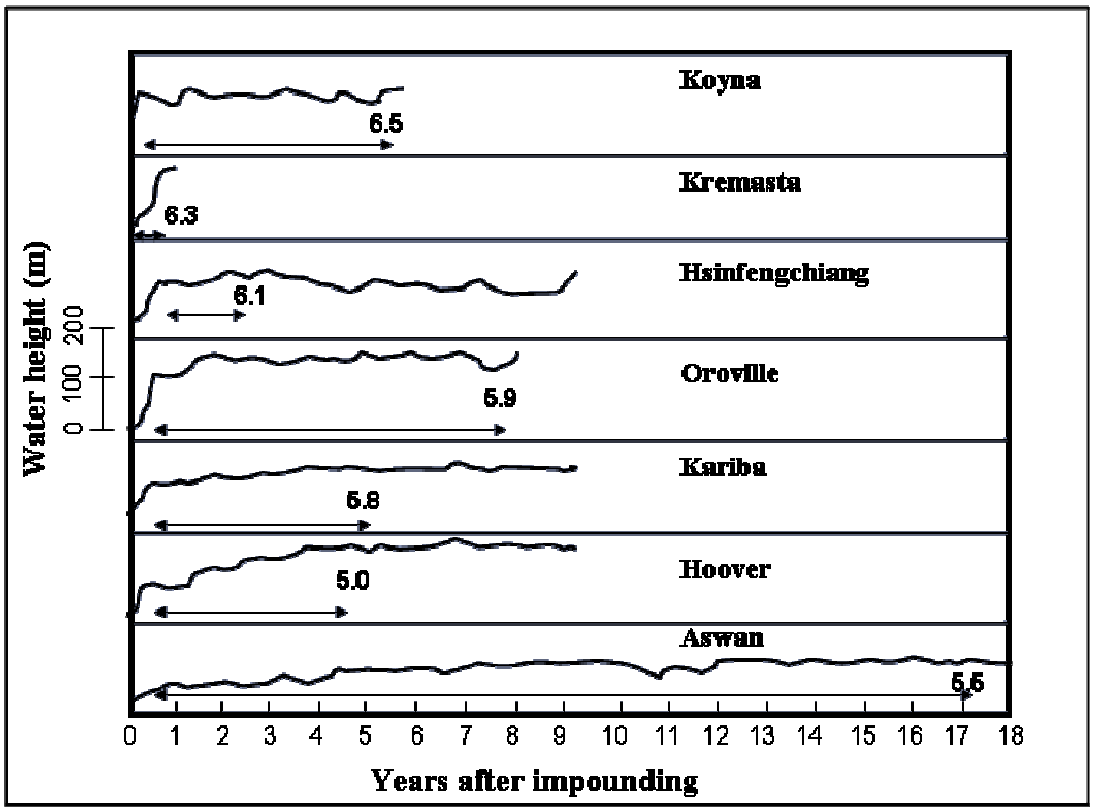

Figure 4.9: Reservoir filling curves, time interval and the magnitude of largest RIS event for seven cases of RIS (modified after Knoll 1992).

A total number of 64 reservoirs (Table 4.2) which have evidenced RIS level II have shown mild to moderate induced seismicity ranging M = 3.1 – 5.9 over a number of years. From the 64 reservoirs, 12 reservoirs, such as Akosombo, Ghana; Aswan, Egypt; Benmore, New Zealand; Coyote Valley, USA; Porto Colombia, Brazil; Varragama, Australia and Volta Grande, Brazil, have displayed seismic events with magnitude of greater than 5.0 (Table 4.1), whereas only 35 reservoirs exhibited microseismicity in the RIS level III ($M \leq 3.0$) apparently due to insufficient detection capability for microseismic activity at distant dam sites (Knoll 1992) that have not been specifically instrumented.

Thus, most of the reservoirs in the data base have shown earthquakes in the magnitude 3.0 to 5.0 though it is obvious that this is a truncated distribution at the lower RIS levels (Figure 4.10). By considering all factors, the maximum height of the reservoir water

column has the principal influence on the occurrence of RIS. An analysis showed by Coates in 1981 (reported in Knoll 1992) that only 0.63% of the world's largest 11,000 dams that are higher than 10 meters have displayed seismicity. However, 10% of the reservoirs more than 90 meters deep have displayed RIS, and 21% of the reservoirs more than 140 meters deep have triggered significant earthquakes (Knoll 1992).

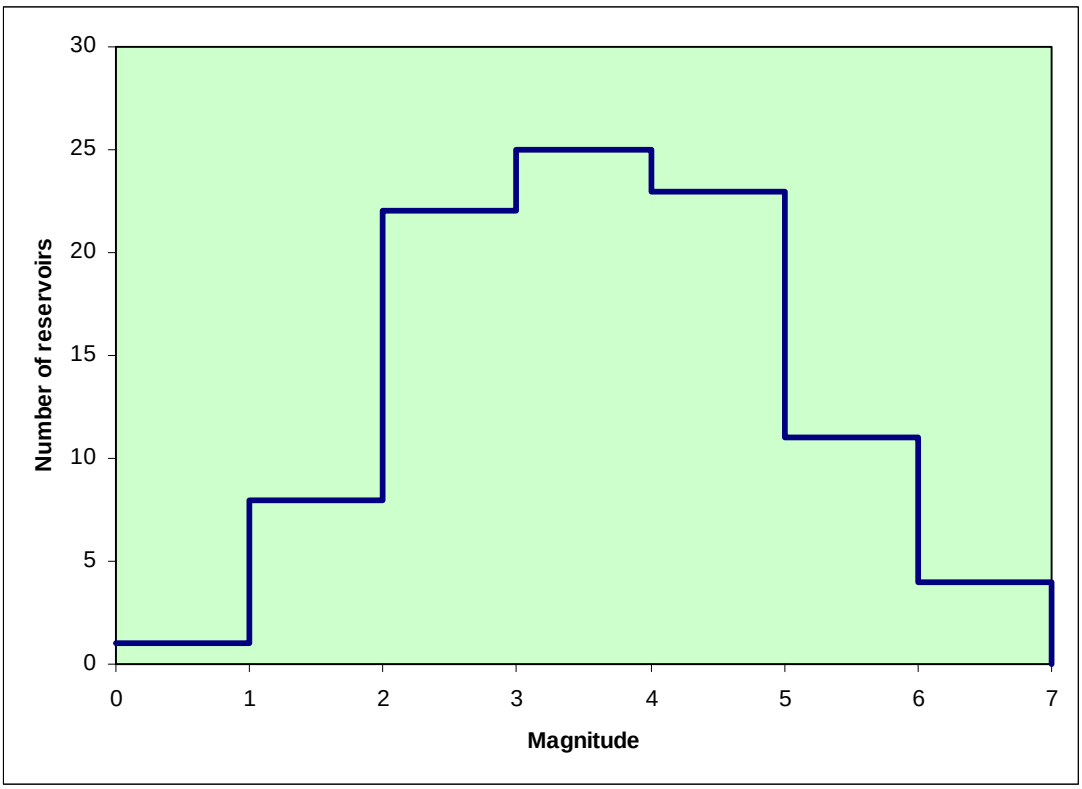

Figure 4.10: Frequency-magnitude distributions of RIS cases (Tables 4.1 & 4.2)

4.7.1 Koyna Reservoir, India

Koyna dam and Koyna reservoir are situated on the western side of India. Koyna reservoir is about 200 kilometers south of Bombay (Mumbai), in the state of Maharashtra as shown in Figure 4.11 (Agrawal et al. 2004). The area was previously understood to be generally aseismic (no detected seismic activity), similar to other regions of the peninsular shield of India (Figure 4.11). Satellite imagery (Figure 4.12) exposes the presence of major lineaments which are trending NW – SE and NE – SW on the plateau. Field observations have confirmed that the lineaments correspond to either shear/fracture

zones or major stress-field induced joint systems. Three major lineaments cross just south of the Koyna dam (Knoll 1992).

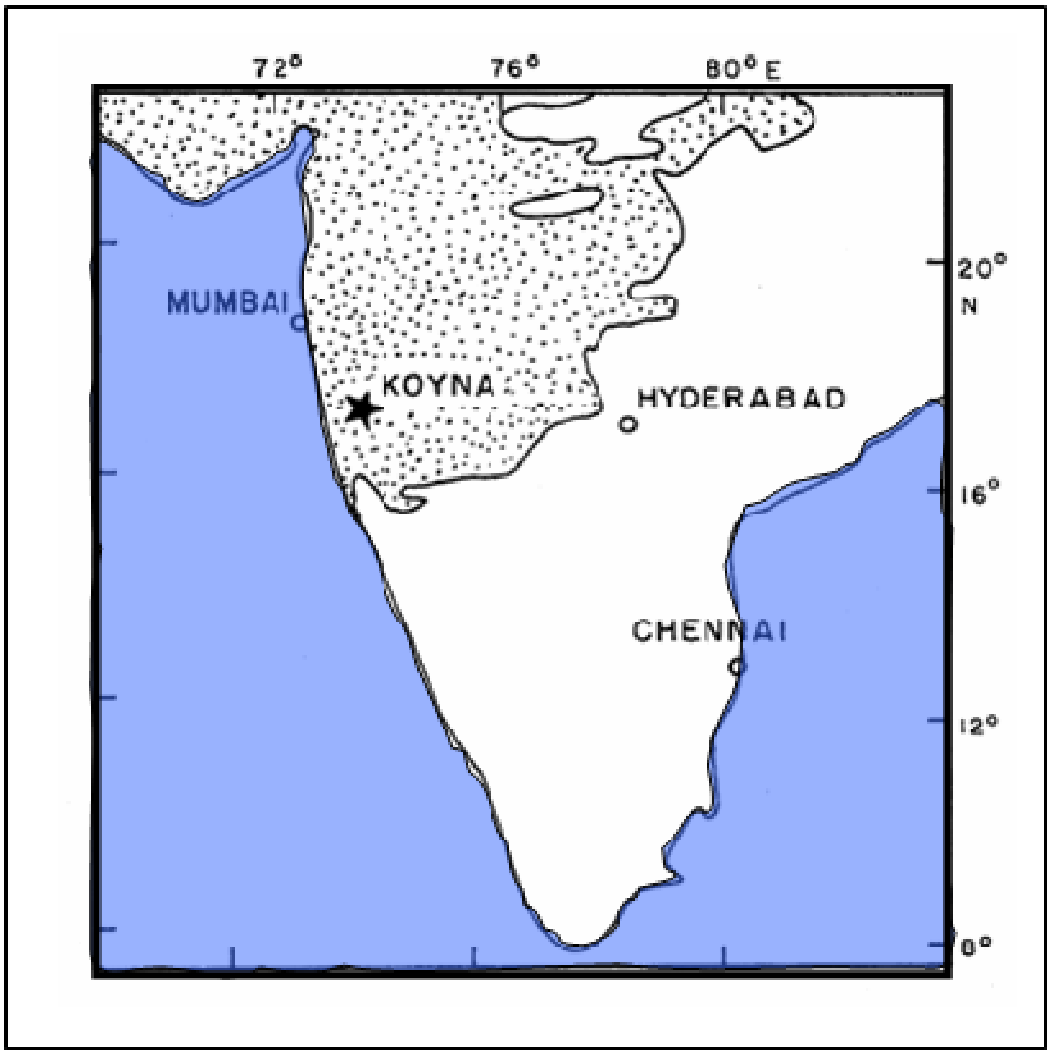

Figure 4.11: Location map of the Koyna region (modified after Agrawal et al. 2004).

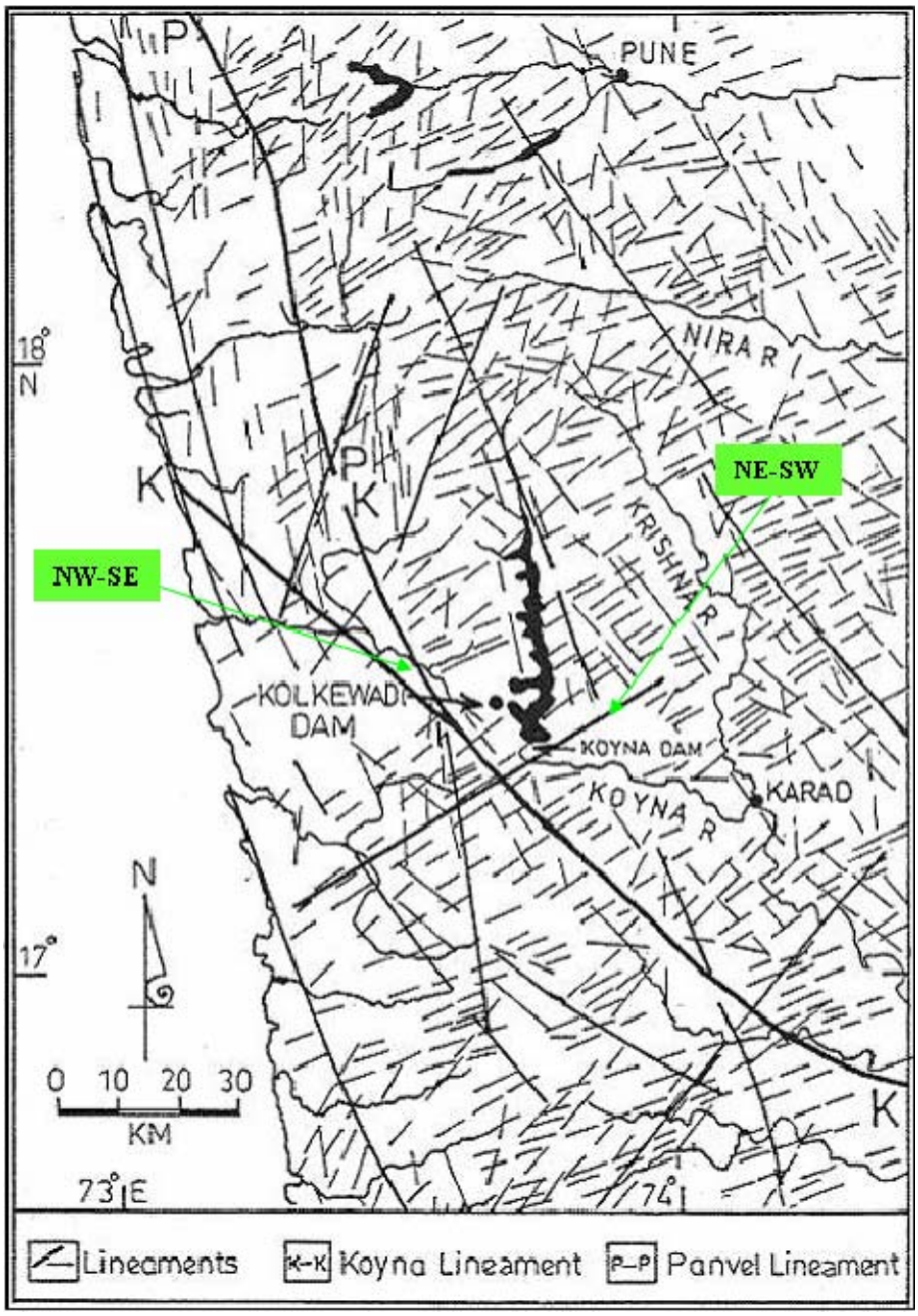

Figure 4.12: Lineament map of the Koyna area, India (modified after Knoll 1992).

Following its initial filling in 1962, the reservoir area started to display very mild induced seismicity accompanied by loud sounds. Five significant earthquakes (M = 4.0 to 5.6) took place in the reservoir region on September 13, 1967 and soon after, on December 10, 1967, a disastrous earthquake with magnitude of 6.5, as shown in Figure 4.13, was

triggered near the dam, causing extensive major and several minor cracks, mostly horizontal (Bradshaw et al. 1997).

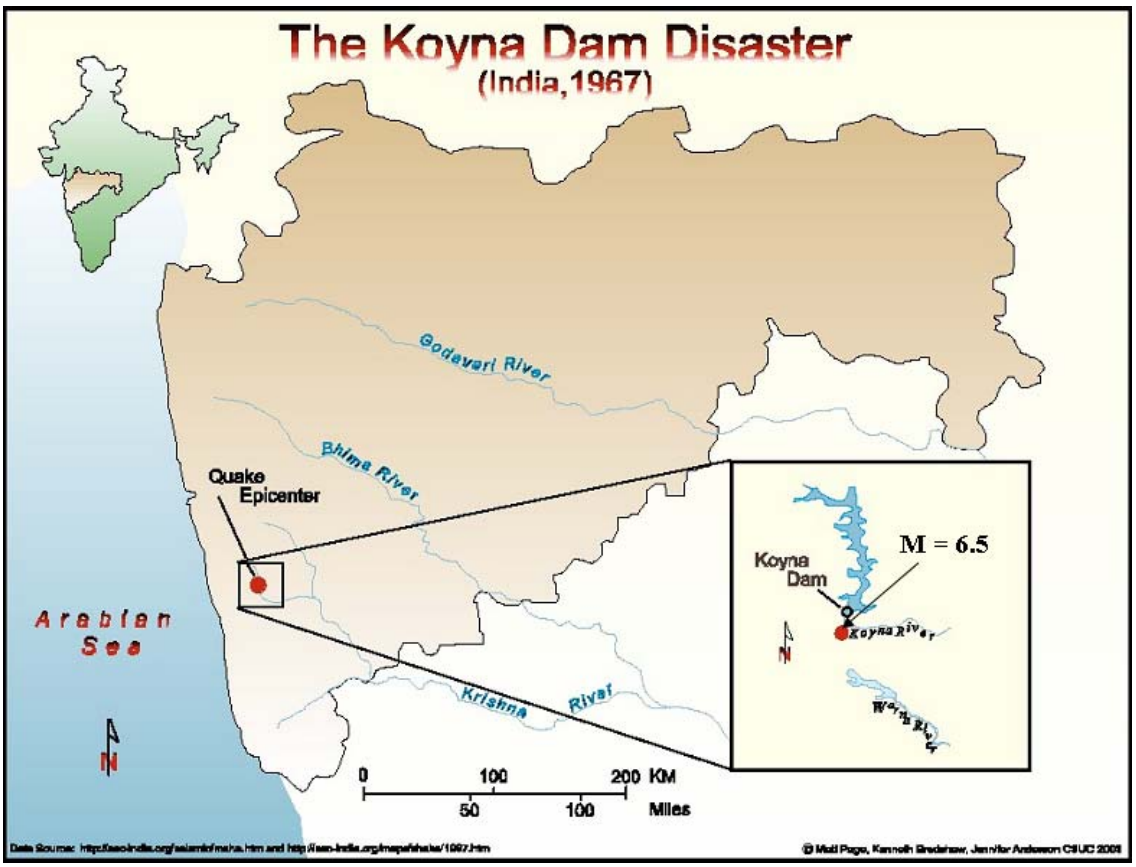

Figure 4.13: Shows the location of the disastrous M = 6.5 earthquake epicenter on December 10, 1967 (modified from Bradshaw et al. 1997).

The table below describes the significant induced seismicity events in the Koyna dam area.

Table 4.3: Seismic events in the Koyna Reservoir, Maharashtra, India (modified after Agrawal, 2004, Bradshaw et al. 997, Knoll 1992)

Date	**Events**
1962	Construction is completed, water impoundment is started.
September 13, 1967	Five significant earthquake observed in the Koyna reservoir.
November 4, 1967	An earthquake with magnitude of 3.2 triggered Maharastra state in Koyna dam area.
December 1, 1967	Magnitude 3.0 earthquake occurred in Koyna reservoir.
December 10, 1967	Magnitude 3.8 earthquake occurred in Koyna reservoir
December 10, 1967 (22:51 UTC)	At 04:21 am local time December 11, 1967, a large earthquake with magnitude of 6.5 occurred in Koyna Nagar near the site of the Koyna dam.
December 11, 1967	Rescue teams are sent off to Koyna Nagar, Army personnel began evacuating residents
December 12, 1967	Newspaper around the world published the first stories of the earthquake. 200 people are confirmed dead.
December 14, (15:06 UTC)	Magnitude 4.1 earthquake aftershocks triggered in the Koyna reservoir area.
December 15, 1967	Numerous aftershocks persisted to shake the Koyna reservoir area.
September 17, 1973	Earthquake with magnitude of 5.2 triggered.
November 14, 1984	Earthquake with magnitude of 5.0 triggered.

In the nearby township of Koyna Nagar, there was entire devastation of single-story masonry buildings, and two hundred people reported dead. Earthquakes with magnitude of 5.2 and 5.0 have been triggered respectively on September 17, 1973 and November 14, 1984. Altogether, about 40 earthquakes with magnitude of 4.0 and above have been observed since the beginning of water impoundment (1962). The induced seismicity in the Koyna reservoir has persisted for about three decades (Agrawal et al. 2004).

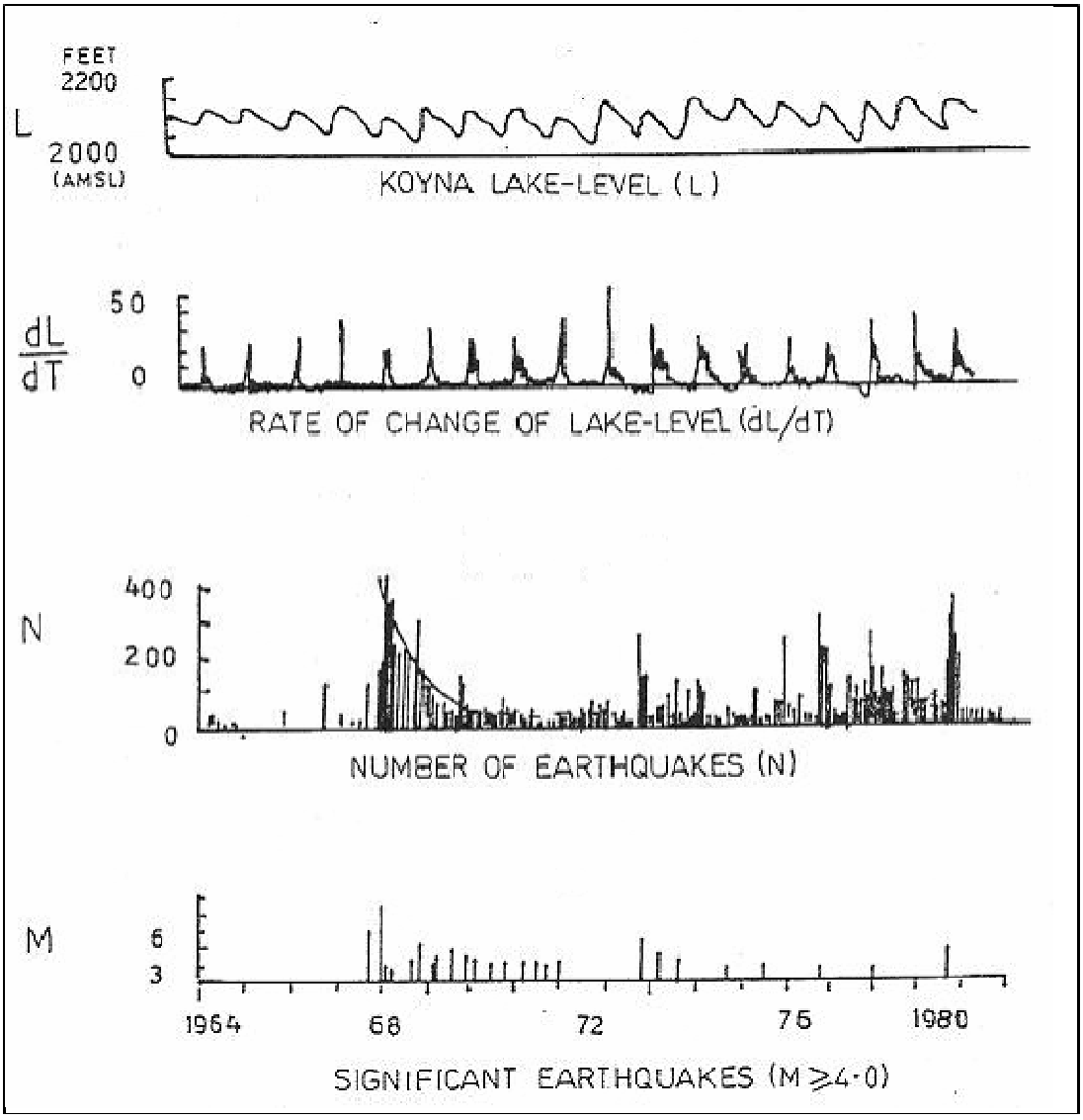

Figure 4.14: Lake level (L), rate of change lake level (dL/dT), and seismicity at the Koyna reservoir (modified after Knoll 1992).

Figure 4.14 exhibits the fluctuation of seismic activity along with the water level over a period of about two decades, as well as the water level rate change, and significant earthquakes with magnitude greater than 4.0. Correspondingly, Figures 4.15a, 4.15b, 4.16a, and 4.16b exhibit the epicentral and focal distributions of seismic activity in the Koyna-Kolkewadi region for the periods 1967 – 73 and 1974 – 81 respectively (Knoll 1992).

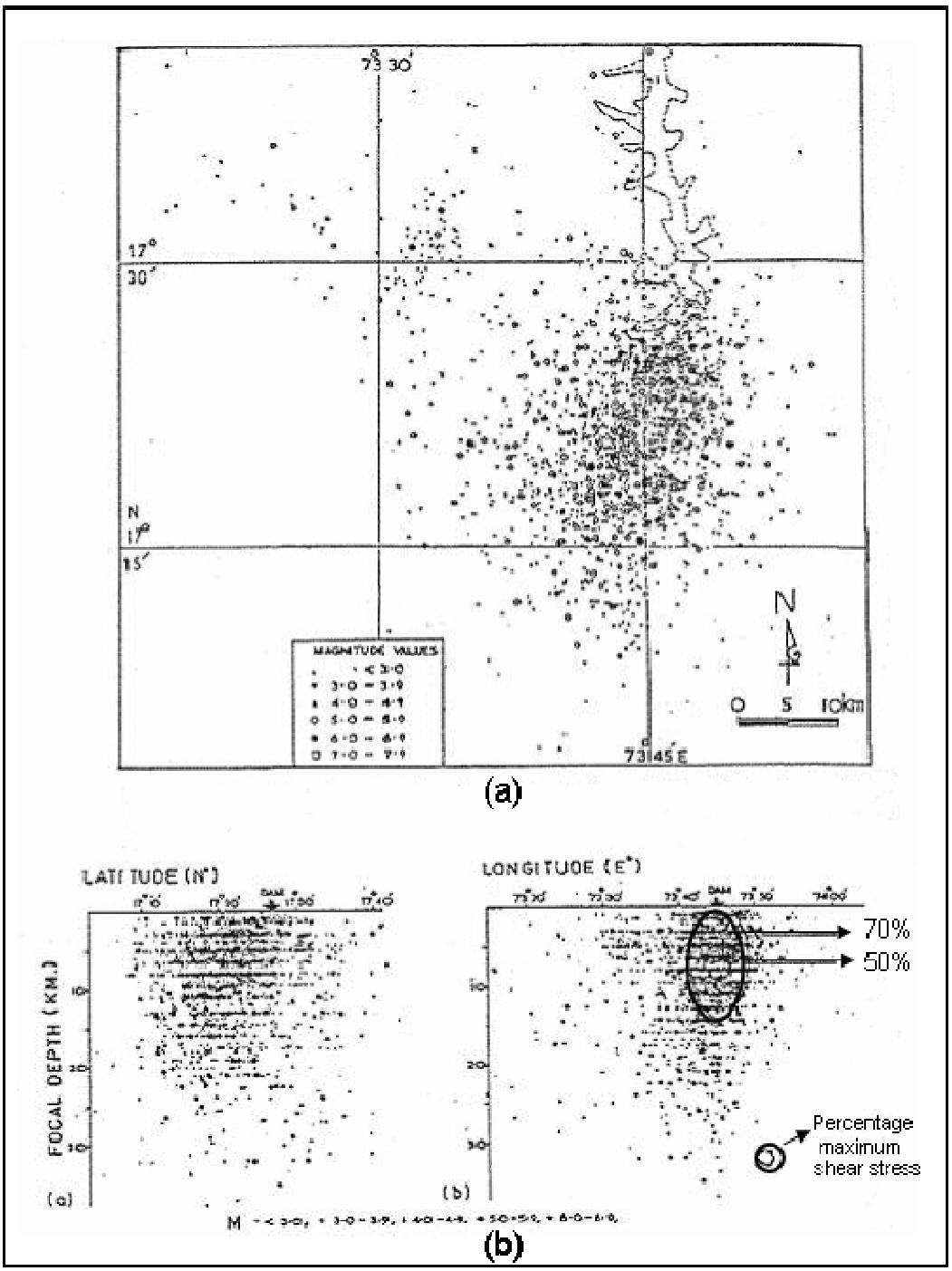

Figure 4.15: Distribution of earthquakes foci in the Koyna-Kolkewadi area from 1967 to 1973 (modified after Knoll 1992).

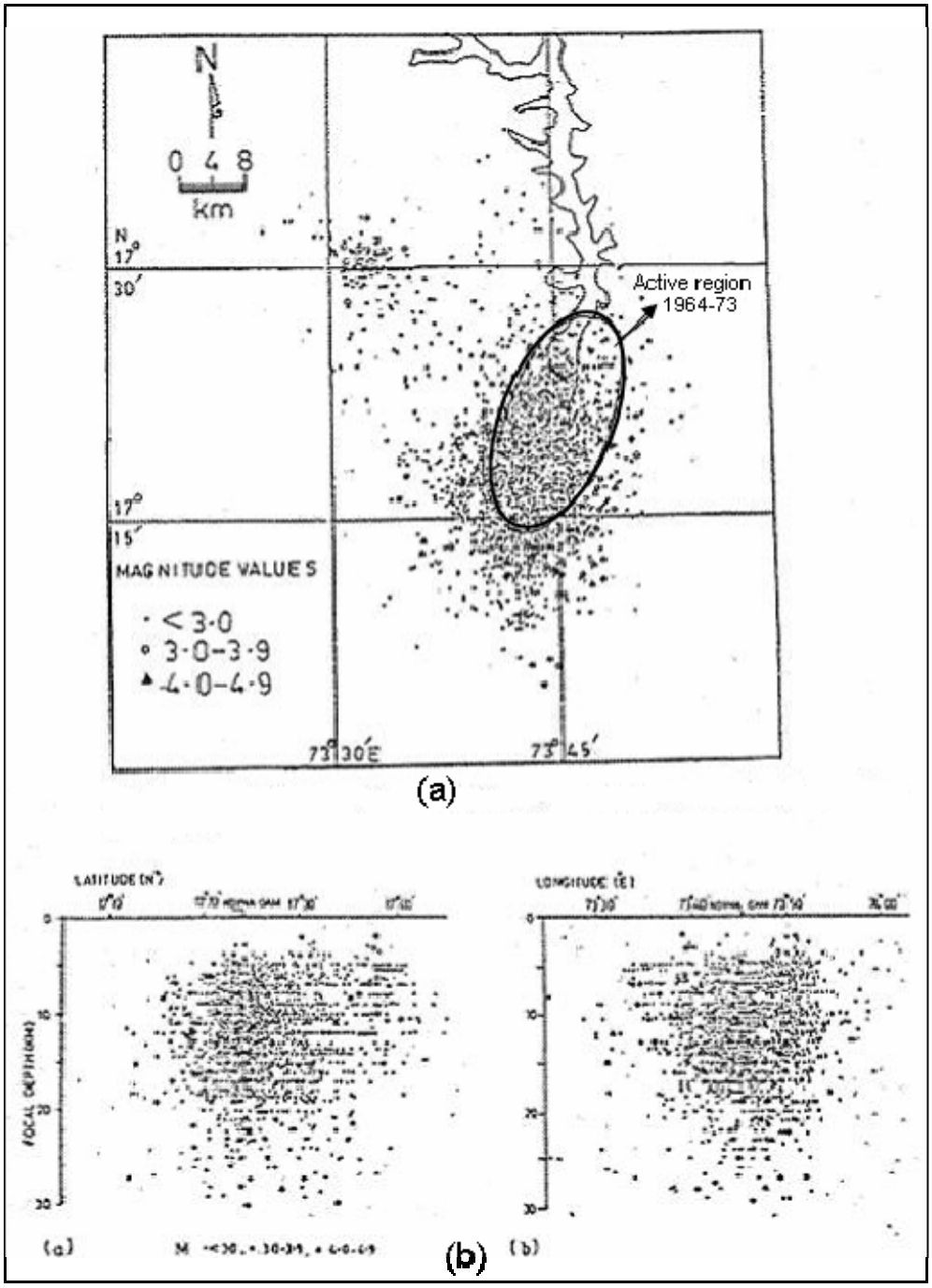

Figure 4.16: Distribution of earthquakes foci in the Koyna-Kolkewadi area from 1974 to 1981 (modified after Knoll 1992).

The great number of triggered earthquakes provided a unique opportunity to precisely estimate *b* value. This is the slope of the frequency magnitude relation, which has been used in many studies in various aspects of seismicity, expressed as the Gutenberg-Richter

equation, log N = a - b M (Knoll 1992). Though the Koyna reservoir is located in a broad aseismic shield region, the post-impoundment period displayed protracted seismicity retained over two and a half decades with infrequent higher magnitude seismic events in 1967, 1973, and 1980. These were preceded by low *b* values, as shown in Figure 4.17 and "…high lake level (L), a higher rate of change of the lake level (dL/dT) (Figure 4.15) and large ground tilt…" (Knoll 1992). Evidently, there is a substantial time lag between the high lake level (L) and the rate of change of the lake level (dL/dT) and the resulting seismic activities (Knoll 1992).

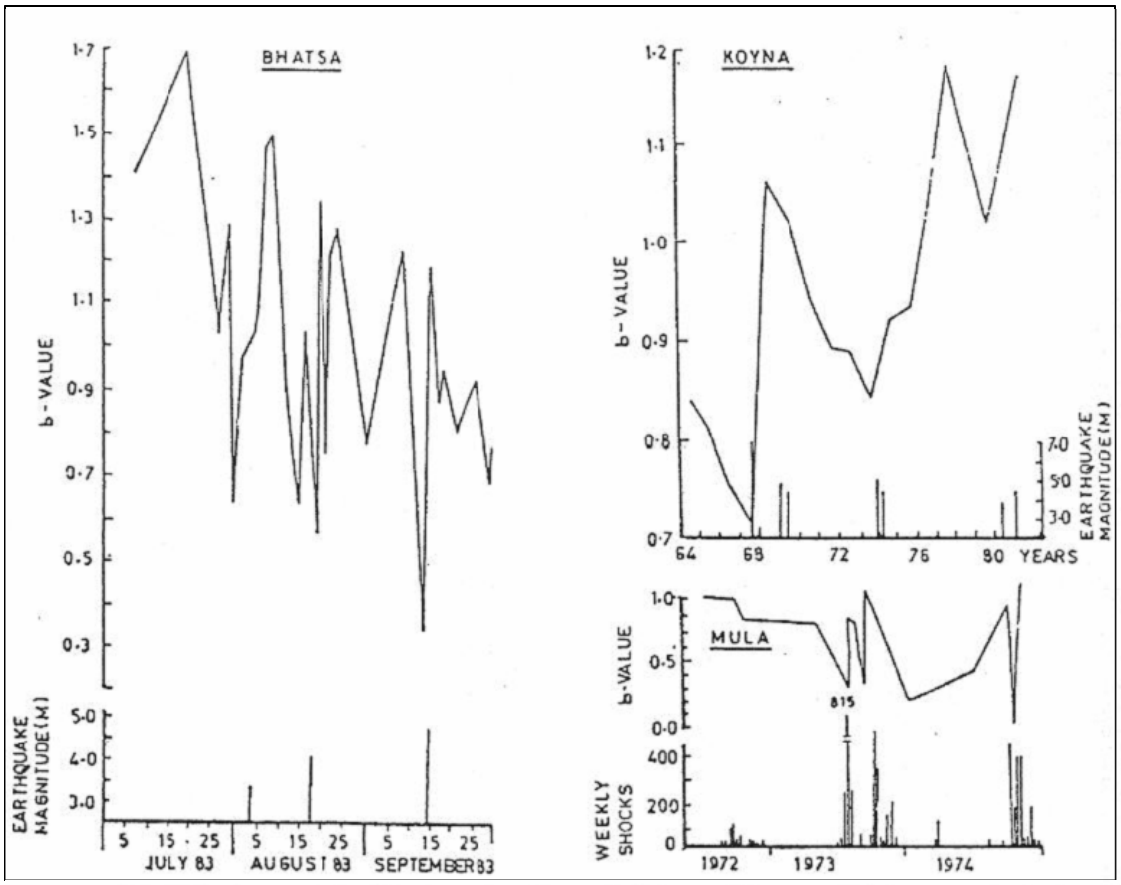

Figure 4.17: *b*-values and significant earthquakes at the Koyna, Bhatsa, and Mula dams, India (modified after Knoll 1992).

4.7.2 Bhatsa Reservoir, India

The Bhatsa reservoir is located in the Deccan Volcanic Province of western India. The dam is about 90 kilometers north-east of Bombay (Mumbai) and about 200 kilometers north of Koyna dam (Rastogi et al. 1986). An isoseismal contour map of the Bhatsa-Khardi area is shown in Figure 4.18 with the lines representing either basic dykes or fracture zones. The Bhatsa dam (number 6 on the figure) is located within a NW – SE direction, 4 km wide strip showing a high density of lineaments, mostly oriented in the same direction (Knoll 1992).

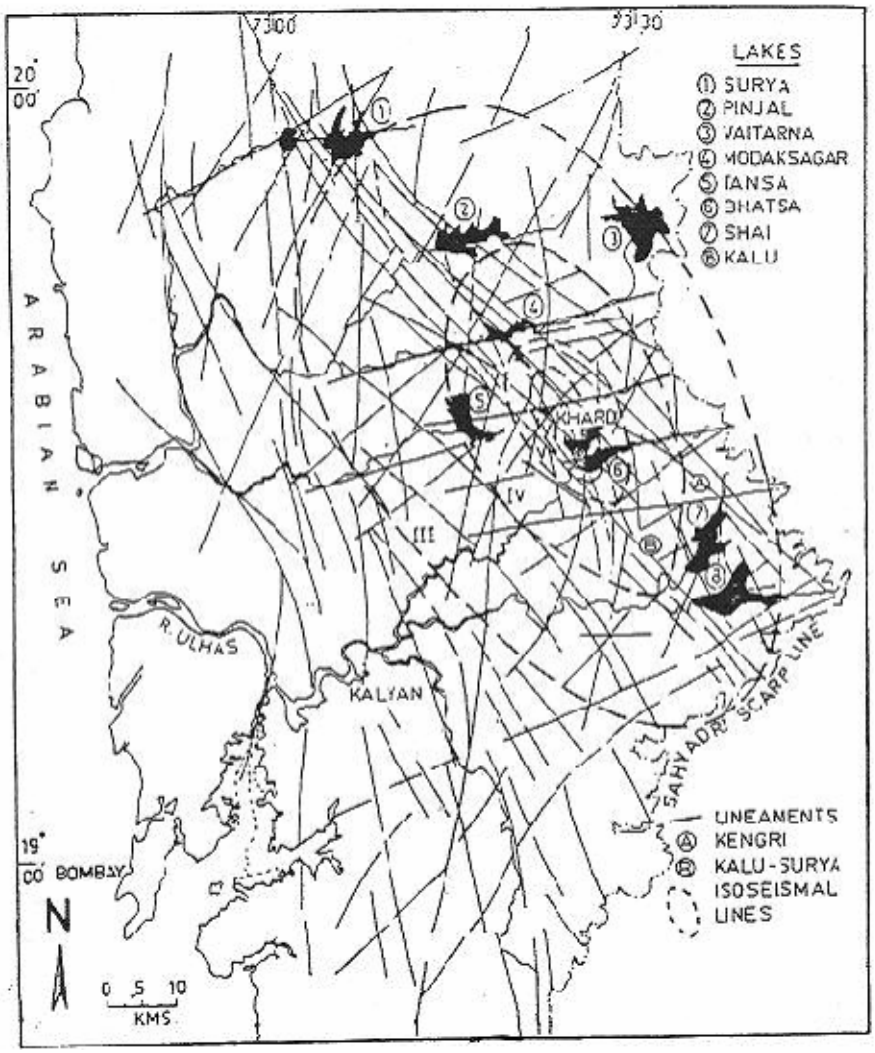

Figure 4.18: A map of the Khardi-Bhatsa region showing isoseismal contours (lines of equal earthquake intensity), India (from Knoll 1992).

The first experience of seismicity around the Bhatsa reservoir area was observed in early 1983 though the impoundment of water behind the dam began in June 1977. In June 1983, the water level was recorded about 92.5 meters above mean sea level[1] and after one month, the water level increased to over 110 meters. An earthquake with magnitude 4.0 triggered on August 17, 1983 and another stronger earthquake with magnitude 4.8 occurred on September 15, 1983. Both earthquakes epicenters are found at Khardi, about 7 km northwest of the dam. There is a significant correlation between the lake level (L), the rate of change of lake level (dL/dT) and resulting seismicity, but with a certain time delay, as shown in Figure 4.19 (Knoll 1992). Seismicity dropped very rapidly after the strongest event (M = 4) in September 1983.

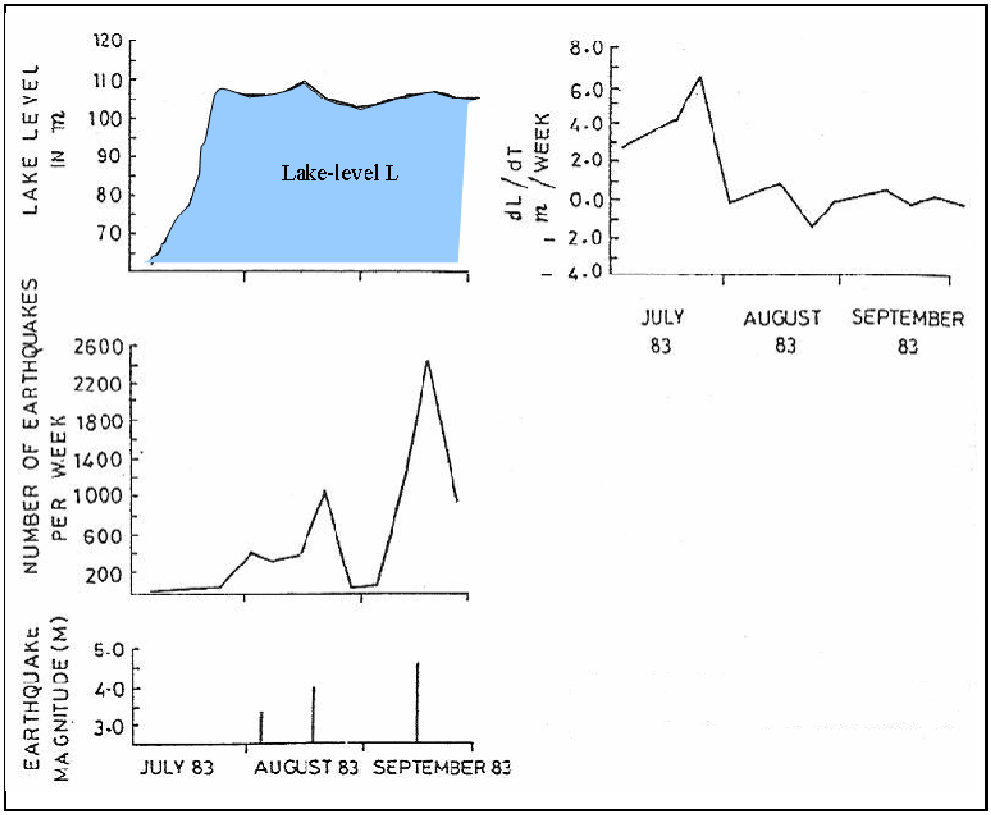

Figure 4.19: Lake level, rate of change of lake level, and seismicity at the Bhatsa reservoir (modified after Knoll 1992).

[1] The article uses mean sea level, but it likely is meant to be above reservoir base level.

4.7.3 Mula Reservoir, India

The Mula reservoir is located in the west central part of the Deccan Volcanic province. Dykes, fractures and ancient basaltic lava flows were recorded in the area of Mula dam. A very low level sesimicity (M < 2.0) was reported after impoundment of the Mula reservoir, in contrast to other case histories of RIS in this area (see Figure 4.20). The RIS activity demonstrated an evident relationship between the lake level (L), rate of change of the lake level (dL/dT) and resulting seismicity during the period 1972 to 1974, as shown in Figure 4.20 (Knoll 1992).

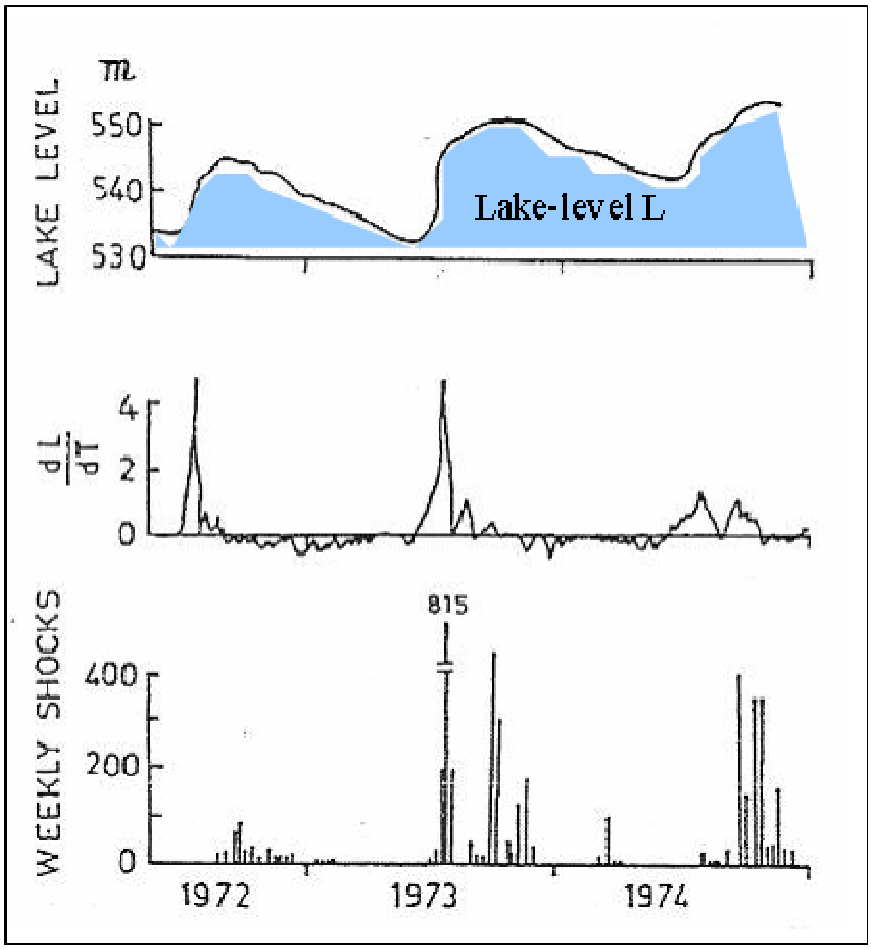

Figure 4.20: Lake level, rate of change of lake level, and seismicity at the Mula reservoir (modified after Knoll 1992).

A large number of microearthquakes were recorded in the vicinity of all the reservoirs (Koyna, Mula, and Bhatsa), and the b value is shown in Figure 4.17. In all cases, low *b* values seem to precede significant seismic events, and thus changes in *b* values seem to act as precursory signals, and it has been suggested that this could be utilized as an effective sign for the prediction of imminent strong reservoir-induced seismicity.

A number of water reservoirs located in different provinces of India have been impounded during the last forty years or so (Figure 4.21), but only 14 reservoirs have been reported with induced seismicity activity, ranging from strong (M = 7.0) to low (M < 2.0). It is, however, quite possible that some of the reservoirs may have triggered low level seismicity (M < 2) that was not detected due to lack of instrumentation in the surrounding area (Knoll 1992).

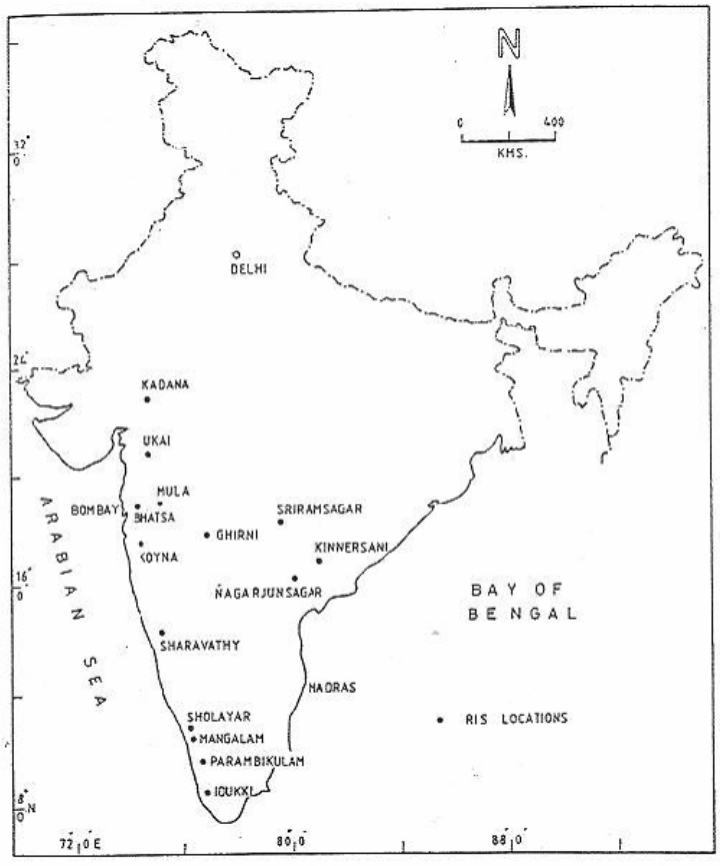

Figure 4.21: Geographical locations of reservoirs showing induced seismicity in India (from Knoll 1992).

4.7.4 Hsinfengchiang Reservoir, China

The Hsinfengchiang (Xinfengjiang) reservoir like the Koyna reservoir is also a prominent case of strong RIS (maximum M = 6.1). It is situated 160 km northwest of Canton in the coastal area, which is considered to be an area of moderate to low seismicity. A number of NE – SW trending strike-slip faults is found in the area surrounding the reservoir, which was initially impounded in 1959. The first earthquake of magnitude 6.1 occurred on March 18, 1962 following a rapid increase of lake level, as shown in Figure 4.22 (Knoll 1992). There were many smaller earthquakes recorded in the reservoir area since the initial filling, with a total number of more than 80,000 during two decades of sustained seismicity following filling of the reservoir. During the main event (M = 6.1), the 80 m high concrete dam experienced damage; later, it was repaired to withstand stronger earthquakes.

RIS activities at Hsinfengchiang are similar to the Koyna reservoir, such as a long duration of induced seismicity over two decades, large earthquake with magnitude of 6.1, many triggered earthquakes ($M \geq 4.0$) being induced following a high rate of change of the water level, low to moderate previous seismic activities of the two sites, numerous microearthquake occurrence following water filling, most epicenters being situated at deeper reservoirs regions, and the great majority of the earthquake foci being within 10 km of surface (Knoll 1992).

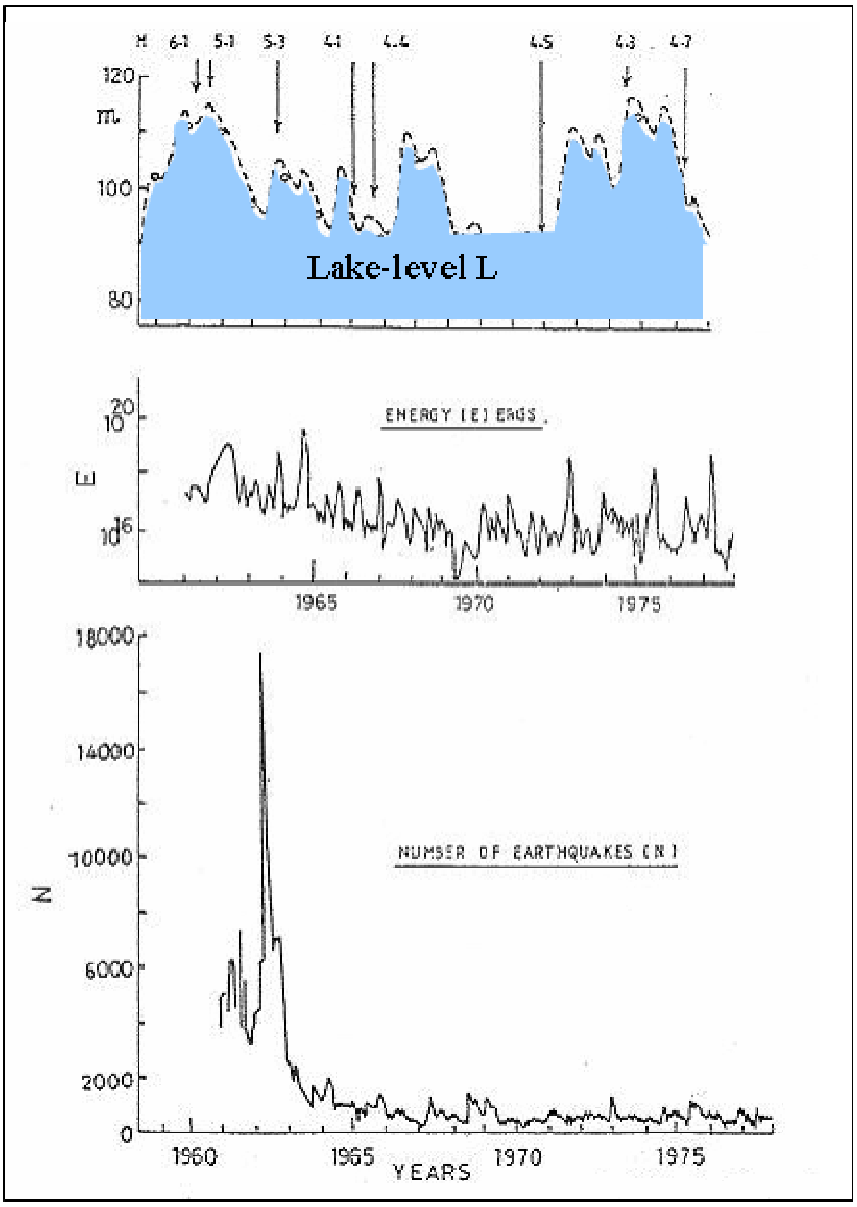

Figure 4.22: Lake level and seismicity at the Hsinfengchiang reservoir, China (modified after Knoll 1992).

4.7.5 Kariba Reservoir, Zambia-Zimbabwe border

The Kariba reservoir is crossed by numerous faults trending in a NE – SW direction. The maximum depth of the Kariba reservoir is 122 m. The area, on Precambrian rock, is not characteristically seismic, but there had been some low-magnitude seismicity epicenters in the reservoir area. The reservoir area started to experience regular earth tremors after

impoundment. The first strong earthquake with magnitude of 5.7 was triggered in 1962 and was followed by three stronger earthquakes M = 6.1, 5.6, and 5.8 in quick progression (Knoll 1992). Seismicity increased sharply in 1963, as shown in Figure 4.23, following the rapid rise of the water level up to 50 m, subsequently decreased gradually, indicating confirmation of triggering of seismicity by the water level fluctuations (Knoll 1992).

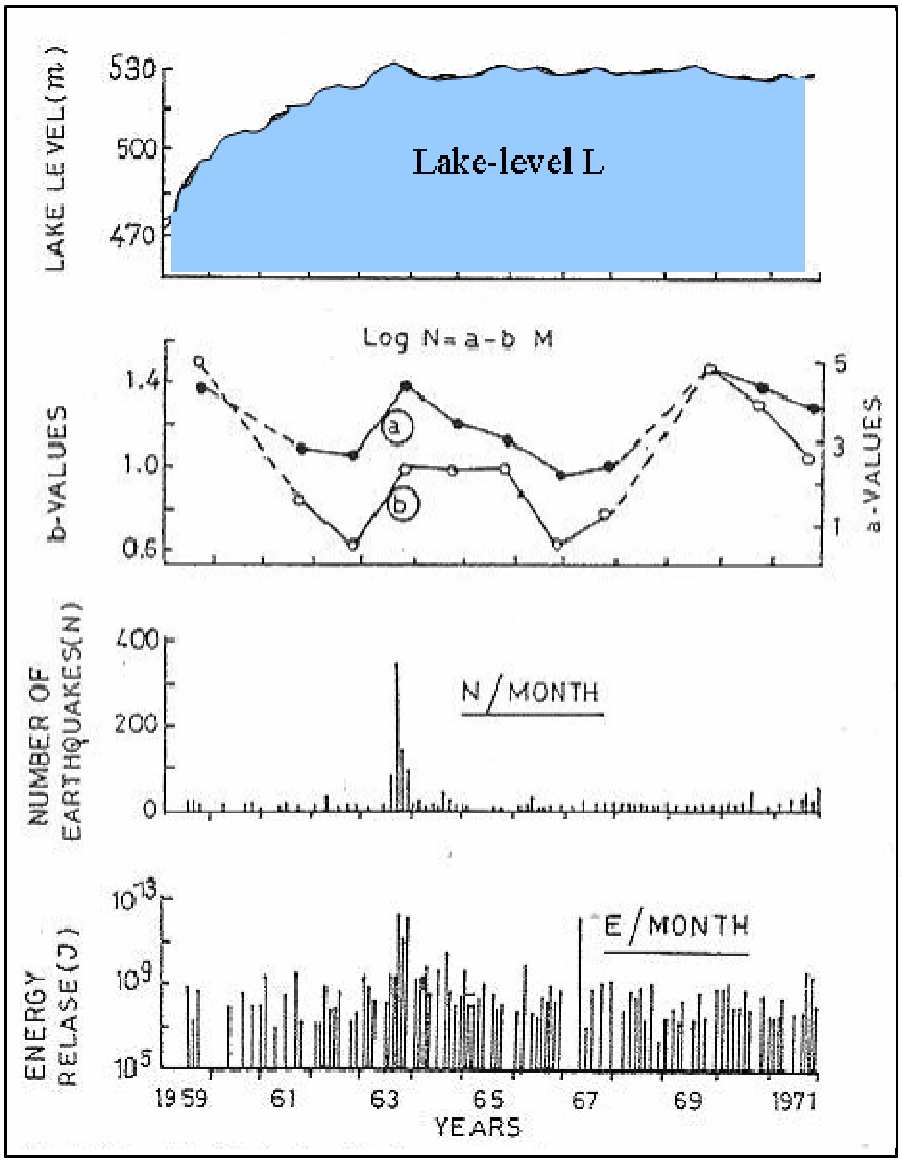

Figure 4.23: Lake level, *b*-values, and seismicity at the Kariba reservoir, Zambia-Zimbabwe border (modified after Knoll 1992).

A correlation between water level and seismicity at the Kariba reservoir is shown in Figure 4.24.

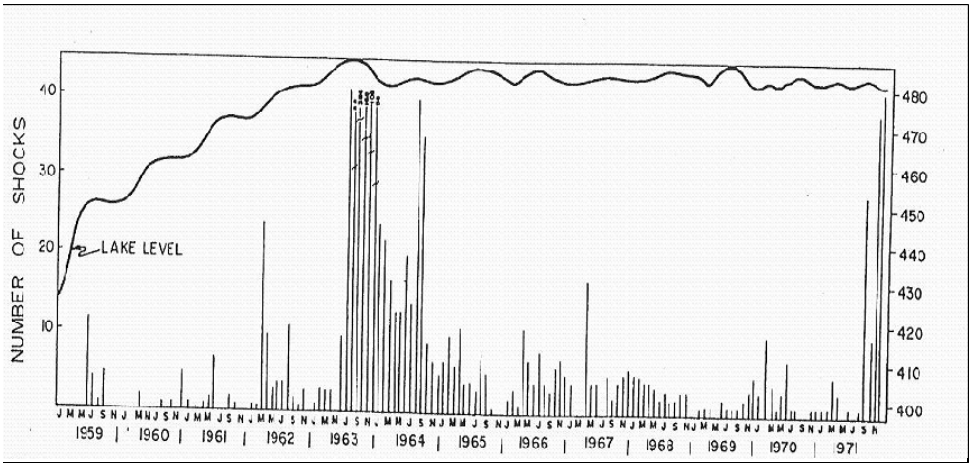

Figure 4.24: Monthly frequency of earthquake and lake level of Kariba reservoir, Zambia-Zimbabwe border (Knoll 1992).

4.7.6 Kremasta Reservoir, Greece

The height of Kremasta dam is 120 m. The Kremasta reservoir is situated on a major N – S trending fault zone within the Macdonian plate and is transversed by many strike-slip and reverse faults trending in N – S and NE – SW directions. The limestone base displaying wide karstification is covered by sandstone, mudstone, siltstone and local conglomerates (Knoll 1992).

Historically, earthquakes are known to have occurred in the area of the Kremasta reservoir but epicenters of past earthquakes were not situated within the reservoir area. The situation changed considerably following the impoundment; earthquake swarms were observed by the end of 1965, and 81 earthquakes of magnitudes of up to 5.0 were triggered during the period January 1 to February 4, 1966. An earthquake with a magnitude of 6.3 also occurred within the reservoir area during this time (Knoll 1992). Studies indicated a close relationship between water level and resulting seismicity as indicated above in Figure 4.9.

4.7.7 Discussion on RIS

The mechanisms by which seismicity is induced have been extensively studied by Talwani and Acree (1984 and 1985); Simpson et al. (1988); and Talwani (1997), amongst others. The most important features involve the disruption of stresses and pore pressures at depths affected by the weight of the water in the reservoir, and the diffusion of extra induced pore pressures to epicenter depths from the reservoir at the surface. Both theoretical and observational studies have indicated that the controlling issues in these processes are "…the pre-existing tectonic stresses and pore pressures, permeability of rock masses and fracture systems, the strength of fault systems, and the relative orientation between the tectonic stresses and potential fault systems" (Assumpção et al. 2002).

Because of the heterogeneous properties of the rocks underneath a reservoir (including factors such as fracture systems, porosity, lithology, permeability, as well as the local stress field) the triggered earthquake (seismicity) can demonstrate intricate temporal and spatial effects in response to the impoundment history. As an example, movement of activity from one region of the reservoir to another can also be experienced because of the complex subsurface, such as in the Acu reservoir, northeast Brazil (Assumpção et al. 2002).

Proposals to categorize the patterns of induced sesimicity into two main components have been described by Simpson et al. (1988) and Talwani (1995, 1997) (reported in Assumpção et al. 2002). The two classifications of Simpson 1988 are "rapid", when activity starts instantly following first impoundment or major variations in water level, and fades away after a few days, and "delayed", when the main sesimicity, including the largest event, occurs a number of years after filling after the water variation take place for a number of annual cycles. Talwani (1995, 1997) characterizes the two classifications as "initial", that is, related to initial filling or large water level changes, and "protracted" occurring only after the effect of the initial seismicity has lessened yet sustained for numerous years without substantial decrease in frequency and magnitude (the hypocenters can be underneath the reservoir or in the vicinity). Although some reservoirs

exhibit only a rapid (initial) response, many reservoirs show a mixed pattern (rapid and delayed), with a later period of activity following the rapid response (Assumpção et al. 2002).

Despite the development attained in explaining the mechanisms of RIS, it may be difficult to predict the incidence of induced seismicity of a future reservoir because of the practical complications in precise mapping in a large volume of rock below the reservoir, particularly with respect to key factors such as *in situ* stress distributions, permeability, and orientations and frequency of fracture systems. From a technical point of view, statistical studies of past cases can be useful for estimation of future reservoirs, but only in a general sense. In this regard, more complete collections of previous cases of RIS worldwide, together with their spatial/temporal pattern, should lead to better evaluation of future reservoirs (Assumpção et al. 2002).

4.8 Summary

The first example of RIS was observed at Lake Mead in the late 1930's. RIS is increased by two factors: the first part can be considered due to the poroelastic effect after impoundment of the reservoir and is known as initial seismicity; the second part can be considered due to pore pressure diffusion coupled with the elastic load and is known as protracted seismicity (Talwani 1997).

The study of rapid response cases showed a tendency for occurrences of small earthquake swarms at shallow depths in the immediate surrounding area or just below the reservoir. In delayed response cases, the larger earthquakes are triggered at greater depth and frequently at some distance (~ 10 km) from the deepest part of the reservoir (Knoll 1992).

Furthermore, RIS depends on the volumetric and depth capacity of the reservoir: the bigger the reservoir, the larger the events that have been observed. In addition, seismicity varies with tectonic activity, with the reservoir's surrounding area, with the lithology of the rocks, with initial stress distribution, with reservoir impoundment rate, and so on. In

general, RIS is a transitory phenomenon which will occur instantaneously after filling of the reservoir, and also after a delay of few years.

It appears that in many areas, the shallow crustal rocks are close to a state of shear slip that can be triggered by a change in pore pressure or total stress. “The energy released in a reservoir triggered earthquake is a normal tectonic strain energy that has been prematurely released because of the reservoir.” (Parry 1995).

Chapter – 5

Geyser Eruption and Remote Seismicity

5.1 Introduction

Geysers, also known as hot springs, are spectacular hydrothermal events, but are not common geologic features. A geyser is linked to a reservoir of hot water that intermittently and explosively ejects part or all of its contents. Activity in most geyser areas ranges over a wide spectrum such as energetically boiling pools, quiescent hot pools, dry steam jets, mud pots, and so on (Rinehart 1980).

Geysers are found only here and there in a few widely separated, highly localized regions. The most famous areas are in Yellowstone National Park in Wyoming, northwestern USA, Iceland, the North Island of New Zealand, Kamchatka Peninsula in northeastern USSR, and Japan. There are isolated geysers in Chile, Mexico, Africa, the Azores, Indonesia, and various Pacific volcanic islands, the People's Republic of China, the Basin and Range Province of western USA, and the Unmak Islands, Alaska. In principle, all geysers are found in volcanic regions that contain large quantities of rhyolite from which the geysers spout; only a few emerge from basalts and andesites (Rinehart 1980).

Microseismicity activity is associated with stress, pressure, and temperature changes in the geyser or the underlying geothermal reservoir. It has been assumed by various authors that conditions in geothermal reservoirs could be changed by arrival of large amplitude surface waves which perhaps altered the permeability by unblocking existing fractures, leading to pressure and stress changes. Thereby, increased activity should be observed in geysers or geothermal reservoirs after a large earthquake event. Because the microseismic activity level in and around a geyser is logically induced by movement of hydrothermal fluids and changes in pore pressure within the geothermal reservoir (Husen et al. 2004), microseismic activity above and around the geyser or the geothermal reservoir can be used during eruptions for monitoring the process, and perhaps linked to teleseismic activity.

It was at one time commonly believed that an earthquake at one location could not trigger earthquakes in distant areas, but after the Landers earthquake in California on June 28,

1992, this hypothesis was shattered. It was observed that the Landers earthquake triggered earthquake swarms more than 1280 km away in Yellowstone National Park (USA), as well as other jolts near Mammoth Lake, California and Yucca Mountain, Nevada. Moreover, in the Yellowstone National Park (USA) area, geyser activity and microearthquake swarms increased after the Denali fault earthquake (Alaska) of November 2, 2002. The Park is about 3100 km distance from the Denali fault epicenter. The Richter magnitudes of the Landers and the Denali fault earthquakes have been recorded as 7.4 and 7.9 respectively (Husen et al. 2004).

Whatever the mechanism, it appears that earthquakes can increase seismic activity at great distances, as shown in Yellowstone National Park after the Denali fault earthquake. To explain the changes in Yellowstone geyser activity that are clearly linked to teleseismic activity, it has been assumed that seismic waves from a large, distant earthquake must jostle the ground, thereby triggering small earthquakes (microseisms) by moving and altering the pressures in the hydrothermal fluids responsible for geysers and hot springs, thus changing the effective stresses (Husen et al. 2004).

5.2 Geyser Fundamentals

Geysers are unusual geological features, and there have been several studies of the conditions that must be present to activate geyser eruptions. It has been observed that at least three essential elements must be met, albeit many other factors are involved that affect the type and frequency of eruptions. The three essential fundamentals needed for a geyser eruption are water supply, heat source, and a reservoir with an associated plumbing system (Rinehart, 1980).

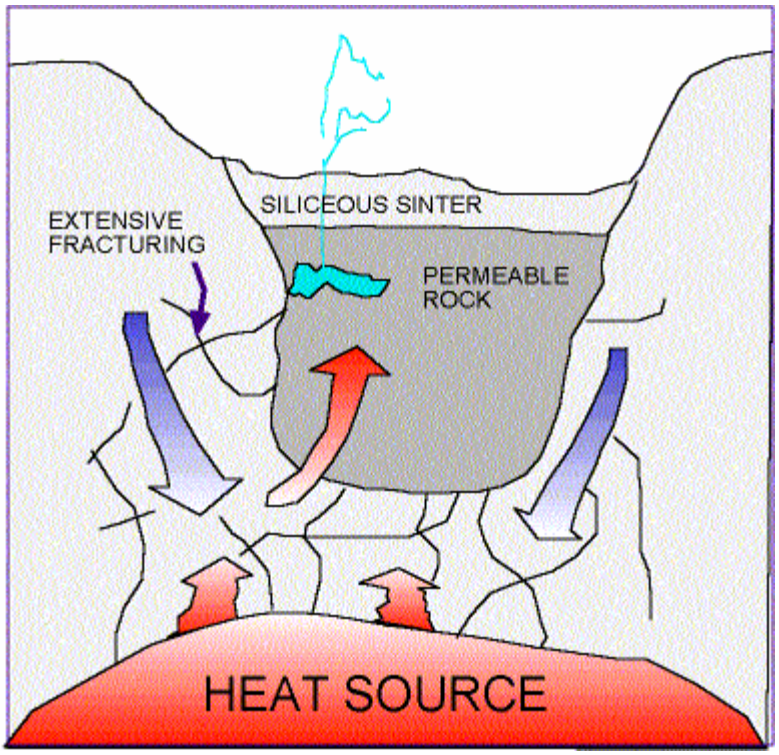

Figure 5.1: Cross-section of typical geyser (after Streepey 1996).

5.2.1 Water Supply

Meteoric water is present in a geyser system. Usually, geyser fields are found near or on the banks of rivers, which thus must play an important role in the geyser's water source. Moreover, a significant contribution is generated by rainfall and circulating groundwater in geysers. Study of the iridium content of water in geysers indicates that groundwater expelled from a geyser can be on the order of 500 years old (Rinehart 1980). This is related to the time that it takes for groundwater in the region where the processes are originating to circulate to the depth of the hot rock (heat source), become heated, and move back up to lower pressures at shallow levels (Streepey 1996) from where the boiling eruption can take place.

5.2.2 Heat Source

Interaction between hot and cool fluids plays a significant role for eruption of water or gas from geysers. The mechanism that is required for continued geyser activity is a

constant and steady supply of heat. It is well documented that every geyser field in the world has been found in the vicinity of volcanic activity and shallow-lying heat sources (Streepey 1996). It is observed that geyser fields are most frequently found near lithospheric plate boundaries, which are typically characterized by active volcanism. Other geyser fields far from plate boundaries are hypothesised to be located above or near hot spots or plumes, such as in Yellowstone National Park. The majority of all geysers are observed to lie within and above large bodies of rhyolite, while a lesser number of fields are coupled with other volcanic rocks such as basalt or andesite (Rinehart 1980).

5.2.3 Reservoirs and Associated Plumbing Systems

The reservoir and plumbing system is the third essential component of geyser systems, although for every geyser, the plumbing system is to be considered extremely complex and geometrically unique. Commonly, six classifications of reservoir have been postulated for most geyser actions (Rinehart 1980). These are shown in Figure 5.2.

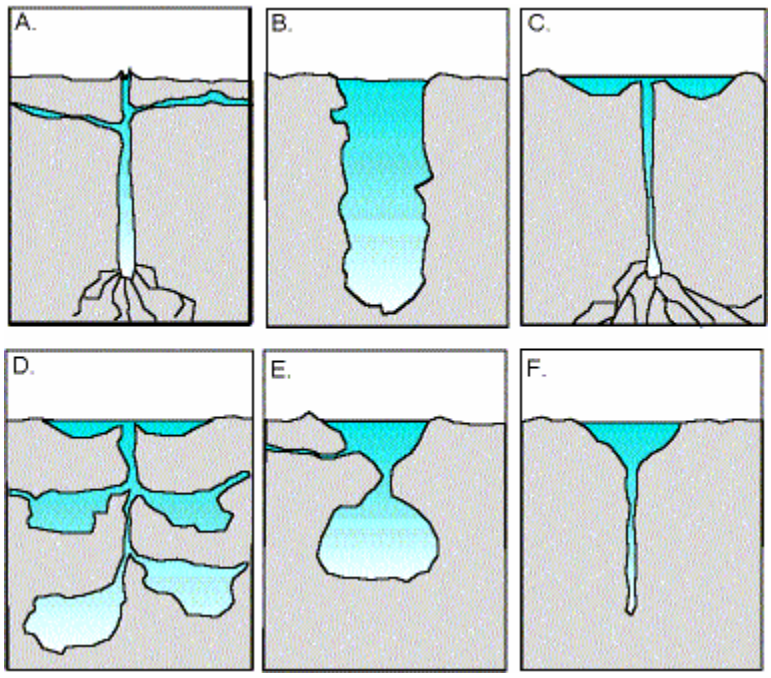

Figure 5.2: The six types of reservoir systems (after Streepey 1996).

5.2.3.1 Type A

The plumbing systems of Type A have usually fairly regular eruption intervals. Such geysers normally have a single standpipe which is connected to an underground reservoir with a raised cone of deposited minerals at the surface. The eruptions of such geysers are typically of considerable height, such as the Old Faithful geyser in Yellowstone National Park (Rinehart 1980). In 1992, a probe carrying temperature and pressure sensors and a video camera was introduced into the standpipe of Old Faithful, and a fairly large cavern filled with vigorously boiling water was found at a depth of 45 feet (14 m) (Bryan 1995).

5.2.3.2 Type B

The eruption of such geysers is quite violent but the time span is short. An example of a geyser that is considered to have this type of plumbing system is Round Geyser in Yellowstone National Park. The eruptions of the Round Geyser occur on the order of every 8 hours, and the eruption height is measured to be about 25 meters (Streepey 1996).

5.2.3.3 Type C

Some geysers, such as Strokkur in Yellowstone National Park, do not build cones but their standpipes have slightly raised rims around the openings and are in pools of water as in Type C of figure 2 (Rinehart 1980). Strokkur's tube is 13.5 m deep and funnel-shaped, 8.3 m in diameter at the top and only 26 cm in diameter 8.3 m down. "This makes their behaviour somewhat different from a purely columnar geyser such as Old Faithful and purely fountain geysers such as the Grand or Great Fountain in Yellowstone" (Streepey 1996).

5.2.3.4 Types D, E, and F

Reservoir systems such as three depicted in the Types D, E, and F of Figure 5.2, are characteristic of fountain geysers such as Grand and Great Fountain, Narcissus Geyser in Yellowstone, and the Great Geysir of Iceland. Geysers that erupt in a series of explosions with intermediate quiet periods are associated with Type D plumbing (Rinehart 1980).

This mechanism is because of a complex set of interconnected reservoirs, which empty in rows as shown in Figure 2. Other configurations for fountain or pool geysers are in Types E and F. The plumbing system for both Types E and F gives rise to long and fairly regular eruptions, but mostly not violent ones (Streepey 1996).

If the three necessary elements are not present in the correct configuration, geysers will not develop, but there could still be a high level of geothermal activity in the area, with hot water circulating up from depths and generating hot springs or ponds, but without exhibiting violent periodic eruptive activity.

5.3 Mechanism of Eruption

Generally, two types of eruptions occur in geyser systems, the first type of geyser erupts from fountain or pool geyser systems and the second type from columnar geyser systems. It is always observed that the reservoir of the geyser is filled slowly with water influx after the reservoir has been depleted by an eruption.

5.3.1 Pool or Fountain Geyser

Pool or fountain geysers are not violent in eruption. It is generally considered that most geyser systems have two separate water sources. One source brings in large amounts of shallow, cool water, and the other source is boiling water from depth, which is smaller in quantity. The water will mix in the reservoir in such a way that the hot, less dense water is moving upward and the cooler dense water is moving downward. The process continues until the reservoir fills and the temperature increases within the reservoir. When water is heated enough that a blob of hot water is moving upward sufficiently rapidly without cooling, it can retain enough energy to turn into steam as it reaches the surface where the pressure is low. This conversion of water to steam leads to an eruption which expels enough water so that the pressure on the hot water in the reservoir is suddenly reduced, allowing part of the water in the reservoir to turn into steam and trigger another eruption. Thus, a series of moderate eruptions is experienced as the pressure is reduced in stages to an equilibrium state (Streepey 1996).

5.3.2 Columnar Geyser

Columnar geysers have a slightly different behaviour than the pool geysers and their eruptions are more aggressive. The hot water in a columnar geyser system is flowing from depth into the geysers' plumbing system and mixes with the cooler water, much in same way as in a pool geyser. When the temperature is high enough for the depth, some of the water is turned into steam bubbles, which begin to rise and are caught in the geyser's plumbing system. The pressure builds up until it lifts water up and out of the channels so the steam bubble can escape. By this process, the boiling temperature of the remaining hot water is lowered by dropping the pressure in the reservoir. This water, which was already boiling before, now boils more vigorously, and forms yet more steam bubbles which occupy a larger volume. The steam expands rapidly and causes the reservoir to empty suddenly, continuing until the reservoir runs out of boiling water or the reservoir temperature is reduced from its boiling point by the influx of cool water from above or laterally (Streepey 1996). Then, after the vigorous eruption is finished, the reservoir begins to refill with a mixture of hot and cold water.

5.4 Behavioural Changes in Geysers

Behavioural variations may occur due to earth tides and earthquakes in geysers. In detailed, it is described below:

5.4.1 Earth Tides

Earth tides, like ocean tides, are described as slow-moving solid body waves with long wavelengths, generated by interactions between the gravitational fields of the earth, sun, and moon. Solid earth tides are analogous to tides in bodies of water, but of much lesser magnitude because of the solidity of the earth. Geyser behaviour can be affected by the earth tides, and there appear to be two different effects at low earth tide and at high earth tide when the sun and moon are aligned to give an additive effect on the earth tide phenomenon.

Low tide effects are thought to be related with squeezing and partial closing of channel openings, restricting the flow of water into reservoirs so that the replenishment rate is reduced. High tides are considered to open fractures somewhat by dilational processes, generating enhanced fluid flow paths. Thus, high earth tides play an important role in changing the rate of flow of water into the geyser plumbing system. Figure 5.3 illustrates a schematic drawing of the effect of earth tides on the permeability of geyser plumbing systems.

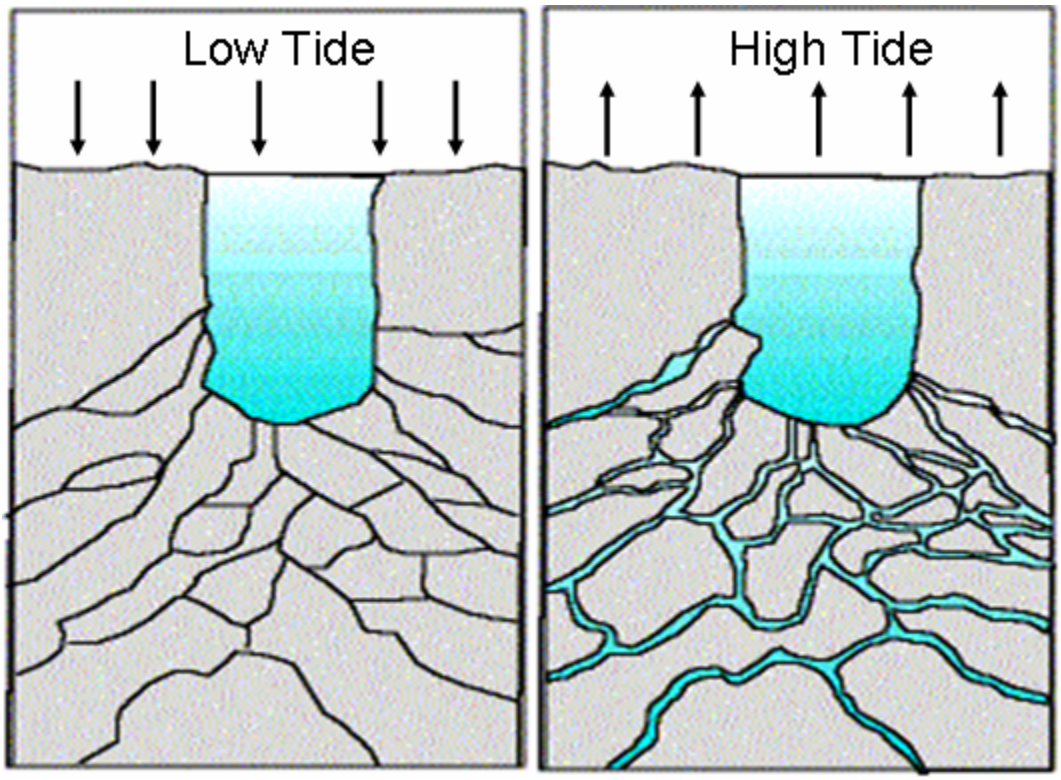

Figure 5.3: Effect of variation in gravity by earth tide forces in modifying crack openings (modified after Streepey 1996)

Many geysers have eruptive time spans that show correlation with earth tides. It has been observed that the increase in the earth tidal force is associated with an increase in the frequency of eruptions of geysers such as Old Faithful, as well as some California geysers (Rinehart 1980). The increase in the earth tidal forces therefore in some way causes a higher rate of eruption, leading to a correlation, or a coupled variation in time, as shown in Figure 5.4.

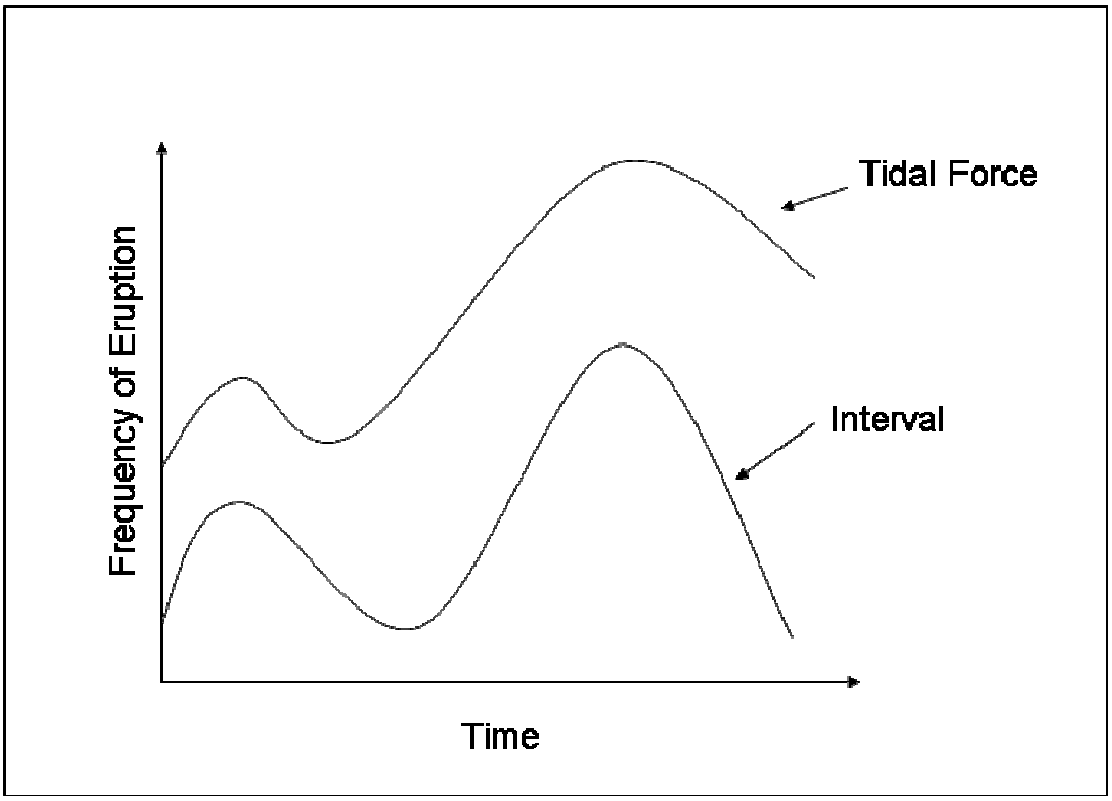

Figure 5.4: Frequency of eruptions of Old Faithful and California Geysers with respect to earth tidal force (modified after Rinehart 1980)

5.4.2 Earthquake Effects

If strains from earth tides are linked to geyser activity, earthquake activity and geyser behaviour could be strongly connected, and this relationship has been studied extensively. Geysers are located typically in tectonically active zones, i.e. earthquake regimes. That means geysers are subjected to the stress and pore pressure changes that precede and follow earthquake activity. The general pattern of change in geyser activity is hypothesized to be related in some direct manner to variations in tectonic forces which can affect the rate of flow of fluids, both gases and liquids, within the fractured and porous rock masses by modifying the dimensions of flow channels (fractured rocks) and pore throats (porous rocks).

It was well documented that in 1959 the Yellowstone geysers were dramatically affected by the nearby Hegben Lake earthquake (Rinehart 1980), which apparently was the largest

recorded earthquake since the park was discovered. The effects were strong likely because the epicenter was so near to Yellowstone. All the geysers erupted in the park and the average water temperature increased an average of 2°C in the geysers after the earthquake, indicating an enhanced rate of heat exchange. Some geysers that had been quiescent became active, suggesting that the hydraulic connectivity and transmissivity of the fluid pathways for these inactive geysers increased temporarily. Interestingly, Old Faithful was the only geyser in Yellowstone that did not erupt anomalously after the Hegben Lake earthquake (Rinehart, 1980). It is speculated that this shows that the changes in geyser activity due to earthquakes are not caused by slip along faults (displacement) so much as by changes in regional strain that affect the apertures of the fractures that control the flow rates into the plumbing system.

As geysers appear to record (i.e. reflect) earthquake activity in a reasonably faithful manner, there have been studies on whether geysers could be used as predictors for earthquake activity. For earthquake mechanisms that may develop very close to the locations of geysers, the hypothesis is the following:

- Earth strains (stored strain energy) that will eventually lead to an earthquake gradually accumulate in the time preceding an earthquake.
- The changes in strain (extensional in some areas, compressional in others) affect the aperture of fractures and fissures in the subsurface that affect water flow rates.
- These changes in flow rates affect the geyser eruption magnitude and recurrence rates.
- Therefore, changes in geyser activity may presage earthquake slip.

However, after detailed studies of geysers by Rinehart (1980), a systematic correlation between earthquakes and geyser activity was not found. On the other hand, more recent studies by Silver and Valette-Silver (1992) indicated that some geysers in California demonstrate observable anomalous activity in a period before the earthquake.

It appears that the hypothesis of local strain associated with earthquakes affecting local geysers is demonstrated, or at least is not contra-indicated. Nevertheless, it is not possible

to accept such a hypothesis for remote earthquakes because the magnitude of elastic earth strains becomes negligible with distance from the incipient trigger point. For example, at the distance between Landers earthquake and the Yellowstone geyser field, the pre-earthquake strains must be far less than the magnitude of the earth tidal strains. Thus, one may suppose that the precursor strain effect only is realistic at a modest distance from the earthquake locus, on the order of perhaps tens to no more that several hundreds of kilometers, depending on the volume of rock being strained by the process.

5.5 Microseismic Activity

Microseismic activity can affect geyser behaviour, although the response of geysers to slow changes in tectonic strains is not well understood. Microseismic activity is not a common feature of geothermal reservoirs but where it occurs it could be in principle linked to changes in reservoir pressure, temperature, and stress-strain behaviour of the associated rocks forming the geyser geothermal regime. For example, shallow injection of fluids is known to trigger microseismic activity (Warpinski et al. 2004), and it is hypothesized that an increasing pressure of the liquids in a fault zone is a potential source for the triggering of earthquakes (Sliver and Valette-Silver 1992). It seems logical to extend these observations to the association of microseismic and geyser activity.

Permeability in geothermal reservoirs is usually due to fractures, as the rocks are most commonly dense or otherwise of low permeability. In geothermal areas, fractures are often blocked by rapid precipitation of silica (SiO_2). The permeability can be altered by loosening or re-fracturing of these deposits, generating reopened existing fractures after an earthquake. This effect may therefore cause changes in geyser eruption intervals or in magnitudes of the eruptions. On the other hand, an earthquake with a different ground movement could conceivably reseal these fractures by increasing the normal stress across the fracture direction, and bring about reductions in permeability. Thus, an earthquake apparently could lead to an increase or a decrease in geyser eruption intervals.

A high shear stress generated by slow earth straining or the sudden release of the high shear stress may increase the permeability along fractures in and around the geothermal

reservoir. In general, if this is true, then any reservoir stress changes may cause changes in geyser activity. Furthermore, stress changes outside the active geothermal reservoir can also lead to induced seismicity where there may be no pore fluid content or pressure changes, with the seismic activity caused by volume changes associated with temperature changes. Temperature changes could be affected by the presence of crystallizing magma beneath the region, such as in Yellowstone caldera (Husen et al. 2004). Crystallizing magma is also associated with a loss of volume (in contrast to water which expands when it freezes), thus if a magma mass is "freezing", shrinkage will lead to stress changes, which in turn may be related to microseismic activity.

It is usually considered that there are two basic mechanisms by which microseismic activity affects geyser behaviour. The first mechanism is related to change in the regional (10 – 100 km) strain field and associated changes in the volumetric flow velocity into the reservoir; as a result, geyser eruption interval is affected. On the other hand, strain changes in microfractures could be causing change in the permeability of the plumbing systems in the geyser reservoirs (Linde and Silver 1989).

As an example, the Denali fault earthquake (Alaska), occurred in 2002 with magnitude of 7.9, and it brought clear changes in geyser activity in Yellowstone National Park (USA) area. A series of small earthquakes were observed in surrounding areas of Yellowstone (Husen et al. 2004), even though the distance is about 3100 km from the Denali earthquake epicenter. Several geysers changed their eruption frequency, and this was postulated to be due to the arrival of low frequency and large amplitude surface waves from the Denali fault earthquake (Husen et al. 2004). If indeed it is surface waves that are responsible, one must assume that the depth of penetration of the surface wave strains is sufficient to affect the rock mass so that geyser activity is altered.

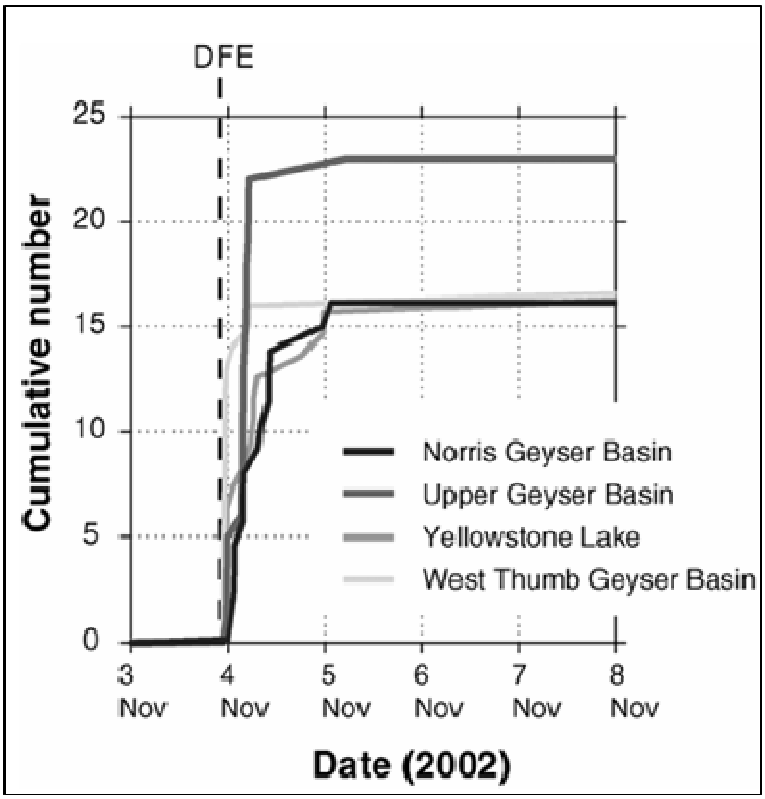

Figure 5.5: Earthquake swarms prior to and after the Denali fault earthquake (modified after Husen et al. 2004).

Earthquake swarms have been observed near to major geyser basins. It is found that these "…swarms were unusual compared to past seismicity in that they occurred…" concurrently in different geyser basins (Husen et al. 2004).

Even though earthquake swarms are frequent in Yellowstone, the seismicity after the Denali earthquake is considered slightly different for two reasons. One is that the microseismic earthquakes (as well as the related changes in geyser activity) occurred simultaneously throughout Yellowstone. Second, the intensity of the triggered earthquakes was high (magnitude of 2) as compared to previous earthquakes (Husen et al. 2004). The earthquakes with magnitude of 1.0 or higher that had been observed before the Denali earthquake "…occurred close to particular hydrothermal systems; however they never occurred simultaneously throughout Yellowstone." (Husen et al. 2004). In recent studies it has been suggested that "…geysers might be less sensitive to elastic

deformation than previously assumed…" (Husen et al. 2004). Moreover it is suggested that the internal dynamic processes (i.e. flow-related processes) of geysers could vary the geyser eruption intervals in response to excitation. The dynamic stresses associated with earthquakes can alter the permeability by opening (dilating) existing fractures in the geothermal system. It is usually assumed that microseismicity is induced by the redistribution of fluids and increases in pore pressure within the geothermal system (Husen et al. 2004).

In any case, the Denali fault earthquake is clear evidence that alterations in a geothermal system can be induced by a large magnitude earthquake event at a great distance, and that there is an important role that geothermal systems play in triggering local microseismic activity (Husen et al. 2004).

5.6 Remote Seismicity

Remote seismicity is associated with earthquake triggering, in which an earthquake can induce or retard seismic activity in surrounding regions or trigger other earthquakes at great distances. It has been observed that a remarkable feature of the 7.4 magnitude Landers earthquake was that it triggered seismic activity (i.e. earthquakes) at remote locations such as in Mammoth Lake, California (approximately 300 km away from the epicenter of Landers earthquake) and Yucca Mountain, Nevada (approximately 320 km away from the epicenter of Landers earthquake) (Landers earthquake (34:20:00N 116:44:00W), Mammoth Lake, California (36:41:00N 116:79:00W), Yucca Mountain, Nevada (36:71:00N 116:29:00W) (Iris.edu. 2004). Another example is the remotely triggered seismicity that was observed in Yellowstone National Park after the Denali fault earthquake (November 2, 2002). Figure 5.6, 5.7, 5.8, 5.9 and 5.10 are the records of the seismcity in Yellowstone from October 23, 2002 to November 25, 2002.

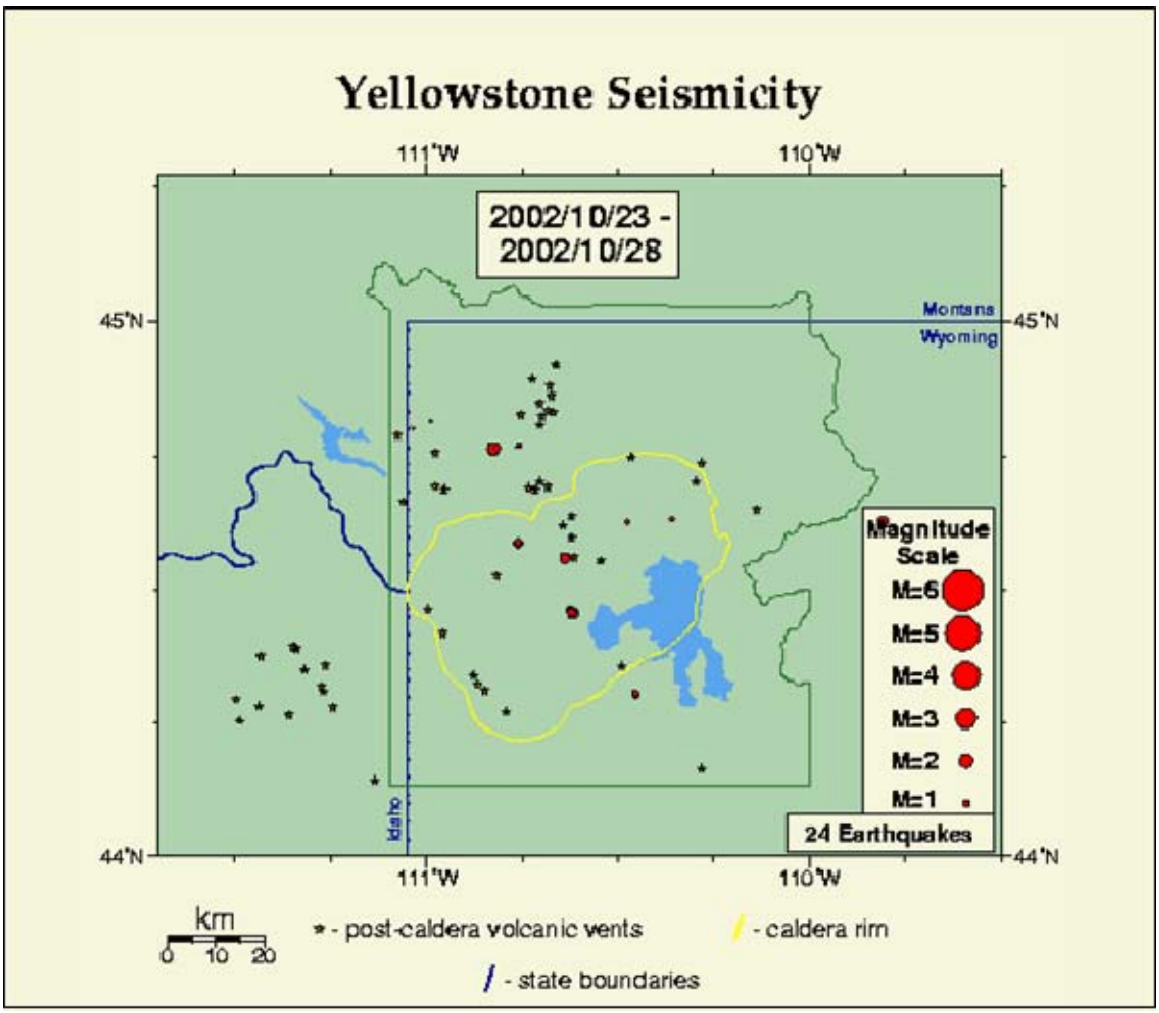

Figure 5.6: Seismicity in Yellowstone from 23/10/02 to 28/10/02 (modified after Utah Mines Edu. 2005)

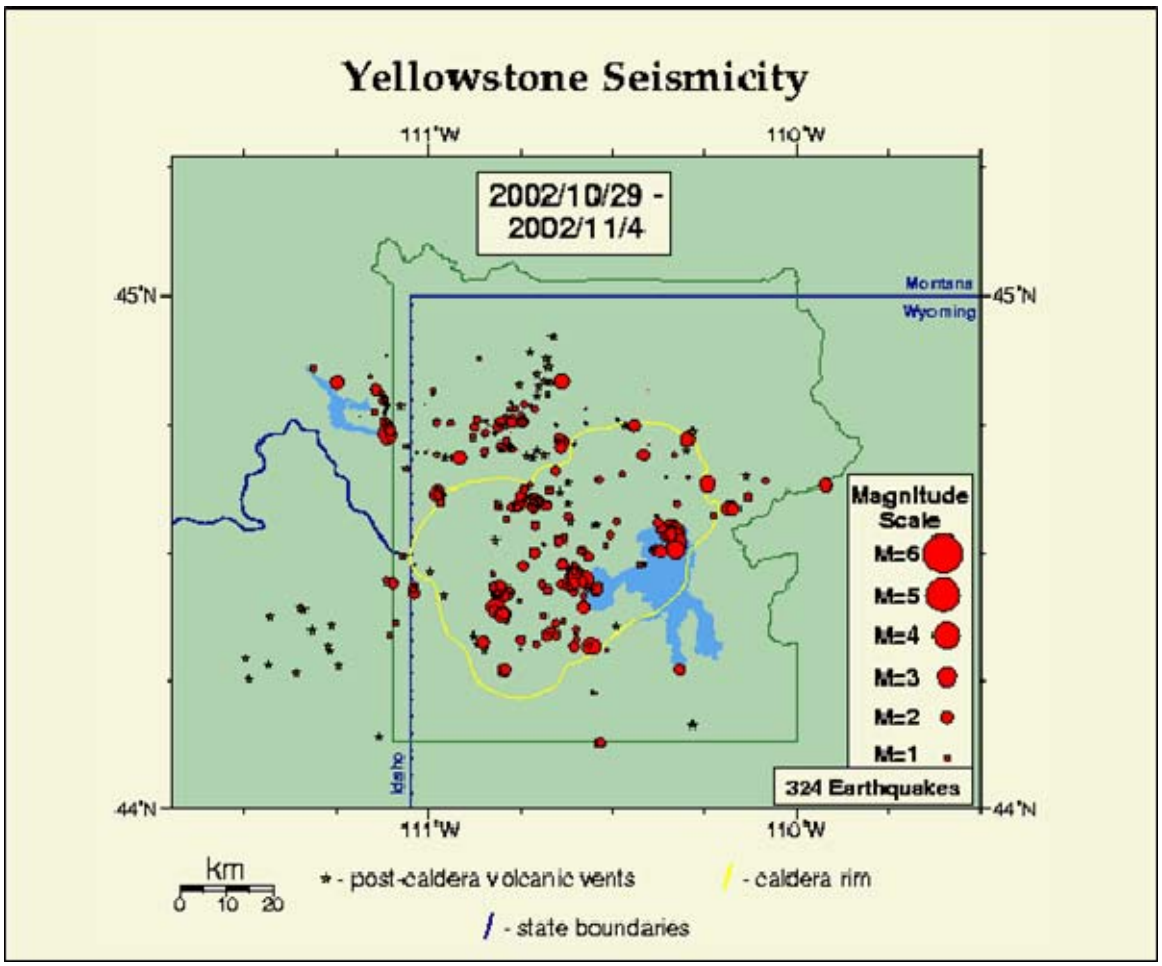

Figure 5.7: Seismicity in Yellowstone from 29/10/02 to 04/11/02 (modified after Utah Mines Edu. 2005)

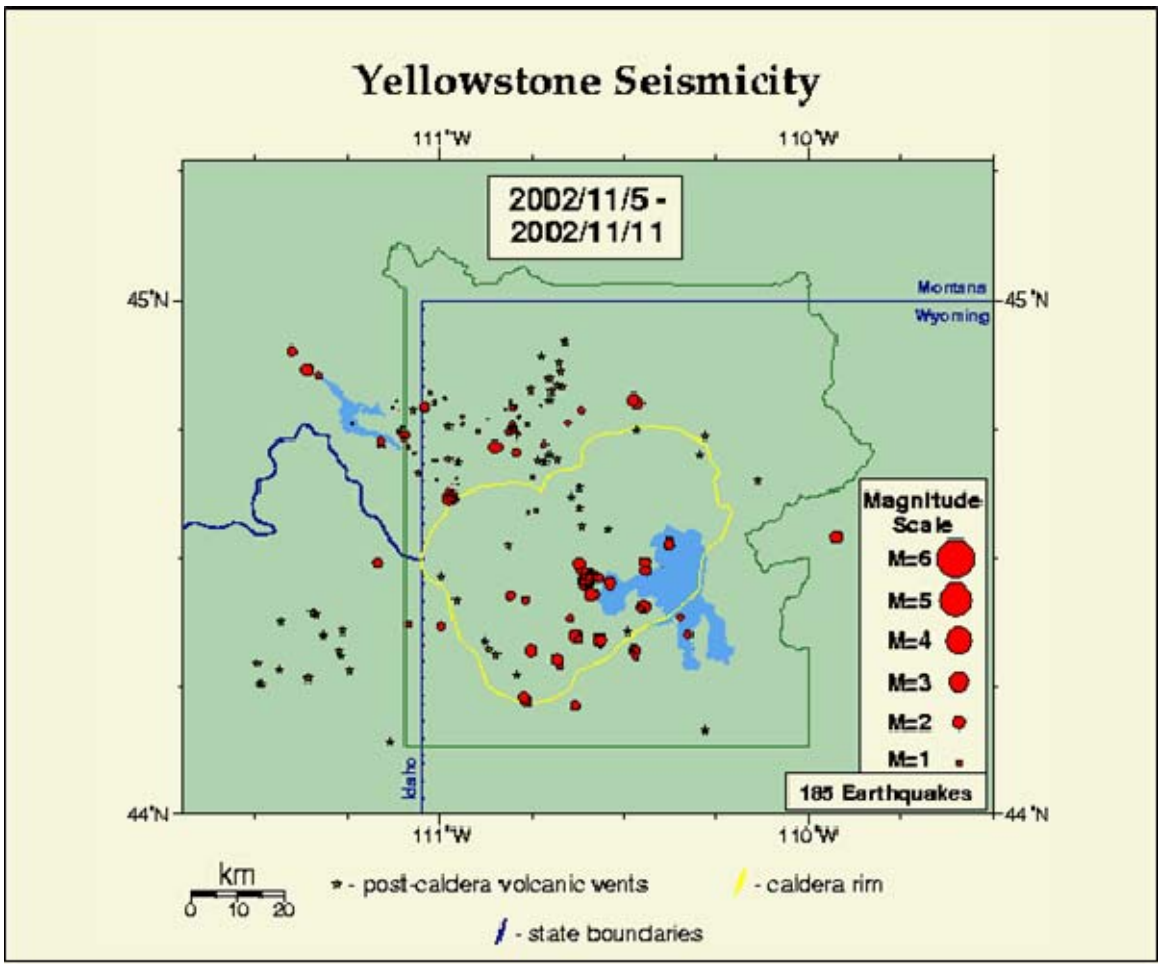

Figure 5.8: Seismicity in Yellowstone from 05/11/02 to 11/11/02 (modified after Utah Mines Edu. 2005)

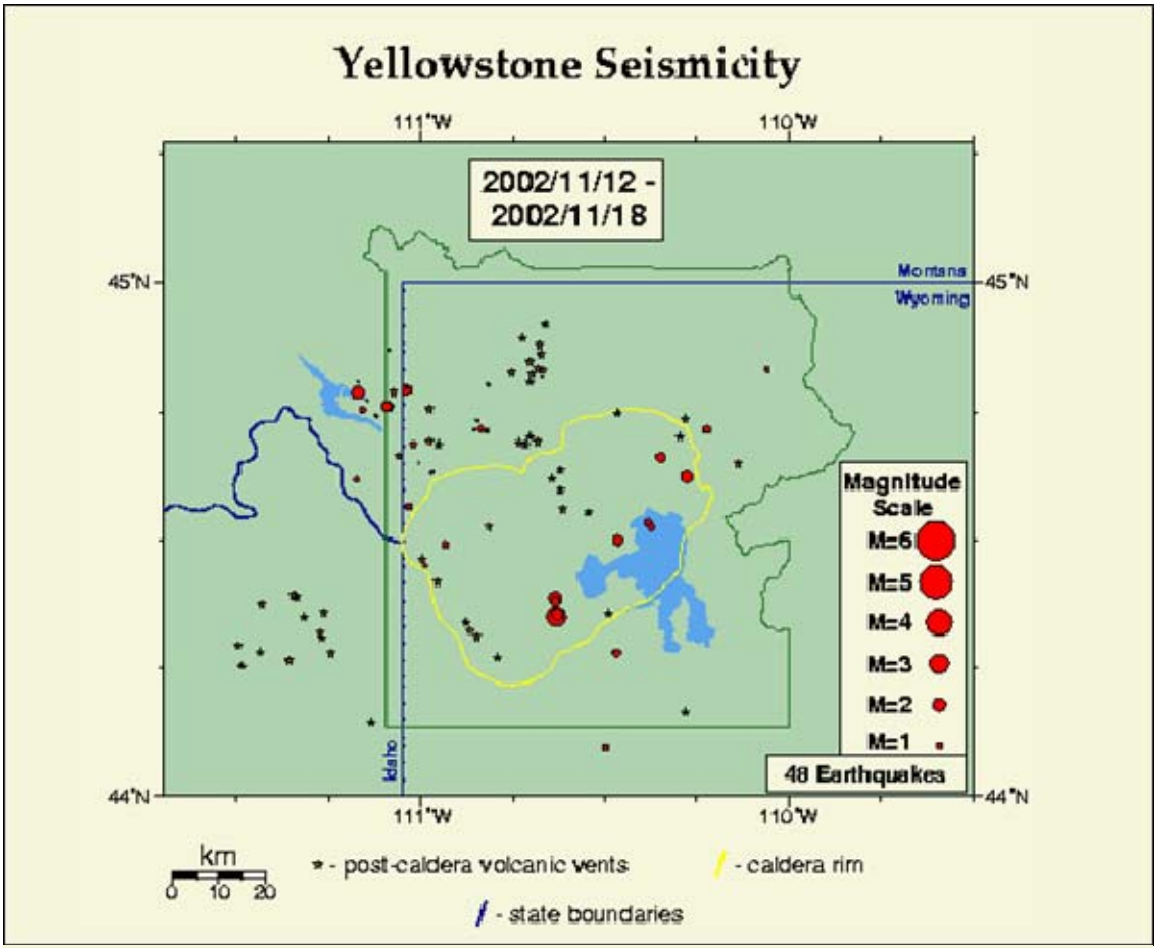

Figure 5.9: Seismicity in Yellowstone from 12/11/02 to 18/11/02 (modified after Utah Mines Edu. 2005)

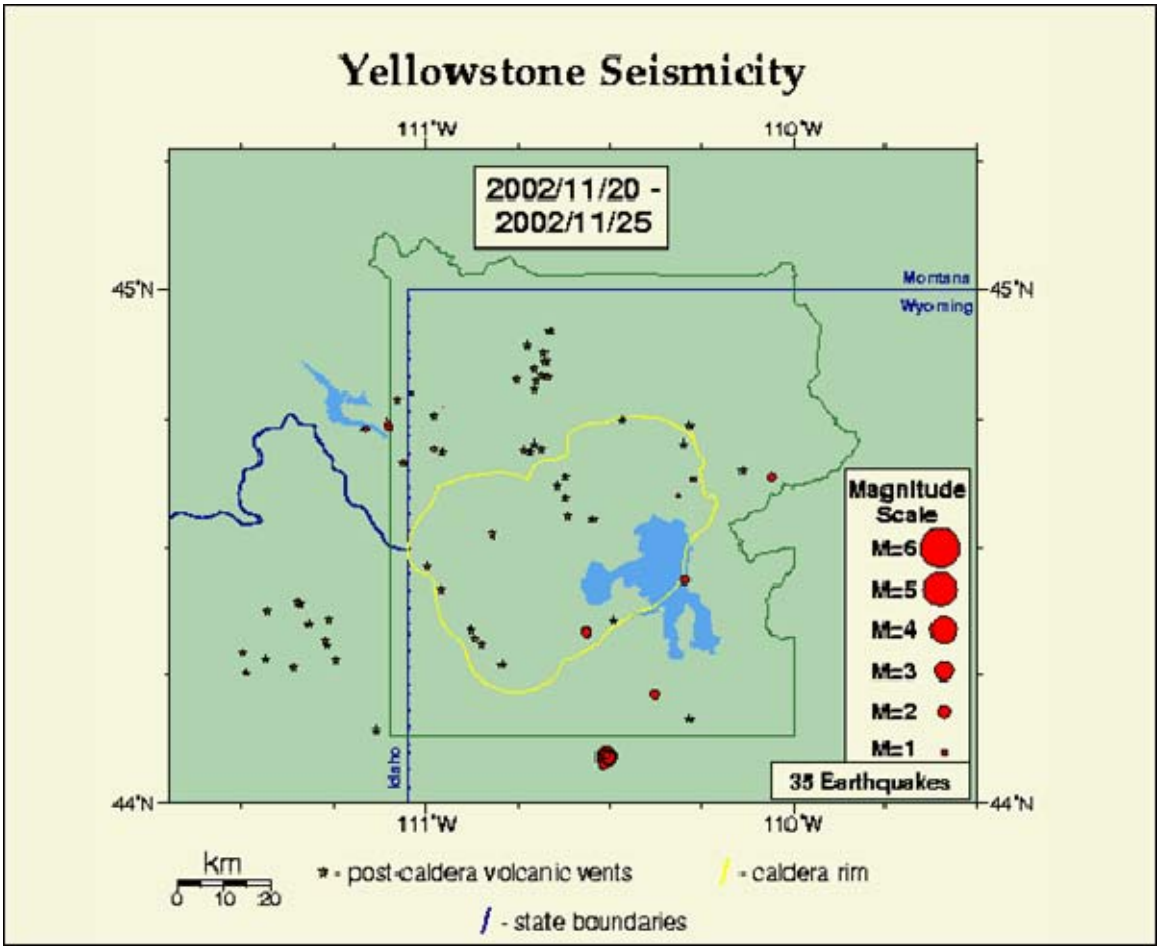

Figure 5.10: Seismicity in Yellowstone from 20/11/02 to 25/11/02 (modified after Utah Mines Edu. 2005)

Figures 5.6 through 5.10 show that the rate of earthquakes increased after the Denali fault earthquake. In Yellowstone, which is considered to be a tectonically active zone, normally fewer than 50 earthquakes would be expected in the week, but after the Denali fault earthquake, the seismicity rate increased enormously, as shown in Figure 5.7. Further, a graph is generated by using the above Figures from 5.6 to 5.10, shown as Figure 5.11, which illustrates that after the Denali earthquake, the seismicity increased and then decayed in Yellowstone National Park. As these data are recorded on a weekly basis, it is not easy to delineate the precise timing of the induced seismicity.

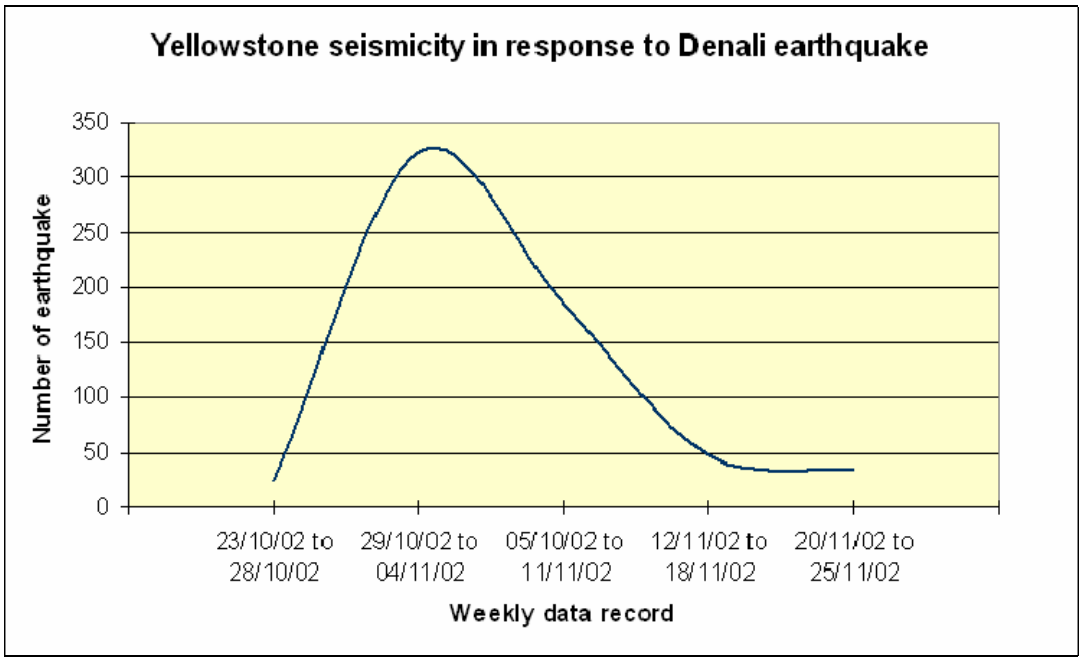

Figure 5.11: Graph shows a dramatic peak in microseismic events at Yellowstone National Park in response to the 2002 Denali earthquake.

A different way of showing this is Figure 5.12, which shows the seismic activity in Yellowstone in 2002. Clearly, sudden increases in local seismicity have occurred. These three peaks (number of earthquakes) show that seismicity temporarily increased in the Yellowstone National Park area after the Denali fault earthquake waves train passed (in early November) as above in figure 5.6 to 5.10 show as well.

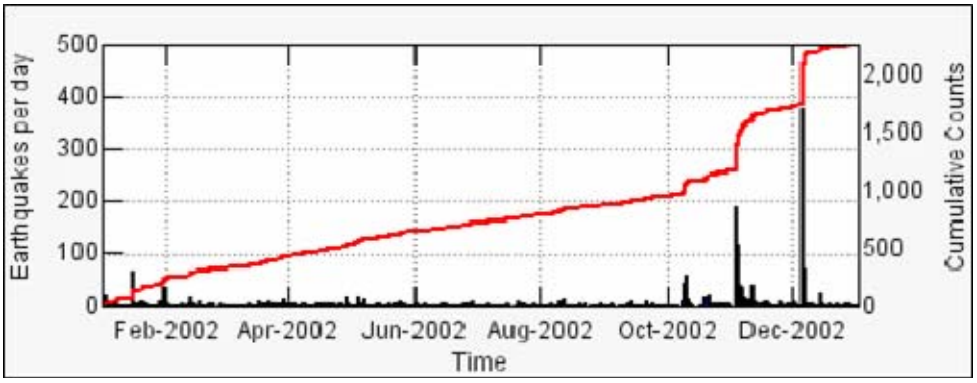

Figure 5.12: A plot of recorded earthquake activity at Yellowstone for the year 2002 (Volcanoes USGS 2005)

5.7 Summary

The mechanism of geyser eruption can be associated with induced seismicity; for example, it is well documented that geysers in Yellowstone generally started to erupt after the Denali fault earthquake (Husen et al. 2004). That means the stress changes and increase in pore pressure within the geyser reservoir played a significant role in aiding eruption of the geysers. Furthermore, it may be assumed that induced dynamic stresses or strains were well above those associated with earth tides because the geyser activity level change was far greater than that correlated to the earth tides. It has been generally considered that hydrothermal fluids transfer dynamic stress changes into sustained stress changes capable of triggering seismicity in geothermal reservoir (Husen et al. 2004).

It is currently not known if remotely triggered seismicity is common or rare. The mechanism of remote seismicity triggering remains uncertain, and may be different among the regions in which earthquakes were triggered, and for different geyser areas. One may consider that not enough past seismic data exists to clearly identify the triggering phenomena on a large scale, but it must be in some way due to the passage of seismic waves released by the earthquakes. These waves transmitted the energy and brought abrupt changes in stresses and pressures within the region, which are demonstrated to be capable to induce seismic activity in the geyser region. However, there seems to be no clear picture of what is the dominant wave source, though it seems clear that the P-wave and the S-waves are insufficient in terms of ground strain magnitudes at teleseismic distances. This leaves the surface waves and the slower waves as possible triggering energy sources.

Chapter – 6

Velocity Data Analysis of Earthquake Interactions

6.1 Introduction

Earthquake triggering is the process by which stress changes or energy emissions can induce or retard seismic activity in the surrounding area or trigger other earthquakes at remote regions. Earthquakes are often intricate in their rupture attributes because of the geometrical irregularity of faults and heterogeneity in a variety of factors in the rupture resistance such as the shear strength and the pore pressure. In many cases this heterogeneity may be highly influential on teleseismic wave propagation, but there nevertheless appears to be a consensus that in some cases, triggered secondary earthquakes can be recognized (Turcotte and Schubert 2002) in seismic analysis.

The soliton wave in a liquid-saturated porous medium is described as a displacement wave (rather than a strain wave) with large amplitude and low frequency; it is highly conservative so that it can travel long distances with small energy or structure loss. This is analogous to a tsunami in deep water that can travel thousands of kilometers with little loss in energy if conditions are appropriate. It is hypothesized that a soliton wave packet, travelling at a velocity of 100-300 m/s, is a possible mechanism of energy transfer that increases the local pore pressure and allows highly stressed faults to be “triggered” by a distant major event (Spanos et al. 2003), leading to a secondary or induced earthquake.

There is evidence of this kind of wave in nature. In the 1964 Alaska earthquake, many water wells in the Great Plains showed a sudden change in the head the day after the earthquake, long after all known body and surface waves had passed (Plafker and Kachadoorian 1966).

There seems to be no clear picture of what is the dominant wave source that leads to these responses, though it seems that the P-waves and the S-waves are insufficient in terms of ground strains. This leaves the surface waves and the slower waves as possible energy sources for triggering induced responses (Spanos et al. 2003).

6.2 Possible Earthquake Interactions

To study possible earthquake interactions analysis, broadband records at teleseismic distances were retrieved from Incorporated Research Institutions for Seismology (IRIS website: http://www.iris.edu/cgi-bin/wilberII_page1.pl), to find evidence of the predicted wave velocity 100-300 m/s. IRIS global seismographic network (GSN) is made up of over 128 permanent surface seismic recording stations covering the Earth's surface as shown in Figure 6.1. IRIS GSN stations continuously record surface seismic data from very broadband seismometers at 20 samples per second (sps), and higher frequency (40 sps) and also strong-motion (1 and 100 sps) sensors are deployed in some locations (IRIS 2004).

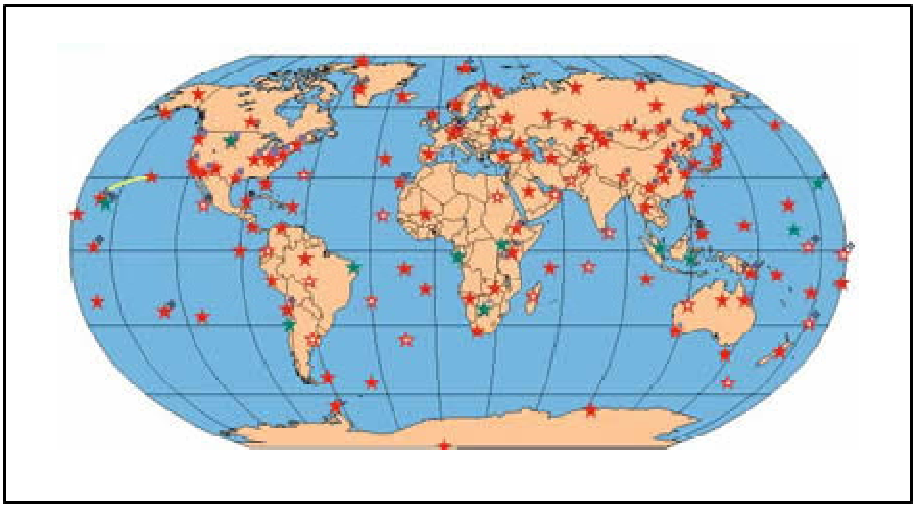

Figure 6.1: Locations of 128 seismic telemetry stations around the world (after IRIS 2004)

A total of 468 earthquakes were recorded with a magnitude 2.8 filter in situ by IRIS in 2003. These seismic event locations are shown in Figure 6.2, 6.3, 6.4, and 6.5, which contain only 2003 data from around the world. In fact, the effective filter cut-off lies somewhere between magnitudes 4.5 and 6, as will be seen later.

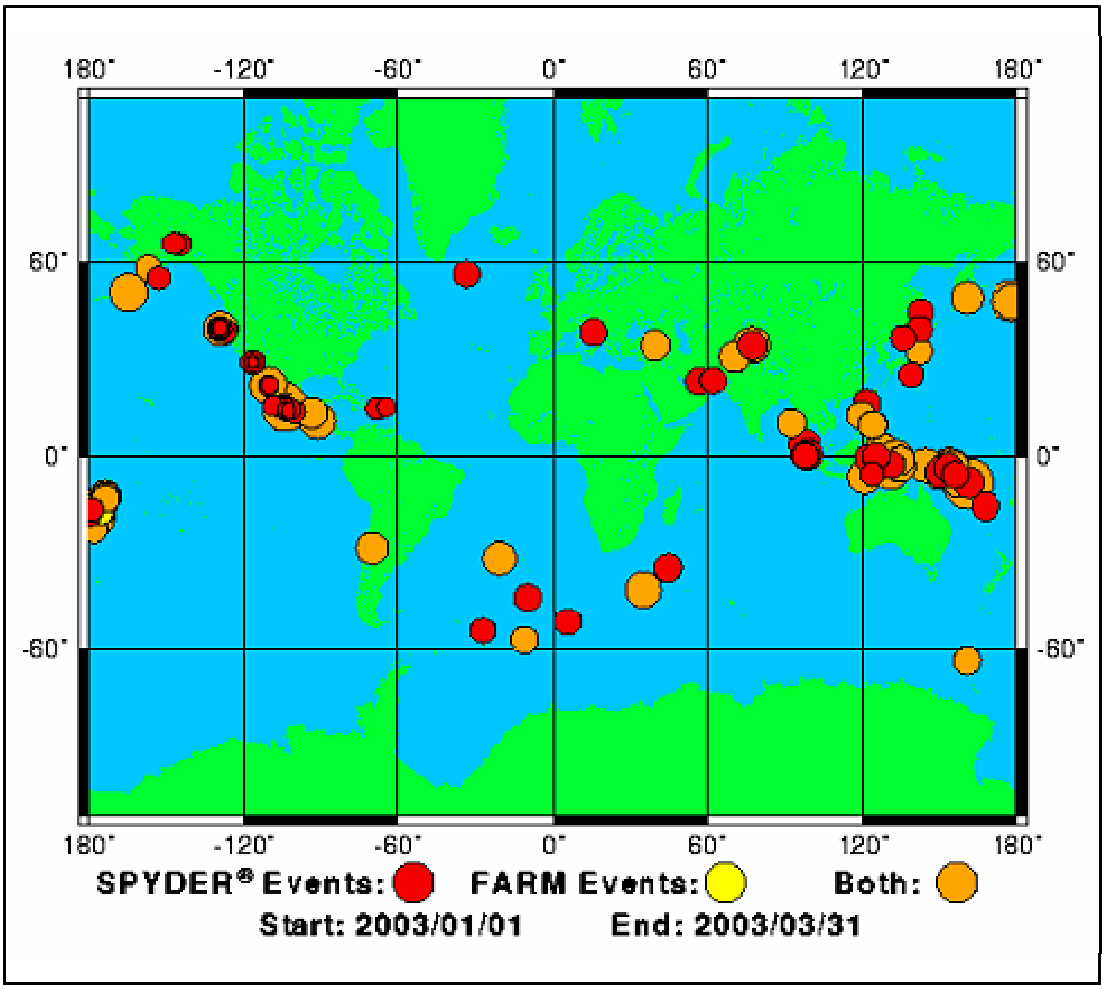

Figure 6.2: Location of earthquakes 01/01/03 to 31/03/03 (from IRIS 2004).

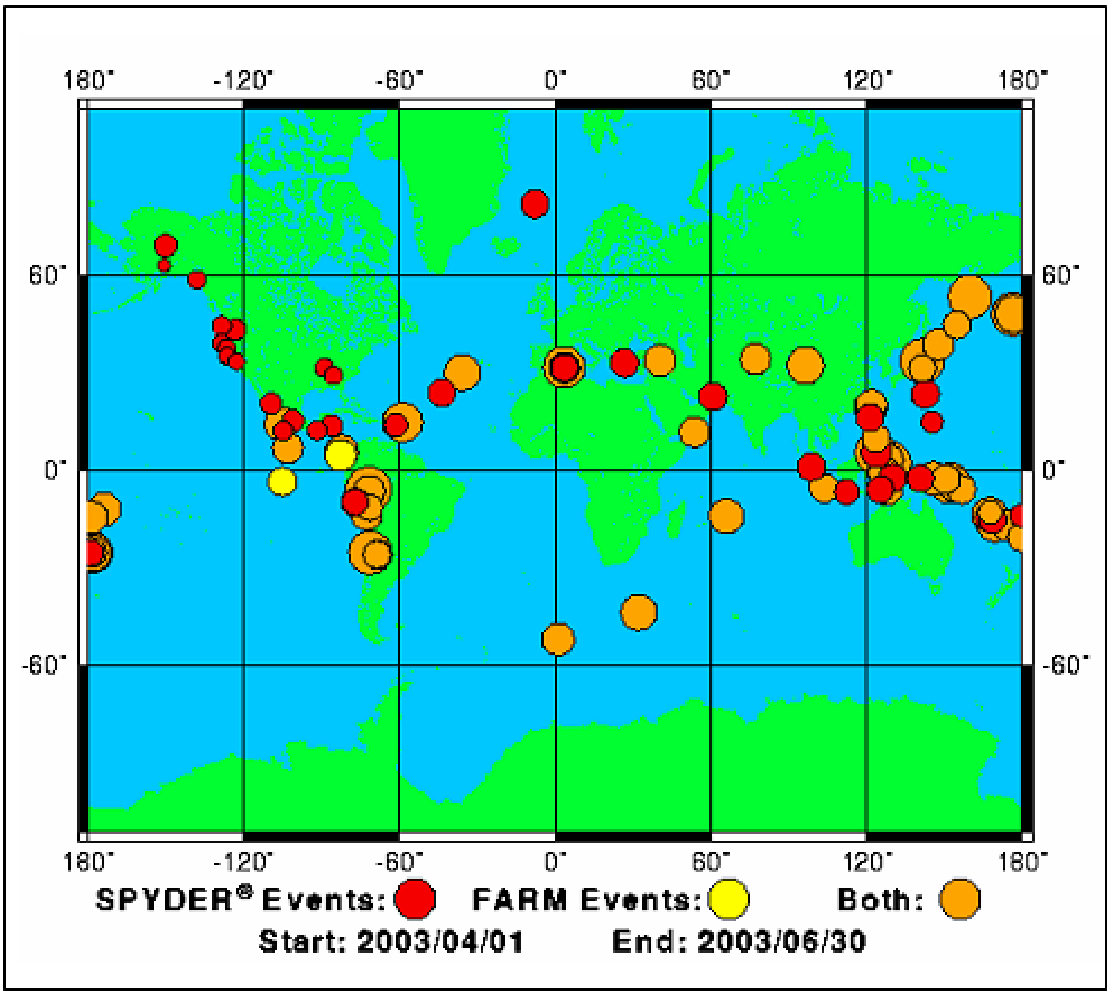

Figure 6.3: Location of earthquakes from 01/04/03 to 30/06/03(modified after IRIS 2004).

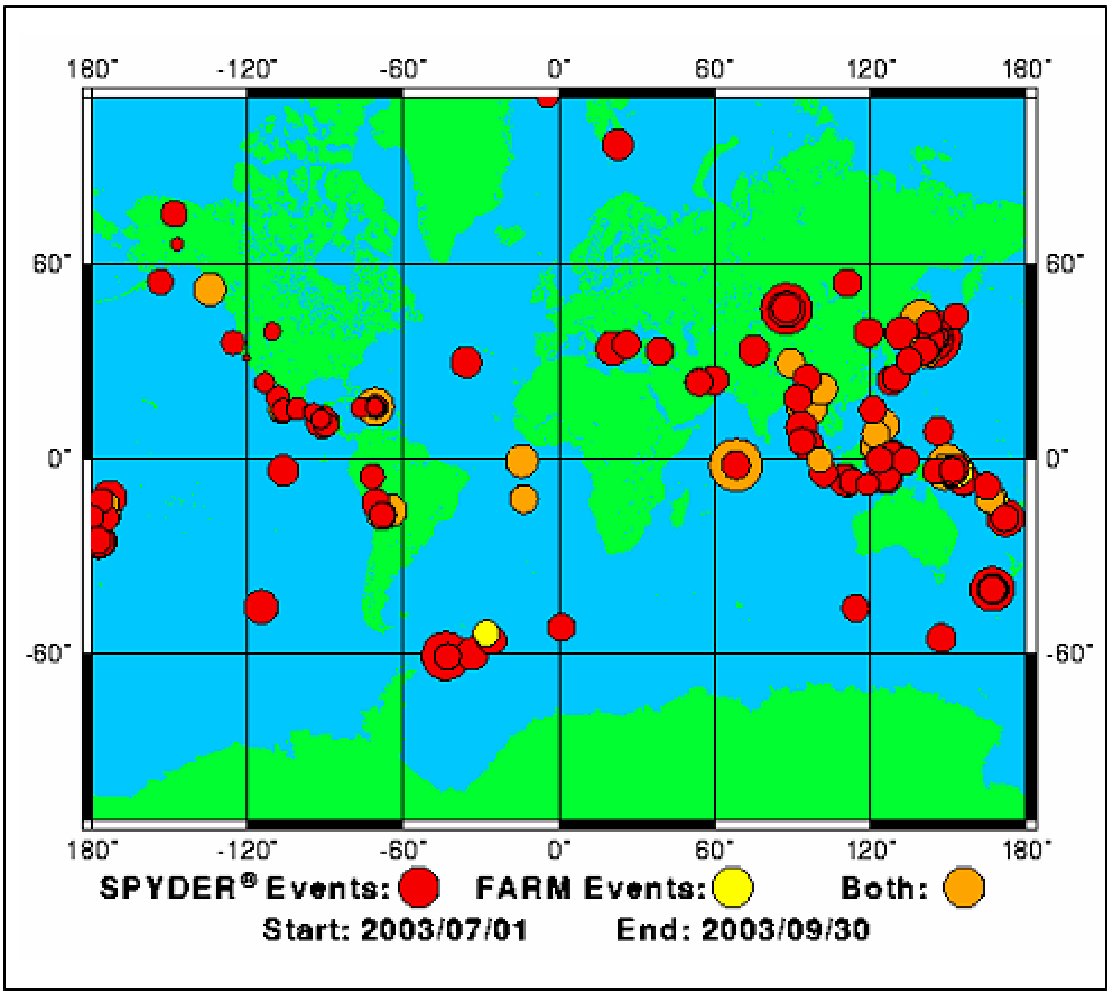

Figure 6.4: Location of earthquakes from 01/07/03 to 30/09/03 (modified after IRIS 2004).

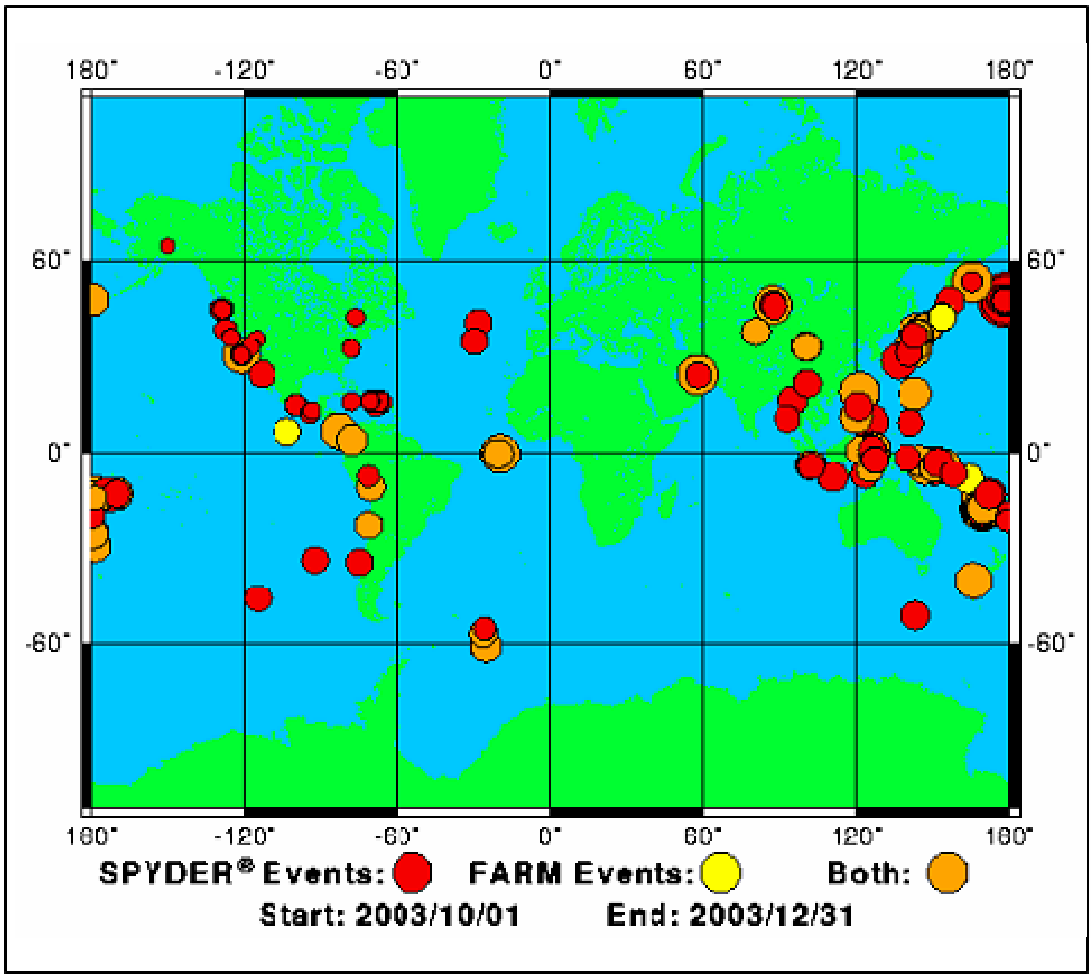

Figure 6.5: Location of earthquakes from 01/10/03 to 31/12/03 (modified after IRIS 2004).

Two data bases are made on EXCEL spreadsheets by putting together the information for the 2003 worldwide earthquakes, such as magnitude, location, latitude, longitude, time, date and depth. One data base (real sequence 2003) contains earthquake interactions velocity data by calculating the velocity between the first earthquake and the second earthquake as occurred in a real succession. In the real sequence, the velocities of a possible triggered event are calculated as the velocities between sequenced events based on the time difference $\Delta t_{21} = t_2 - t_1$, $\Delta t_{32} = t_3 - t_2$, etc., for a sequence such as such as 1-2, 2-3, 3-4, 4-5, and so on, as shown in Figure 6.6.

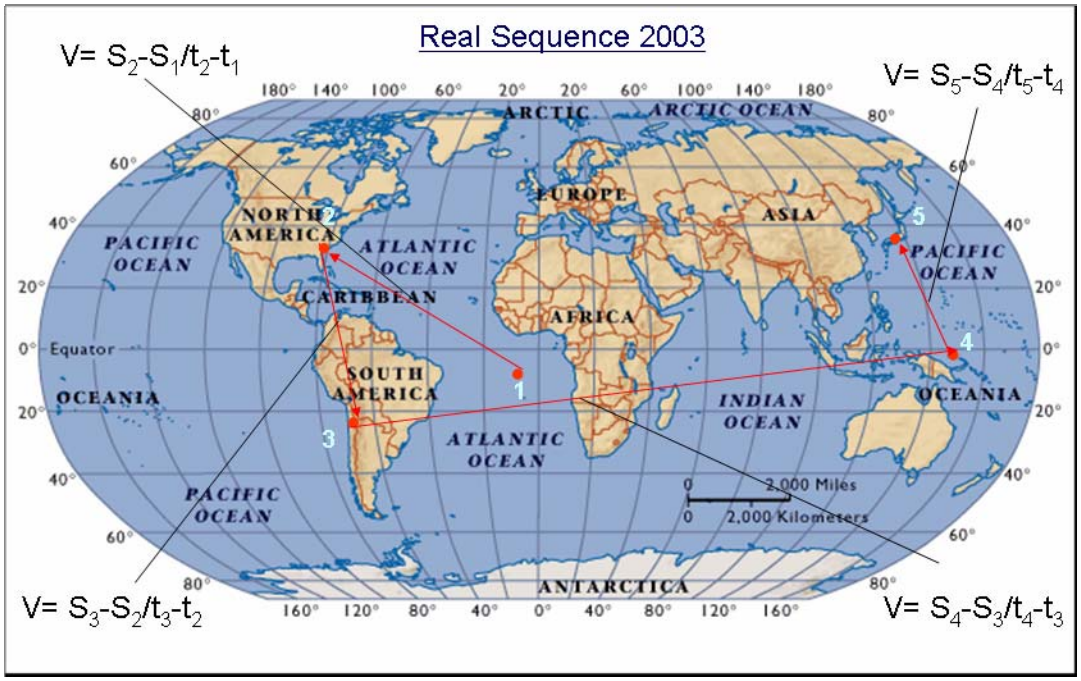

Figure 6.6: Example showing how the velocity of earthquake interactions was calculated in the real sequence 2003 data base (modified after Mapquest 2002).

Another data base (K-Q cases in 2003) is made by calculating the velocity between an assumed primary earthquake (K) and its set of possible secondary earthquakes (Q1, Q2, Q3…) and so on, as shown in Figure 6.7. In this case, the velocities are calculated from the time differences $\Delta t_{KQ1} = t_{Q1} - t_K$, $\Delta t_{KQ2} = t_{Q2} - t_K$, and so on.

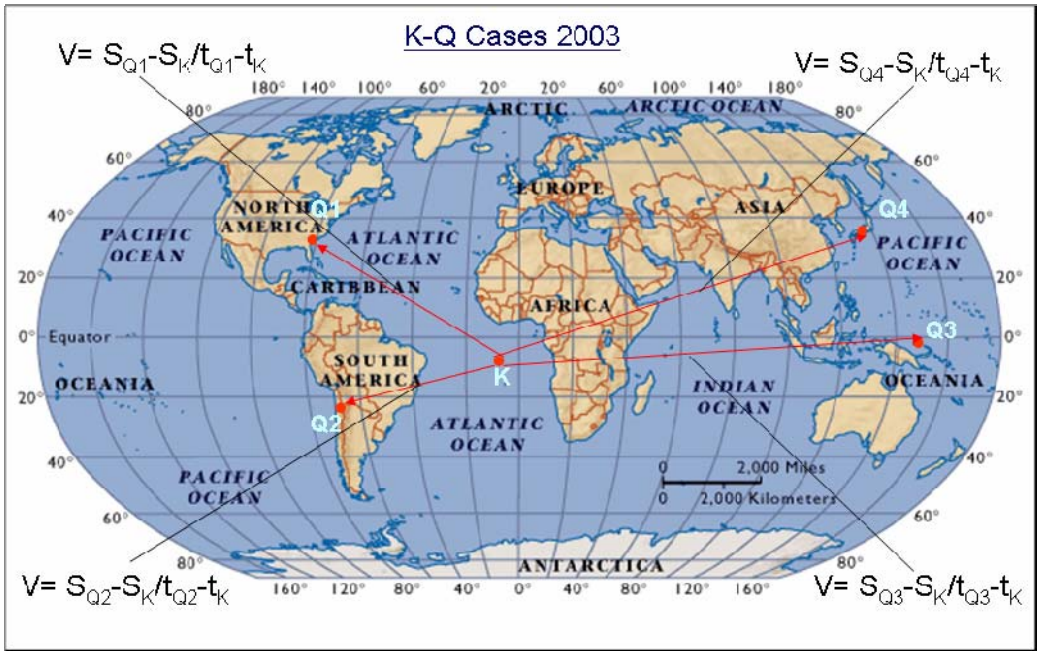

Figure 6.7: Example showing how the velocities of possible earthquake interactions in the K-Q Cases 2003 data base were calculated (modified after Mapquest 2002).

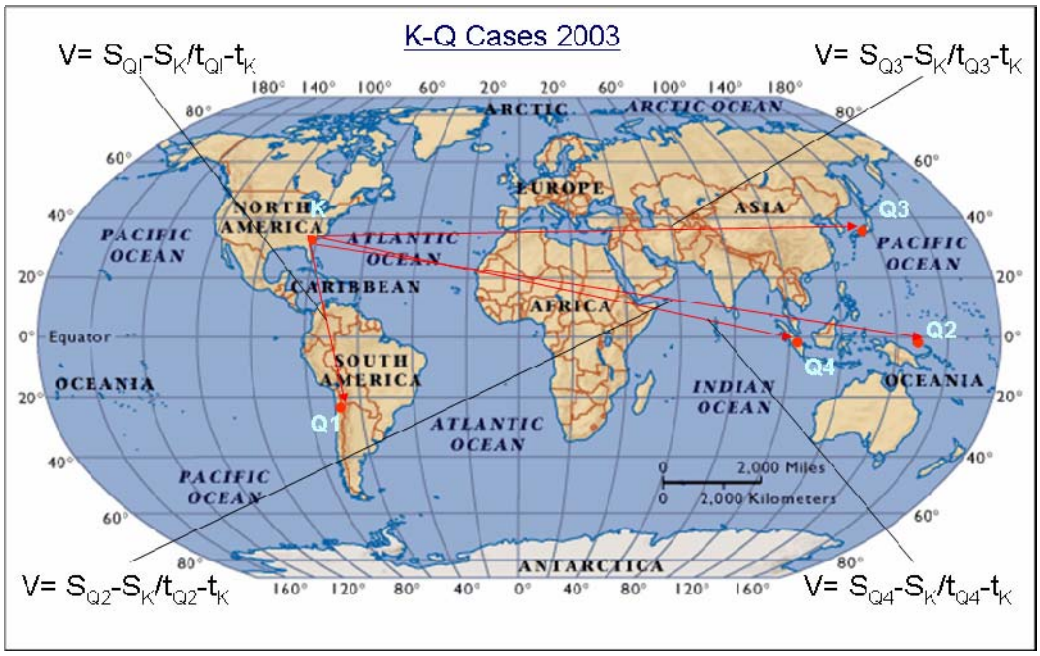

Figure 6.8: Another example showing how the velocities of possible earthquake interactions in the K-Q Cases 2003 data base were calculated (modified after Mapquest 2002).

The distances in both data bases, such as between Earthquake #1 and Earthquake #2 in the real sequence data base, or between the K earthquake and the possible secondaries Q1, Q2, Q3…, are calculated by using the algorithm found at website http://www.indo.com/cgi-bin/dist.

6.2.1 Velocity Analysis

To explore earthquake interactions by using velocity data analysis from real sequence 2003 data base, a graph is plotted, shown in Figure 6.9. The graph shows that possible earthquake interactions (triggers) decrease as we increase the velocity range of seismic waves, as expected of course. This plot is independent of the type of seismic wave, such as P-wave, S-wave, Love wave and Raleigh wave, although all of these have velocities greater than about 2 km/s (2000 m/s). A plot of this type has to show a hyperbolically decaying shape so that the probability of an earthquake being triggered by a very high velocity wave (e.g. 10 km/s) must approach zero. The plot does indeed show this structure. Although the shape of the decay curve with increasing velocity has not been determined mathematically, this figure shows what appears to be an unusually large number of triggers in the soliton velocity range.

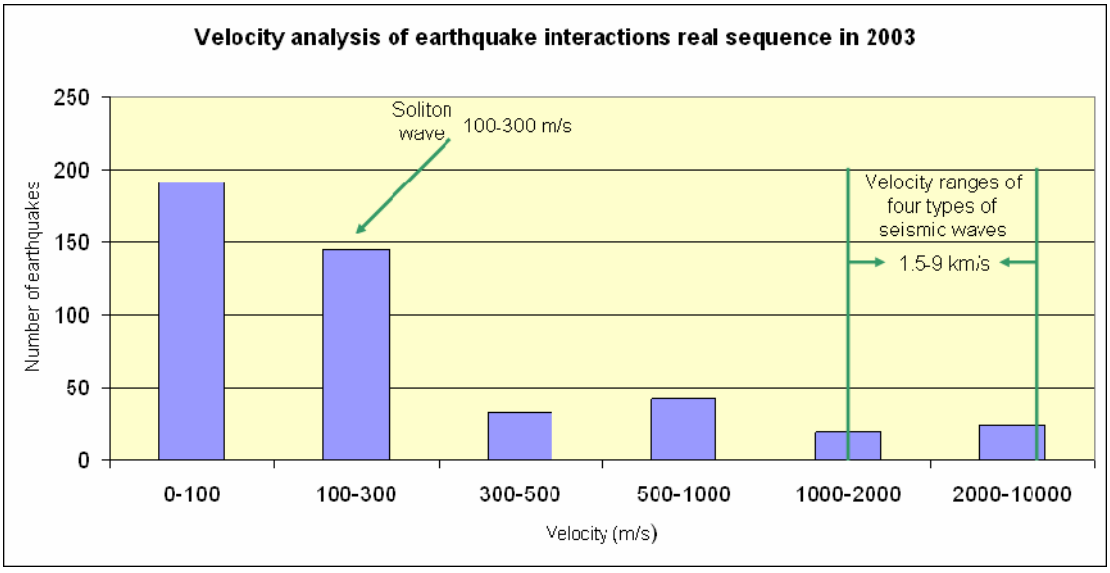

Figure 6.9: Graph showing distribution of possible earthquake trigger interactions with velocities of different seismic waves included.

145 earthquakes interactions can be considered in the range of a possible response to a soliton velocity range (100-300 m/s). Remember that P-waves travel with 5-7 km/s velocity, S-waves with 3-4 km/s velocity, and other surface waves in the range of 2-4 km/s velocity after an earthquake, depending on the structures and materials these waves pass through (Braile 2005). Earthquake interactions that could be attributed to energy transmitted at the velocities of these are few in number. Of course, the small strains at teleseismic distances of these high velocity waves because of with geometric spreading and attenuation suggest that it is difficult on the basis of known geophysics hypotheses to attribute even this low number to a physical origin associated with the primary. In other words, in a large data set of earthquakes, there is always some probability of finding a hypothesized secondary earthquake in any velocity range (although less and less at high velocities). Clearly, at best, only a few numbers of earthquake interactions at high velocities are found by analyzing the graph.

Seismic strain waves are high frequency and short wavelength waves, whereas a soliton wave is low frequency and long wavelength; this means soliton waves can carry more energy and therefore possess a greater possibility to trigger seismic events either nearby or remotely after a major earthquake. Further, seismic wave amplitudes generally decay exponentially with increasing travel distance because of intrinsic absorption and scattering loss due to distributed heterogeneities in the Earth (Sato and Fehler 1998), whereas solitons must propagate more conservatively, similar to tsunamis, and must travel great distances with small energy loss because the wavelengths are so long. Finally, it is important to mention again that the strain waves at high frequency are extremely unlikely to cause changes in pore pressure or stress that could trigger any secondary event, but the soliton wave carries with it, because it is a liquid displacement wave, the potential to affect the pore pressure at a distance. If the earth is “critically organized” (many faults just at the point of rupture, awaiting a small trigger), a small n crease in pore pressure could suffice as a trigger.

If the above graph (Figure 6.9 is generated on logarithmic scale as shown in Figure 6.10), a smooth decay line is found, which means that possible earthquake interactions are decreasing as expected with increasing seismic waves velocity ranges, but there is also a

broad bump in the range 100-300 m/s velocity, rather than a smooth decline. The small bump to the right is not large in view of the sample base, and it may not be significant, but the 100-300 m/s bump appears to be significant, although at this time it is not known how to test this statistically.

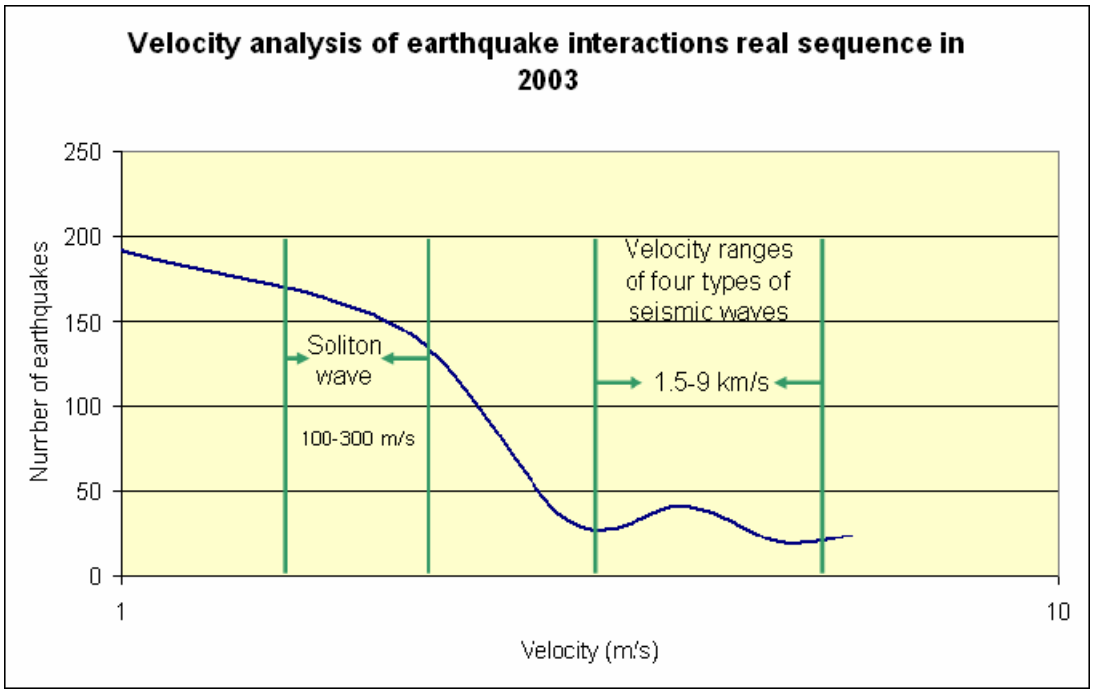

Figure 6.10: Graph shows distribution of possible earthquake interactions with velocities of different seismic waves in a logarithmic scale.

Another graph is plotted by using K-Q cases in the 2003 data base on the basis of different seismic wave velocities as shown in Figure 6.11. This illustrates more or less the same picture as in Figure 6.9. The probability of earthquake interactions in response to a soliton-sourced trigger is not proven conclusively by this data analysis, but there are definitely some reasonably strong suggestions. Note that if a triggering mechanism was being carried great distances by surface waves (extremely unlikely because their amplitude decays exponentially with depth), there would be a bump in the 2-4 km/s range, and if S-waves were the trigger (again unlikely because of the extremely small strains), the bump would be in the 3-5 km/s range. Such evidence cannot be seen.

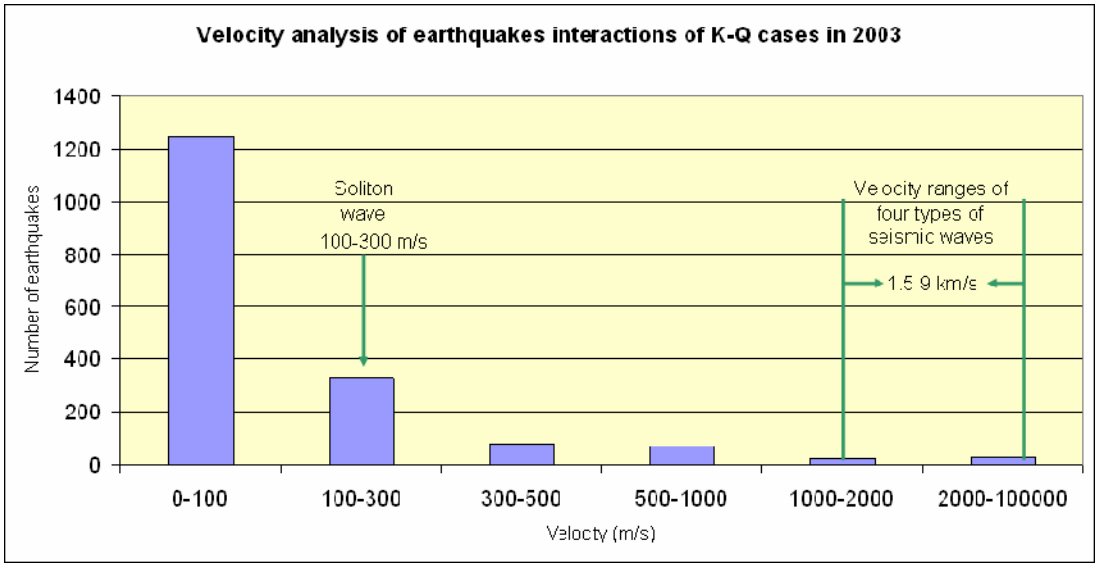

Figure 6.11: Graph shows distribution of possible earthquake interactions with velocities of different seismic waves.

If the above graph (Figure 6.11) is generated on logarithmic scale as shown in Figure 6.12, it is found that earthquake interactions are decreasing smoothly with increasing seismic waves velocity values. In this case, there is no bump in the soliton velocity range, and a very small bump in the S and P-wave range. Obviously, these results are not clear-cut, but neither do they disprove the soliton hypothesis.

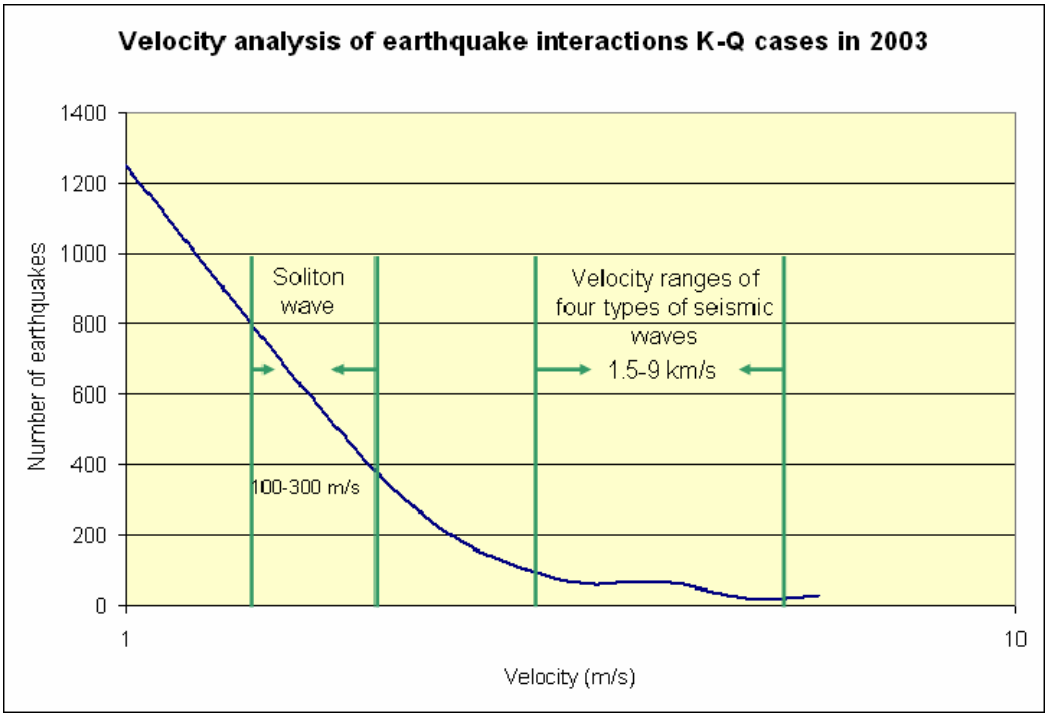

Figure 6.12: Graph shows distribution of possible earthquake interactions with different seismic wave velocities in a logarithmic scale.

It remains a reasonable hypothesis that a large earthquake can trigger sympathetic secondary earthquakes at near or far distances due to the emission of energy in a soliton packet. It is also likely that large earthquakes (M > 5) have more probability for triggering earthquakes at remote distance instead of small (M < 5) earthquakes because attenuation of the seismic waves in small earthquakes is rapid due to heterogeneity of the Earth. The recorded earthquakes that occurred show most in the range 5-6 (Figure 6.13), but that is largely because smaller earthquakes simply did not register on enough stations to be included in the data base, which again relates to the attenuation with distance. In other words, somewhere around magnitude 5-5.5 appears to be the actual magnitude filter for the IRIS database. This is unfortunate, as one would in general suspect that only smaller earthquakes would be triggered by a large primary, but if most earthquakes less than 5.0 are absent, smaller secondaries cannot be picked up on IRIS.

A table of earthquake interactions (found in the Appendix) is created in which (K) primary earthquake may be considered to trigger (Q1, Q2, Q3…) secondary earthquakes

at 100-300 m/s. In the table, earthquakes with magnitude of 5 to 6 are indicated as being possible primaries that could trigger secondary earthquakes in most cases. In other words, there are possible secondaries in the right soliton velocity range.

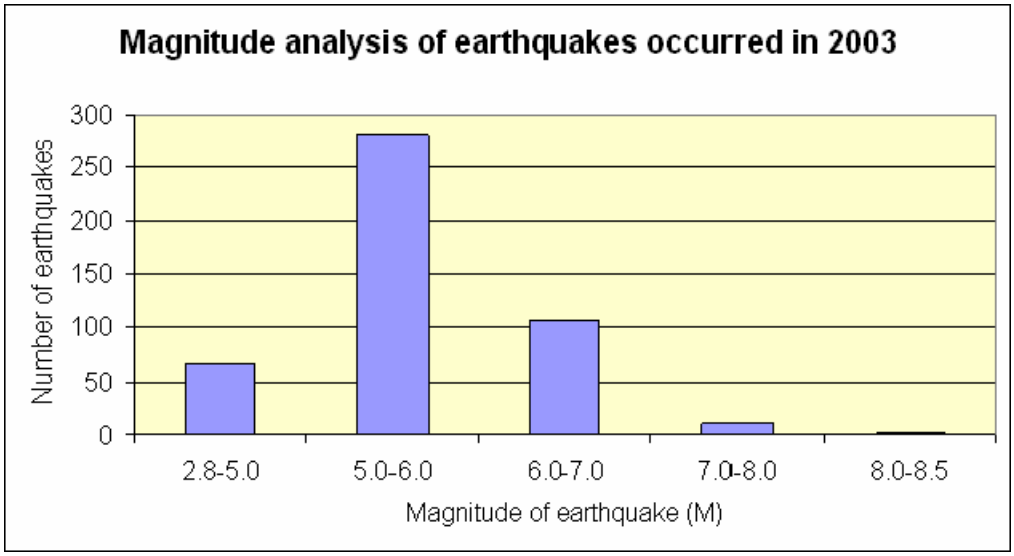

Figure 6.13: Graph illustrates earthquakes occurring in 2003 with different magnitude.

In view of a reasonable supposition that bigger earthquakes, such as earthquakes with magnitude of 6 or greater, are more likely to trigger secondary earthquakes at remote distances, a graph is plotted as shown in Figure 6.14 by using the real sequence data base for magnitude 6 and greater.

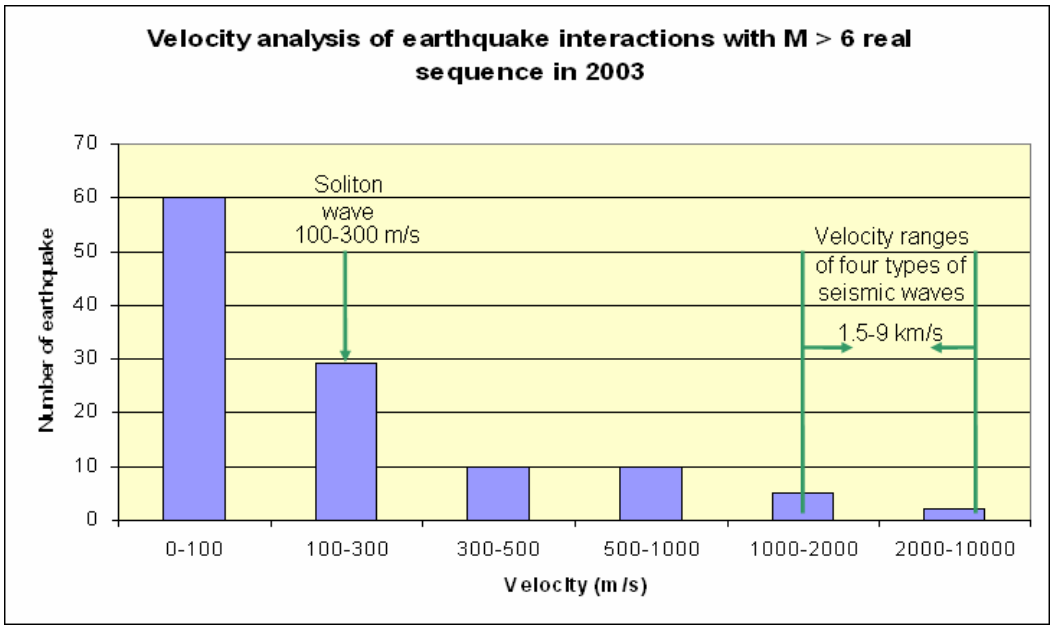

Figure 6.14: Graph showing distribution of possible earthquake interactions with velocities of different seismic waves, magnitude 6 and over.

The above graph (Figure 6.14) is plotted on a logarithmic scale, as shown in Figure 6.15.

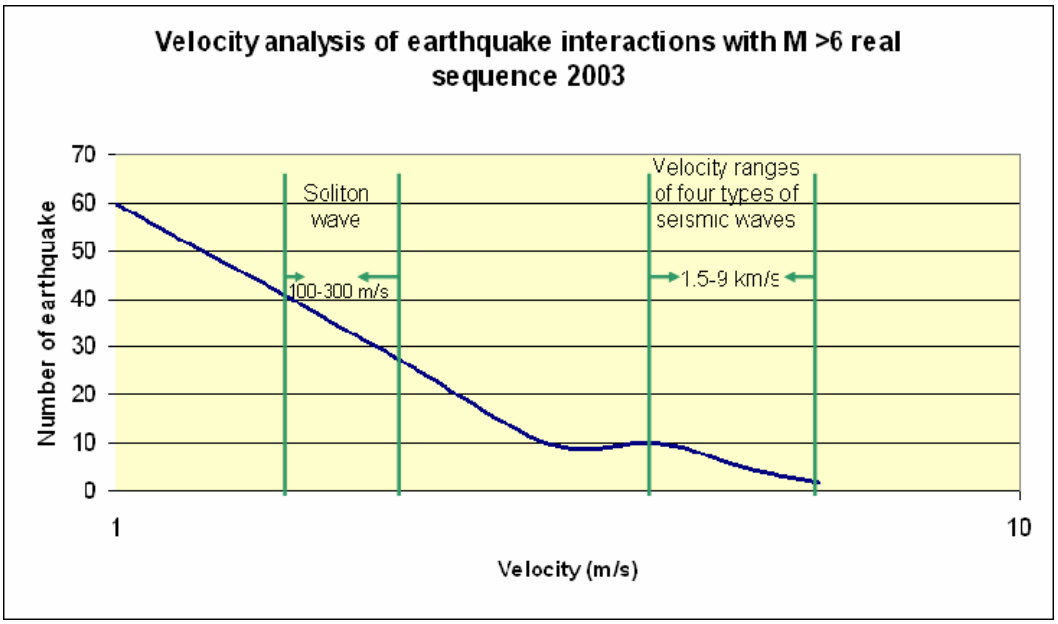

Figure 6.15: Graph showing distribution of possible earthquake interactions with different seismic wave velocities in logarithmic scale.

These two graphs (Figure 6.14 and 6.15), if compare with Figure 6.9 and 6.10, the broad bump diminished in the range of soliton wave velocity range and other seismic waves velocities range remain same. A small bump in the range of 2-4 km/s exists in the otherwise smooth decline of the frequency plot.

Similarly, the possible earthquake interactions with primaries only of magnitude of 6 or above are plotted using the K-Q cases 2003 data base, as shown in Figure 6.16. This Figure plotted on a logarithmic scale, shown in Figure 6.17.

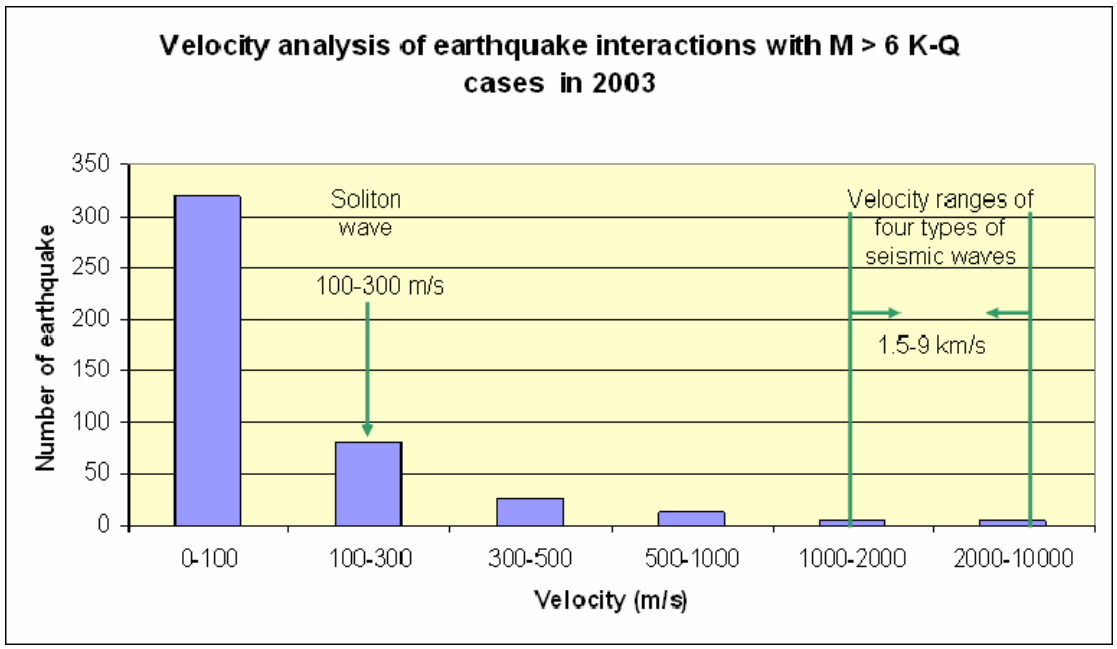

Figure 6.16: Graph shows distribution of earthquake interactions with velocities of different seismic waves.

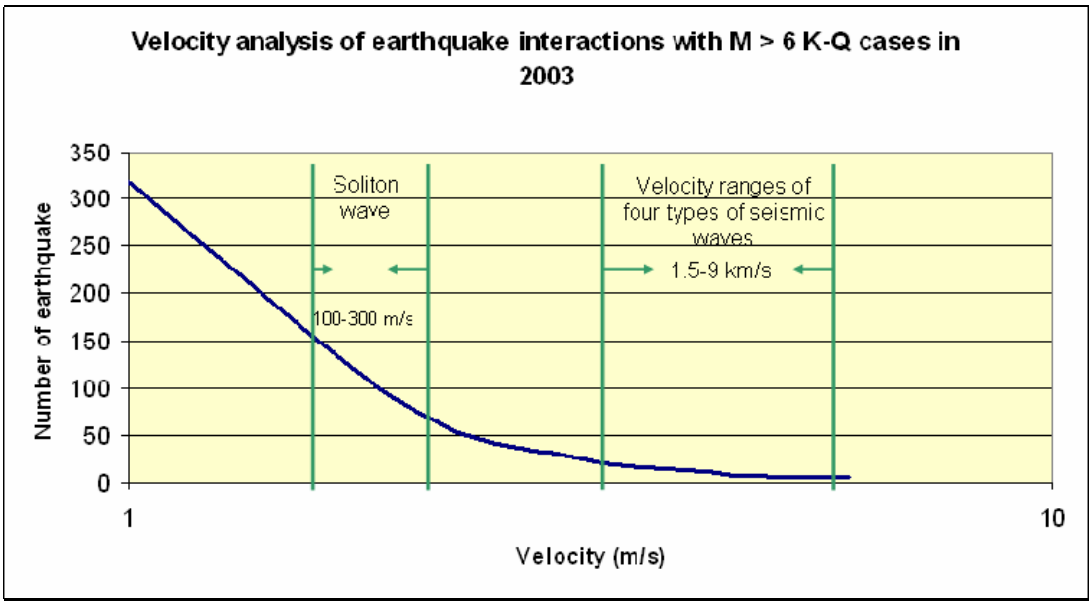

Figure 6.17: Graph shows distribution of earthquake interactions with different seismic wave velocities in logarithmic scale.

Comparison these two graphs (Figure 6.16 and 6.17) with Figure 6.11 and Figure 6.12, no significant changes are observed and they give an analogous picture to the previous plots, although in Figure 6.17, any "bump" at higher velocities has totally disappeared. Therefore, these results show that hypothesis remains a possibility, but there are issues that exist with the data and the approach to the analysis.

Some cases are shown in Figures 6.18, 6.19, 6.20, and 6.21, where a K earthquake may well have emitted the necessary secondary earthquake trigger (Q1, Q2, Q3…) within the assumed velocity range, simply for illustration.

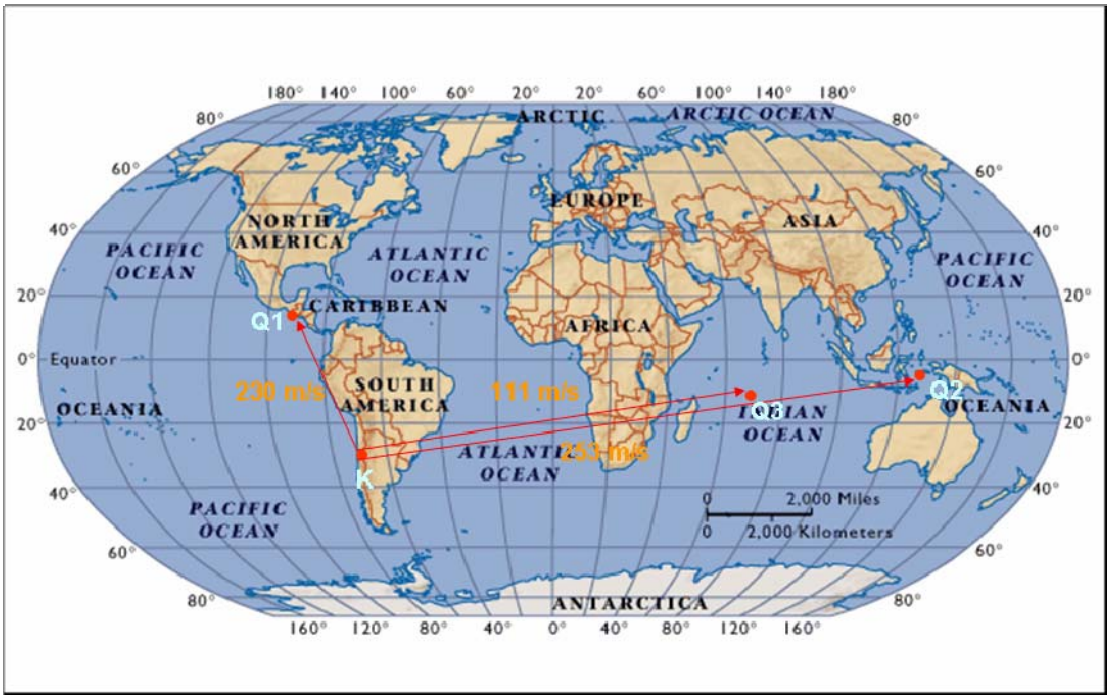

Figure 6.18: Interactions between (K) primary earthquake and Q1, Q2, and Q3 secondary earthquakes in response to velocities of an assumed soliton wave packet (modified after Mapquest 2002).

In Figure 6.18 it is considered that a primary earthquake occurred on May 27, 2003 at San Juan province, Argentina, with magnitude of 5.7 that may have promoted three secondary earthquakes, Q1 at Mexico-Guatemala border region, Q2 at Java, Indonesia, and Q3 at Mauritius-Reunion region with 230 m/s, 253 m/s, and 111 m/s respectively.

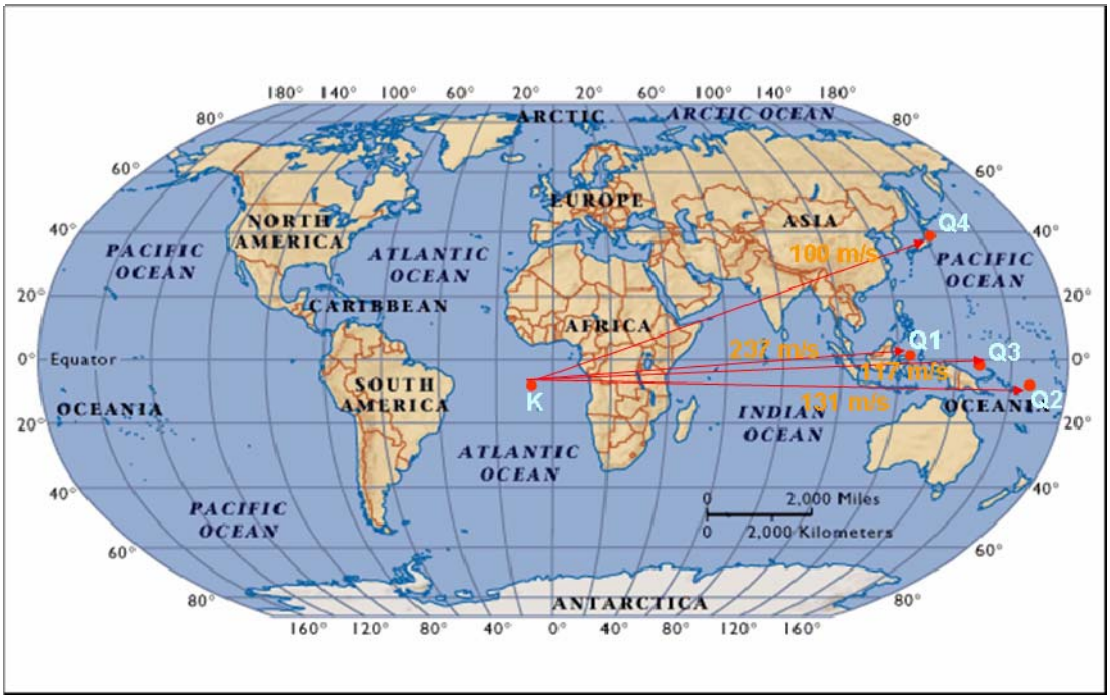

Figure 6.19: Interactions between (K) primary earthquake and possible Q1, Q2, Q3, and Q4 secondary earthquakes triggers at a velocity characteristic of the soliton wave packet (modified after Mapquest 2002).

It is assumed that a primary earthquake occurred on July 23, 2003 at Southern Mid-Atlantic Ridge, with magnitude of 5.6 that may have triggered four secondary earthquakes, Q1 at Minahassa Peninsula Sulawesi, Indonesia, Q2 at Santa Cruz Islands region, Q3 at New Ireland region Papua New Guinea, and Q4 at Eastern Honshu, Japan, with 237 m/s, 132 m/s, 118 m/s and 100 m/s respectively, as shown in Figure 6.19.

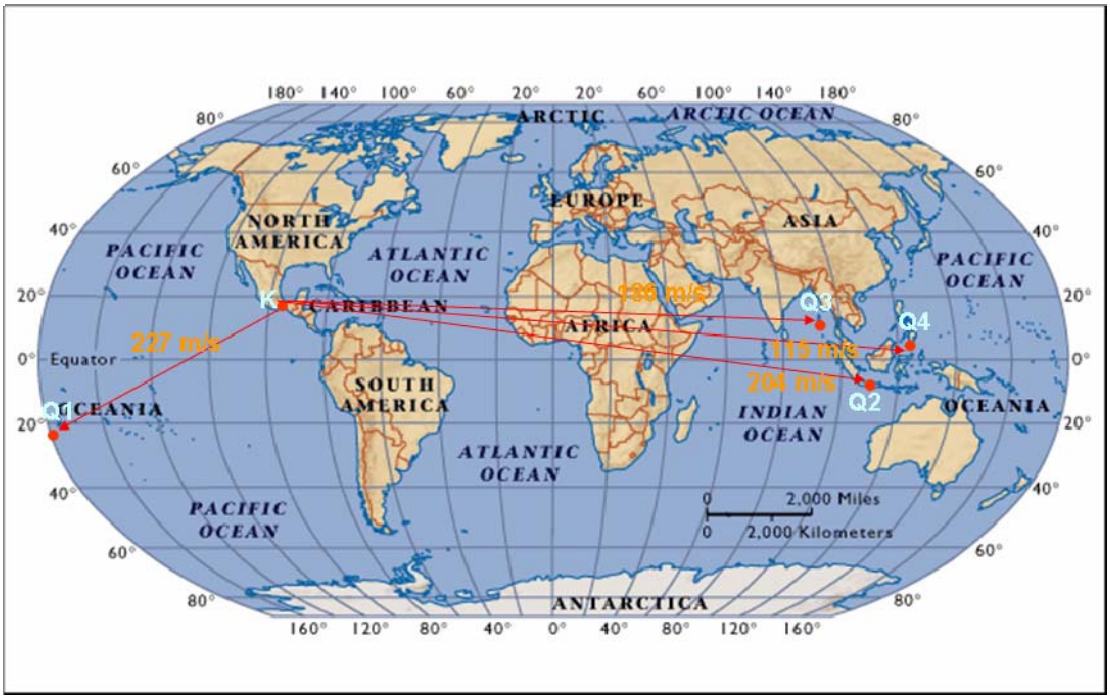

Figure 6.20: Interactions between (K) primary earthquake and Q1, Q2, Q3, and Q4 secondary earthquakes in response to soliton wave packet (modified after Mapquest 2002).

In Figure 6.20 it is also considered that a primary earthquake occurred on November 19, 2003 at Guerrero, Mexico, with magnitude of 4.8 that may have promoted four secondary earthquakes, Q1 at South of Fiji Islands, Q2 at South of Java, Indonesia, Q3 at Andaman Islands, India, and Q4 at Northern Molucca Sea, Indonesia with 227 m/s, 204 m/s, 186 m/s and 115 m/s respectively.

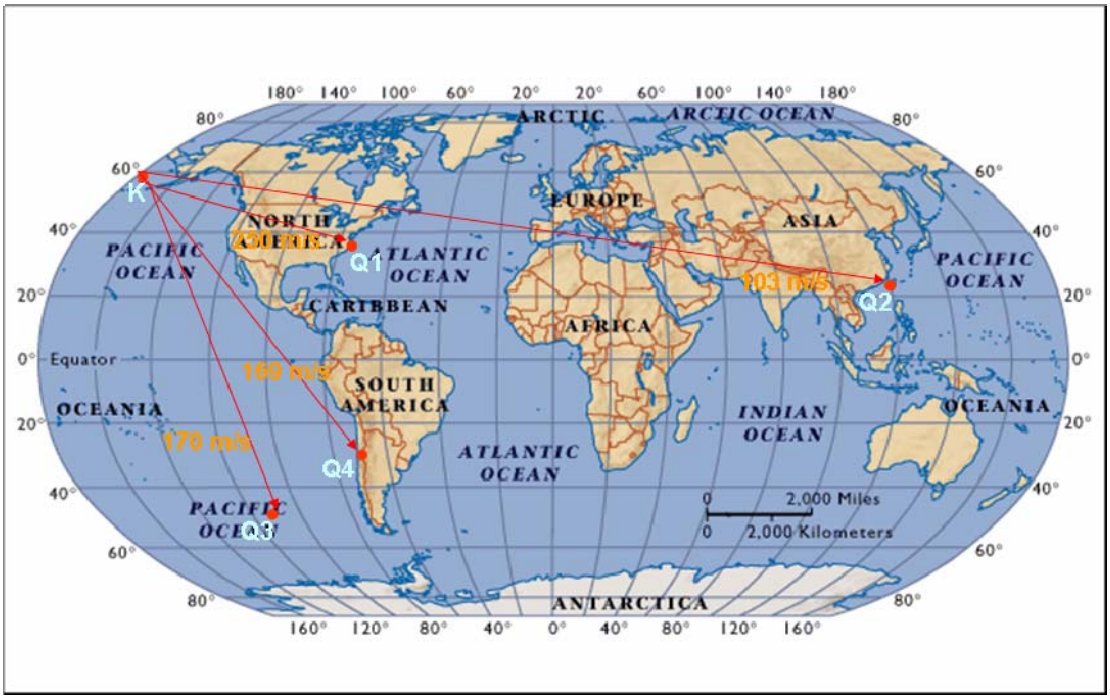

Figure 6.21: Interactions between (K) primary earthquake and Q1, Q2, Q3, and Q4 secondary earthquakes in response to soliton wave packet (modified after Mapquest 2002).

It is considered that a primary earthquake occurred on December 9, 2003 at Aleutian Islands, with magnitude of 6 that may have triggered promoted four secondary earthquakes, Q1 at Virginia, Q2 at Taiwan, Q3 Southern East Pacific Rise, and Q4 at near coast of Northern Chile, with 250 m/s, 103 m/s, 170 m/s and 160 m/s respectively, as shown in Figure 6.21.

6.2.2 Depth Analysis

A graph is plotted to find out how many earthquakes in 2003 occurred at what depth according to the Earth's interior classification, as shown in Figure 6.22. It is observed that most of earthquakes normally occurred at 0-40 km deep into the Earth. This zone is made of crustal rocks which have microscopic cracks and pores which are undoubtedly liquid saturated (Sato and Fehler 1998). Soliton excitation can increase the pore pressure and therefore can alter the effective stress field, and this process may lead to the trigger of an

earthquake or fault slip in the rocks (or microseismic, geyser and water level activity). The distant earthquake or fault can only be triggered if the primary emits the right frequencies at a large enough amplitude to cause a large soliton to be emitted and to intersect a critically stressed zone at a remote place.

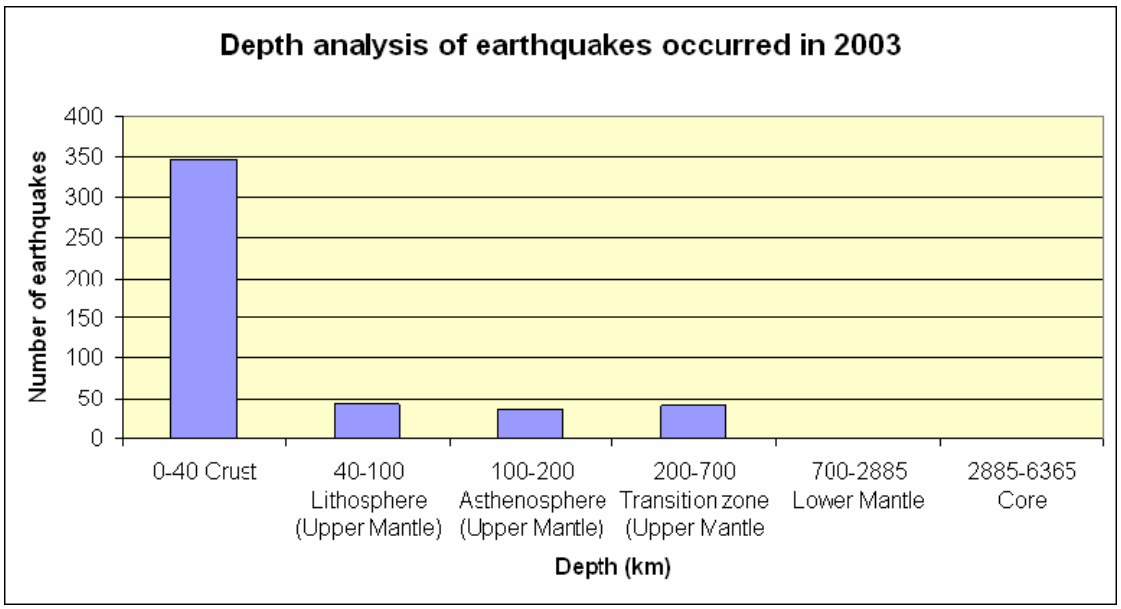

Figure 6.22: Graph showing earthquakes at different depths in the Earth, 2003.

A small number of earthquakes occurred in the lithosphere, asthenosphere, and transition zones. At these depths, it is not likely that there is interconnected pore space that would permit a large soliton (water-solid coupling) to be emitted by the source. Also, once below a depth of 40 km, the magnitude of earthquakes drops rapidly. Furthermore, seismic waves are generally reduced in energy by travelling deep within the Earth due to the presence of heterogeneous material. Therefore, most of earthquakes are triggered in the crustal zone where there is potentially a pressure effect from the soliton energy. Of course, in the lower mantle and core zone, no seismic events are found because high temperature and pressure within solid rocks leads to viscous flow rather than stick-slip behaviour.

6.3 Hydrological Responses

Fluid level changes in wells have been observed worldwide at remote distances after large earthquakes, such as in the United States, where water level fluctuations were recorded in 716 wells after the Alaska earthquake of magnitude 8.5 in 1964 (Beresnev and Johnson 1994). Moreover, it has been observed that water level fluctuations have been noticed to take place long after P-wave, S-wave, surface wave, Stoneley wave, and others waves had passed (Plafker and Kachadoorian 1966).

For an example, water level changes occurred in observation well Vw-1 (Van Wert County), USA in response to the Alaska earthquake (ONDR 2006). The Vw-1 well is the most sensitive well in the network to earthquakes and it fluctuated 5.8 feet, as shown in Figure 6.23. This fluctuation is clearly affected by the energy emitted from the epicenter of the earthquake, and these waves as they passed through the area apparently caused an alternating contraction and expansion of the aquifer material which resulted in the water level rises and dips in the well. However, no known earthquake wave has such a low frequency of dilation and contractile excitation. Of course, an alternative explanation is that pore pressure responses could be the source of this behaviour, and the pore pressures are affected by the soliton wave packet transit.

By interpreting the graph, it seems that the water level began to rise approximately 10 or 12 hours after the Alaska earthquake. Well Vw-1 is located about 4812 km away from the earthquake, as the location of Alaska earthquake has occurred on the global coordinate of 61.04° N 147.73° W (Christensen 2006) and Vw-1 well is located on 40.13° N 84.52° W (Mapquest 2002). Interaction between the earthquake (Alaska earthquake) and the water level flux (Vw-1 well) is with a 111 m/s velocity, which is in the soliton wave velocity range (100-300 m/s) and can be considered as a possible connection among them due to a soliton wave packet (Figure 6.23 shows the time window of arrival of a soliton packet with respect to the timing of the primary earthquake.

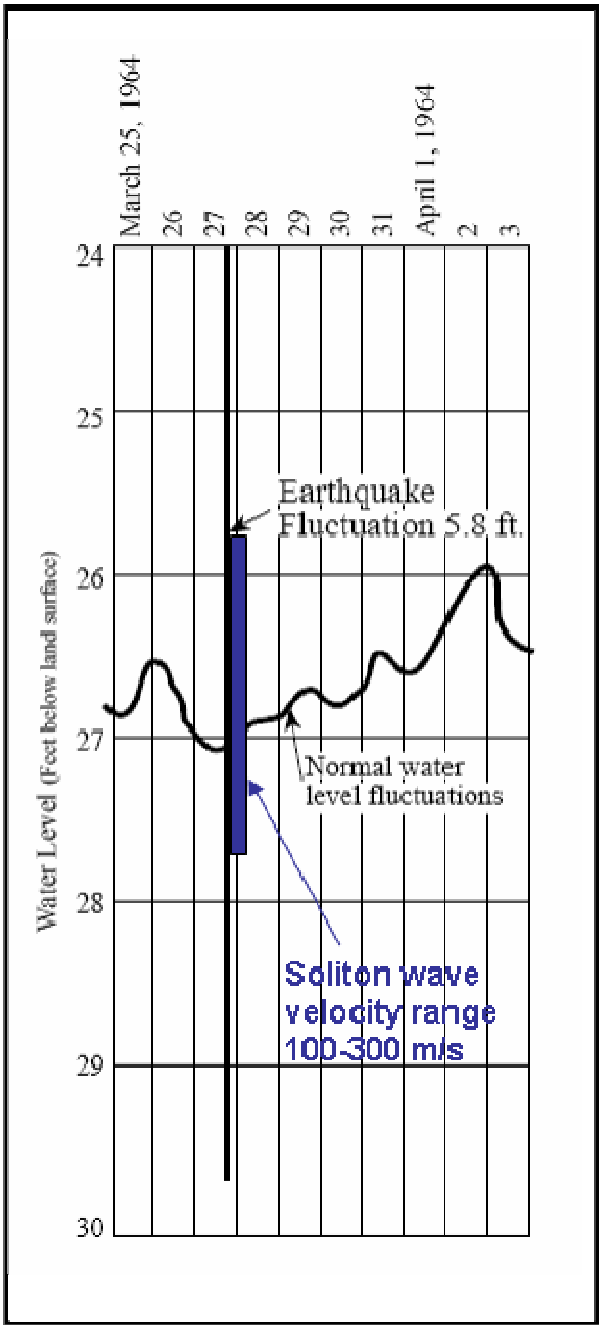

Figure 6.23: Water level rises of 5.8 feet in well Vw-1feet in response to Alaska earthquake (ODNR 2006).

If the fluctuation had occurred due to P-wave, S-wave and other waves, it would be evidenced as a rise or a fall within an hour of the event, as these waves propagate with 1.5-9 km/s speed, which is clearly not the case here. Furthermore, temporal but relatively short-period water level variations depend on other factors such as direction and

magnitude of seismic waves and the structure of the reservoirs. Therefore, interaction between earthquakes and hydrological changes may be due to soliton waves, which is a reasonable postulation but not yet proven because of a lacking of precise timing data for wells. There is other evidence to support the existence of a low velocity energy transmission speed. (There is clear need for a detailed timing study of well data with respect to large and relatively shallow earthquakes.)

Water level fluctuations have been observed in 18 wells at the Eskisehir region, NW Turkey in response to the Izmit earthquake which occurred on August 17, 1999 with magnitude of 7.4 and the Duzce earthquake which occurred on November 12, 1999 with magnitude of 7.2, as shown in Figure 6.24. These wells are situated 118-216 km away from the epicenters (Yaltirak et al. 2005).

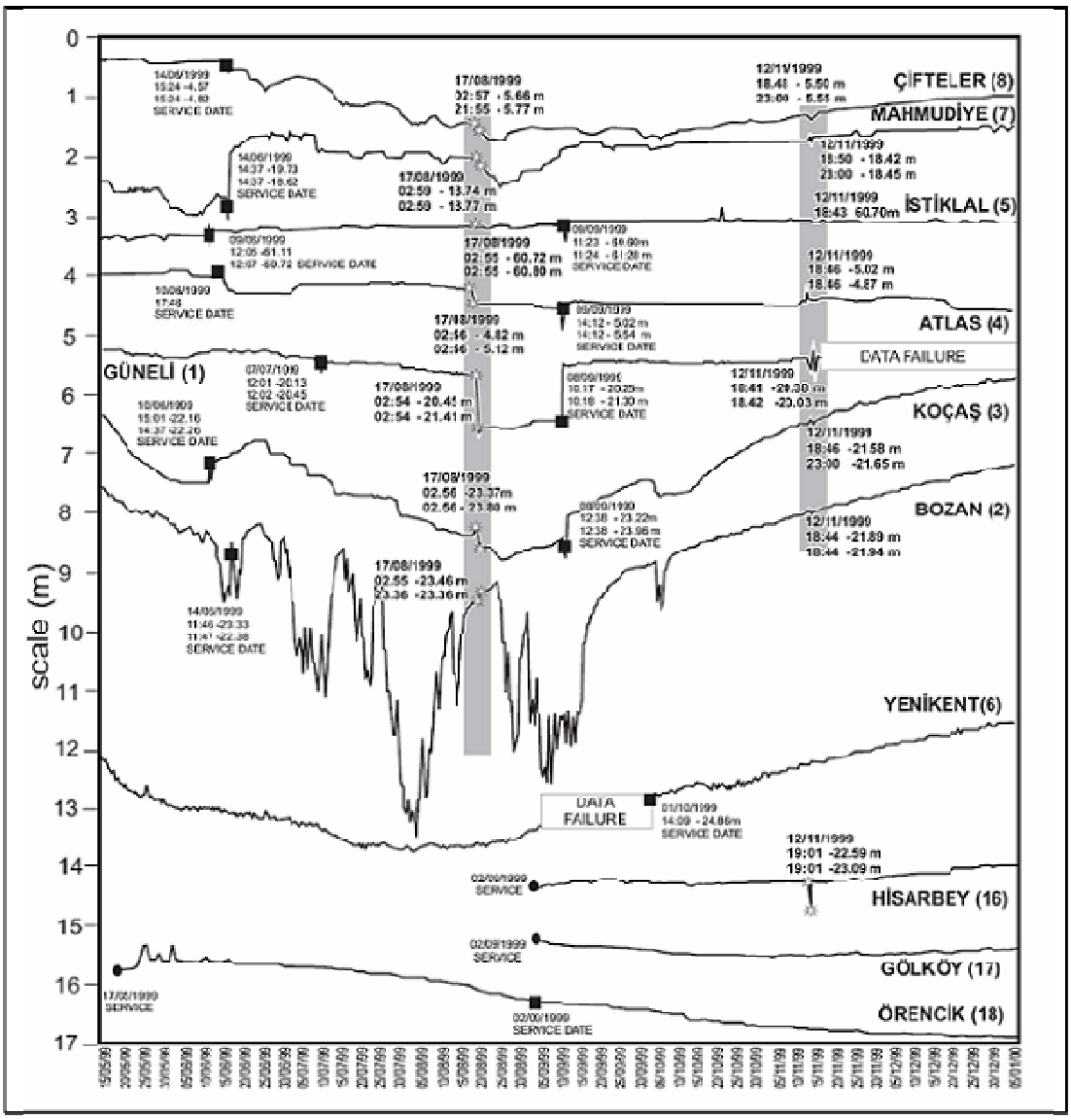

Figure 6.24: Water level variations in wells at Eskisehir area, NW Turkey in response to Izmit and Duzce earthquakes (Yaltirak et al. 2005)

Yaltirak claims that the changes in water level in wells at Eskisehir region shows through a common computer whether due to coseismic deformation or surface waves (Yaltirak et al. 2005).

In another example of water level changes in response to remote distance earthquakes, groundwater observation wells in Virginia, Florida (USA) displayed significant

fluctuations in response to the large Indonesian earthquake triggered on December 26, 2004 with magnitude of 8.5, as shown in Figure 6.25 (McBride 2005). The earthquake resulted in destructive tsunamis transmitted throughout the Indian Ocean. The wells are located 16617 km away from the epicentre, yet one well demonstrated a sudden rise in water level of approximately 2 feet. The well did not regain totally from the seismic waves intrusion for approximately 5 hours. An abrupt rise in water level of about 0.25 to 0.5 feet has been recorded in four wells at west-central Florida, as shown in Figure 6.18. The water levels did not recover completely from the seismic disturbance for almost 24 hours (McBride 2005).

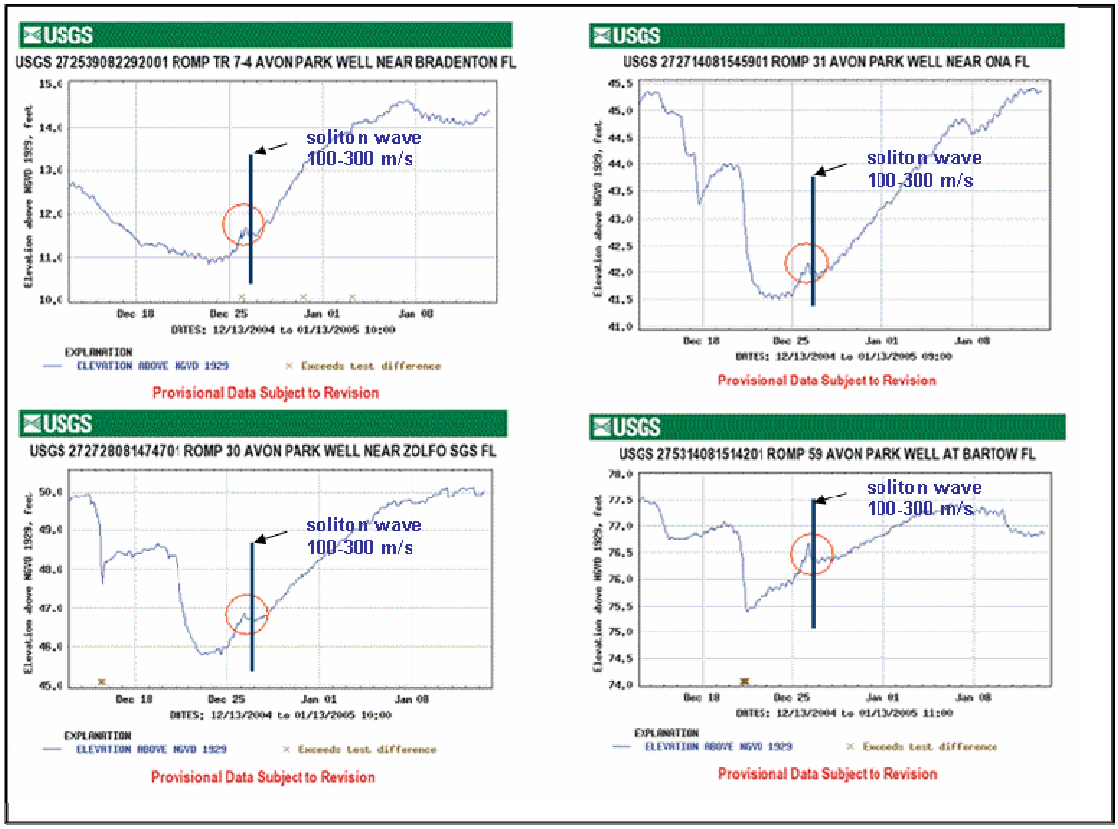

Figure 6.25: Water level variations shows in wells at Florida region in response to the 2004 Boxing Day Indonesian earthquake, blue bars represent the arrival window of a soliton wave with v = 100-300 m/s (McBride 2005).

The above Figure 6.25 shows that the water level fluctuations in Florida wells may be due to the arrival of a soliton wave packet generated from the Indonesian earthquake. The blue bars are marked approximately at the timing for the soliton wave velocity range. In general, based on these figures, a slightly higher velocity of energy transmission than the soliton wave seems to be the case.

More examples of water level variation in response to earthquakes are discussed in Chapter 3. It is still unclear what kind of wave is responsible for the alteration of water level in wells and flow rates in streams. As a general conclusion from these and other studies, the magnitude and perseverance of liquid level fluctuations in wells in response to earthquakes are related with the earthquake magnitude and depth, the distance from the epicenter, the hydrological environment, and whether the rock mass is a consolidated rock or an unconsolidated sediment.

6.4 Summary

The velocity data analysis in the above graphs, as shown in Figure 6.9, 6.10, 6.11, 6.12, 6.14, 6.15, 6.16 and 6.17 provide some support that a soliton energy packet propagating with 100-300 m/s velocity can induce sympathetic earthquakes, as much earthquake interaction is found in this range, and there is little or no evidence that any other velocity range is preferred. Other seismic waves propagate too fast, at a velocity range from 1.5 to 9 km/s, and it is appears to be unlikely, given the data base, that these waves can trigger other secondary earthquakes, as only a few cases in above graphs are found (expected just from random fluctuations). There are also physical arguments against the other body waves and surface waves as triggers (strain amplitude, depth of penetration).

Some limitations are encountered in trying to find demonstrate the existence of a soliton wave using a data base such as the IRIS system. It does not record earthquakes with magnitude of less than 2.8, and from Figure 6.13 it appears that the real effective filtering level is around a magnitude of 5.0 or a little higher. Thus, there is no certainty that a shallow earthquake of magnitude 5.0 in a remote location is actually recorded on the IRIS data base for 2003. This means that potentially triggered earthquakes of lower magnitude

are not reliably and consistently sampled. If a large earthquake occurs that might trigger secondary earthquakes with magnitude of less than this limit of 4.5-5 at a remote distance, these earthquakes are not recorded. This restriction impairs the use of IRIS to reveal the existence of soliton wave. It would perhaps have been best to look at large earthquakes worldwide, but examine only possible secondaries in a highly monitored region such as the United States or Europe.

In this thesis, only one year of earthquake interactions on IRIS is analyzed, but for better science, the data base must be expanded more than 20 years of earthquake interactions, perhaps with magnitude of 7 or above, which is more likely to be a mechanism of triggering a sufficiently large amplitude soliton wave packet.

Seismic coupling among earthquakes is possibly excited by the soliton phenomenon. The velocity of the soliton depends on the compressibility of the liquids and the matrix, as well as the liquid viscosities and the permeability of the material. It can only travel in a porous and permeable zone, but it does tend to be internally reflected in these zones (wave-guide effects?) because it does not travel into less permeable or impermeable rocks, because in these cases fluid may not move into and out of the pores. If fluid moves into and out of the pores, a broad frequency excitation process such as an earthquake promotes propagation of a soliton that is similar to a tsunami, and can travel great distance with a small loss of energy. This chapter has not proven the existence of the soliton as a trigger, but it has pointed out directions to take, and has shown some intriguing information that is suggestive of a low-velocity triggering mechanism.

Chapter – 7

Conclusions and Future Work

7.1 Conclusions
7.2 Future Work

7.1 Conclusions

After qualitative and quantitative analysis of earthquake interactions and hydrological changes in response to a hypothesized soliton wave packet the following conclusions and future work can be seen.

- The new dynamic-diffusion theory by Spanos predicts the existence of a low velocity wave called a soliton wave, which appears to provide a mechanism for the transmission of a suitable amount of energy into remote systems; its existence cannot be derived from Biot-Gassmann and Darcy flow formalism.
- The dynamic-diffusion theory predicts that this kind of wave can be found only in cases of liquid-solid coupling. The excitation of a soliton wave can be generated only when pore liquid performs incompressibly, as the soliton is a displacement wave like a tsunami.
- The results from the graphs illustrate that earthquake interactions may be due to a soliton wave. The graphs give a reasonable window of possible trigger velocities to support the hypothesis but not prove it. The frequency of earthquake interactions due to the predicted velocity of a soliton wave ~100-300 m/s is higher than the other seismic waves such as P-wave, S-wave, and surface waves, as these waves are propagating geometrically with approximately 1.5 to 9 km/s after a seismic event. Hence the probability of secondary earthquakes in response to a primary earthquake may be due to a soliton wave.
- The sensors (geophones, hydrophones, seismometer e.g.) are not installed under the water table or liquid-solid coupling zone (saturation zone) in current seismic recording systems. Thus, it is hard to detect the soliton wave and the recording is not long enough to identify its existence in coda because the soliton wave is a slow wave (100-300 m/s) as compared to other seismic waves (1.5-9 km/s).
- Geyser eruption activity can be affected in response to soliton wave because the study of geyser eruption behaviour showed that after passing the wave train, the frequency of geyser eruption has been increased, it is still unclear that what kind of wave alters the frequency of geyser eruption due to absence of timing data.

- Fluid level fluctuation in wells or in streams is reported due to earthquakes. The precise timing data is unavailable so it is hard to confirm what kind of wave has potential to promote the changes.
- It is also found that generally big (M > 5) earthquakes seem to trigger secondary earthquakes and alter fluid levels in wells and even to induce remote microseismicity.

7.2 Future Work

- New displacement (soliton wave) theory experiments should be executed in the laboratory for better understanding its mechanism and effects.
- The soliton wave detection may be found if highly precise accelerometers or pressure sensors which can measure at low frequency range from 10^{-2} to 10^{0} Hz are placed under the water table, in the liquid-saturated zone (porous media zone).
- Seismic recording systems must be measured in long time span recording of the earthquakes to accomplishment of better science. Therefore a soliton wave existence may be discovered as a long wavelength response if the sensors are properly coupled to the liquid-solid phases.
- An array of highly precise sensors, properly located, should be placed over tectonically active zones to obtain more useful information about the physical mechanisms.
- Fluid wells should be monitored continuously and timing data must be recorded precisely in response to earthquakes for obtaining the phenomenological approach data needed to verify velocities.
- The possible earthquake interactions data base should be expanded to cover a longer time period, perhaps 20 years, and perhaps the analysis should be limited to only large earthquakes with magnitude of 6 and above (or 7 and above).
- Because triggered secondary earthquakes are not likely to be large ones, it is suggested that the secondary data base be generated from an area that has more detailed seismic coverage for low magnitudes, such as the USA.

Appendix

Possible Earthquake interactions Velocity Data

Possible earthquake interactions velocity data is produced by calculating velocity between (K) primary earthquake and (Q1, Q2, Q3…) secondary earthquakes. The distance between K and Q is calculated by using website http://www.indo.com/cgi-bin/dist. The velocity is computed by using following equation:

$$V = \frac{S}{T} = \frac{Q - K}{Qt - Kt}$$

Table A-1: Earthquake interactions K-Q cases due to a hypothesized soliton excitation with a velocity range of 100-300m/s.

No.	K Primary earthquake location	K Magnitude (M)	K Depth (km)	Q Secondary earthquake location	Q Magnitude (M)	Q Depth (km)	Velocity (m/s)
1	Southern Mid-Atlantic Ridge	5.6	10	Near coast of Michoacan, Mexico	4.3	33	132
2	Near coast of Michoacan Mexico	4.3	33	Fiji Islands region	6	377	156
3	Central Alaska	5.1	5	1.Luzon Philippine Islands 2.Chile-Argentine border region	5.6 6	33 111	186
4	Chile-Argentina border region	6	111	Tonga Islands	5.6	33	119
5	Fiji Islands Region	5.8	33	Guerrero Mexico	5	62.1	111
6	Northern Sumatra Indonesia	5.8	33	Guerrero Mexico	5	62.1	222
7	Guerrero Mexico	5	62.1	New Ireland region P.N.G	6.6	71.9	299
8	Kodiak Island region	5.1	32.3	Off coast of Oregon	5.3	10	288
9	Coast of Oregon	4.9	10	Coast of Oregon	6	10	106
10	Solomon Island	7.5	33	Solomon Island	6.3	10	187
11	Near coast of Guatemala	6.3	33	Fiji Island region	5.1	512.7	143
12	Fiji Island region	5.1	512.7	1. Near coast of Jalico, Mexico 2. Near coast of Jalico, Mexico	5.5 5.1	10 10	118 115
13	Near coast of Michoacan, Mexico	4.7	33	Near coast of Michoacan, Mexico	4.7	33	187
14	Northern Sumatra, Indonesia	5.8	33	1. Near coast of Jalico, Mexico 2. Near coast of Jalico, Mexico 3. Near coast of Michoacan, Mexico	5.5 5.1 4.3	10 10 10	272 264 143
15	Turkey	6	10	Prince Edward Island region	6.2	10	213
16	Prince Edward Island region	6.2	10	Minahassa peninsula Sulawesi	5.5	33	153
17	South Sandwich Island region	5.3	76.7	1.Tonga Island 2. Sakhalin Island	5.5 5.4	113.7 33	248 150
18	Tonga Island	5.5	113.7	1.South Indian ridge 2.Sakhalin Island	5.6 5.4	10 33	237 107
19	South of Fiji Island	5.2	591.9	1.Southern Iran 2.Bouvet Island region	5.5 5.5	33 10	210 101
20	Tonga Island	5.5	33	Bouvet Island region	5.5	10	169
21	Southern Iran	5.5	33	1.Bouvet Island region 2.Luzon Philippine Island	5.5 5.6	10 10	225 103
22	Samara Philippine Island	6.3	10	Virgin Island	4.6	43.6	104
23	Revilla Gigedo Island region	4.6	10	Hokkaido Japan region	5.4	212	116
24	South of Fiji Island	5.2	253.8	Southern California	5.2	2.9	116
25	Southern California	4.5	3	Southern Xingjian China	6.3	33	106
26	Southern California	3.4	5	Southern Xingjian China	6.3	33	194

27	Southern Xingjian China	6.3	33	Southern California	4.5	3.9	124
28	Irian Jaya region Indonesia	5.7	33	Southern mid Atlantic ridge	5.7	10	121
29	Banda Sea	5.1	585.2	Southern mid Atlantic ridge	5.7	10	203
30	Halmahera Indonesia	6.1	33	Kermadec Island region	5.5	147.9	234
31	New Ireland region P.N.G.	6.8	33	Southern Xingjian China	5.7	33	119
32	New Britain region P.N.G.	5.9	33	South Xingjian China	5.7	33	124
33	Southern Xingjian China	5.7	33	Gulf of California	6.1	10	185
34	Gulf of California	6.1	10	1.Balleny Island region 2.Irian Jaya region Indonesia	5.6 6.2	10 33	126 111
35	Tonga Island	6.1	274.6	Off east coast of Kamchatka	5.8	33	181
36	South western Atlantic Ocean	5.5	10	1.Rat Island Aleutian Island 2.Rat Island Aleutian Island	6.8 6.2	33 33	174 147
37	Sea of Japan	5.3	362.1	Solomon Island	5.9	33	231
38	Vanuatu Island region	5.7	39.3	Southern Molucca Sea	5.5	33	142
39	Andaman Island India	5.7	33	1.Solomon Island 2.Gurrero Mexico	5.5 4.8	33 33	227 164
40	Solomon Island	5.5	33	Gurrero Mexico	4.8	33	175
41	Tonga Island	5.9	40.9	1.Hindu Kush region Afghanistan 2.Adriatic Sea	5.8 5.5	33 33	185 187
42	Hindu Kush region Afghanistan	5.8	33	Adriatic Sea	5.5	33	220
43	Adriatic Sea	5.5	33	1.Seram Indonesia 2.New Britain region P.N.G.	6 6	33 33	136 124
44	Seram Indonesia	6	33	New Britain region P.N.G.	6	33	107
45	Northern mid Atlantic ridge	5.6	10	South of Fiji Island	5.3	478.6	255
46	Northern Alaska	5	16	South of Fiji Island	5.3	55.6	193
47	Vanuatu Island region	5.6	33	Near east coast of Honshu Japan	5.5	55.6	124
48	Aegean Sea	5.6	10	South of Panama	6.1	10	106
49	Qinghai Island region	6.2	14	1.Bouvet Island region 2.Southern Alaska	6 3.8	10 61	270 109
50	Western Brazil	5.9	545.7	1.South west of Sumatra Indonesia 2.Kuril Island	5.7 6	33 62.5	142 103
51	Tonga Island	6	33	Southern Xingjian China	5.6	10	101
52	New Ireland region P.N.G.	5.7	33	Prince Edward Island	6.1	10	136
53	Vanuatu Island	5.5	87.2	San Juan province Argentina	5.5	115.4	165
54	San Juan province Argentina	5.5	115.4	Fiji Island	6	564.2	221
55	Northern Algeria	6.7	10	South eastern Alaska	4.5	5.2	259
56	Northern Algeria	5.7	10	South eastern Alaska	4.5	5.2	262
57	South of Panama	5.9	10	Arabian Sea	5.8	10	280
58	Near east coast of Honshu Japan	6.9	52.8	1.Halmahera Indonesia 2.San Juan province Argentina 3.Mexico-Guatemala border region	7 5.7 4.6	33 117.9 200	119 206 109
59	Halmahera Indonesia	7	33	1.Mexico-Guatemala border region 2.Northern Algeria	4.6 5.8	200 10	209 163
60	Mindanao Philippine Island	6.8	559.7	1.Mexico-Guatemala border region 2.Northern Algeria	4.6 5.8	200 10	263
61	San Juan province Argentina	5.7	117.9	1.Mexico-Guatemala border region 2.Jawa Indonesia 3.Mauritius reunion region	4.6 5.2 5.9	200 65.9 10	230 253 111
62	Mexico-Guatemala border region	4.6	200	Mauritius reunion border	5.9	10	197
63	Northern Algeria	5.8	10	1.Mauritius reunion region 2.Near coast of Peru	5.9 5.6	10 41.4	108 103
64	Java Indonesia	5.2	65.9	1.Near coast of Peru 2.Vancouver Island region	5.6 4.6	41.4 10	243 128
65	Near coast of Peru	5.6	41.4	Vancouver Island region	4.6	10	295
66	Vanuatu Island	5.6	35	1.Off coast of Oregon 2.Off coast of Mexico 3.Caibbean Sea	4.5 5.8 4.9	10 10 10	166 147 125
67	Near coast of Peru	5.8	33.1	Off coast of Oregon	4.5	10	189
68	Off coast of Oregon	4.5	10	1.Caribbean Sea 2.Kermadec Island New Zealand	4.9 5.8	10 114	121 140
69	Off coast of Mexico	5.8	10	Kermadec Island New Zealand	5.8	114	160
70	Kermadec Island New Zealand	5.8	114	Tennessee	4.5	10	119
71	Tennessee	4.5	10	New Britain region P.N.G.	6.7	33	296

72	Banda Sea	5.5	33	Taiwan region	5.5	33	218
73	Central east Pacific rise	5.7	10	Solomon Island	5.7	404.9	124
74	Western Brazil	6.7	553	1.Near coast of central Chile	6.9	36.9	99
				2.Banda Sea	5.9	165.5	189
75	Off coast of Michoacan Mexico	4.7	10	Banda Sea	5.9	165.5	185
76	Near coast of central Chile	6.9	36.9	Banda Sea	5.9	165.5	234
77	Rat Island Aleutian Island	6.9	30	Southern Iran	5.6	61.9	137
78	Mariana Island	4.9	400	Northern mid Atlantic ridge	5.5	10	192
79	Southern Iran	5.6	61.9	Northern mid Atlantic ridge	5.5	10	146
80	Northern mid Atlantic ridge	5.5	10	Luzon Philippine Island	5.6	10	116
81	Off coast of northern California	4.3	10	Luzon Philippine Island	5.6	10	281
82	Near north coast of New Guinea	6.1	33	Leeward Island	5.1	33	141
83	Leeward Island	5.1	33	1.Celebes Sea	6	607.9	163
				2.Samar Philippine Island	5.8	33	112
84	Celebes Sea	6	607.9	Off coast of central Mexico	5.1	10	156
85	Samara Philippine Island	5.8	33	Off coast of central Mexico	5.1	10	272
86	Off coast of central Mexico	5.1	10	1.Hokkaido Japan region	5.7	23.1	141
				2.Tonga Island	5.7	33	97
				3.New Britain region P.N.G.	5.5	33	98
87	Hokkaido Japan region	5.7	23.1	New Britain region P.N.G.	5.5	33	113
88	Tonga Island	5.7	33	1.New Britain region P.N.G.	5.5	33	163
				2.Svalbard region	5.8	10	154
89	New Britain region P.N.G.	5.5	33	Svalbard region	5.8	10	177
90	Turkey	5.6	10	1.Xizang	5.7	33	130
				2.Western Brazil	5.2	517.5	97
91	Vanuatu Island	5.7	86.2	1.Xizang	5.7	33	296
				2.Western Brazil	5.2	517.5	120
92	Xizang	5.7	33	1.Western Brazil	5.2	517.5	223
				2.Chiapas Mexico	4.6	139.1	117
93	Western Brazil	5.2	517.5	1.Near north coast of New Guinea	5.4	45.1	155
				2.Ryuyu Island	5.5	60	121
94	Chiapas Mexico	4.6	139.1	1.Near north coast of New Guinea	5.4	45.1	250
				2.Ryukyu Island	5.5	60	144
95	Near north coast of New Guinea	5.4	45.1	Ryukyu Island	5.5	60	132
96	Southern Iran	5.5	10	Negros Philippine Island	5.6	33	98
97	Southern Iran	5.5	10	Negros Philippine Island	5.6	33	101
98	Turkey	5.5	10	El Salvador	5.2	33	174
99	El Salvador	5.2	33	1.Southern Sumatra Indonesia	5.3	145.8	223
				2.Carlberg ridge	7.6	10	103
100	Carlsberg ridge	7.6	10	Off coast of Jalico Mexico	5.2	33	106
101	Carlsberg ridge	5.6	10	Off coast of Jalico Mexico	5.2	33	122
102	New Britain region P.N.G.	6.3	190.1	Minahassa peninsula Sulawesi	5.5	33	137
103	Yunnan China	5.9	10	1.Nicobar Island	5.5	10	157
				2.Minahassa peninsula Sulawesi	5.5	33	233
				3.Vanuatu Island	5.7	33	167
104	Nicobar Island India	5.5	10	Vanuatu Island	5.7	33	258
105	Minahassa peninsula Sulawesi	5.5	33	Vanuatu Island	5.7	33	158
106	Vanuatu Island	5.7	33	Southern mid Atlantic ridge	5.6	10	126
107	Southern mid Atlantic ridge	5.6	10	1.Minhassa peninsula Sulawesi	5.7	33	237
				2.Santa Cruz Island region	5.5	68.6	132
				3.New Ireland region P.N.G.	6.4	50.6	118
				4. Eastern Honshu Japan	5.5	33	98
108	Santa Cruz Island region	5.5	68.6	1.New Ireland region P.N.G.	6.4	50.6	108
				2.Eastern Honshu Japan	5.5	33	157
109	New Ireland region P.N.G.	6.4	50.6	1.Eastern Honshu Japan	5.5	33	227
				2.Eastern Honshu Japan	6.1	6	101
				3.Near east coast of Honshu Japan	6.1	33	101
110	Eastern Honshu Japan	5.4	33	1.Fiji Island region	5.8	199.5	121
				2.Fiji Island region	5.2	412.8	107
111	Tonga Island	5.3	226.1	Near southeast coast of Russia	6.7	481.4	142
112	India-Bangladesh border region	5.6	10	Near southeast coast of Russia	6.7	481.4	192
113	Fiji Island region	5.8	199.5	Fiji Island region	5.2	412.8	117
114	Bouvet Island region	5.5	10	1.Cuba region	4.7	10	252
				2.Kodiak Island region	5.3	33	101

115	Northern mid Atlantic ridge	5.8	10	Kodiak Island region	5.3	33	216
116	Kodiak Island region	5.3	33	1.Scotia Sea 2.Scotia Sea	7.3 5.4	10 10	183 137
117	Halmahera Indonesia	6	33	West of Macquarie Island	5.7	10	140
118	Halmahera Indonesia	5.5	10	West of Macquarie Island	5.7	10	141
119	Off coast of Jalico Mexico	5	10	1.West of Macquarie Island 2.Andaman Island India	5.7 5.9	10 101.1	285 221
120	Sumba region Indonesia	5	10	Greece-Albania border region	6.1	10	252
121	Greece-Albania border region	6.1	10	1.Off coast of northern California 2.Baja California Mexico	5.1 4.7	3.7 10	103 109
122	Baja California Mexico	4.7	10	North eastern China	5.7	24.4	114
123	Eastern Xizang-India border region	5.6	33	Fiji Island region	5	605.2	103
124	Fiji Island region	5	605.2	Southern Iran	5.7	20	102
125	Southern Iran	5.7	20	Northern Alaska	5.4	10	127
126	Northern Alaska	5.4	10	South Island New Zealand	5.5	26	109
127	Irian Jaya region Indonesia	5.5	33	South Island New Zealand	5.5	26	251
128	Java Indonesia	5.3	33	Near coast of Peru	5.6	31.2	206
129	Near coast of Peru	5.6	31.2	Banda Sea	6	410.2	139
130	Southern east Pacific	6.1	10	Central California	2.9	8.4	209
131	Southern Xingjian China	5.8	33	Tonga Island	6.2	10	187
132	South Island New Zealand	5.8	10	Northern Sumatra Indonesia	5.8	134.3	149
133	Northern Sumatra Indonesia	5.8	134.4	Central east Pacific rise	5.8	10	197
134	Central east Pacific rise	5.8	10	1.South Sandwich Island region 2.Southern Sumatra Indonesia	5.7 5.6	33 33	182 140
135	South Sandwich Island region	5.7	33	1.Southern Sumatra Indonesia 2.Loyality Island region 3.Loyality Island region	5.6 5.5 6.4	33 33 33	165 141 141
136	Southern Sumatra Indonesia	5.6	33	1.Loyalty Island region 2.Loyalty Island region	5.5 6.4	33 33	179 178
137	Loyalty Island region	5.5	33	Java Indonesia	5.9	46.9	109
138	Loyalty Island region	6.4	33	Java Indonesia	5.9	46.9	109
139	South of Australia	5.5	10	Mexico-Guatemala border region	4.6	179.7	149
140	Lake Baikal region Russia	5.6	33	Chile-Bolivia border region	6.1	127.3	132
141	South Sandwich Island region	5.4	116.8	Myanmar	6.7	10	158
142	Myanmar	6.7	10	Dominican Republic region	4.4	10	255
143	North of Association Island	6	10	1.Dominican Republic region 2.Dominican Republic region 3.Dominican Republic region	5.1 4.4 4.7	10 10 10	292 157 137
144	Dominican Republic region	5.1	10	New Ireland region P.N.G.	5.8	94.1	237
145	Hokkaido, Japan region	5.5	33	North of Svalbard	4.8	10	194
146	Hokkaido, Japan region	5.7	33	North of Svalbard	4.8	10	215
147	Hokkaido, Japan region	4.8	10	North of Svalbard	4.8	10	220
148	Tonga Island region	5.6	33	Hokkaido Japan region	5.6	33	113
149	North of Svalbard	4.8	10	Hokkaido Japan region	5.6	33	103
150	South western Siberia, Russia	7.5	17.6	Ryukyu Island	5.7	10	106
151	South western Siberia, Russia	5.7	33	Ryukyu Island	5.7	10	126
152	South western Siberia, Russia	6.3	33	Hokkaido Japan region	5.5	33	127
153	Hokkaido, Japan region	5.9	33	Scotia Sea	6	10	171
154	Hokkaido, Japan region	5.6	33	Scotia Sea	6	10	207
155	Kuril Island	5.3	117.6	1.New Britain region P.N.G. 2.Kermadec Island New Zealand 3.Kermadec Island New Zealand	5.6 6.3 6	33 33 33	103 116 110
156	New Britain region P.N.G.	5.6	33	1.Kermadec Island New Zealand 2.Kermadec Island New Zealand	6.3 6	33 33	183 154
157	Scotia Sea	6	10	1.Kermadec Island New Zealand 2.South western Siberia Russia	5.5 6.6	33 10	192 266
158	Central Alaska	4	70	Banda Sea	5.5	531.1	132
159	Santa Cruz Island region	5.8	33	Chiapas Mexico	4.5	149.6	167
160	Samoa Island region	6.1	33	Chiapas Mexico	4.5	149.6	234
161	Chiapas Mexico	4.5	149.6	1.Hokkaido Japan region 2.Hokkaido Japan region 3.Hokkaido Japan region	6.6 5.8 5.7	33 33 33	180 143 99
162	Hokkaido Japan region	5.8	33	Off coast of northern California	4.6	33	117

163	Hokkaido Japan region	5.7	33	Off coast of northern California	4.6	2.5	283
164	Off coast of northern California	4.6	2.5	Mindoro Philippine Island	6.1	33	188
165	Hokkaido Japan region	5.7	33	Fiji Island region	5.2	600	109
166	Fiji Island region	5.2	600	Southern Quebec Canada	4.5	18	273
167	Southern Quebec Canada	4.5	18	Fiji Island region	6	33	134
168	Fiji Island region	5.8	600	Dominican Republic region	4.7	10	139
169	Dominican Republic region	4.6	10	Yunnan, China	5.6	10	167
170	Dominican Republic region	4.7	10	1.Solomon Island 2.Southern Sumatra Indonesia	6.4 5.7	133.9 33	134 134
171	Solomon Island	6.4	133.9	1.Southern Sumatra Indonesia 2.Dominican Republic region	5.7 4.5	33 10	226 199
172	Southern Sumatra Indonesia	5.7	33	Dominican Republic region	4.5	10	300
173	South Sandwich Island region	5.4	142.2	Near north coast of Iran Jay	5.6	10	109
174	Off coast of Mexico	5.6	10	1.Russia-Mongolia border region 2.Western Caroline Island	5.5 5.5	10 33	170 118
175	Eastern New Guinea region P.N.G.	6.3	33	Russia-Mongolia border region	5.5	10	186
176	Russia-Mongolia border region	5.5	10	1.Western Caroline Island 2.Rat Island Aleutian Island	5.5 5.6	33 33	240 153
177	New Britain region	6	53.1	Dominican Republic region	4.8	10	208
178	Kuril Island	5.8	69.3	South Sandwich Island region	5.9	33	156
179	South Sandwich Island region	5.9	33	Off east coast of Honshu Japan	6.6	33	253
180	Off east coast of Honshu Japan	5.7	10	Off east coast of Honshu Japan	6.4	10	163
181	Near west coast of Colombia	6	33	1.Northern Molucca Sea 2.Vanuatu Island	5.9 6	10 112.6	151 104
182	Northern Molucca Sea	5.9	10	1.Vancouver Island region 2.South Sandwich Island region	4.6 5	10 33	100 101
183	Vanuatu Island	6	112.6	Kuril Island	5.7	66.7	128
184	Kuril Island	5.7	66.7	Vancouver Island region	4.6	10	134
185	Central mid Atlantic ridge	6.6	10	1.Kermadec Island region 2.Kermadec Island region 3.Volcano Island region	5.9 5.8 6.1	33 33 112.6	105 101 101
186	Kermadec Island region	5.9	33	Northern Molucca Sea	6.2	33	175
187	Kermadec Island region	5.8	33	1.Northern Molucca Sea 2.Off coast of central Chile	6.2 5.5	33 31.6	212 241
188	Near coast of Chiapas Mexico	4.7	33	Off coast of central Chile	5.5	31.6	199
189	Volcano Island region	6.1	112.6	1.Northern Molucca Sea 2.Gulf of California	6.2 5.5	33 10	142 275
190	Northern Molucca Sea	6.2	33	Near south coast of Honshu Japan	6.4	391.1	129
191	Off coast of central Chile	5.5	31.6	West of Macquire Island	5.7	10	99
192	Gulf of California	5.5	10	West of Macquire Island	5.7	10	170
193	Near south coast of Honshu Japan	6.4	391.1	West of Macquire Island	5.7	10	148
194	Vanuatu Island region	6.1	33	Near east coast of Honshu Japan	5.6	38.9	133
195	Near east coast of Honshu Japan	5.6	38.9	Tonga Island region	5.8	33	172
196	Tonga Island region	5.8	33	1.Nevada USA 2.Nevada USA	4.5 5.7	4.3 8.4	178 164
197	South western Siberia Russia	5.7	10	Rat Island Aleutian Island	5.2	33	260
198	Rat Island Aleutian Island	5.7	33	Samara Philippine Island	6.3	33	119
199	Samara Philippine Island	6.3	33	Guerrero Mexico	4.8	90	189
200	Guerrero, Mexico	4.8	90	1.South of Fiji Island 2.South Java Indonesia 3.Andaman Island India 4.Northern Molucca Sea	5.4 5.8 5.5 5.5	480.7 10 33 33	227 205 186 115
201	South of Fiji Island	5.4	480.7	1.South of Java Indonesia 2.Andaman Island India 3.Northern mid Atlantic ridge	5.8 5.5 5.5	10 33 10	198 236 176
202	South Java Indonesia	5.8	10	1.Northern mid Atlantic ridge 2.Cuba region	5.5 4.6	10 10	256 135
203	Andaman Island India	5.5	33	1.Northern Molucca Sea 2.Northern mid Atlantic ridge 3.Cuba region	5.5 5.5 4.6	33 10 10	100 223 124
204	Northern Molucca Sea	5.5	33	Cuba region	4.6	10	178

205	Nevada USA	4.5	10	New Britain region	5.8	33	109
206	Flores region Indonesia	5.7	33	West Chile rise	5.5	10	146
207	South of Fiji Island	5	493.6	1.Komandorsky Island	6.6	10	122
				2.Mona passage	5.2	50.8	135
				3.Mona Passage	4.7	33	130
208	Mona passage	5.2	50.8	Komandorsky Island	4.8	10	111
209	Mona Passage	4.7	33	Komandorsky Island	4.8	10	115
210	Andrean of Island Aleutian Island	6	52.5	1.Virginia USA	4.5	5	251
				2.Taiwan	6.6	33	103
				3.Southern east Pacific rise	5.5	10	170
				4.Near coast of northern Chile	5.5	41.2	160
211	Virginia, USA	4.5	5	1.Southern east Pacific rise	5.5	10	227
				2.Near coast of northern Chile	5.5	41.2	133
				3.Luzon Philippine Island	5.7	10	198
212	Near coast of north Chile	5.5	41.2	1.Samoa Island region	5.6	33	141
				2.Halmahera Indonesia	5.8	33	116
213	Luzon Philippine Island	5.7	10	Samoa Island region	5.6	33	144
214	Samoa Island region	5.6	33	Halmahera Indonesia	5.8	33	103
215	New Britain region P.N.G.	5.8	49.1	1.Myanmar	5.7	33	101
				2.Vancouver Island region	5	10	114
216	Central mid Atlantic ridge	5.8	10	Hokkaido Japan region	5.7	33	168
217	Hokkaido, Japan region	5.7	33	1.Central California	6.5	7.6	204
				2.Central California	4.7	0	201
				3.Central California	4.6	5	193
				4.Central California	4.5	4.9	103
218	Central California	6.5	7.6	Central mid Atlantic ridge	5.8	10	289
219	Central California	4.7	0	1.Central mid Atlantic ridge	5.8	10	293
				2.Azores Island region	5.5	10	114
220	Central California	4.6	5	1.Central mid Atlantic ridge	5.8	10	303
				2.Azores Island region	5.5	10	
221	Central California	4.5	4.9	1.Azores Island region	5.5	10	249
				2.Central California	4.9	6.9	134
222	Central mid Atlantic ridge	5.8	10	1.Azores Island region	5.5	10	160
				2.Central California	4.9	6.9	249
				3.Southern Sumatra Indonesia	5.5	33	128
223	Azores Island region	5.5	10	Southern Sumatra Indonesia	5.5	33	180
224	Central California	4.9	6.9	Southern Sumatra Indonesia	5.5	33	234
225	Southern Sumatra Indonesia	5.5	33	1.Mona Passage	5	141.1	263
				2.Panama-Costa Rica border region	6.5	33	274
226	Mona passage	5	141.1	1.Loyalty Island region	6.5	10	280
				2.Loyalty Island region	5.9	10	238
227	Panama-Costa Rica border region	6.5	33	1.Loyalty Island region	6.5	10	249
				2.Loyalty Island region	5.9	10	210
				3.Southern Iran	6.7	33	210
228	Southern Iran	6.7	33	1.Loyalty Island region	6.6	10	188
				2.Loyalty Island region	6.1	10	136
229	Southern Iran	5.4	33	1.Loyalty Island region	6.6	10	200
				2.Loyalty Island region	6.1	10	142
				3.Loyalty Island region	7	10	100
230	Loyalty Island region	6.6	10	Off coast of Oregon	5	10	151
231	Loyalty Island region	6.1	10	Off coast of Oregon	5	10	259
232	Off coast of Oregon	5	10	Minahassa peninsula Sulawesi	5.5	74.6	225
233	Loyalty Island region	7	10	Peru-Brazil border region	4.9	562.8	227
234	Peru-Brazil border region	4.9	562.8	1.Hokkaido, Japan region	5.8	33	228
				2.Loyalty Island region	5.8	10	121

References

1. Agrawal, P. K., Pandey, O. P., and Chetty T. R. K. 2004. Aeromagnetic anomalies, lineaments and seismicity in Koyna-Warna region. Journal of Indian Geophysical Union, Vol. 8, No. 4, pp. 229 – 242.
2. Allen, E. T. and Day, A. L. 1927. Steam wells and other thermal activity "The geysers California". Published by the Carenegie Institution of Washington, pp. 106.
3. Allis, R. G. 1982. Mechanism of induced seismicity at the geysers geothermal reservoir, California. Geophysical Research Letters, Vol. 9, No. 6, pp. 629-632.
4. Ammon, C. J. 2006. Seismic waves and earth's interior. URL: http://eqseis.geosc.psu.edu/~cammon/HTML/Classes/IntroQuakes/Notes/waves_and_interior.html accessed on Jan 14 2006.
5. Assumpção, M., Marza, V., Barros, L., Chimliganond, C., Soares, J. E., Carvalho, J., Caixeta, D., Amorim, A., and Cabreal, E. 2002. Reservoir induced seismicity in Brazil. Pure and Applied Geophysics, Vol. 159, pp. 597 – 617.
6. Beresnev, I., and Johnson, P. 1994. Elastic wave stimulation of oil production: A review of methods and results. Geophysics, Vol. 59, No. 6, pp. 1000 – 1017.
7. Berkeley 2003. URL: http://www.lbl.gov/Science-Articles/Archive/ESD-shake-rattle-flow.html accessed on February 11, 2005.
8. Bradshaw, K., Page, M., and Anderson, J. 1997. Cartography student at California State University. URL: http://www.hubcat.org/Andrienne/Koyna/Koyna_home.htm accessed on September 20, 2005.
9. Braile, L. W. 2005. Seismic wave demonstrations and animations. URL: http://www.eas.purdue.edu/~braile/edumod/waves/WaveDemo.htm accessed on Jan 13, 2006.
10. Brodsky, E., Roeloffs, E., Woodcock, D., and Gall, I. 2003. A mechanism for sustained groundwater pressure changes induced by distant earthquakes. Journal of Geophysical Research, Vol. 108, No. B8, pp. 2390.
11. Bryan, T. S. 1995. The geysers of Yellowstone, 3rd Edition. University press of Colorado, pp. 463.

12. Chadha, R. K. 1995. Role of dykes in induced seismicity at Bhatsa reservoir, Maharashtra, India. Pure and Applied Geophysics, Vol. 145, No.1, pp. 155 – 165.
13. Chen, Q., and Nur, A. 1992. Pore fluid effects in anisotropic rocks: Mechanisms of induced seismicity and weak faults. Pure and Applied Geophysics, Vol. 139, No. 3, pp. 463 – 479.
14. Chia, Y. P., Wang, Y. S., Huang, C. C., Chen, J. S., and Wu, H. P. 2002. Coseismic changes of groundwater level in response to the 1999 Chi-Chi earthquake. Western Pacific Earth Sciences, Vol. 2, No. 3, pp. 261 – 272.
15. Christensen, D. 2006. The great Alaska earthquake of 1964. URL: http://apsn.awcable.com/1964.htm accessed on April 13, 2006.
16. Dusseault, M. B., Davidson, B., and Spanos, T. J. T. 2000. Pressure pulse: the ups and downs of starting a new technology. Journal of Canadian technology, Vol. 39, No. 4.
17. Dusseault, M. B. 2004. Lecture notes. University of Waterloo.
18. Evans, J. R., Julian B. R., Foulger, G. R., and Ross, A. 1995. Shear wave splitting from local earthquake at the geyser geothermal field, California. Geophysical Research Letters, Vol. 22, No. 4, pp. 501 – 504.
19. Geoff, F. E., Donnelly, J. M., Thompson, J. M., and Hearn, B. C. Jr. 1977. Geothermal prospecting in the geyser clear lake area, Northern California. Geological Society of America, Vol. 32, No. 5, pp. 509 – 515.
20. Geilikman, M. B., Spanos, T. J. T., and Nyland, N. 1993. Porosity diffusion in fluid-saturated media. Tectonophysics, Vol. 217, pp. 111 – 115.
21. Guha, S. K. and Patil, D. N. 1992. Canadian induced sesimicity research group (CISRG database) URL: http://www.telusplanet.net/public/retom/index.htm accessed on March 23, 2005.
22. Gupta, H. K. 1992. Reservoir induced earthquakes. Elsevier Science publishers B. V., Amsterdam, The Netherlands, pp. 364.
23. Hays, W. W. 1981. Facing geologic and hydrologic hazards -- Earth science considerations. U.S. Geological Survey Professional Paper 1240B, pp. 108.

24. Helmstetter, A., Kagan, Y., and Jackson, D. 2004. Earthquake probabilities based on earthquake interactions. European Geosciences Union, Geophysical Research, Vol. 6, pp. 539.

25. Huang, F. Q., Chen, Y., Li, M., Xu, G. M., and Yan, R. 2004. Response changes of water levels to the Chi-Chi earthquake and their dynamical implications. Institute of Geophysics, China earthquake administration, Beijing 100081(China), correspondence author email: hfquiong@seis.ac.cn.

26. Husen, S., Taylor, R., Smith, R. B., and Healer, H. 2004. Changes in geyser eruption behaviour and remotely triggered seismicity in Yellowstone National Park produced by 2002. Geological Society of America, Vol. 32, No. 6, pp. 537 – 540.

27. Husen, S., Weimer, S., and Smith, R. B. 2004. Remotely triggered seismictiy in the Yellowstone National Park Region by the 2002 M_w 7.9 Denali fault earthquake, Alaska. Bulletin of the Seismological Society of America, Vol. 94, No. 6B, pp. S317 – S331.

28. IRIS. 2004. URL: http://www.iris.edu/cgi-bin/wilberII_page1.pl> accessed November 12, 2004.

29. Janetski, C. J. 2002. Indians in Yellowstone National Park. University of Utah press, USA, pp. 145.

30. Kayen, R., Tanaka, Y., Kishida, T., and Sugimoto, S. 2002. Liquefaction potential of native ground in west Kobe, Japan by the spectral analysis of surface waves methods. URL: http://walrus.wr.usgs.gov/geotech/liquefaction/ > accessed on April 12, 2005.

31. Kearey, P., and Brooks, M. 1996. An introduction to geophysical exploration. Blackwell publishing, pp. 254.

32. Kerr, R. A. 1998. Can great quakes extend their reach? Science, Vol. 280, No. 5367, pp. 1194 – 1195.

33. King, C. Y., Azuma, S., Igarashi, G., Ohno, M., Saito H., and Wakita, H. 1999. Earthquake related water level changes at 16 closely clustered wells in Tono, central Japan, Journal of Geophysical Research, Vol. 104, No. B6, pp. 13,073 – 13,082.

34. King, C. Y., Koizumi, N. and Kitagawa, 1995. Hydrogeochemical anomalies and the 1995 Kobe Earthquake. Science, 269, pp. 38 – 39.
35. Kissling, H. 2001. Postseismic fluid flow after the large subduction earthquake of Antofagasta, Chile, Geology, Vol.29, No.9, p. 847-850.
36. Knoll, P. 1992. Induced seismicity, Central institute for physics of the earth, Potsdam. A.A.Balkema, Rotterdam, Netherlands, pp. 469.
37. Krotz, D. 2003. Shake, rattle and flow. URL: http://www.lbl.gov/Science-Articles/Archive/ESD-shake-rattle-flow.html> accessed on February 11, 2005.
38. Linde, A.T., and Silver, P.G. 1989. Uplift data and the great 1960 Chilean aseismic slip. Geophysical Research Letters, Vol. 16, pp. 1305 – 1308.
39. Manga, M., Brodsky, E., and Boone, M. 2003. Response of stream flow to multiple earthquakes. Geophysical Research Letter, Vol.30, No.5, pp. 1024.
40. Mapquest 2002. URL: http://go.hrw.com/atlas/norm_htm/world.htm accessed on June 03, 2004.
41. Marzocchi, W., Selva, J., Piersanti, A., and Boschi, E. 2003. On the long-term interaction among earthquakes: some insight from a model simulation. Journal of Geophysical Research, Vol. 108, No. B11, pp. 2538.
42. Matsumoto, N., Kitagawa, G., and Roeloffs, E.A. 2001. Hydrological response to earthquakes in Haibara well, central Japan – I, groundwater level changes using state space decomposition of atmospheric pressure, rainfall and tidal responses. Geophysical Journal International, Vol. 155, pp. 885 – 898.
43. McBride, W. S. 2005. USGS Florida groundwater monitoring wells respond to Indonesian earthquake. URL: http://fl.water.usgs.gov/Tampa/earthquakeresponse.html accessed on April 15, 2006.
44. Montgomery, D.R., and Manga, M. 2003. Stream flow and water well responses to earthquakes. Science, Vol. 300, pp. 2047 – 2049.
45. Muco, B. 1998. Twenty years seismic monitoring of induced seismicity in northern Albania. Pure and Applied Geophysics, Vol. 153, No. 1, pp. 151 – 162.
46. ODNR. 2006. Ohio department of natural resources. URL: http://www.dnr.state.oh.us/water/ accessed on 13 April 2006.

47. Panfilov, V. S., and Sobolev G. A. 1995. Unstable steam-water convention as possible trigger to earthquakes. Pure and Applied Geophysics, Vol. 145, No. 1, pp. 139 – 147.

48. Parnell, J. 1994. Geo-fluids: origin, migration, and evolution of fluids in sedimentary basins. Geological society special publication no.78, published by the geological society, London, UK.

49. Parotidis, M., Shapiro, S. A., and Rothert, E. 2004. Pore Pressure diffusion and interpolate earthquake swarms. Geophysical Research Abstracts, Vol. 6, pp. 01861.

50. Parry, R. H. G. 1995. Mohr circles, stress paths and geotechnics. Published by E & FN Spon, an imprint of Chapman & Hall, London, UK.

51. Piccinelli, F. G., Mucciarelli M., Federico P., and Albarello, D. 1995. The microseismicity network of the Ridracoli Dam, north Italy: data and interpretation. Pure and Applied Geophysics, Vol. 145, No. 1, pp. 97 – 108.

52. Plafker, G., and Kachadoorian, R. 1966. Geologic effects of the March 1964 Earthquake and associated seismic sea waves on Kodiak and nearby Islands Alaska. U.S. Geological Survey Professional Paper, 543-D, pp. 46.

53. Rajendran, K. 1995. Sensivity of a seismically active reservoir to low-amplitude fluctuations: Observations from Lake Jocassee, south Caroline. Pure and Applied Geophysics, Vol. 145, No. 1, pp. 87 – 95.

54. Rajendran, K. and Harish, C.M. 2000. Mechanism of triggered seismicity at Koyna: An evaluation based on relocated earthquakes. Current Sciences, Vol. 79, No. 3, pp. 358 – 363.

55. Rastogi, B.K., Chadha, R.K., and Raju, I.P. 1986. Seismicity near Bhatsa reservoir, Maharashtra, India. Physics of the Earth and Planetary Interiors, Vol. 44, No. 2, pp. 179 – 199.

56. Rastogi, B. K., Chadha, R. K, and Sarma, C. S. P. 1995. Investigations of June 7, 1988 earthquake of magnitude 4.5 near Idukki Dam in southern India. Pure and Applied Geophysics, Vol. 145, No. 1, pp. 109 – 122.

57. Raval, U. 1995. Seismicity of the Koyna region and regional tectonomagmatism of the Wester Margin, India. Pure and Applied Geophysics, Vol. 145, No. 1, pp. 175 – 192.

58. Rinehart, J. S. 1980. Geysers and geothermal energy, Springer-Verlag New York, printed in United States of America 98765431, pp. 233.

59. Robertson, C. E. 2001. The interior of the Earth. URL: http://pubs.usgs.gov/gip/interior/ accessed on November 7, 2005.

60. Roeloffs, E. 1996. Poroelastic techniques in the study of earthquake related hydrologic phenomena. Advances in Geophysics, Vol. 37, pp. 135 – 195.

61. Roeloffs, E. 1998. Persistent water level changes in a well near Parkfield, California, due to local and distant earthquakes. Journal of Geophysical Research, Vol.103, No. B1, pp. 869 – 889.

62. Roeloffs, E., Sneed, M., Galloway, D. L., Sorey, L. M., Farrar, C. D., Howle, J. F, and Hughes, J. 2003. Water level changes induced local and distant earthquakes at Long Valley caldera, California. Journal of Volcanology and Geothermal Research, Vol. 127, pp. 269 – 303.

63. Rutledge, J. T., Stark, M. A, Fairbanks, T. D., and Anderson, T. D. 2000. Near surface microearthquakes at the geysers geothermal field, California. Submitted to Pure and Applied Geophysics, LAUR no. 00-1554.

64. Saar, M. O., and Manga, M. 2003. Seismicity induced by seasonal groundwater recharge at Mt. Hood, Oregon. Earth and Planetary Science Letters, pp. 605 – 618.

65. Sato, H. and Fehler, M. C. 1998. Seismic wave propagation and scattering in the heterogeneous earth. Springer-Verlag, New York, Inc. pp. 308.

66. Scholz, C. H. 1988. Mechanisms of seismic quiescences. Pure and Applied Geophysics, Vol. 126, No. 2 – 4, pp. 701 – 718.

67. Scholz, C. H. 2002. The Mechanics of Earthquakes and Faulting, 2nd edition. Printed in the United Kingdom at the University Press, Cambridge, 471 p.

68. Sciencedaily. 2003. Charting seismic on water levels can refine earthquake understanding. URL:

http://www.sciencedaily.com/releases/2003/06/030627000320.htm accessed on April 13, 2006.

69. Shen, L. Y., and Chang B. Q. 1995. Application of stress pore pressure coupling theory for porous media to the Xinfengjiang reservoir earthquake. Pure and Applied Geophysics, Vol. 145, No. 1, pp. 123 – 137.

70. Simpson, D. W., Leith, W. S., and Scholz, S. K. 1988. Two types of reservoir induced seismicity. Bulletin Seismology Society of America, Vol. 78, pp. 2025 – 2040.

71. Simsek, S. 2003. Geothermal activity at earthquake zones and using of geothermal energy on the earthquake area. Hacettepe University, International research and application center for Karst water resources (UKAM), 06532 Beytepe, Ankara, Turkey.

72. Sleep, H. N., and Fujita, K. 1997. Principles of geophysics. Blackwell publishing, pp. 586.

73. Sliver, P. G. and Valette-Silver, N. J. 1992. Detection of hydrothermal precursors to large northern California earthquakes. Sciences, Vol. 257, pp. 1363 – 1368.

74. Sneed, M., Galloway, D. L, and Cuuningham, W. L. 2003. Earthquake – Rattling the earth's plumbing system. U.S. geological survey, information services Box 25286, Denver Federal Center, Denver, CO 80225, fact sheet 096 – 03 URL: http://water.usgs.gov/pubs/fs/fs-096-03/ accessed on February 12, 2005.

75. Spanos, T. J. T. 2002. The thermophysics of porous media. Corporate blvd., Boca Raton, Florida, printed in United States of America, pp.1 – 220.

76. Spanos, T. J. T, Dusseault, M. B., Udey, N. 2003. Fundamental thermodynamic requirements for porous media description. Proc. Int. Conf. on THMC processes in geo-systems, Stockholm, pp. 511-519.

77. Srivastava, H. N., Bhattacharaya, S. N., Sinha, R. K. C., Mahmoud, S. M., and Yunga, S. 1995. Reservoir associated characteristics using deterministic Chaos in Aswan, Nurek and Koyna reservoirs. Pure and Applied Geophysics, Vol. 145, No. 1, pp. 209 – 217.

78. Stein, S., and Wysession, M. 2003. An introduction to seismology, earthquakes, and earth structure. Blackwell publishing, pp. 498.

79. Streepey, M. 1996. Tectonophysics Group, University of Michigan, Department of Geological Sciences, 2534 C.C. Little Building, Ann Arbor, MI 48109-1063, USA. URL: http://www.umich.edu/~gs265/geysers.html accessed November 2, 2004.

80. Talwani, P. and Acree, S. 1984/1985. Pore pressure diffusion and the mechanism of reservoir induced seismicity. Pure and Applied Geophysics, Vol. 122, pp. 947 – 964.

81. Talwani, P. 1995. Speculation on the causes of continuing seismicity near Koyna reservoir, India. Pure and Applied Geophysics, Vol. 145, No. 1, pp. 168 – 174.

82. Talwani, P. 1997. On the nature of reservoir induced seismicity. Pure and Applied Geophysics, Vol. 150, No. 3 – 4, pp. 473 – 492.

83. Talwani, P. 2000. Seismogenic properties of the crust inferred from recent studies of reservoir-induced seismicity, application to Koyna. Current Science, Vol. 79, No. 9 – 10. pp. 1327 – 1333.

84. Thomson, J. J. 1997. Earth's interior and plate tectonics. URL: http://www.solarviews.com/eng/earthint.htm accessed on October 12, 2005.

85. Tsukuda, T. 1997. Sizes and some features of luminous sources associated with the 1995 Hyogo-ken Nanbu earthquake. Journal of Physics of the Earth, Vol. 45, pp. 73-82.

86. Turcotte, D. L. and Schubert, G. 2002. Geodynamics 2nd edition. Cambridge University press, UK, pp.456.

87. USGS. 2005. Volcanoes hazards. URL: http://volcanoes.usgs.gov/yvo/2004/faq_yearlyeq.html accessed March 11, 2005.

88. UtahMinesEdu. 2005. Remote seismicity. URL: http://www.mines.utah.edu/~ggcmpsem/UUSATRG/Seis/Yellowstone/Yellreadymadepost.cgi accessed March 11, 2005.

89. Voisin, C., Cotton, F., and Carli, S. D. 2004. A unified model for dynamic and static stress triggering of aftershocks, antishocks, remote seismicity, creep events, and multisegmented rupture. Journal of Geophysical Research, Vol. 109, B06304.

90. Waite, G. P., and Smith, R. B. 2004. Seismotectonics and stress field of the Yellowstone volcanic plateau from earthquake first-motion and other indicators. Journal of Geophysical Research, Vol. 109, B02301.

91. Wakita, H. 1975. Water wells as possible indicators of tectonic strain. Science, 189, pp. 553 – 555.

92. Warpinski, N. R., Wolhart, C. A., and Wright, S. L. 2004. Analysis and prediction of microseismicity induced by hydraulic fracturing. Society of Petroleum Engineers, Vol. 9, No. 1, pp. 24 – 33.

93. White, D. E. 1967. Some principles of geyser activity mainly from steamboat spring Nevada. American Journal Sciences, Vol. 265, pp. 641 – 684.

94. Wood, R. M. and King, G. C. P. 1993. Hydrological signatures of earthquake strain. Journal of Geophysical Research, Vol. 98, No. B12, pp. 22,035 – 22,068.

95. Wu, R. S. and Aki, K. 1988. Introduction seismic wave scattering in three dimensionally heterogeneous Earth. Pure and Applied Geophysics, Vol. 128, No.1-2, pp. 1 – 6.

96. Yaltirak, C., Yalcin, T., Yuce, G., and Bozkurtoglu, E. 2005. Water-level changes in shallow wells before and after the 1999 Izmit and Duzce earthqukes and comparison with long-term water-level observations (199902004), NW Turkey. Turkish Journal of Earth Sciences, Vol. 14, pp. 281-309.